

# Gelsolin Amyloidosis: a Diagnostic and Therapeutic Nanobody Approach



ir. Adriaan Verhelle

promotor: prof. dr. Jan Gettemans

Thesis submitted to fulfill  
the requirements for achievement of the degree of  
Doctor in Biomedical Sciences

Faculty of Medicine and Health Sciences  
Department of Biochemistry  
Ghent University

*'The absolute worst thing that you ever can do, in my opinion,  
in bringing science to the general public, is be condescending or judgmental.  
It is so opposite to the way science needs to be brought forth.'*

- Brian Greene

*'We live in a special time,...  
the only time where we can observationally verify  
that we live in a special time'*

- Lawrence M. Krauss

**Promoter:**

**Prof. dr. Jan Gettemans**  
Nanobody lab  
Department of Biochemistry  
Faculty of Medicine and Health Sciences  
Ghent University, Belgium

**Dean:**

**Prof. dr. Piet Hoebeke**

**Rector:**

**Prof. dr. Anne De Paepe**

# Gelsolin Amyloidosis: a Diagnostic and Therapeutic Nanobody Approach

**ir. Adriaan Verhelle**

Promoter: Prof. dr. Jan Gettemans

Thesis submitted in fulfilment of the requirements  
for the degree of Doctor (PhD) in Biomedical Sciences

## **Dutch translation of the title**

Gelsoline amyloidose: een diagnostische en therapeutische benadering met nanobodies

## **Cover Illustration**

The cover illustration shows a picture of the monument to the laboratory mouse. This sculpture is located in front of the Institute of Cytology and Genetics at the Russian Academy of Sciences in Novosibirsk, Siberia, Russia. The monument depicts an anthropomorphic mouse, with glasses and a lab coat, knitting a DNA double helix. It is dedicated to all the laboratory mice - and in a broader sense all laboratory animals - which, although involuntary, gave their life to science. In the same way, this cover illustration is meant as a humbling reminder of all the mice which were used during the course of this PhD. The original picture was processed with a charcoal image filter.

## **Reference**

Verhelle Adriaan (2017), Gelsolin Amyloidosis: a Diagnostic and Therapeutic Nanobody Approach. PhD thesis. Ghent University.

## **Printing**

University Press, Zelzate

The author and the promoter give the authorization to consult and to copy parts of this work for personal use only. Every other use is subject to the copyright laws. Permission to reproduce any material contained in this work should be obtained from the author.

Author  
Adriaan Verhelle

Promoter  
Jan Gettemans

## **Members of the examination committee**

### **Prof. dr. Bruno Verhasselt**

*Chairman*

Department of Clinical chemistry, microbiology and immunology  
Faculty of Medicine and Health Sciences  
Ghent University, Belgium

### **Dr. Lennart Zabeau**

Department of Biochemistry  
Faculty of Medicine and Health Sciences  
Ghent University, Belgium

### **Prof. dr. Patrick Santens**

Department of Internal medicine  
Faculty of Medicine and Health Sciences  
Ghent University, Belgium

### **Dr. Elke Decrock**

Department of Basic Medical Sciences  
Faculty of Medicine and Health Sciences  
Ghent University, Belgium

### **Prof. dr. Els Van Damme**

Department of Molecular biotechnology  
Faculty of Bioscience Engineering  
Ghent University, Belgium

### **Prof. dr. Sophie Hernot**

Department of Medical Imaging and Physical Sciences  
Faculty of Medicine and Pharmacy  
Vrije Universiteit Brussel (VUB), Belgium

### **Prof. dr. Jan Gettemans**

*Promoter*

Department of Biochemistry  
Faculty of Medicine and Health Sciences  
Ghent University, Belgium





# Table of Contents

<b>Table of Contents</b>	<b>i</b>
<b>Preface</b>	<b>vi</b>
<b>List of abbreviations</b>	<b>x</b>
<b>Summary &amp; Samenvatting</b>	<b>1</b>
1 Summary	3
2 Samenvatting	6
<b>I General introduction</b>	<b>9</b>
1 Introduction to the actin skeleton and gelsolin	11
1.1 The Cytoskeleton . . . . .	11
1.1.1 Actin . . . . .	12
1.1.2 Gelsolin . . . . .	16
2 Introduction to amyloid disease	24
2.1 Amyloidosis . . . . .	24
2.1.1 Protein synthesis . . . . .	24
2.1.2 Protein quality control . . . . .	27
2.1.3 Amyloidosis . . . . .	31

---

<b>3</b>	<b>Introduction to gelsolin amyloidosis</b>	<b>36</b>
3.1	Gelsolin amyloidosis . . . . .	36
3.1.1	Discovery . . . . .	36
3.1.2	Epidemiology & genealogy . . . . .	36
3.1.3	Clinical features . . . . .	37
3.1.4	Molecular mechanism . . . . .	40
3.1.5	Diagnosis and treatment . . . . .	44
3.1.6	Mouse model . . . . .	44
<b>4</b>	<b>Introduction to nanobodies</b>	<b>45</b>
4.1	Antibodies and their fragments . . . . .	45
4.1.1	Conventional antibodies . . . . .	45
4.1.2	Discovery of nanobodies . . . . .	47
4.1.3	Structure and characteristics of nanobodies . . . . .	47
4.1.4	Nanobody production . . . . .	50
4.2	Applications of nanobodies . . . . .	50
4.2.1	Research . . . . .	50
4.2.1.1	Crystallography . . . . .	50
4.2.1.2	Intrabodies . . . . .	50
4.2.2	Diagnostics . . . . .	51
4.2.2.1	Biosensors . . . . .	51
4.2.2.2	<i>In vivo</i> imaging . . . . .	51
4.2.3	Therapeutics . . . . .	52
4.2.3.1	Multidomain nanobodies . . . . .	52
4.2.3.2	Cancer therapy . . . . .	52
<b>II</b>	<b>Preceding work &amp; Scope</b>	<b>54</b>
<b>1</b>	<b>Introduction</b>	<b>56</b>
<b>2</b>	<b>Preceding work</b>	<b>57</b>
2.1	Extracellular targeting of the AGel pathological pathway . . . . .	57
2.2	Intracellular targeting of the AGel pathological pathway . . . . .	59

---

<b>3</b>	<b>Scope of the thesis</b>	<b>63</b>
<b>III</b>	<b>SPECT/CT imaging in the AGel mouse model</b>	<b>66</b>
<b>1</b>	<b>Non-invasive imaging of amyloid deposits in a mouse model of AGel using <sup>99m</sup>Tc-modified nanobodies and SPECT/CT</b>	<b>68</b>
1.1	Abstract . . . . .	68
1.2	Introduction . . . . .	69
1.3	Materials & Methods . . . . .	70
1.3.1	Antibodies and reagents . . . . .	70
1.3.2	Generation of FAF gelsolin-specific nanobodies . . . . .	70
1.3.3	cDNA cloning . . . . .	70
1.3.4	Purification of the nanobodies . . . . .	70
1.3.5	Serum stability assay . . . . .	71
1.3.6	Radiolabeling with <sup>99m</sup> Tc . . . . .	71
1.3.7	Single-photon emission computed tomography/X-ray tomography imaging experiments . . . . .	71
1.3.8	Immunofluorescence . . . . .	72
1.3.9	Statistical analysis . . . . .	73
1.4	Results . . . . .	73
1.4.1	Nanobody stability and labeling . . . . .	73
1.4.2	Follow-up study of GSN Nb11-expressing AGel mice with <sup>99m</sup> Tc-FAF Nb1 SPECT/CT image analysis . . . . .	79
1.4.3	Correlation between SPECT/CT signal and <i>in vivo</i> binding site levels . . . . .	80
1.5	Discussion . . . . .	83
1.6	Conclusion . . . . .	85
1.7	Acknowledgements . . . . .	86
<b>IV</b>	<b>Nanobody gene therapy against gelsolin amyloidosis via adeno-associated viruses</b>	<b>88</b>
<b>1</b>	<b>AAV9 delivered bispecific nanobody attenuates amyloid burden in the gelsolin amyloidosis mouse model.</b>	<b>90</b>
1.1	Abstract . . . . .	90

---

1.2	Introduction . . . . .	90
1.3	Materials & Methods . . . . .	92
1.3.1	Antibodies and reagents . . . . .	92
1.3.2	Generation of gelsolin-specific nanobodies . . . . .	92
1.3.3	cDNA cloning . . . . .	92
1.3.4	Purification of recombinant PG*, C68 and nanobodies . . . . .	93
1.3.5	ELISA . . . . .	93
1.3.6	WB with bispecific Nb11-FAF nanobodies as primary antibody . . . . .	93
1.3.7	<i>In vitro</i> MT1-MMP sensitive linker assay . . . . .	93
1.3.8	<i>In vitro</i> Furin/MT1-MMP assay . . . . .	93
1.3.9	HEK293T cell culture, transfection and microscopy . . . . .	94
1.3.10	HEK293T medium analysis . . . . .	94
1.3.11	AAV9 gene therapy intervention study . . . . .	95
1.3.12	SPECT/CT imaging . . . . .	96
1.3.13	Muscle contractile properties . . . . .	96
1.3.14	Immunofluorescence . . . . .	96
1.4	Results . . . . .	97
1.4.1	Production of the bispecific nanobody . . . . .	97
1.4.2	Bispecific gelsolin nanobodies merge the binding characteristics of their monovalent constituents <i>in vitro</i> . . . . .	98
1.4.3	The MT1-MMP peptide linker is functional in an <i>in vitro</i> setup . . . . .	98
1.4.4	Bivalent Nb11-FAF Nb protects D187N plasma gelsolin against combined furin/MT1-MMP proteolysis . . . . .	100
1.4.5	Furrin assay in HEK293T cells - Bivalent Nb11-FAF Nbs inhibit furin proteolysis . . . . .	102
1.4.6	Bispecific Nb11-FAF1 gene therapy in AGel mice via AAV9 . . . . .	106
1.4.7	AAV9-Nb11-FAF1 displays therapeutic properties in AGel mice . . . . .	107
1.5	Discussion . . . . .	111
1.6	Conclusion . . . . .	113
1.7	Acknowledgements . . . . .	113

---

V	Discussion	115
1	Where are we now	117
2	SPECT/CT imaging of amyloid deposits in the AGel mouse model	119
3	AAV9 gene therapy with bispecific Nb11-FAF1 nanobody in AGel mice	122
4	General conclusion and future prospects	125
	Bibliography	131
VI	Dankwoord	160
	Bedankt!	162
	Curriculum Vitae	166

# PREFACE



# Preface

In science we have to be particularly cautious about 'why' questions. When we ask, 'Why?' we usually mean 'How?' If we can answer the latter, that generally suffices for our purposes.

---

*Lawrence M. Krauss*  
*A Universe from Nothing*

The origin of modern science dates back to 16th century Europe, when Nicolaus Copernicus dared to defy the anthropocentric view imposed by the Catholic church. His lifework, '*De revolutionibus orbium coelestium*', shook the foundations of religious orthodoxy that had held society in its grasp throughout the Dark Ages. Despite the ferocious attempts of the Roman Inquisition to nip this new movement in the bud, the power of inductive reasoning proved to be an unstoppable force. Gaining more and more momentum via the sequential, mind-blowing - but at that time utterly controversial - insights of Giordano Bruno, Galileo Galilei, Johannes Kepler and Isaac Newton, humanity had finally broken out of the clerical yoke and launched itself into a new era fueled by freethinking rational minds. In the following 5 centuries scientific discoveries were translated into practical application and infiltrated every aspect of our daily lives.

Since then, every scientific breakthrough started out as a simple question regarding why - or more accurately how - some natural process happens the way it does. Scientists have the irresistible need to completely dismantle every natural phenomenon into all its individual compartments. During this process, the emergence of more and more detailed knowledge inevitably raises numerous side questions, all of which have to be answered. Ultimately, after years of copious experiments, the final detail reveals itself. The scientists take a step back and marvel how all the pieces fall into place.

The story of Gelsolin amyloidosis - the main scope of this manuscript - is not different. In the decennia after this disease was first described in a patient, a troop of scientists have meticulously unraveled this pathology to the molecular level.





# LIST OF ABBREVIATIONS



# Abbreviations

<sup>111</sup> Ln	Artificial isotope of indium
26S	26 Svedberg
3D	Three-dimensional
8 kDa	8 kDa amyloidogenic fragment of gelsolin
<sup>99m</sup> Tc	Metastable nuclear isomer of technetium-99
9q34	Position 34 on the long arm of chromosome 9
$\beta$ 2AR	$\beta$ -2 adrenergic receptor
$\mu$ M	Micromolar
A	Adenine
AA	Amino Acid
ABPs	Actin binding proteins
ADP	Adenosine diphosphate
AGel	Gelsolin amyloidosis
Arp2/3	Actin-related proteins 2 and 3
ATP	Adenosine triphosphate
C	Cytosine
C68	68 kda C terminal fragment of gelsolin
Ca <sup>2+</sup>	Calcium in its +2 oxidation state
CG	Cytoplasmic gelsolin
CLD	Corneal lattice dystrophy
CNX	Calnexin
CRT	Calreticulin
C-terminus	Carboxylic group terminus of a polypeptide
DNA	Deoxyribonucleic acid
EGTA	Ethylene glycol-bis( $\beta$ -aminoethyl ether)-N,N,N',N'-tetra-acetic acid
ELISA	Enzyme-linked immunosorbent assay
ERAD	Endoplasmatic-reticulum-associated protein degradation
ER	Endoplasmic reticulum

---

ES cells	Embryonic stem cells
Fab	Antigen-binding fragment
F-actin	Filamentous actin
FAF	Familial amyloidosis of the Finnish type
FRs	Framework regions
G	Guanine
G1-6	One of the six globular domains that comprise gelsolin
G2 phase	Cell cycle Gap2 phase
G-actin	Globular actin
GSN	Gelsolin gene
GSN <sup>-/-</sup>	Gelsolin gene knock-out
HCAbs	Heavy chain antibodies
HIF-1	Hypoxia-inducible factor 1
Hsp40	Heat shock protein 40
Hsp70	Heat shock protein 70
IPODs	Insoluble protein deposits
JUNQ	Juxta nuclear quality control compartment
kb	Kilobase
kcal	Kilocalorie
kDa	Kilodalton
kg	Kilogram
log <sub>10</sub>	Decimal logarithm
LPA	Lysophosphatidic acid
LPS	Lipopolysaccharide
mAbs	Monoclonal antibodies
MCK	Muscle creatine kinase
Mda	Megadalton
mg/l	Milligram per liter
Mg <sup>2+</sup>	Magnesium in its +2 oxidation state
M	Molar
MT1-MMP	MT1 matrix metalloproteinase
nABPs	Nuclear actin binding proteins
nm	Nanometer
N-terminus	Amine group terminus of a polypeptide
PAF	Platelet activating factor
PET	Positron emission tomography
PG	Plasma gelsolin
PG*	Mutant plasma gelsolin
pH	Decimal logarithm of the hydrogen concentration

---

PIP <sub>2</sub>	Phosphatidylinositol 4,5-bisphosphate
PMEL	Pigment cell-specific pre-melanosomal protein
pp60 <sup>c-src</sup>	Proto-oncogene tyrosine-protein kinase Src
PYK2	Protein tyrosine kinase 2 beta
RNA	Ribonucleic acid
sIBM	Sporadic inclusion body myositis
SPECT	Single-photon emission computed tomography
SR	Signal recognition particle receptor
SRP	Signal recognition particle
T	Thymine
TGF $\beta$	Transforming growth factor $\beta$
TLR	Toll-like receptor
U	Uracil
UGGT	(UDP)-glucose:glycoprotein glucosyltransferase
UPR	Unfolded protein response
UPS	Ubiquitin proteasome system
VH	Variable domain of the heavy chain
VHH	Variable domain of the heavy chain of heavy chain antibodies
VL	Variable domain of the light chain



# SUMMARY & SAMENVATTING





# 1

## Summary

Gelsolin amyloidosis (AGel), formerly known as familial amyloidosis Finnish type (FAF), is a debilitating, autosomal, dominantly heritable, incurable disease caused by a point mutation - most commonly G654A/T - in the *GSN* gene. As a result, gelsolin's second domain loses part of its intrinsic stability and can adopt an intermediate state during  $\text{Ca}^{2+}$  activation. This aberrant conformation exposes an otherwise buried furin cleavage site. During secretion, mutant plasma gelsolin encounters furin in the trans-Golgi network. Proteolysis produces a C-terminal, 68 kDa fragment - C68 - which, upon secretion in the extracellular matrix, gets cleaved by MT1-MMP-like proteases. With this, 8 and 5 kDa amyloidogenic fragments are produced which, in time, start to polymerize into amyloid fibrils and which eventually form amyloid plaques. Patients, of whom the majority is found in Finland, experience a triad of ophthalmological, neurological and dermatological symptoms. At the moment, treatment is purely symptomatic; eye drops, corneal transplantation and plastic surgery. Therapies involving the inhibition of furin and/or MT1-MMP have been suggested. However, tampering with these key proteases will almost surely result in severe unwanted side effects. In our lab we therefore redirected our attention towards mutant plasma gelsolin. Nanobodies were developed against both gelsolin and the 8 kDa amyloidogenic fragment. Upon *in vitro* screening a chaperone for mutant plasma gelsolin - Nb11 - and chaperones for C68 - FAF Nb1, 2 and 3 - (partly) protected their antigen against furin and MT1-MMP respectively. Intraperitoneal injection with FAF Nb2 and *in vivo* expression of Nb11 in the AGel mouse model both resulted in a reduced deposition of the amyloidogenic 8 kDa fragment. In this thesis we further explored the potential of these nanobodies in regard to AGel therapeutics.

In a first study the imaging potential of the FAF nanobodies was explored. The rationale for this was that, up until now, the efficacy of AGel therapeutics under development could only be measured via end-stage animal trials. With the already characterized FAF Nbs - raised against the 8 kDa amyloidogenic gelsolin fragment - we set out to shed light on this black box hurdle. Coupled to  $^{99\text{m}}\text{Tc}$ , all three nanobodies rendered clear, low background, SPECT/CT images of the gelsolin

---

amyloid buildup in A $\beta$  mice. Based on its superior signal-to-noise ratio and signal specificity, FAF Nb1 was chosen as the most promising candidate. A follow-up study involving A $\beta$  mice expressing the therapeutically active Nb11 demonstrated that, besides rendering qualitative images, FAF Nb1 can also provide quantitative data. Indeed, comparison of quantified SPECT/CT images, biodistribution analysis and immunofluorescent histology revealed similar patterns in signal increase. Furthermore, a correlation plot showed a positive relationship between  $^{99m}\text{Tc}$ -FAF Nb1 uptake and *in vivo* gelsolin amyloid buildup.

In a second study the two types of therapeutic chaperone nanobodies - Nb11 shields mutant plasma gelsolin from furin and FAF Nb1, 2 and 3 shield C68 from MT1-MMP - were combined into a single bispecific format. The FAF Nbs were linked head-to-tail to Nb11 via a MT1-MMP sensitive linker. We hypothesized that during secretion, the bispecific Nb would encounter mutant plasma gelsolin in the trans-Golgi network and (partly) shield it from furin degradation. Upon secretion in the extracellular matrix, the MT1-MMP sensitive linker would serve as a decoy and, at the same time, release the FAF Nb moiety, which would then shield (the lower amount of) C68 from MT1-MMP degradation. Overall this double hit strategy would result in a significant decrease in amyloidogenic 8 kDa peptide production. *In vitro*, a combination of Nb11 and FAF Nb1 proved to be the most potent. As this approach requires intracellular delivery of the protective bispecific nanobody, adeno-associated virus serotype 9 (AAV9) gene therapy seemed an appropriate and clinically relevant method of administration during an intervention study in A $\beta$  mice. FAF Nb1 based SPECT/CT imaging, and immunohistochemistry evinced a significant decrease in gelsolin amyloid buildup, which translated in improved muscle contractile properties.



# 2

## Samenvatting

Gelsoline amyloïdose is een slopende, autosomaal, dominant overerfbare, ongeneeselijke ziekte die veroorzaakt wordt door een punt mutatie - hoofdzakelijk G654A/T - in het *GSN* gen. Vanwege deze mutatie verliest het tweede domein van gelsoline een deel van zijn intrinsieke stabiliteit en neemt een intermediaire conformatie aan tijdens  $\text{Ca}^{2+}$  activatie. In deze abberante conformatie komt een anderzijds begraven furine knipplaats aan het oppervlakte te liggen. Tijdens secretie colocaliseert mutant plasma gelsoline met furine in het trans-Golgi netwerk. Proteolyse resulteert in de vorming van een C-terminaal, 68 kDa fragment - C68 - dat op zijn beurt, bij secretie in de extra cellulaire matrix, verknipt wordt door *MT1-MMP like* proteasen. Hierbij worden 8 en 5 kDa amyloïdogene fragmenten vrijgesteld die, op termijn, polymeriseren in amyloïd fibrillen die finaal samenklitten in amyloïd plaques. Patiënten, waarvan de meerderheid terug te vinden is in Finland, ervaren een triade van oftalmologische, neurologische en dermatologische symptomen. Momenteel wordt enkel symptomatisch behandeld; oogdruppels, cornea transplantatie en plastische chirurgie. Therapeutica gebaseerd op de inhibitie van furine of MT1-MMP werden reeds naar voor geschoven. Echter, inhibitie van deze proteasen zal nagenoeg zeker resulteren in ernstige, ongewenste neveneffecten. Op basis hiervan richtten we onze aandacht op mutant plasma gelsoline. Nanobodies werden ontwikkeld tegen zowel gelsoline en het 8 kDa amyloïdogene fragment. *In vitro* screening identificeerde één chaperone nanobody voor mutant plasma gelsoline - Nb11 - en drie voor C68 - FAF Nb1, 2 en 3 - die hun antigeen (gedeeltelijk) beschermen tegen respectievelijk furine en MT1-MMP. Intraperitoneale injectie met FAF Nb2 en *in vivo* expressie van Nb11 in het AGel muis model resulteerde in beide gevallen in een verminderde afzetting van het amyloïdogene 8 kDa fragment. In dit proefschrift werden deze nanobodies verder getest op hun potentiëel binnen de AGel diagnostiek en therapie.

In een eerste studie werd het potentieel van de FAF nanobodies binnen de amyloïd beeldvorming verkend. De motivering hiervoor was dat, tot nu toe, de werkzaamheid van potentiële AGel therapeutica enkel kon worden nagegaan via *end-stage* dierenproeven. Met de reeds gekarakteriseerde FAF Nbs - opgewekt tegen het 8 kDa amyloïdogene gelsoline fragment - op zak namen we het op

ons om dit obstakel weg te werken. Gekoppeld aan  $^{99m}\text{Tc}$  produceerden alle drie de nanobodies scherpe, SPECT/CT beelden van de gelsoline amyloïd afzettingen in AGel muizen. Op basis van zijn superieure *signal-to-noise* ratio en signaalspecificiteit werd FAF Nb1 gekozen als het meest veelbelovende nanobody. In een *follow-up study* met AGel muizen die Nb11 expresseren, werd duidelijk dat FAF Nb1 eveneens bruikbaar is voor kwantitatieve beeldvorming. Inderdaad, een vergelijking van SPECT/CT kwantificatie, biodistributie data en immunofluorescente histologie resulteerde in gelijkaardige patronen van signaal toename. Daarenboven, correlatieplots toonden een positief verband aan tussen  $^{99m}\text{Tc}$ -FAF Nb1 opname en *in vivo* gelsoline amyloïd afzetting.

In een tweede studie werden de twee types therapeutische chaperone nanobodies - Nb11 die mutant plasma gelsoline afschermt van furine en FAF Nb1, 2 en 3 die C68 afschermen van MT1-MMP - samengevoegd in één bispecifiek nanobody. De FAF Nbs werden kop-staart verbonden met Nb11 met behulp van een MT1-MMP gevoelige linker sequentie. De hypothese was dat, tijdens secretie, het bispecifieke nanobody mutant plasma gelsoline zou binden in het trans-Golgi netwerk en (gedeeltelijk) behoeden voor furine degradatie. Vervolgens zou, bij secretie in de extracellulaire matrix, de MT1-MMP gevoelige linker optreden als afleiding en simultaan instaan voor de vrijstelling van het FAF Nb fragment. Dit laatste zou dan op zijn beurt instaan voor de afscherming van (de reeds lagere hoeveelheid) C68 tegen MT1-MMP proteolyse. Deze *double hit* strategie zou resulteren in een significante reductie van de geproduceerde hoeveelheid 8 kDa peptide. *In vitro*, gaf een combinatie van Nb11 en FAF Nb1 het beste resultaat. Gezien deze strategie een intracellulair actieve component bevat, leek adeno-geassocieerd virus serotype 9 (AAV9) genterapie een toepasselijke en klinisch relevante toedieningsmethode tijdens een interventie studie in AGel muizen. FAF Nb1 gebaseerde SPECT/CT beeldvorming en immunohistochemie toonden een significante reductie in de gelsoline amyloïd afzetting aan. Deze resultaten werden ondersteund door verbeterde spiercontractie parameters.



# **PART I**

## GENERAL INTRODUCTION





# 1

## Introduction to the actin skeleton and gelsolin

### 1.1 The Cytoskeleton

One of the most striking features of living organisms is their ability to move; bacteria follow chemical gradients, plants have parts that respond to touch, moisture and/or light and the majority of animals have the ability to roam freely, at least during one stage of their life cycle. On the cellular level this movement is the result of an immense array of interactions with the cytoskeleton. Every organism is a specific combination of the basic building block of life: the cell. Although they come in more than 200 different forms and sizes (bionumbers ID 103626) - ranging from the tadpole shaped sperm cell being only 60  $\mu\text{m}$  to neurons of almost one meter (bionumbers ID 104901) - their basic design is identical. In essence a cell is a bubble of viscous, protein-rich liquid, the cytoplasm, contained in a lipid bilayer called the plasma membrane. Internally, more lipid bilayers define separate compartments in which the key functions for survival are performed. (i) The nucleus holds the DNA, the molecule which encodes all the information necessary to build a complete organism. When needed, pieces of this information get translated into RNA, a messenger molecule able to leave the nucleus. (ii) The protein production center is formed by the ribosomes, the endoplasmic reticulum (ER), Golgi apparatus and all the associated transport vesicles. Ribosomes translate the information - coded in the DNA/RNA - into proteins which are released into the cytoplasm or further mature in the ER and Golgi apparatus and get distributed to their final location. Proteins can hold many functions, from simple building blocks for structures such as hair or skin to miniature copy machines which duplicate DNA when a cell is about to divide. (iii) The mitochondria are the power stations of the cell. The fact that these essential structures still hold their own DNA is a remnant of their bacterial origin. In these structures, sugars react with oxygen forming carbon dioxide, water and energy. The latter is stored under

the form of adenosine triphosphate (ATP), the number one energy transfer molecule<sup>1</sup>.

In order for this system of data copying in the nucleus, translation by the ribosomes and distribution by the Golgi apparatus - all fueled by the energy generated in the mitochondria - to run smoothly, evolution has employed a cellular framework called the cytoskeleton. This vast network of fibrous structures serves several important functions. (i) The cytoskeleton defines the overall shape of cells which stands in a close relationship to its function. (ii) Being a dynamic structure, breakdown at one side of a cell and buildup on the opposite site enables certain cell types to move in a specific direction. (iii) Subsets of these fibrous structures serve different functions. The microtubules can be used as roadways for transport proteins such as kinesin and dynein whereas intermediate filaments and microfilaments grant tensile strength and pressure resistance to cells.

### 1.1.1 Actin

Microfilaments are also called actin filaments as they are primarily composed of polymerized actin, combined with a whole array of interacting proteins. In any eukaryotic cell, actin is the most abundant protein - ranging from 25% in muscle cells to about 1-5% in liver cells [2, 3] - and can be visualized with specific fluorescent dyes such as phalloidin (**Figure 1.1**).

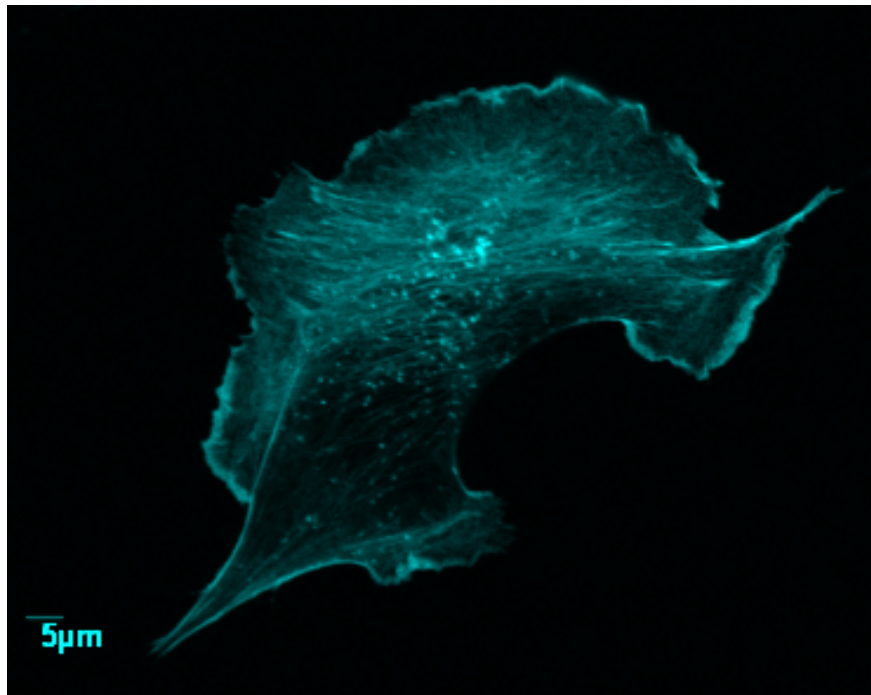


**Figure 1.1: Phalloidin staining of the cytoskeleton.** Phalloidin selectively binds to filamentous actin and prevents depolymerization. Using fluorescently labeled derivatives of phalloidin microscopic images can be taken of the actin cytoskeleton, as depicted here in blue [4].

---

<sup>1</sup>I would like to emphasize that this description is an oversimplification of all the intricate structures and processes contained within a cell. For more details I kindly refer to the book *Molecular Biology of the Cell* from Alberts *et al.*, 2002 [1] and other similar outstanding literature.

The amino acid (AA) sequence of actin is heavily conserved in the eukarya - the domain of life including all life forms comprised of (a) nucleated cell(s) (**Figure 1.2**) - and differs no more than 20% between any two species. It is however an oversimplification to talk about actin as a specific protein. It is better to consider it as a family of actin proteins since in mammals 6 and in some plants even 60 isoforms are expressed [1, 5]. The six isoforms can be subdivided in two groups, (i)  $\alpha_{\text{skeletal}}$ -actin,  $\alpha_{\text{cardiac}}$ -actin,  $\alpha_{\text{smooth}}$ -actin and  $\gamma_{\text{smooth}}$ -actin are primarily expressed in cardiac, skeletal and smooth muscle cells whereas (ii)  $\beta_{\text{cyto}}$ -actin and  $\gamma_{\text{cyto}}$ -actin are ubiquitously expressed. Compared to one another these different isoforms share at least 93% identity [6].

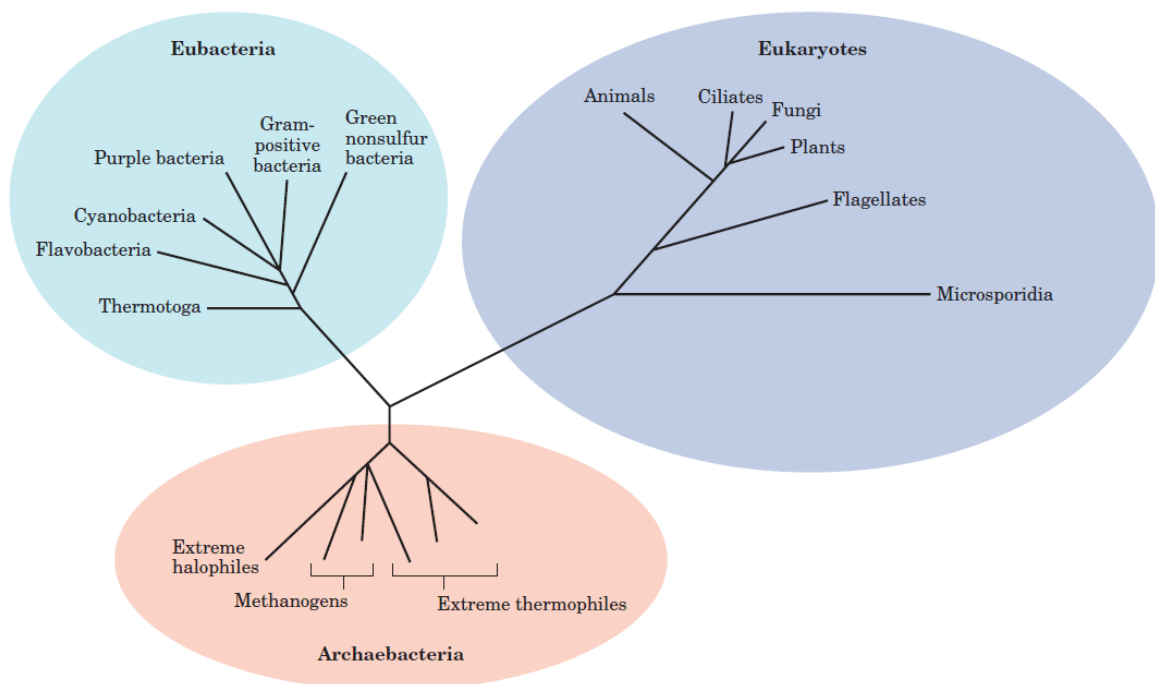


**Figure 1.2: The classification of life in three domains** - bacteria, archaea and eukarya - was introduced by Carl Woese in 1977. It underlines the fundamental difference between the two prokaryotic groups, with the archaea being closer related to the eukarya than the bacteria. Figure adapted from Lehninger Principles of Biochemistry, Sixth Edition [7].

The actin cytoskeleton is not a rigid, defined structure. There is a constant dynamic balance between assembly and disassembly. If one would isolate a single actin filament, called F-actin, it would appear to move forward in a specific direction<sup>2</sup>. This optical illusion is due to the fact that actin is not an equilibrium polymer. Indeed, as G-actin starts to polymerize, the on- and off-rates differ between both ends of the filament. In order to compensate for this thermodynamic

<sup>2</sup>Indeed, as the more critical reader may point out, this is an oversimplification. In order to observe this phenomenon, the F-actin filaments need to be placed in a solution containing 0.1  $\mu\text{M}$  G-actin - the critical concentration for treadmilling - otherwise the filament would also increase (higher concentrations) or decrease (lower concentrations) in size.

imbalance, actin utilizes its ATPase activity [8]. Actin monomers have the capacity to bind ATP. After being assembled at the barbed end, G-ATP-actin will slowly hydrolyze to form F-ADP-actin thereby releasing a phosphate group and energy. At the pointed end, the opposite takes place. F-actin disassembles, thereby releasing G-ADP-actin. With the help of profilin this G-ADP-actin can exchange its ADP for ATP and the process starts over. This unceasing flux of actin from the pointed end to the barbed end, called treadmilling, is the driving force behind actin-based cell motility (**Figure 1.3**) [9]. Besides energy in the form of ATP, this actin polymerization process also requires  $Mg^{2+}$ . This divalent cation serves as a cofactor - a non-protein compound required by a protein to perform its biological function - for actin's ATPase activity.

This actin polymerization process is carefully controlled and guided towards the desired end structures by a broad range of actin binding proteins (ABPs). More than 160 identified ABPs are involved in actin (de)polymerization, bundling, stability, fragmentation and crosslinking [3]. According to their specific functions, the ABPs have been divided into seven groups (**Table 1.1**).

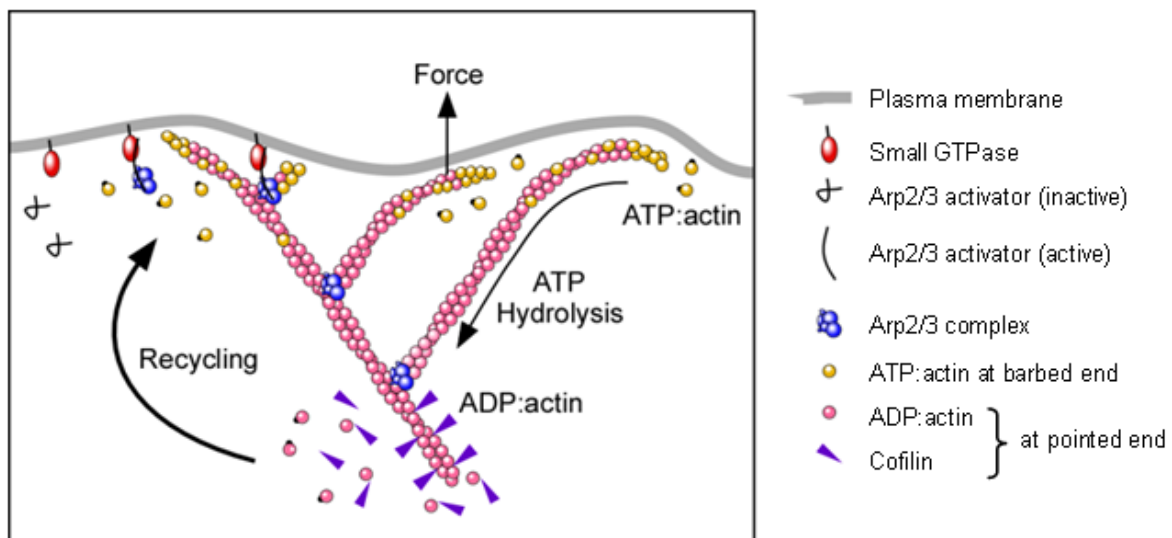


**Figure 1.3: Actin treadmilling.** The dynamic equilibrium of actin filaments results in a constant turnover of actin monomers. At the pointed end, G-ADP-actin is released and recycled back into ATP-actin via phosphorylation. At the barbed end this ATP-actin polymerizes into F-actin, thereby elongating the actin-filament. This process results in a directional force enabling the cell - or individual organelles - to move into a specific direction. Over time the incorporated ATP-actin monomers will be hydrolyzed back into ADP-actin and the cycle can repeat itself. Depolymerization at the pointed end is accelerated by cofilin while the branching towards the barbed-ends is facilitated by Arp2/3, which is activated via an Arp2/3 activator and Small GTPases [10].

**Table 1.1:** Actin binding protein groups

Group type	Function	Examples
Monomer-binding proteins	Sequestration of G-actin and prevention of its polymerization	Thymosin $\beta$ 4, DNase I
Filament depolymerizing proteins	Induction of the conversion of F- to G-actin	CapZ, Cofilin
Filament end-binding proteins	Capping of the actin filament ends, thereby preventing the exchange of monomers	Tropodomulin, CapZ
Cross-linking proteins	Facilitating the formation of filament bundles, branching filaments, and formation of three-dimensional networks	Arp2/3
Stabilizing proteins	Binding to the sides of actin filaments and preventing depolymerization	Tropomyosin
Motor proteins	Transportation of vesicles across F-actin filaments	Kinesin, dynein
Filament severing proteins	Shortening the average length of filaments by binding to the side of F-actin and cutting it into two pieces	Gelsolin

Adapted from dos Remedios *et al.*, 2003 [11].

A key member of the filament severing group, gelsolin, has several mutants which cause a disease known as gelsolin amyloidosis. This affliction is essentially the main topic of this PhD and will be rigorously discussed in Chapter 3. But first the native function of gelsolin and a phenomenon known as amyloidosis will be discussed.

### 1.1.2 Gelsolin

Gelsolin was first described in 1979 by Yin and Stossel as a protein able to liquefy solid actin gels: the gel-sol reaction, hence the name [12]. It is the founding member of the gelsolin superfamily; a group of  $\text{Ca}^{2+}$ -regulated actin binding proteins with the ability to sever, cap and/or nucleate actin. These proteins are highly conserved in the animal kingdom and contain three or more prototypical 'gelsolin-like' domains. The basic architecture of such a globular 'gelsolin-like' domain consists of a central, five or six-stranded  $\beta$ -sheet packed between a long, roughly parallel and a short, roughly perpendicular  $\alpha$ -helix (**Figure 1.4**) [13, 14]. Gelsolin is composed of six such domains (G1-6) - each domain is about 120-130 amino acids long - which, in a  $\text{Ca}^{2+}$ -free environment, are closely packed together. Given the great homology between domain 1-2-3 and domain 4-5-6 respectively, gelsolin seems to have evolved through a gene triplication followed by a gene duplication. The single, 70 kb gelsolin gene (*GSN*), located on chromosome 9q34 contains 14 exons and gives rise to three gelsolin isoforms via multiple transcription initiation sites and alternative splicing [15]. The two main isoforms; plasma gelsolin (PG, 84 kDa) and cytoplasmic gelsolin (CG, 82 kDa) are ubiquitously expressed and differ from one another at two points. (i) PG contains an N-terminal extension of which 24 amino acids remain present after cleavage of the ER signal peptide<sup>3</sup>. (ii) Of the five cysteine residues, two of them form a disulfide bond in PG - Cys<sup>188</sup> with Cys<sup>201</sup> - whereas in CG they are all in the free thiol form [16]. The third isoform, gelsolin-3 (82 kDa), has until now only been detected in brain oligodendrocytes, lungs and testis tissue. Just like PG it contains an N-terminal extension, albeit only 11 residues long [17].

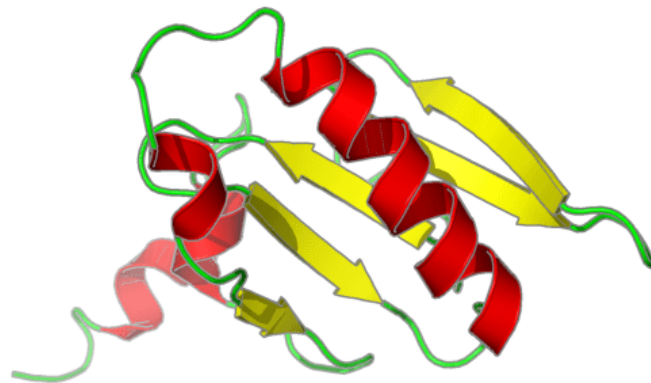


**Figure 1.4: Schematic representation of a gelsolin domain.** A gelsolin domain consist of a five or six-stranded  $\beta$ -sheet (yellow, five stranded) sandwiched between a long, roughly parallel (red, right helix) and a short, roughly perpendicular  $\alpha$ -helix (red, left helix). Unpublished figure from Van Overbeke *et al.*, 2015 [18].

<sup>3</sup>An ER signal peptide is a short peptide sequence - usually between 5 and 30 amino acids - used to tag proteins which are destined for the secretory pathway which begins in the ER.

To our current knowledge the overall structure and activity regulation of the isoforms is essentially identical. As we proceed with the disquisition of the structure and activity regulation, I will therefore simply refer to both isoforms as 'gelsolin'.

### Ca<sup>2+</sup> activation

Given the catalytic nature of gelsolin, its function is tightly regulated by both Ca<sup>2+</sup>, pH levels, phosphatidylinositol 4,5-biphosphate and lysophosphatidic acid. All six gelsolin domains contain a type-2 Ca<sup>2+</sup> binding site, each having a different affinity (**Figure 1.6**). Upon sequential binding of Ca<sup>2+</sup> to each one of these domains, gelsolin will unfold its globular inactive state, thereby bringing its actin binding regions to the surface. This process involves the unfolding/relocation of three latches (**Figure 1.5A**) - (i) the tail latch formed by the C-terminus and G2 domain, (ii) the G1-G3 latch and (iii) the G4-G6 latch - and can be divided in several stages based on the required concentration of Ca<sup>2+</sup>. (i) 0.2  $\mu$ M Ca<sup>2+</sup>: G6 binds Ca<sup>2+</sup> thereby straightening its major helix and destabilizing the G4-G6 latch. The tail latch is weakened [19]. (ii) 2  $\mu$ M Ca<sup>2+</sup>: G4 binds Ca<sup>2+</sup>, G4 and G5 shift and the G4-G6 latch further weakens. The tail latch is now fully released [19]. (iii) 100  $\mu$ M Ca<sup>2+</sup>: G5 binds Ca<sup>2+</sup>, by that stabilizing its interface with G4 and locking the G4-G6 latch in an open state. Simultaneously, G3 binds Ca<sup>2+</sup> thereby straightening its long helix and opening the G1-G3 latch. The latter reveals the cryptic, high affinity Ca<sup>2+</sup>-binding site on G2 [20]. This site cooperatively binds Ca<sup>2+</sup> and pushes G2-G3 towards its active conformation. Once activated, G2 releases its Ca<sup>2+</sup> ion. (iv) From 0.6 mM Ca<sup>2+</sup> onwards: G1 binds Ca<sup>2+</sup> and gets locked into position via the G1-G2 linker. Gelsolin is ready to strike and sever F-actin. Upon interaction with actin, two more Ca<sup>2+</sup> binding sites come into play. These so called type-1 Ca<sup>2+</sup>-binding sites are sandwiched between the actin:G1 and actin:G4 interfaces. In other words, these Ca<sup>2+</sup>-binding sites are a conjunction between gelsolin and actin residues and most likely have an influence on the affinity between the two during F-actin severing [21]. This process happens in three stages (**Figure 1.5B**). (i) The activated G2-G3 - step (iii) of the activation process - binds to F-actin via G2. (ii) Binding of G2 induces G6, the G1-G2 and G3-G4 linker to wrap around the filament, enabling G1 and G4 to move towards the cleavage site. (iii) G1 and G4 cleave F-actin. Gelsolin remains bound thereby preventing polymerization at the newly formed barbed end. This action is called capping<sup>4</sup>.

---

<sup>4</sup>Although I have described this entire process of gelsolin activation and F-actin severing/capping in a discrete number of individual steps, it is important to realize that this is a model derived from *in vitro* observations using carefully controlled amounts of Ca<sup>2+</sup>. In reality, *in vivo*, this is a continuous process which takes place in a fraction of a second. The cell does not contain individual compartments with all the specific concentrations mentioned in the text.



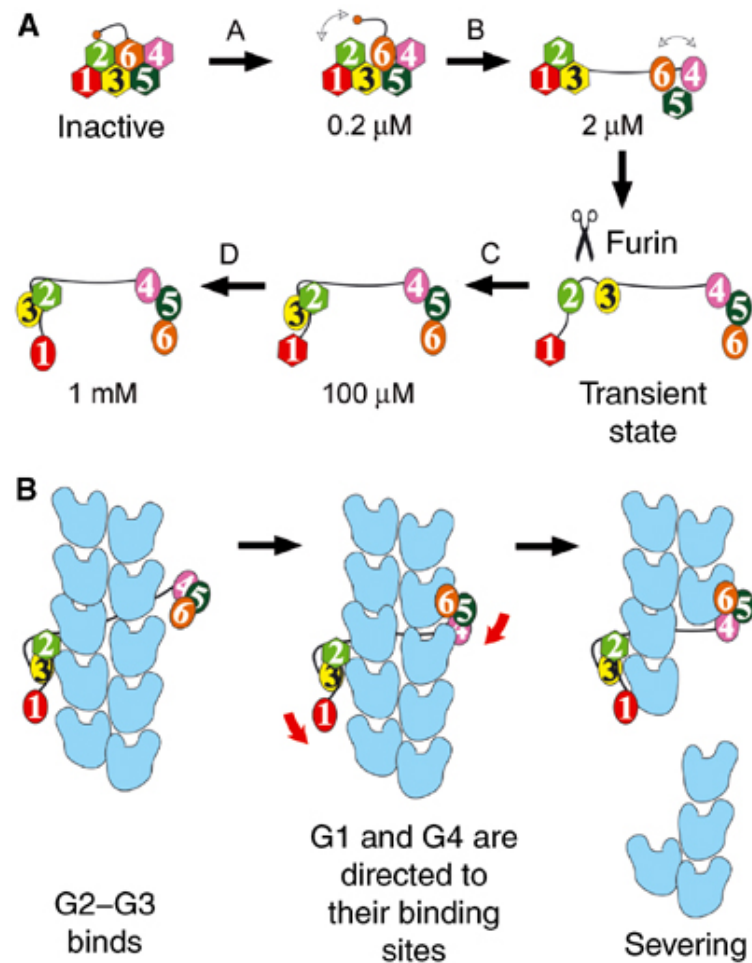


**Figure 1.5: Schematic representation of gelsolin activation (panel A) and its actin severing activity (panel B).**  $\text{Ca}^{2+}$ -free gelsolin domains are represented as hexagons.  $\text{Ca}^{2+}$ -activated domains are represented as ovals. Actin subunits are represented as light blue U-shapes. For each step which requires  $\text{Ca}^{2+}$ , the needed ion concentrations are indicated. Given the high  $\text{Ca}^{2+}$  concentration in the blood compared to the cytoplasm's carefully controlled  $\text{Ca}^{2+}$  concentration, this stepwise representation of gelsolin's activation is more representative for the cytoplasmic isoform than it is for the plasma variant. Figure adapted from Burtnick *et al.*, 2004 [22].

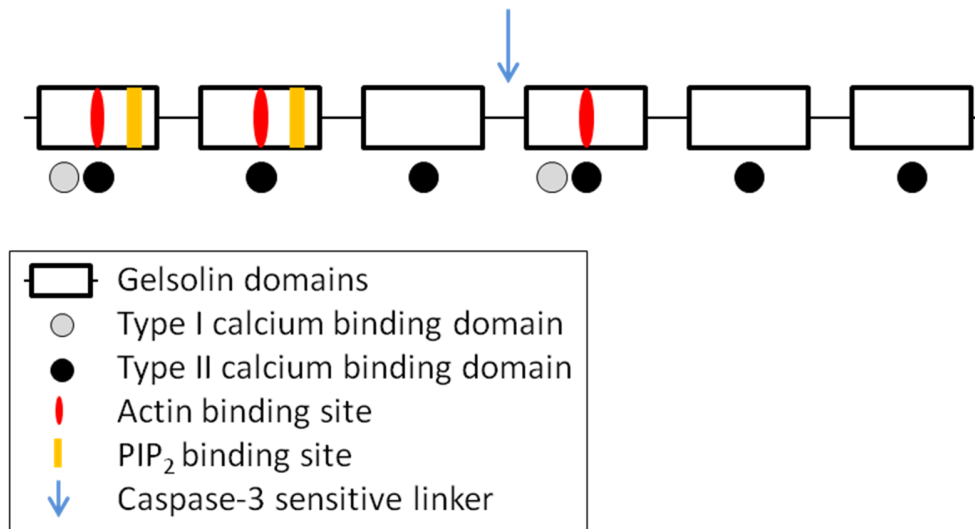


**Figure 1.6: Schematic representation of gelsolin.** Black boxes represent the six gelsolin domains. Ca<sup>2+</sup>-binding sites (grey and black dots), actin-binding sites (red), PIP<sub>2</sub>-binding sites (yellow) and caspase-3 sensitive linker (blue arrow) are indicated [23].

In distinction to the two destructive functions described above, gelsolin has, at least *in vitro*, a constructive capacity; nucleation [24]. Gelsolin has the ability to bind two actin monomers, thereby bringing them in close proximity. Onto this complex, actin polymerization can be performed, forming a new F-actin filament. It is highly unlikely that this process also takes place *in vivo*. In eukaryote cells G-actin is bound to either thymosin-b4 or profilin, rendering it unfit for pointed end growth from a gelsolin-actin nucleus [25]. Rather, *in vivo* actin nucleation is ascribed to the Arp2/3 complex and formins [26].

### Physiological Ca<sup>2+</sup>

The tight regulation of gelsolin's activity by Ca<sup>2+</sup> is not a peculiarity. In fact, Ca<sup>2+</sup> is one of the most important intracellular messenger ions in a plethora of cellular processes. Its intracellular distribution is therefore meticulously regulated.

Blood plasma contains 2.5 mM Ca<sup>2+</sup> of which 1.2 mM is free, unbound. Intracellular free Ca<sup>2+</sup> is used to regulate all sorts of intracellular processes via numerous proteins with the ability to buffer Ca<sup>2+</sup>. They reside in the different organelles and differ in their buffering capacity and response to Ca<sup>2+</sup> [27]. Hence, each organelle is characterized by a specific Ca<sup>2+</sup> concentration and Ca<sup>2+</sup>-response. One thing all these Ca<sup>2+</sup>-buffering proteins do have in common is the fact that they aren't merely Ca<sup>2+</sup>-buffers. These multifunctional proteins are of major importance in processes such as apoptosis, gene transcription, mitochondrial metabolism and protein folding [28]. The latter can be directly linked to the activation of CG (discussed above) and protein folding which will be discussed in Chapter 2.

Zooming in on PG, two organelles are of major importance; the endoplasmic reticulum and Golgi apparatus. As will be explained in more detail in subsection 2.1.1 *Protein synthesis*, PG travels through the ER and Golgi apparatus during its synthesis. Simultaneously it will adopt its correct folding and eventually gets secreted into the bloodstream where it can achieve its active conformation.

The ER represents the largest intracellular  $\text{Ca}^{2+}$ -buffer; 1 mM  $\text{Ca}^{2+}$  of which 200  $\mu\text{M}$  is unbound [28]. The majority of the ER  $\text{Ca}^{2+}$ -binding proteins serve as folding chaperones for proteins like PG. Calreticulin, which binds 50% of the ER  $\text{Ca}^{2+}$ , and BiP are two examples of such chaperones and will be discussed in more detail in subsection 2.1.1 *Protein synthesis*.

The Golgi apparatus has also been identified as a  $\text{Ca}^{2+}$ -buffer; 2 to 300  $\mu\text{M}$   $\text{Ca}^{2+}$ . Calnuc, also known as nucleobinding, is the primary  $\text{Ca}^{2+}$ -binding protein in the Golgi apparatus and shows some homology to Calreticulin [29]. It has been postulated that this protein may serve both as a  $\text{Ca}^{2+}$ -buffer,  $\text{Ca}^{2+}$ -sensor and interacts with a large number of other proteins [30].

#### PIP<sub>2</sub> and LPA regulation

The  $\text{Ca}^{2+}$  activation of gelsolin is meticulously counterbalanced by the inhibitory actions of phosphatidylinositol 4,5-bisphosphate (PIP<sub>2</sub>) and lysophosphatidic acid (LPA). The phospholipid PIP<sub>2</sub> is a minor component of cell membranes, enriched in certain areas, where it serves a key role in a number of signaling pathways and is considered one of the fundamental regulators of the subcortical actin network in eukaryotes [31]. In gelsolin, two amino acid stretches - G1: AA 135-149 and G2: AA 150-169 - have been identified as PIP<sub>2</sub>-binding motifs (**Figure 1.6**) [32, 33]. Corresponding regions have also been detected in all other members of the gelsolin superfamily. As PIP<sub>2</sub> is incorporated in the plasma membrane, binding to gelsolin sequesters the latter, making it unavailable for  $\text{Ca}^{2+}$  activation, thereby inhibiting actin-severing. When bound to PIP<sub>2</sub>, gelsolin - and a number of other ABPs - readily undergo phosphorylation by pp60<sup>c-src</sup> and PYK2 which further decreases its affinity for actin<sup>5</sup> [34, 35]. In addition, PIP<sub>2</sub> is able to disrupt gelsolin's capping function, by that actively promoting actin polymerization [36]. Hydrolysis of PIP<sub>2</sub> releases gelsolin from the plasma membrane, allowing  $\text{Ca}^{2+}$  mediated reactivation of gelsolin's actin severing and capping functions.

LPA, a phospholipid which contains the same uncommon phosphomonoester as PIP<sub>2</sub> in its head-group, has similar effects on gelsolin regulation as PIP<sub>2</sub>. Additionally, LPA directly influences a number of intracellular components with a pivotal role in signal transduction; n-chimaerin, G-proteins, protein kinase C, etc. [37–39]. Interestingly, the same peculiar phosphomonoester group can also be found in lipopolysaccharides (LPS) - large molecules consistent of a lipid and a polysaccharide present in Gram-negative bacteria. In fact, gelsolin has a higher affinity for LPS

---

<sup>5</sup>Phosphorylation is a common post-translational modification in which a phosphate group is transferred from ATP to one (or several) of the amino acids in a protein. This charged group induces conformational changes which may (de)activate a protein or modify its function.

than for PIP<sub>2</sub> or LPA [40]. Gelsolin-LPS binding impedes LPS-mediated thrombin inhibition, LPS-induced actin remodeling and collagen-induced platelet activation pathways independent of toll-like receptors (TLR) [40]. Despite the fact that gelsolin itself does not affect bacterial growth, this evidence does suggest that interaction with LPS inhibits the inflammatory and coagulatory effect of the latter.

### Regulation by pH

The earlier discussed activation of gelsolin by Ca<sup>2+</sup> can, at least *in vitro*, be overruled. The pH value - a negative log<sup>10</sup> scale of the proton concentration specifying the acidity of a solution (acidic < 7 < basic) - of our extracellular fluids fluctuates around a value of 7.4. In such an environment gelsolin requires at least 10 μM of Ca<sup>2+</sup> for activation. *In vitro*, lowering the value to pH 6.5 reduces this to 3 μM Ca<sup>2+</sup>. At pH values below 6.0, gelsolin severing activity has even been observed in solutions containing EGTA<sup>6</sup>. Dynamic light scattering experiments suggest that the increased proton concentrations induce conformational changes in gelsolin similar to the ones induced by Ca<sup>2+</sup>-binding [41]. Furthermore, slightly acidic pH levels boost PIP<sub>2</sub> binding affinity [42]. These findings suggest that gelsolin integrates Ca<sup>2+</sup>, PIP<sub>2</sub>/LPA and pH signals in order to fine-tune its activity status.

### Functions of gelsolin

**Cell motility & invasion:** During different stages of development, several types of eukaryotic cells are able to move freely throughout the body. Cells migrate to their final location during embryogenesis, immune cells search and destroy pathogens and cancers cells may one day leave their tissue of origin ready to colonize the rest of the patient's body. Their movement resembles the crawling motion of amoebas and is fueled by the polarized polymerization/depolymerization of the actin skeleton (**Figure 1.3** and **1.7**). CG is a key regulator of these actin remodeling processes and it plays a substantial role in cellular movement. This was first demonstrated in NIH 3T3 fibroblast; overexpression<sup>7</sup> of CG resulted in an increased motility [43]. More elaborate evidence came from gelsolin null mice (GSN<sup>-/-</sup>) in which osteoclasts are unable to form podosomes - cell adhesion structures involved in cell motility and invasion - resulting in a defect basal and osteopontin-induced motility [44]. Also, during neuronal growth, cone formation and retraction is delayed [45] and fibroblasts show defective chemotaxis resulting in delayed wound healing [46]. Thus, even though GSN<sup>-/-</sup> mice are viable - at least in a mixed strain background - and phenotypically healthy, they display several cellular defects which prove lethal at perinatal and early postnatal stages [47].

---

<sup>6</sup>EGTA is a chelating agent capable of binding all the Ca<sup>2</sup> ions present in the solution, making them unavailable for other processes.

<sup>7</sup>During overexpression, cells are stimulated to abundantly express an artificial gene.

**Apoptosis:** The bodies of full-grown, multicellular organism are not static. Every cell will eventually be replaced via a mechanism of programmed cell death called apoptosis. This process involves a cascade of breakdown processes whereby no lysis products are released onto the surrounding cells, as is the case in necrosis. Instead the cell will disintegrate in a large amount of apoptotic bodies - small vesicles containing (partly) degraded cell matter - which are then engulfed by macrophages and recycled. Apoptosis is strictly regulated by caspases; a family of cysteine-aspartases. One member, caspase-3, is able to cleave gelsolin in half (Asp<sup>352</sup>-Gly<sup>353</sup>). The N-terminal half (G1-G3) hereby no longer requires Ca<sup>2+</sup> for activation and, in the case of CG, will induce uncontrolled actin cytoskeleton breakdown, one of the first steps of apoptosis. Intriguingly, full length CG has been shown to inhibit apoptosis in murine hearts, Jurkat T cells and in studies with the GSN<sup>-/-</sup> mice [48–52].

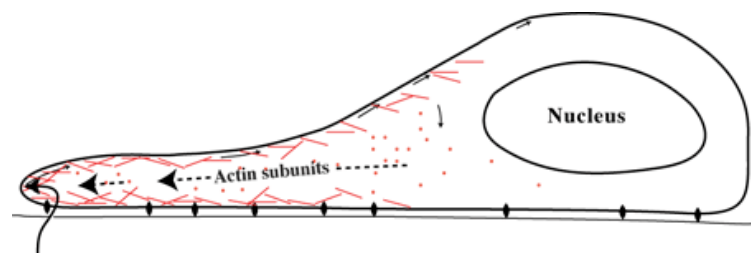


**Figure 1.7: Cell motility by actin polymerization.** The constant directional turnover of actin filaments allows cells to migrate into a specific direction [53].

**Cancer:** The duality of gelsolins' pro- and anti-apoptotic properties, discussed in the previous paragraph, sow controversy regarding its role in tumor formation. During the initial stages of tumor development, cancerous cells play it safe and downregulate gelsolin expression [54], as was observed in breast, pancreas, stomach, bladder, colon, kidney, ovary and colon cancer. Low levels of CG enable a rapid expansion without the risk of gelsolin-related apoptosis or growth inhibition. Indeed CG has the ability to induce cell cycle arrest at the G2 phase [55, 56]. In later stages - during the transition to a malignant and/or metastatic cancer - cancer cells change strategy and start to overexpress gelsolin. Most probably this is due to the increased need for cell motility [54].

**Signal transduction:** In 1987 it came to light that cofilin plays a role in the intranuclear actin modulation [57]. Since then profilin, supervillin, CapG and plastins have been added to the list of nuclear actin binding proteins (nABPs). These proteins normally reside in the cytoplasm but during stress- or hormone-induced cellular differentiation they can migrate into the nucleus. The way in which this is achieved is still under investigation. The same capacity has been observed for CG in differentiated endothelial cells [58] and serum-starved NR6 fibroblasts [59]. CG also has a role in several signal transduction pathways. For example, it interacts with the testosterone-bound androgen receptor, facilitates its nuclear translocation and enhances its transcriptional activity [60]. Furthermore, an interaction between hypoxia-inducible factor 1 (HIF-1) - a transcription

factor and key regulator of cell metabolism under hypoxic conditions - and CG has been reported [61]. Additionally, gelsolin involvement has been reported in EGF-mediated motility [62, 63], the Ras-PI3K signaling pathway [64, 65], PI3K modulated osteoclast function [66] and many more.

**Extracellular actin scavenging:** During inflammation or injury vast amounts of actin are released into the bloodstream, an environment which promotes the polymerization into F-actin. This process would drastically increase the blood viscosity if left unchecked. This is where, hypothetically, the secreted plasma isoform of gelsolin comes into play. Its primary function is the removal of this excess actin via its actin scavenging and severing activity. This hypothesis is backed by the observed lower levels of free PG during hepatic failure, malaria, acute lung injuries, myonecrosis and cardiac injury [67–70]. Moreover, patient injuries accompanied by a prolonged reduction in PG-levels correlate with a poor outcome or even death [71]. This may be explained by the fact that PG binds to inflammatory messenger molecules such as lysophosphatidic acid and platelet activating factor (PAF), thereby keeping the inflammation contained. As PG gets depleted during injury, these molecules are no longer sequestered, opening the doors for uncontrolled immune reactions throughout the body [72].

# 2

## Introduction to amyloid disease

### 2.1 Amyloidosis

Having dissected gelsolin, the first part of this PhD thesis' major topic, let's move on to the second; amyloidosis. This term is best known in regard to Alzheimer's disease. As our life expectancy rose, so did the prevalence of this debilitating and eventually lethal neurodegenerative disease. In this Chapter I will show that this is just one member of a large group of amyloid diseases and provide detailed insight into the nature of the common causative agent; amyloid. In Chapter 3 both concepts will come together in the disquisition of a disease called gelsolin amyloidosis.

#### 2.1.1 Protein synthesis

Before we are able to talk about amyloid, we have to go back to the central dogma of molecular biology which states that information flows from DNA to RNA to protein<sup>1</sup>. DNA or deoxyribonucleic acid is a double stranded, linear molecule composed of four nucleobases; cytosine (C), adenine (A), guanine (G) and thymine (T). In the same way digital data is essentially stored in large arrays of zeros and ones, so is all the information that defines a person stored in large arrays of C's, A's, G's and T's<sup>2</sup>. DNA molecules are safely locked away in the nucleus. Whenever a fragment of this DNA information is needed a RNA polymerase copies it into RNA or ribonucleic acid. This process is called transcription. Just as DNA, RNA is composed of four nucleobases,

---

<sup>1</sup>This flow of information, formulated by Francis Crick in 1958 is not completely correct. In 1970 it was adjusted as by then it had become clear that information can also flow from RNA to DNA or from RNA to RNA.

<sup>2</sup>In recent years it has become clear that DNA contains extra layers of information in the form of methyl groups placed both on the cytosines and histone proteins. This new scientific field is called epigenetics and has significantly enhanced our understanding of how genotypes relate to phenotypes [73].

however instead of thymine, uracil (U) is used. Moreover, RNA is single stranded and, contrary to DNA, able to leave the nucleus. In the cytosol, protein-coding RNA molecules will associate with ribosomes - ribonucleoproteins able to translate RNA coded information into an amino acid sequence - and translation will commence. Every triplet of RNA bases - called codons - codes for one of the 20 canonical amino acids used in eukaryotes<sup>3</sup>. This process heralds an important shift in information. The information, linearly stored in DNA and RNA gets translated into an amino acid chain which, when fully matured, will adopt a specific 3D structure directly correlated to the protein's function (**Figure 2.1**)<sup>4</sup>. In every organism, proteins perform a vast array of functions, including, but not limited to, the formation of rigid structures - e.g. keratin in hair and nails - transportation of molecules and other particles - e.g. hemoglobin ships oxygen from the lungs throughout the body - and catalyzing chemical reactions. Proteins serving this latter function are called enzymes.

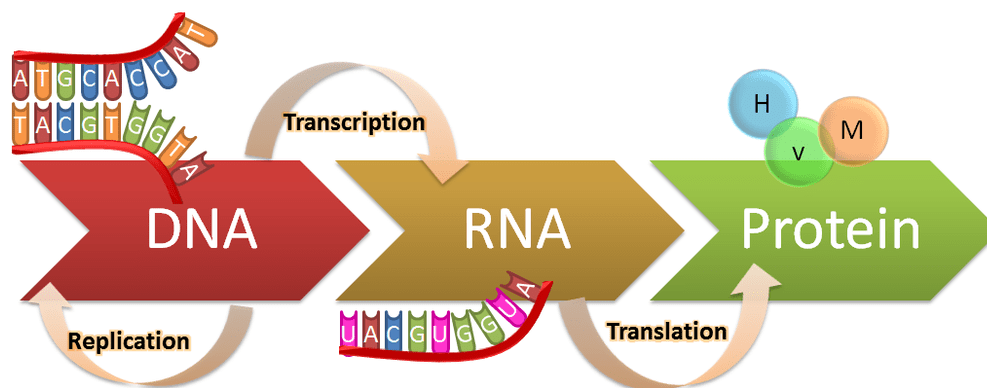


**Figure 2.1: The central dogma in biology; information generally flows from DNA to RNA to protein.** In preparation to cell division, the double stranded DNA gets duplicated in a process called replication. Information coded by the DNA can only leave the nucleus after it has been copied into a single stranded RNA molecule; transcription. Every RNA coding for a protein will be translated. Each RNA-nucleobasetriplet codes for a single amino acid. The resulting peptide will adopt its native 3D conformation resulting in a functional protein [76].

In the early days of molecular biology, it was common belief that the primary structure of a protein - the linear sequence of amino acids joined by covalent bonds - contained all the information necessary to migrate towards the final 3D structure [77, 78]. To a certain degree this is true. The presence of hydrophilic/hydrophobic and negatively/positively charged side chains is sufficient to induce the local formation of  $\alpha$ -helices and  $\beta$ -strands/sheets. These secondary structures can self-assemble into a denser tertiary state. Larger proteins which consist of multiple subunits will fit their individual parts together forming a quaternary structure. However, this entire process is

<sup>3</sup>Selenocysteine, although present in 25 human proteins is not directly coded by DNA [74].

<sup>4</sup>As always there are exceptions. Secondary structures in DNA and RNA molecules serve specific functions and micropeptides, although lacking significant secondary structures, have been shown to be biologically active [75].



stochastic. Starting from its initial primary structure, the proteins sample several conformations in search for a thermodynamically favorable outcome. As they migrate through the folding landscape, there is a risk of getting stuck in local energy minima representing partly folded states, or worse, drifting off course towards non-functional oligomers, amorphous aggregates or amyloid fibrils (**Figure 2.2**). By now we know that a great deal of proteins rely on chaperones; proteins which assist them during the folding process, guiding them towards their native state.

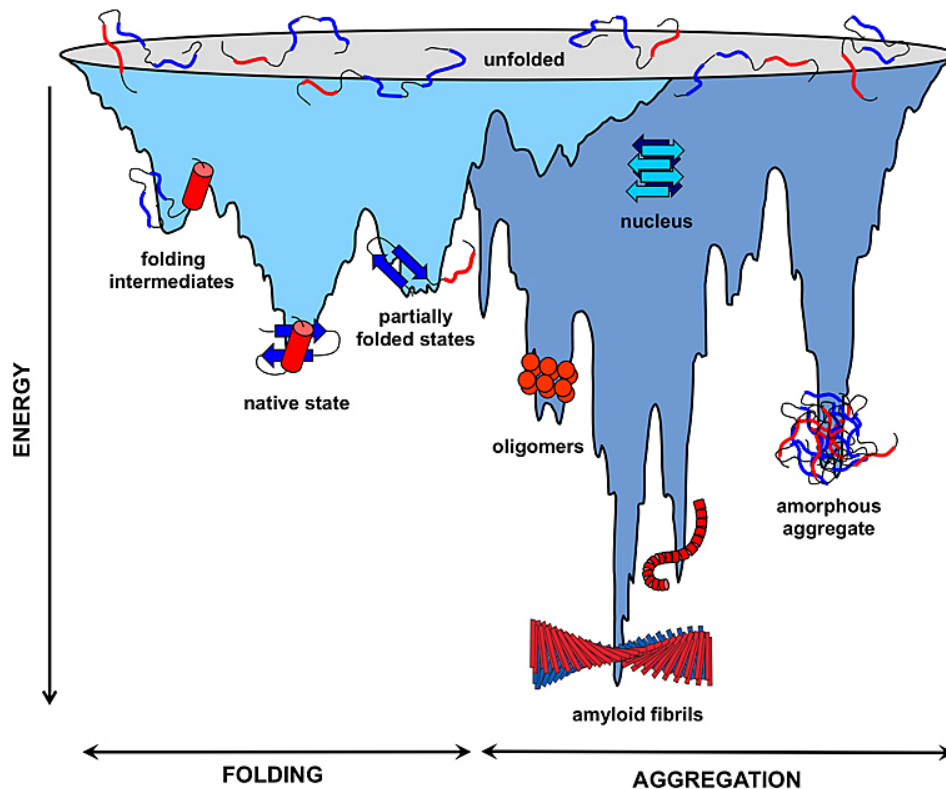


**Figure 2.2: The protein folding landscape.** The folding process of newly synthesized polypeptides is a thermodynamically driven process during which several conformations in the folding landscape are sampled in a search towards the native state. The presence of local thermodynamical minima entail the risk of getting trapped in a partially folded state. Chaperones serve to prevent or overcome such bottlenecks. However, if, for whatever reason, the folding mechanism fails, evidence suggests that each protein could adopt aggregated and amyloidogenic conformations as these represent thermodynamically stable configurations [79].

### Secretory protein synthesis

The synthesis of secretory proteins is essentially the same as for any other protein. The only difference lies in the fact that secretory proteins contain a hydrophobic N-terminal signal sequence that directs them toward the endoplasmic reticulum (ER) (**Figure 2.3**). Upon translation, the signal sequence is recognized by a signal recognition particle (SRP). Translation is put on hold and the entire complex is guided towards the ER. As the SRP interacts with the SRP receptor (SR), the emerging polypeptide can enter the ER. The SRP/SR complex dissociates from the

signal sequence and translation resumes. The folding process starts in concert with translation and, just as for cytosolic proteins, may require the assistance of chaperone proteins.

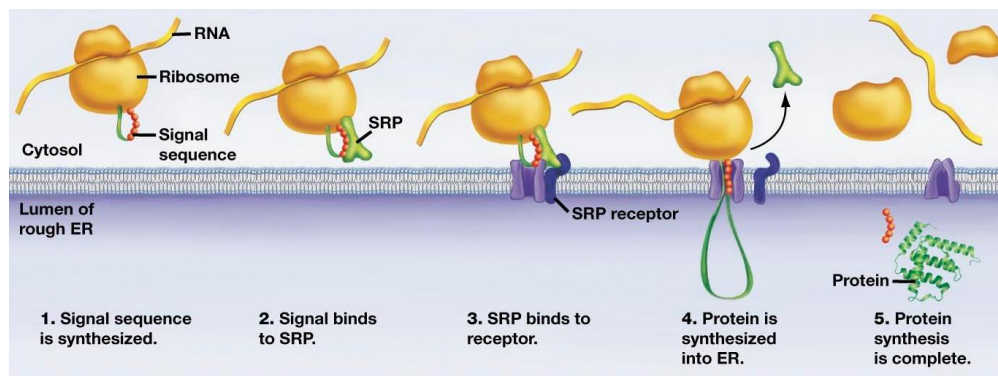


**Figure 2.3: Cotranslational uptake in the ER.** During translation of RNA coding for secretory proteins, the first translated stretch of amino acids contains a signal sequence which is recognized by the SRP. Binding of the SRP halts translation and targets the entire complex (ribosome bound to RNA and the nascent polypeptide chain) towards the translocon; a protein-conducting channel (represented as a purple cylinder) via docking with the SRP receptor. Upon release of the SRP, translation continues. The nascent polypeptide is cotranslationally guided through the translocon into the ER lumen where protein folding takes place [80].

### 2.1.2 Protein quality control

At any given time, a single human cell contains several billion proteins. Each of which, on average, required 3000 ATP molecules to make. Maintaining a proteome of this magnitude requires a constant translation by about 3 million ribosomes at a rate of six amino acids per second [81]. This machinery consumes up to 75% of the cell's energy [82, 83]. Thus, it is in the cell's best interest to optimize every step. Remarkably the translation process itself is extremely efficient. By contrast, folding proteins into their functional, native state frequently fails. Moreover, the more than 300 different types of posttranslational modification, 35 types of oxidative damage and more than 10 types of carbonylation make protein maintenance a heavy burden [5]. During the course of evolution several mechanisms have been developed to enhance folding efficiently and dispose of proteins lost beyond repair.

#### Quality control at the ribosomes

Translational errors can have devastating effects on protein stability. A single mutation changes the free energy with about 0.5-5 kcal/mol [84]. Therefore ribosomes are assisted by a cohort of nearly 300 proteins which restrict the misincorporation to about 1/10,000 amino acids. A second effective way in which translational errors can be minimized is optimization of the mRNA codon use. The hypothesis that 'the use of codons that slow translation increases proper folding'

has been demonstrated by incorporating wobble codons in the luciferase gene<sup>5</sup> [85]. A slower translation broadens the timeframe during which chaperones can bind to aggregation-prone amino acid stretches. Also, during times of stress, cells will actively slow down or pause translation. On the other hand, a rapid translation may prevent the formation of intermediate folding states, thereby increasing the fraction of proteins reaching their native fold. The take home message is that the rate of translation itself may significantly affect the folding efficiency.

Cotranslational folding is another means to avoid incorrect folding. As single proteins can be as large as 3.7 MDa [86], sequential translation and folding would leave hydrophobic stretches exposed for a prolonged period of time, increasing the risk for aberrant folding intermediates. In eukaryotes chaperones like heat shock protein 40 and 70 (Hsp40, Hsp70) will bind to nascent polypeptides and chaperone the cotranslational folding process.

Despite the high translational efficiency, up to 15% of nascent proteins are cotranslationally tagged for degradation. The majority of these are associated with truncated mRNAs or difficult to translate sequences leading to ribosome stalling. How such ribosomes are detected is still under investigation. What is known is that nascent proteins in stalled ribosomes get ubiquitinated via the ribosome-associated E3 ligase Hel3, targeting them for degradation by the ubiquitin proteasome system (UPS).

#### Incorrectly folded protein and the ubiquitin proteasome system

Eventually, any protein not reaching its native conformation or losing it due to oxidative damage will be marked by ubiquitin. This highly conserved, small - 76 amino acids - protein is first activated by E1, a ubiquitin activating enzyme. Next it is attached to E2, a ubiquitin carrier protein which is recognized by E3. The latter is a ubiquitin protein ligase which has the ability to recognize misfolded proteins and tag them with ubiquitin transferred from E2 (**Figure 2.4**). Any E1 can bind with several E2s, which in turn can bind hundreds of E3s. This hierarchical system allows a tight regulation of the ubiquitin pathway [87]. Soluble, ubiquitinated proteins or protein aggregates will be sequestered in the juxtannuclear quality control compartment (JUNQ) [88]. This non-membrane bound cellular site is associated with copious chaperones and proteasome complexes. The local high concentration of chaperones and misfolded proteins may increase the possibility of refolding. If the chaperone machinery does fail, degradation by the 26S proteasome follows<sup>6</sup>. The proteasome consist of a 20S central hollow cylinder composed of 2 times 14 different polypeptides. Both ends are equipped with two 19S caps. Subunits in the central core have trypsin-like, chymotrypsin-like and post-glutamyl activity. During the ATP-consuming protein degradation, the ubiquitin peptides get recycled.

<sup>5</sup>The term wobble refers to abnormal base pairing between the mRNA codon and tRNA anticodon. There are  $4^3=64$  possible mRNA codons, yet most organisms contain no more than 45 different tRNAs. Non-Watson-Crick base pairing - guanine with uracil or hypoxanthine (a sixth nucleobase) with uracil, adenine or cytosine - fix this discrepancy.

<sup>6</sup>Svedberg, S, is a non-SI unit for sedimentation rate. This unit correlates with the size and shape of a particle, in this case a protein.

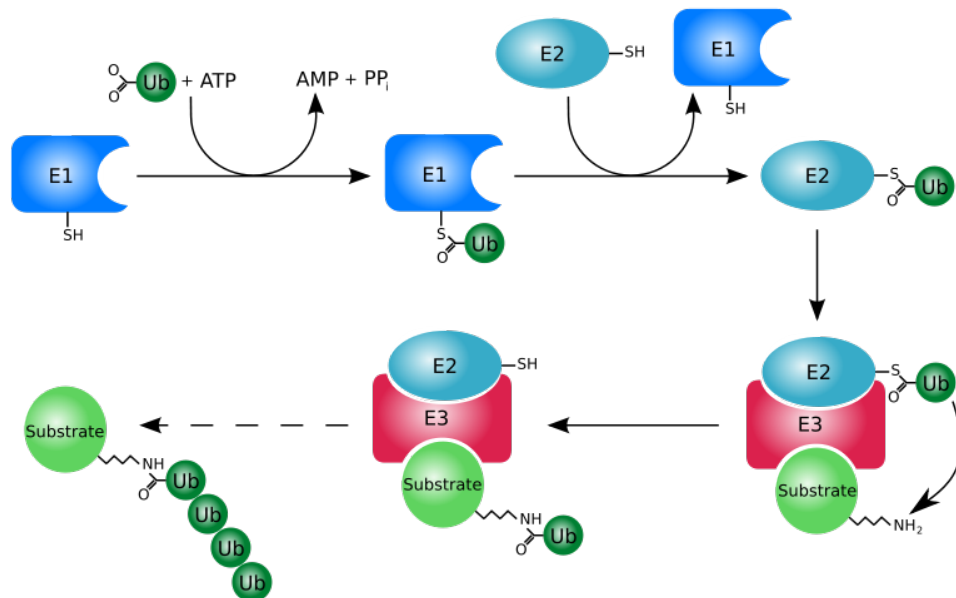


**Figure 2.4: Ubiquitination.** Using ATP E1 binds a ubiquitinating protein. This ubiquitinating-activating enzyme E1 then transfers ubiquitinating to E2 which forms a complex with E3. The latter is able to recognize proteins destined for ubiquitinylation and catalyzes the transfer of ubiquitin from E2 to the target protein. This cycle is repeated until the target protein is tagged by a polyubiquitinating chain [89].

Together with JUNQ a second distinct, non-membrane bound, cytoplasmic structure was discovered [88]. In contrast to JUNQ it contains highly insoluble aggregates and amyloid. A single cell can contain several of these insoluble protein deposits (IPODs). Although the association with chaperones like Hsp104, 70 and 40 [90] indicates an effort to disaggregate the content, most IPOD protein is highly terminal and should be degraded.

### Autophagocytosis

Given the presence of insoluble protein deposits, it is clear that the ubiquitin-proteasome system has its limits. This is in sharp contrast with autophagocytosis, a lysosomal degradation pathway which not only targets protein aggregates but also entire organelles [91]. This disposal mechanism allows (i) cells to dispose of defective organelles and protein aggregates, (ii) remove and recycle superfluous structures and macromolecules during differentiation and (iii) survive times of nutrient deprivation or environmental stress [92].

In mammalian cells, three types of autophagy are known. (i) Chaperone-mediated autophagy which sequesters protein(aggregates) via their KFERQ-like motif using heat shock cognate 70 and other co-chaperones. (ii) Microautophagy, a process especially important during cellular starvation. Here, cytoplasmic material is engulfed via membrane invagination. In general this type of autophagy is non-selective. (iii) Macroautophagy which differs from the other two due to the *de novo* formation of phagophores. More specifically macroautophagy relies on the formation

of a double membrane around the target molecule or organelle which will later on fuse with the lysosomal membrane.

All three types of autophagy rely on an array of associated proteins and lysosomal proteases to recognize, transport, dispose and recycle the targeted substances. Therefore it should not come as a surprise that mutations in the lysosomal pathway have been associated with neurodegenerative diseases. For example, Gaucher disease - a deficiency of glucocerebrosidase due to a mutation in the *GBA1* gene - is considered to be a major risk factor for the development of Parkinson's disease [93].

Consequently, in neurodegenerative diseases heavily stocked IPODs can still be found in the cells of infected tissues. Incapable of degrading the amyloidogenic deposits associated with these diseases, the cells isolate them in IPODs as a last resort [88].

Endoplasmic-reticulum-associated protein degradation (ERAD) and unfolded protein response (UPR)

During translation, proteins processed by the ER get decorated with glycans; covalently bound carbohydrate structures of major importance in a plethora of cellular functions, one of them being protein folding. Calnexin (CNX) and calreticulin (CRT), two lectins - proteins able to recognize specific carbohydrate structures - are at the center of a glycan based ER protein folding/refolding treadmill. In the ER, newly formed proteins are equipped with Glc3Man9GlcNAc2 - a branched polysaccharide chain consisting of 3 glucose, 9 mannose and 2 N-acetylglucosamines. Should the protein not fold correctly, sequential glucose trimming by  $\alpha$ -glucosidase I and II exposes the Glc1Man9GlcNAc2 epitope recognized by calnexin and calreticulin. Via their chaperone domain these lectins will attempt to steer the bound protein towards its native fold. Next  $\alpha$ -glucosidase II will remove the last glucose moiety. If the native fold was achieved, the protein can proceed through the secretory pathway. If not, glucosyltransferase will reglycosylate and another CNX/CRT cycle will take place (**Figure 2.5**). Terminally unfolded proteins will be transported back into the cytosol, ubiquitinated and targeted to the proteasome, as described above.

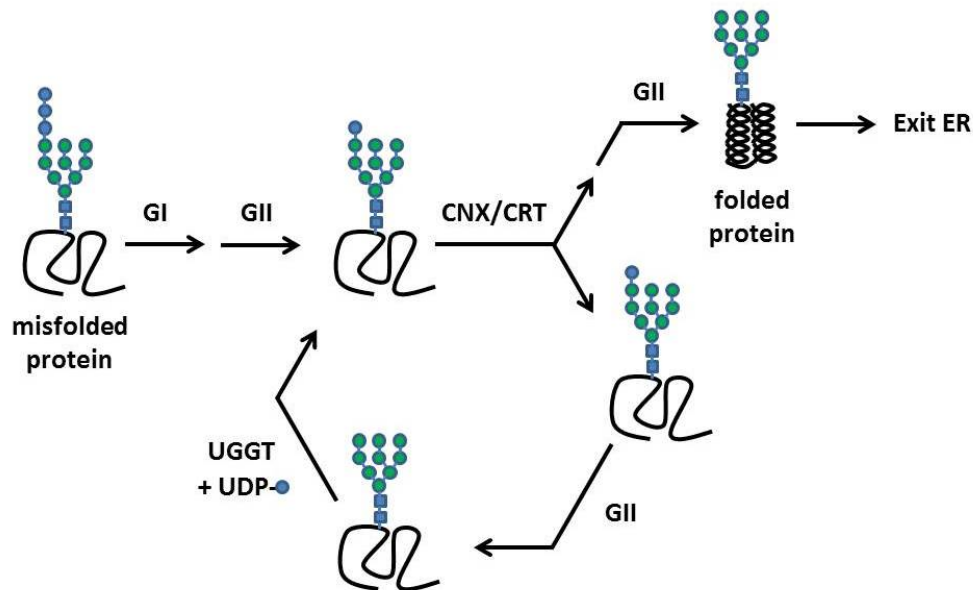


**Figure 2.5: The calnexin/calreticulin cycle.** The glycans of misfolded glycoproteins are trimmed by  $\alpha$ -glucosidase I and II, enabling these glycoproteins to enter the calnexin/calreticulin cycle after which  $\alpha$ -glucosidase II will remove the last glucose moiety. When interaction with these chaperones results in a native conformational fold the glycoprotein can exit the ER. If not it will be recognized by (UDP)-glucose:glycoprotein glucosyltransferase (UGGT), reglycosylated and enter another CNX/CRT cycle [94].

If, for whatever reason, the CNX/CRT cycle proves insufficient, the unfolded protein response is initiated. UPR will (i) halt protein translation, (ii) degrade misfolded proteins and (iii) increase the expression of the molecular chaperone BiP, an ER-variant of HSP70. If however the cell is still unable to reverse the ER protein stress, UPR will eventually initiate apoptosis.

### 2.1.3 Amyloidosis

A very peculiar form of protein (mis) folding is amyloid. In 1854 Rudolf Virchow examined human brain tissue and discovered deposits with similar iodine staining as cellulose-like materials in plants which he named *corpora amylacea* [95]. In the following decades comparable reaction patterns were discovered in other diseased organs and were likewise referred to as amyloid. Although the original cranial structures described by Virchow turned out to be polymeric carbohydrates [96], hence the positive iodine staining and the term amyloid (meaning starch-like), the later discovered deposits in other diseased organs were of proteinaceous nature. Nonetheless, the term amyloid stuck.

Using X-ray diffraction patterns and electron microscopy, the underlying universal structure of amyloid was unraveled. Individual proteins, or protein fragments, are assembled into  $\beta$ -sheets. These  $\beta$ -sheets come together to form an amyloid protofibril in which the sheets run parallel and the individual protein strands perpendicular to the protofibril direction (**Figure 2.6**). Such an

arrangement is referred to as cross- $\beta$ -sheets. Several of these  $\pm 4$  nm wide protofibrils align in parallel and form a mature amyloid fibril containing a slight twist in the same way a rope consists of individual fibers twisted together (**Figure 2.7**). Over time all these amyloid fibrils will become tangled, forging dense networks known as amyloid plaques. Mature amyloid can be stained with Congo red thereby displaying green birefringence under polarized light (**Figure 2.8**).

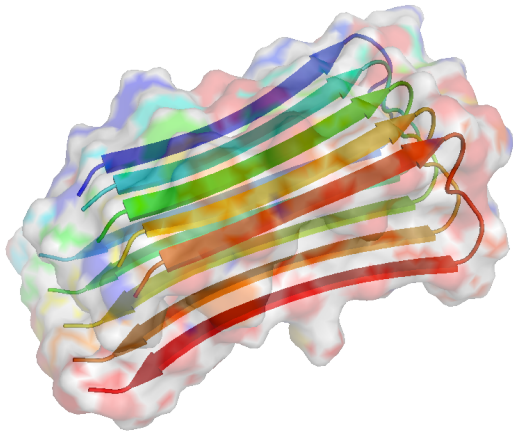


**Figure 2.6: Cross  $\beta$ -sheets.** Amyloidogenic protein (fragments) form  $\beta$ -sheets and align themselves perpendicular to the fibril axes of the protofibril [97].

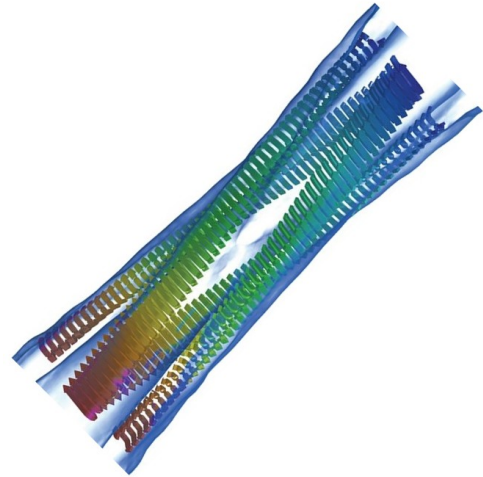


**Figure 2.7: Amyloid fibrils.** Protofibrils allineate with a slight twist into mature amyloid fibrils [98].

The above described amyloid structure and staining characteristics (**Figure 2.8**) are common to all known forms of amyloid, independent of the constituent protein. Variation has however been observed at the protofibril level. Indeed, (i) individual strands may run parallel or antiparallel, (ii)  $\beta$ -sheets may be stacked parallel or antiparallel and (iii) inter-sheet packing may be face-to-face or face-to-back [99].

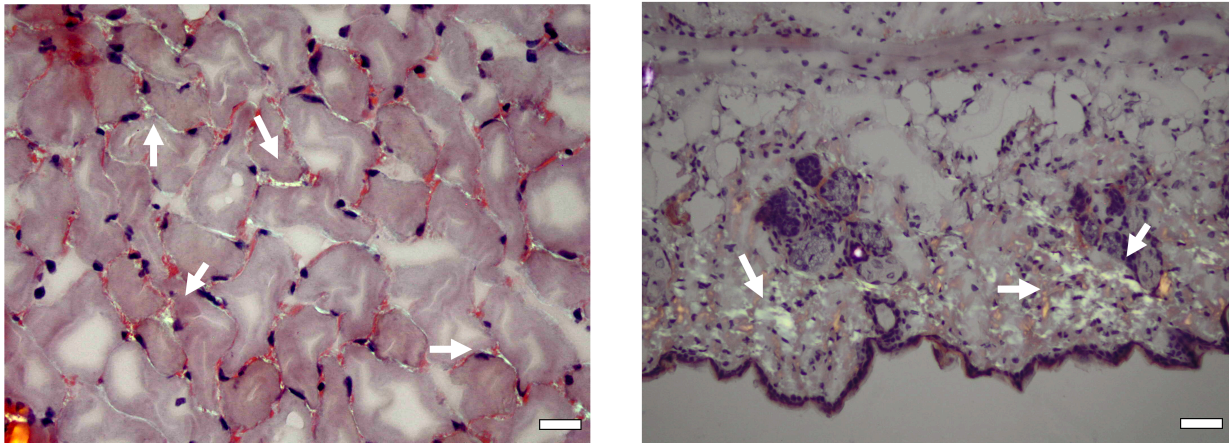


**Figure 2.8: Congo red stained amyloid.** Congo red displays apple-green birefringence under polarized light when bound to mature, cross- $\beta$ -sheet amyloid fibrils (indicated by white arrows). Congo red is therefore still the golden standard for amyloid detection. The gelsolin amyloidosis mouse model (discussed later in this manuscript) displays Congo red positive amyloid buildup starting from the age of 12 months in both muscle (left panel, scale bar = 100  $\mu$ M) and skin (right panel, scale bar = 30  $\mu$ M) tissue. Unpublished figure from Van Overbeke *et al.*, 2014 [100].

### Pathological amyloid

To date, 35 diseases associated with extracellular fibril proteins have been identified. Their nomenclature is based on the precursor protein. These afflictions can be subdivided into classes depending on whether amyloid deposition is systemic or localized, and whether the illness is hereditary or acquired. A subset of these amyloidosis also display intracellular protein inclusion bodies exhibiting amyloidogenic properties [101].

The precursor proteins (**Table 2.1**) differ greatly in regard to their native function, structure, length, hydrophobicity,... . Depending on the disease it may either be the WT protein, a mutant form or an aberrant fragment which polymerizes into amyloid fibrils. Exactly how or why these proteins bypass the complex protein quality control system is, at least for now, still quite obscure. What we do know is that, at a certain point, defective folding of the precursor protein seems to overload the system, thereby initiating their accumulation and subsequent aggregation into amyloid fibrils. Once formed, these prove to be highly stable. Over time considerable amounts of amyloid can infiltrate tissues and organs - in AL amyloidosis, livers weighing up to 15 kg have been reported<sup>7</sup> [102] - thereby debilitating the patient or inducing life-threatening organ failure. Why amyloid is deposited in specific locations is still under investigation. At the moment our best guess is the combined action of specific production sites and interaction with tissue specific components such as heparin sulfate proteoglycans.

<sup>7</sup>A normal liver weighs about 1,2 - 1,4 kg in woman and 1,4 - 1,5 kg in men.



**Table 2.1:** Amyloid fibril proteins and their precursors in human.

<b>Fibril protein</b>	<b>Precursor protein</b>	<b>Systemic and/or localized</b>
AL	Immunoglobulin light chain	S, L
AH	Immunoglobulin heavy chain	S, L
AA	(Apo) Serum amyloid A	S
ATTR	Transthyretin, wild type	S
	Transthyretin, variants	S
A $\beta$ 2M	$\beta$ 2-Microglobulin, wild type	S
	$\beta$ 2-Microglobulin, variant	S
AApoAI	Apolipoprotein A I, variants	S
AApoAII	Apolipoprotein A II, variants	S
AApoAIV	Apolipoprotein A IV, wild type	S
AApoCII	Apolipoprotein C II, variants	S
AApoCIII	Apolipoprotein C III, variants	S
AGel	Gelsolin, variants	S
ALys	Lysozyme, variants	S
ALECT2	Leukocyte chemotactic factor-2	S
AFib	Fibrinogen $\alpha$ , variants	S
ACys	Cystatin C, variants	S
ABri	ABriPP, variants	S
ADan*	ADanPP, variants	L
A $\beta$	A $\beta$ protein precursor, wild type	L
	A $\beta$ protein precursor, variant	L
A $\alpha$ Syn	$\alpha$ -Synuclein	L
ATau	Tau	L
APrP	Prion protein, wild type	L
	Prion protein variants	L
	Prion protein variant	S
ACal	(Pro)calcitonin	L
AIAPP	Islet amyloid polypeptide**	L
AANF	Atrial natriuretic factor	L
APro	Prolactin	L
Alns	Insulin	L
ASPC***	Lung surfactant protein	L
AGal7	Galectin 7	L
ACor	Corneodesmosin	L
AMed	Lactadherin	L
AKer	Kerato-epithelin	L
ALac	Lactoferrin	L

Table 2.1: Continued

<b>Fibril protein</b>	<b>Precursor protein</b>	<b>Systemic and/or localized</b>
AOAAP	Odontogenic ameloblast-associated protein	L
ASem1	Semenogelin 1	L
AEnf	Enfurvitide	L

\*ADan is the product of the same gene as ABri, \*\*Also called amylin, \*\*\*Not proven by amino acid sequence analysis. Adopted from Sipe *et al.*, 2016 [101].

### Functional amyloid

Interestingly a genome-wide analysis revealed that almost all proteins hold the capacity to form amyloid [79]. In fact, in bacteria, fungi and yeast, the controlled production of amyloid serves a function in, among other things, biofilm formation, modulation of water surface tension, regulation of stop-codon read-through and fungal coat formation. In insects and fish, functional amyloid is present in eggshells and spider silk [103]. Even in human melanocytes, amyloid fibrils of pigment cell-specific pre-melanosomal protein (PMEL) are employed as scaffolds on which melanin is deposited. The production of PMEL fibrils is tightly regulated and compartmentalized as any mutation results in the formation of pathogenic PMEL amyloid [104, 105]. The discovery of functional amyloid, combined with its high biophysical stability fuels the development of new nanomaterials such as bioactive matrixes, nanowires, biosensors and carbon-amyloid hybrid materials [106–108].

# 3

## Introduction to gelsolin amyloidosis

### 3.1 Gelsolin amyloidosis

Chapter 3 gelsolin amyloidosis; in this chapter the information regarding gelsolin and amyloid given in Chapter 1 and 2 respectively, will merge.

#### 3.1.1 Discovery

In 1969 the Finnish ophthalmologist Jouko Meretoja first described a new familial amyloidosis syndrome characterized by corneal dystrophy, cranial neuropathies and skin affliction [109]. Over the years this syndrome came to be known under many different names; Meretoja's disease, amyloid polyneuropathy type IV, gelsolin related amyloidosis, corneal lattice dystrophy type II, familial amyloidosis of the Finnish type (FAF) and gelsolin amyloidosis (AGel). It wasn't until 1990 that the role of gelsolin in AGel was demonstrated. Two independent research groups had isolated and sequenced the amyloid fibrils from patient tissues [110, 111]. The fragments appeared to be an internal part of a gelsolin variant having an aspartate to asparagine mutation at position 187 of the primary structure of gelsolin. AGel therefore seemed to arise from an abnormal internal degradation from this gelsolin variant.

In the following years, the role of gelsolin, the genetic cause and pathogenic pathway were further elaborated.

#### 3.1.2 Epidemiology & genealogy

Before the standardized nomenclature for amyloid diseases, AGel was known as familial amyloidosis of the Finnish type referring to the fact that AGel patients show a prominent clustering in Southeastern Finland. This, combined with the Mendelian segregation and genetic homogeneity

amongst different families lead to the hypothesis that all patients could be traced back to a single ancestral mutation; G654A<sup>1</sup>. However, soon after the original report from Meretoja, AGel was correctly diagnosed in several countries across Europe, the Americas and the Far East. Of special interest are (i) Danish, Czech, Korean and Brazilian families carrying a G654T mutation [112–115] and (ii) American families with a G588A or (iii) C633A mutation. Contrary to the clinical similarity (discussed below) between the two most common mutations (G654A and G654T), the more recently discovered mutant forms (G588A and C633A) are only associated with renal amyloidosis [116, 117]. Furthermore no genealogical ties could be found between afflicted families outside of Finland. Taken together it is more likely that the worldwide prevalence of gelsolin amyloidosis is due to sporadic mutations. The founder affect observed in Finland may be the result of a genetic bottleneck.

Estimations regarding the number of AGel patients are scarce and range from 400 patients [118] to 1000 gene carriers [119]. Although, given the rather mild symptoms in young and middle-aged patients, and the obscurity of AGel amongst physicians, the actual number of patients/gene carriers is most likely significantly higher.

### 3.1.3 Clinical features

The majority of AGel patients is heterozygous. Their first symptom, corneal lattice dystrophy, manifests at the age of 25-30 years [109]. In the following decades cranial neuropathy and cutis laxa will, slowly, but surely, set in. The severity of this triad of clinical manifestations vary significantly among patients. Patients of high age may be (i) visually impaired or completely blind, (ii) suffer from minor facial sensory loss or severe sensory ataxia - loss of sensory input into the control of movement - with complete loss of ambulation - the ability to freely move about [120] - and (iii) be affected by negligible laxity of facial skin or suffer a major socio-aesthetic handicap [121]. The exact cause behind the large interpatient symptom variability is yet to be determined. On average, the life expectancy of AGel patients is somewhat shortened compared to the general population [119–121] as a minor subset of patients develops life threatening renal and cardiac amyloidotic complications between the age of 40 and 50 [119, 121, 122]. On the other hand, in homozygous patients, symptoms can manifest as early as at age of 13 and progress significantly faster. A fatal outcome before the age of 30 is no exception [119, 123].

#### Ophthalmological findings

Gelsolin related corneal lattice dystrophy (CLD type II) - the appearance of AGel fibrils in the cornea rendering it opaque, thereby reducing the patients vision - is often the first symptom in AGel patients [109], manifesting in the 3<sup>rd</sup> decade of life (**Figure 3.1**). Homozygous patients can

---

<sup>1</sup>The X-number-Y notation should be read as: ‘nucleotide X at position “number” was replaced by nucleotide Y’.

already be affected at the age of 12 [123, 124]. Typically only the peripheral cornea is affected whereas the central cornea remains largely free from any fibril deposits. Common complaints are eye dryness, photophobia - intolerance to strong visual light - and temporary visual impairment in the morning [109, 118, 124–127]. Furthermore, optical nerve damage and stromal fibrosis may, in aged individuals, lead to blindness [128, 129].

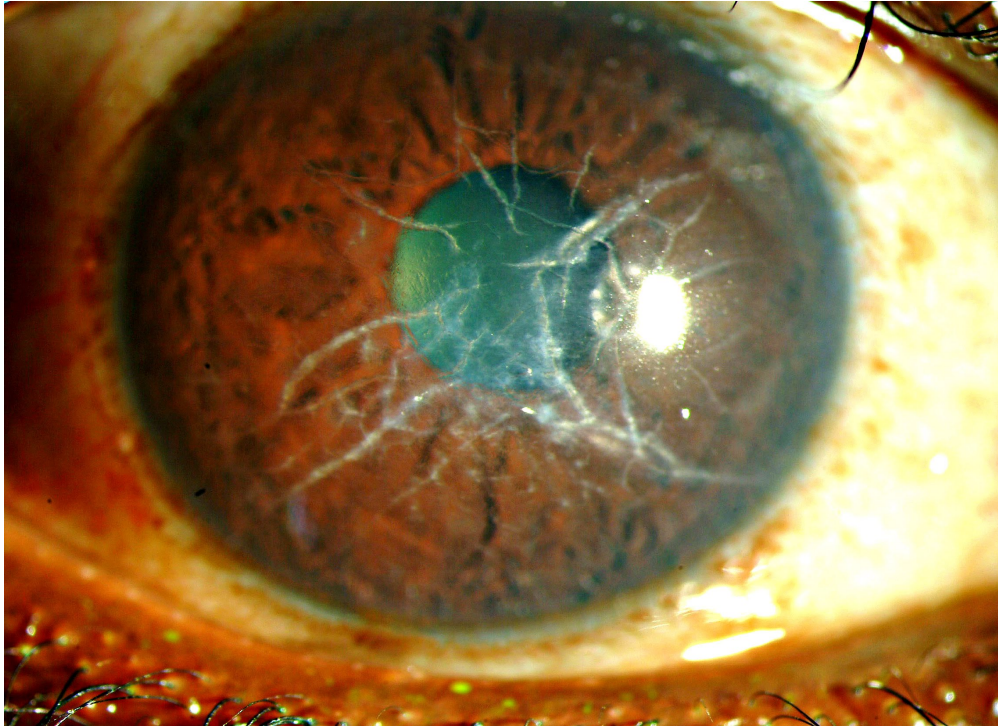


**Figure 3.1: Corneal dystrophy.** Fibrous amyloid deposits in the corneal result in corneally dystrophy. These deposits appear centrally at a young age and spread outwards over the years [130].

#### Neurological findings

Around their 4<sup>th</sup> and 5<sup>th</sup> decade of life, AGel patients slowly develop a progressive cranial neuropathy specifically affecting the facial nerves [109, 112, 125, 131] (**Figure 3.2a**). It may initially be asymmetrical and only involve the upper branches, but will eventually progress to facial diplegia - paralysis of both sides of the face - accompanied with facial myokymias - involuntary quivering of the facials muscles [118]. At advanced age patients may suffer from severe macroglossia or tongue atrophy (**Figure 3.2b**), dysarthria - motor speech disorder -, dysphagia - difficulty in swallowing - and drooling which significantly affects their quality of life. Furthermore involvement of proximal nerves and posterior columns of the spinal cord can result in balance problems and ataxia with occasionally complete loss of ambulation [118, 120, 124, 128, 131–134].

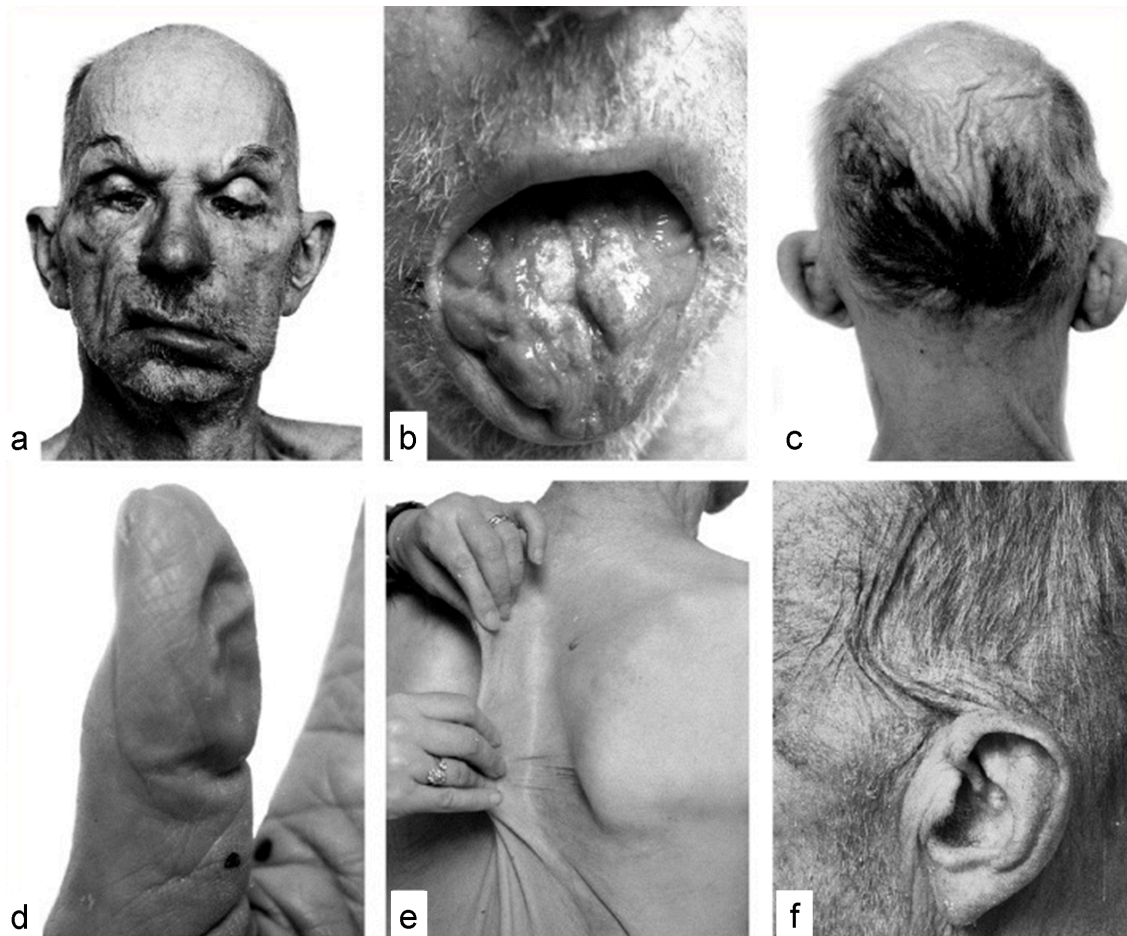


**Figure 3.2: Gelsolin amyloidosis patient.** Typical clinical characteristics of gelsolin amyloidosis: (a) Droopy facial expression due to affliction of the facial nerves, (b) macroglossia and (c-f) cutis laxa affecting the scalp, fingers, back and facial skin [121].

### Dermatological findings

The most distinctive clinical feature of AGel is progressive premature facial aging [135] caused by abnormal skin laxity or cutis laxa (**Figure 3.2c-f**). From their 5<sup>th</sup> decade of life onwards, patients are burdened with a loose, thickened scalp and forehead skin [109, 118]. Later in life lower parts of the face, back, hands, elbows and knees are also affected accompanied with dryness, itching, increased vulnerability and abnormal scarring of the afflicted areas. The facial skin laxity combined with the facial palsies and muscular atrophy encumbers patients with a permanent sad facial expression. Once again, in homozygous patients this process is severely expedited.

### Cardiological and renal findings

Although clinically detectable amyloid cardiomyopathy is uncommon in middle-aged patients, cardiac arrhythmias may necessitate a pacemaker in AGel patients before the age of sixty [136, 137]. Homozygotes can already experience cardiac problems in their thirties [123].

Renal involvement is quite variable amongst patients. Carriers of the G654A/T mutations mostly manifest only minor intermittent proteinuria - the presence of excess protein in the urine - at advanced age [125, 138]. In contrast, as mentioned earlier, symptoms of G588A or C633A patients seems to be almost exclusively nephrological. Their severe renal amyloidosis necessitates dialysis and eventually kidney transplantation [116, 117]. Once more, homozygous patients draw the short stick. Already in their teens proteinuria manifests itself. By the age of 20 this can progress into a severe nephritic syndrome [123, 139].

### 3.1.4 Molecular mechanism

#### Production of amyloidogenic gelsolin fragments

At the moment there are four known mutations resulting in gelsolin related amyloidosis; D187N, D187Y, G167R and the recently discovered N184K<sup>2</sup> (**Figure 3.3**) [113, 116, 117]. The first two, D187N/Y, affect the vast majority of patients. The replacement of the charged aspartic acid (D) by the uncharged asparagine (N) or hydrophobic tyrosine (Y) results in the loss of a Ca<sup>2+</sup> binding site - formed by D187, E209 and D259 - in the second gelsolin domain [14]. Due to this, G2 is able to adopt a partly folded, intermediate state between the active and inactive conformation of gelsolin [22]. This process negatively influences the overall stability of the protein, rendering an otherwise buried cryptic furin cleavage site - R169-V-V-R172-A173 - susceptible to aberrant proteolysis in the trans-Golgi network [20].

---

<sup>2</sup>In the context of proteins the X-number-Y notation should be read as: ‘amino acid X at position “number” was replaced by amino acid Y’.

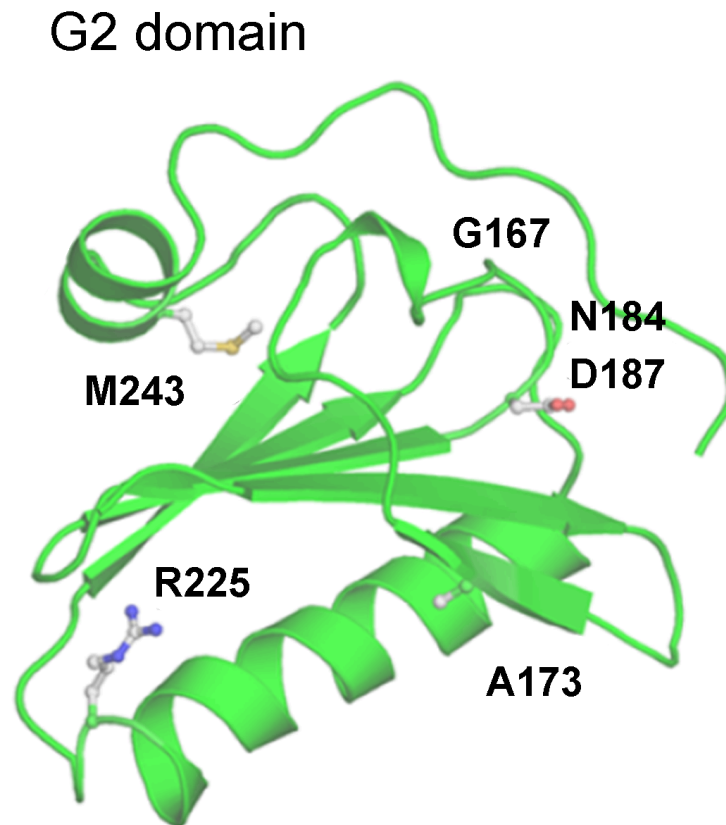


**Figure 3.3: Gelsolin amyloidosis, involvement of the G2 domain** The entire molecular mechanism behind AGel is played out in the second gelsolin domain, depicted here as a ribbon cartoon. Indicated in this figure are the three mutation sites (G167, N184 and D187), the furin cleavage site (A173) and the two MT1-MMP cleavage sites (R225 and M243). Figure adapted from Van Overbeke *et al.*, 2015 [18].

Furin is a membrane bound member of the proprotein convertase family, active in the endosomal and lysosomal pathway. It shuttles between the trans-Golgi network and the cell surface whilst activating a wide range of serum proteins, hormones and receptors [140–142]. During secretion, PG naturally encounters furin without any consequence since wild type gelsolin is already correctly folded due to high  $\text{Ca}^{2+}$ -levels in the ER/Golgi compartments. PG\* on the other hand is susceptible to pathological furin processing due to its induced structural intermediate state. The scissile bond between R172 and A173 is cleaved (**Figure 3.3**), thereby releasing a 68 kDa C-terminal fragment [143]. During secretion, this aberrant C68 constitutes a substrate for MT1-MMP-like proteases present in the extracellular matrix. MT1-MMP-like proteases are members of the matrix-metalloprotease family [144]. They play a pivotal role in protein degradation processes during embryonic development and tissue remodeling. Here however, 8 kDa (AA 173-243) and 5 kDa (AA 173-225) gelsolin amyloidogenic peptides are generated (**Figure 3.3** and **3.4**). Over time, the 8 and 5 kDa fragments start to aggregate in a cross- $\beta$  sheet configuration, a hallmark of amyloid fibrils with the former being the major component of gelsolin amyloid in patients.



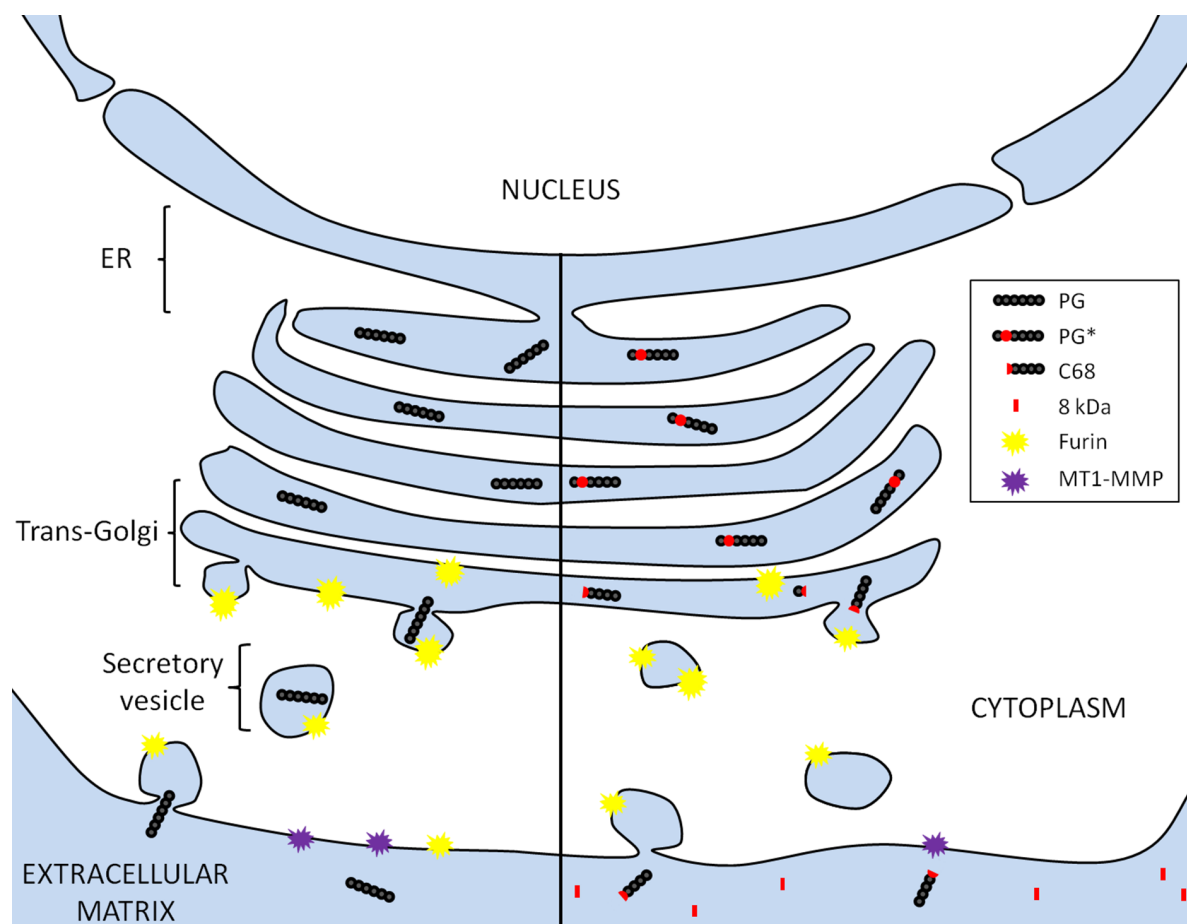


**Figure 3.4: Molecular characteristics of AGel: non-pathological versus pathological PG processing.** The left side depicts the non pathogenic synthesis and secretion of wild type PG via the ER and Golgi-network. On the right, the mechanism for PG\* is depicted. Furin cleaves PG\* in the trans-Golgi network, thereby releasing a C68 fragment. During secretion, C68 is cleaved by MT1-MMP-like proteases, forming 8 and 5 kDa amyloidogenic fragments in the extracellular matrix [23].

Although the more recently discovered G167R and N184K mutations result in the same aberrant proteolytic cascade as described above, their causative mode of action is less clear. The latter is associated with a triad of G2 amino acids - Q164, K166, and D187 - linked by hydrogen bonds which strongly contribute to the stability of G2's  $\beta$ -sheet [14] (**Figure 3.5**). The exchange of the uncharged asparagine (N) by the positively charged lysine (K) could disrupt this stability locus. The same may be true for the G167R gelsolin variant. Although it does not participate in the hydrogen bonding, replacing glycine (G) - the smallest amino acid - by the positively charged arginine (R), may displace it's neighboring amino acid K166. As the latter is part of the hydrogen bound quartet (**Figure 3.5**), this may once again, although indirectly, disrupt the stability of G2. More in to depth structural analysis of these mutants is necessary to reveal their true mode of action and could throw light on why G167R and N184K patients only seem to present nephrosis.

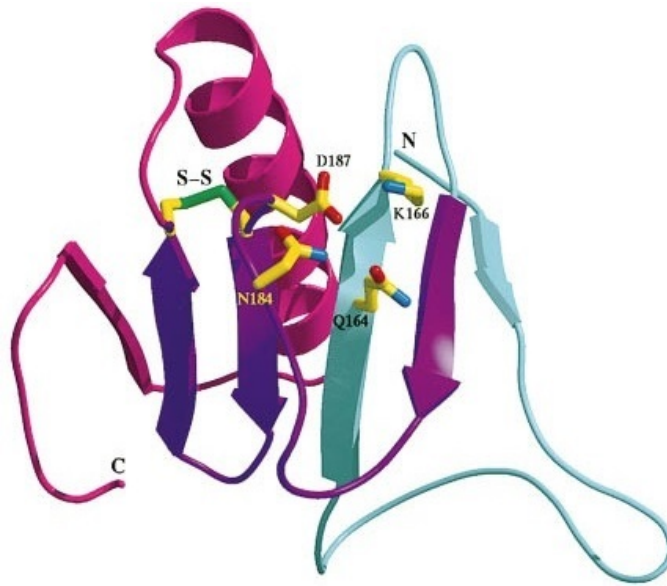


**Figure 3.5: Structure of gelsolins G2 segment.** Q164, K166 and N184 are within binding distance to the amyloidosis mutation site D187. The 8 kDa amyloidogenic fragment consists of colored red and purple. It contains the disulphide bond which may help to stabilize the amyloidogenic fragment. Figure adapted from Burtnick *et al.*, 1997 [14].

Plasma gelsolin is the sole source of amyloid in AGel

As all gelsolin isoforms are transcribed from the same gene, the AGel mutations are present in each one. Nevertheless, PG is the sole source of amyloid. Taking a second look to the aberrant proteolytic cascade described above offers a straightforward explanation for this phenomenon. Furin, the protease responsible for the production of C68, the first step in the AGel pathway, shuttles between the Golgi-network and the plasma membrane. Therefore, PG, the secreted isoform, is the only one who encounters this proprotein convertase. Although CG is not involved in amyloid formation [145], the loss of G2 stability negatively affects its actin binding and severing capacity. The same holds true for the fraction of mutant PG that is secreted intact. In patients, impairment of these actin-related functions results in an altered platelet shape [146]. Furthermore, the observation that neuronal cells, transfected with mutant CG, display a reduced plasticity [147] may suggest altered, gelsolin related, intraneuronal processes in AGel patients. At the moment, little is known regarding the gelsolin-3 variant nor the effects of AGel mutations on its function.

### 3.1.5 Diagnosis and treatment

The clinical diagnosis of AGel most commonly starts with the detection of corneal lattice dystrophy (**Figure 3.1**) [118]. Together with cutis laxa and bilateral facial pareses (**Figure 3.2**), it forms a triad of consistent features differentiating AGel from other amyloid disorders<sup>3</sup>. The diagnosis can be easily confirmed using molecular genetics. In older or homozygous patients renal amyloidosis resulting in proteinuria can also be a first clue [121].

No specific treatment is currently available. Only symptomatic treatments are being offered to improve the overall quality of life. Most important is good ophthalmological care ranging from eye drops to corneal transplantation. Next to that, aesthetic surgery is often needed to ameliorate the patients' overall confidence as the facial pareses and cutis laxa burden the patients with a constant droopy facial expression [135].

Although therapeutic strategies involving the inhibition of protease activity have been suggested, unwanted side-effects are to be expected given the major physiological roles of furin and MT1-MMP [143, 144]. Tackling the problem the other way round by directly shielding PG\* from degradation, proved to be a more valuable route, as will be discussed later in this manuscript.

### 3.1.6 Mouse model

To further study the molecular aspects of AGel and to test different therapeutic avenues, two animal models were set up. In a first attempt, the gene coding for the 8 kDa amyloidogenic fragment was successfully transferred into the genome of *Drosophila melanogaster*. Unfortunately AGel amyloid deposition could not be detected [121].

As of 2009, a mouse model is available that faithfully recapitulates the entire proteolytic cascade of human PG\* [148]. Following electroporation of the human plasma GSN cDNA (carrying the G654A mutation) into mouse ES cells, a transgene animal was obtained where gelsolin is expressed under control of a muscle creatine kinase (MCK) promoter. PG\*, C68 and the 8 and 5 kDa amyloidogenic fragments were detected in the heart, skeletal muscle, diaphragm and skin. Plasma samples contain both full length PG\* and C68. With age, increasing amounts of gelsolin-positive amyloid deposits can be seen in the endomysium. Eventually the phenotype of old homozygous AGel mice starts to resemble sporadic inclusion body myositis (sIBM)<sup>4</sup> with accompanied muscle weakness [148].

---

<sup>3</sup>As G167R and N184K patients only present nephrosis, their diagnosis is more challenging. The few reported patients were correctly diagnosed after laser microdissection of an amyloid deposit followed by mass spectrometry. DNA sequencing was performed to confirm gelsolin involvement. As no more than a handful of such patients is known, this subsection focuses on the D187N/Y patients.

<sup>4</sup>Sporadic inclusion body myositis is an acquired muscle disorder characterized by progressive weakness and degeneration of the muscles.

# 4

## Introduction to nanobodies

### 4.1 Antibodies and their fragments

In general, when people get sick, their physician will prescribe a certain medicine which they can get at the pharmacy in the form of a suspension or tablets. These readily available therapeutics consist of relatively simple organic molecules and are known as small compounds. Since, in the majority of cases, these are easily absorbed in the intestinal tract, such medicines can be taken orally. Despite the fact that small compounds able to inhibit furin or MT1-MMP like proteases are frequently being used for research purposes, they have no clinical value. Since both furin and MT1-MMP perform key cellular functions, tinkering with their activity would result in serious, unwanted, side effects. This has been evinced in mouse trials where furin knockout mice proved to be unviable [149] and MT1-MMP knockout mice, although viable, were burdened with dwarfism, arthritis, osteopenia - low bone mineral density - and several connective tissue defects [150]. We therefore redirected our attention away from these proteases. Instead we explored whether it was possible to directly shield PG\* without having to interfere with the normal function of both furin and MT1-MMP. We chose to work with nanobodies, a derivative from a special kind of antibody, discovered right here in Belgium.

#### 4.1.1 Conventional antibodies

Despite the many physical barriers, from time to time, viruses, bacteria and other parasites are able to invade our body. Through the course of evolution an ingenious system has been developed which specifically targets and removes these pathogens. Macrophages form the first line of defense. These cells are part of the innate immune system and are able to recognize, engulf and digest - a process known as phagocytosis - a wide array of substances, cell debris and pathogens. When this innate immunity proves insufficient, a second, specific line of defense comes into play; the adaptive immune system. Two types of adaptive immunity can be distinguished.

(i) The cell mediated immune response is carried out by T-lymphocytes. When activated, T-cells start to proliferate and generate cytotoxic T-cells and T-helper cells. (ii) The humoral immune response, executed by B-lymphocytes. Upon activation, these cells produce vast amounts of antibodies and keep record of the antigens they encounter, thereby ensuring a faster reaction in the case of a recurrent infection.

Antibodies or immunoglobulins are large, multichain, Y-shaped glycoproteins with the ability to recognize and bind specific molecular patterns - called antigens - on pathogens. They do this via their antigen-binding site - Fab variable regions - at the tips of their 'Y-structure'. Such interactions between antibodies and antigens can neutralize pathogens, activate the complement system and agglutinate and/or precipitate antigens<sup>1</sup>.

Since the introduction of hybridoma technology in 1975, monoclonal antibodies (mAb) have become an indispensable tool in fundamental research and all sorts of clinical applications [152]. Fusing mice B-cells with myeloma cells - immortal B-cell cancer cells - produces a hybrid cell line - hence the name hybridoma - which continuously secretes antibodies. This ability to mass produce antibodies against a plethora of proteins, carbohydrates, nucleic acids and haptens gave rise to molecular diagnostic tests such as ELISA, Western blotting, immunohistochemistry and immunofluorescence. Antibodies in the clinic are used in diagnostic applications by linkage to radioactive or fluorescent moieties. Furthermore they are also being applied therapeutically, be it directly or as a means for drug delivery. As the applications became more and more sophisticated and diversified, the potential pitfalls of this technology also surfaced. First, the production of vast amounts of monoclonal antibodies (mAbs) is very expensive. Second, the mAb format is hard to manipulate to obtain site specific linkage to other molecules such as fluorophores and radioactive nuclids. Last but not least, mAbs hold the potential of evoking an immune response rendering the therapy ineffective. This last hurdle has been addressed with the production of so called humanized antibodies. These second generation antibodies contain a humanized antigen-binding fragment (Fab). Third generation antibodies go one step further and also include an engineered Fc domain to improve the therapeutic activity in patients. Particularly in subpopulations expressing low affinity variants of the Fc receptor [153].

Conventional antibodies (**Figure 4.1**) are comprised of 2 heavy and 2 light chains. This multichain nature is one of the major hurdles when trying to manipulate mAb. Attempts have been made to bypass this by producing mAb fragments such as antigen-binding fragments and single chain variable fragments (scFv). The first, Fab, is composed of the variable and first constant domain of a heavy chain, combined with the variable and constant domain of a light chain. The second, scFv, only contains the variable parts of the heavy and light chain but these are interconnected via a linker. Although these smaller formats ameliorated some of the problems posed by classical mAbs, their production still proved to be troublesome and the functionality of the original mAb

---

<sup>1</sup>As a complete description of the fascinating immune system would fill this entire manuscript, I would like to refer those readers who desire a more in to depth exposition about the immune response to the book *Immunobiology* from Murphy, 2011 [151].

was (partly) lost in some cases.

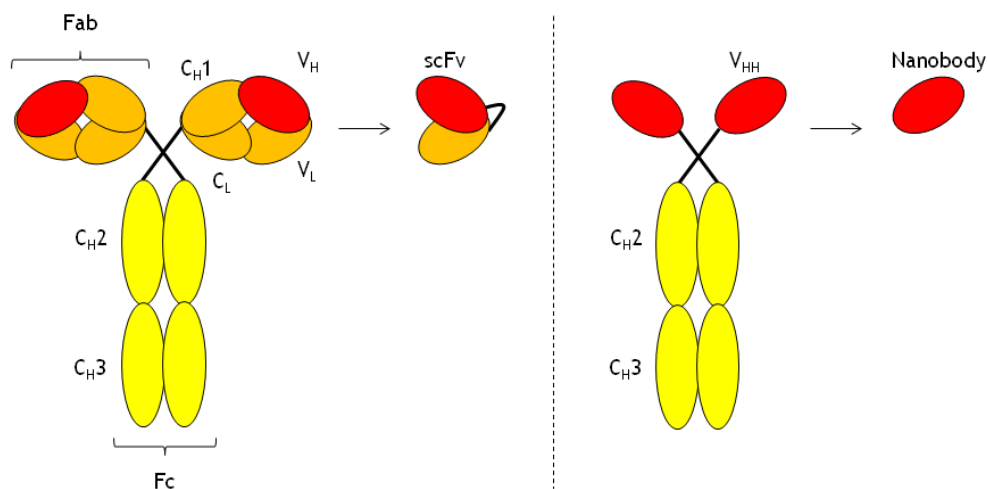


**Figure 4.1: Schematic representation of a conventional and a heavy-chain antibody.** A conventional antibody (left) consists of two heavy chains ( $C_{H3}$ ,  $C_{H2}$ ,  $C_{H1}$  and  $V_H$ ) and two light chains ( $C_L$  and  $V_L$ ). Fragment antigen-binding (Fab) and single-chain variable fragment (scFv) are built from a subset of these domains but retain their binding characteristics when recombinantly expressed. Heavy-chain antibodies (right) only consist of two heavy chains ( $C_{H3}$ ,  $C_{H2}$  and  $V_{HH}$ ). A nanobody corresponds with the variable part of the heavy chain of a heavy-chain antibody ( $V_{HH}$ ) and is the smallest, single-domain, natural, antigen binding fragment which remains fully functional when recombinantly expressed [23].

#### 4.1.2 Discovery of nanobodies

By a stroke of luck in 1993, a new type of antibody was discovered in the blood of *Camelus dromedaries* (**Figure 4.1**) [154]. These antibodies consist solely of two heavy chains, hence they were named heavy chain antibodies (HCAs). Their paratope - the region which interacts with the antigen - is no longer formed by a combination of a heavy and light chain variable fragment but consists exclusively of the variable fragment of a heavy chain. The single domain nature of this paratope offered the natural solution which researchers had been looking for. It has since been named variable domain of the heavy chain of heavy chain antibodies, VHH in short or Nanobody® ([www.ablynx.com](http://www.ablynx.com)). Since their discovery these HCAs have been detected in the blood of all Camelidae family members, nurse sharks, wobbegongs and ratfish [155, 156].

#### 4.1.3 Structure and characteristics of nanobodies

The most important novelty about nanobodies was, and still is, the fact that they are the smallest - 2.5 by 4 nm - single domain, natural, antigen-binding fragments available. Their basic structure consist of two  $\beta$ -sheets - one with four and one with five  $\beta$ -strands - who take on the same immunoglobulin fold like the variable domains of conventional antibodies (**Figure 4.2**). Nanobodies

contain four conserved regions - framework regions (FRs) - separated by three complementarity-determining regions (CDRs) (**Figure 4.3**). In dromedary, the CDR3 sequences are on average longer (16-18 AA) compared those of regular human antibodies (12 AA) [157]. Not only does this compensate for the absence of a light chain, it also allows the CDR3 to form protruding loops which are able to bind cryptic epitopes.

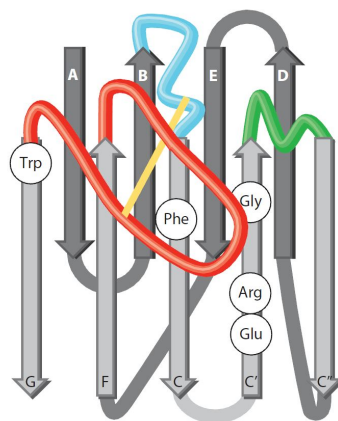


**Figure 4.2: Schematic of the nanobody structure.** The framework regions (grey) encompass nine  $\beta$ -strands which form two  $\beta$ -sheets connected by the CDR loops (blue = CDR1, green = CDR2 and red = CDR3). Several amino acids are often replaced compared to conventional antibodies in order to increase solubility (indicated with their respective three-letter codes). Figure adapted from Muyldermans *et al.*, 2013 [158]

In conventional antibodies a VH and VL fragment interact via their FR2 region to form the paratope. As VHHs do not interact with a VL, their previously hydrophobic FR2 region contains four hallmark mutations - V37F/Y, G44E/Q, L45R/C and W47G/S/L/P - rendering it more hydrophilic, which greatly enhances the solubility of isolated VHH domains [159].



**Figure 4.3: Schematic, linear representation of a nanobody.** CDR regions (blue, green and red) form the linker between the framework regions (grey). In a heavy-chain antibody, the  $V_{HH}$  does not associate with a  $V_L$ . In order to maintain solubility, several amino acids have therefore been substituted in the second framework region (purple diamonds). Figure adapted from Muyldermans *et al.*, 2009 [160]

The above described unique, single domain nature of nanobodies translates into valuable properties, absent in conventional antibodies and their derived antigen-binding fragments.

**Table 4.1:** Biophysical, biochemical and functional characteristics of nanobodies

Property	
Proteolytic resistance	Nbs retain functional activity in gastric and jejuna fluid and display resistance against degradation by pepsin, trypsin and chymotrypsin [161].
Thermal stability	Nanobodies display high $T_m$ values (60 – 80°C) and retain functionality after exposure to elevated temperatures of up to 90°C [162, 163].
pH	Nanobodies are resistant to extremes of pH [159]
Chemical denaturation	Nbs are exceptionally resistant to chemical unfolding with $C_m$ values of 2.3 – 3.3 M and $\geq$ M in high salt (GdmCl) and urea conditions [163].
Refolding capacity	Thermal unfolding of several nanobodies was shown to be fully reversible (in contrast to conventional antibody-derived fragments) [164, 165].
Solubility	Nanobodies were soluble at concentrations of >3 mM without any signs of aggregation [157, 166, 167].
Cloning	A single exon of 450 bp encodes for the VHHs, which enables easy cloning, engineering, optimization, tailoring and generation of Nbs [168].
Expression yield	Recombinant Nbs can be obtained at levels up to 10 mg/L when expressed in <i>E. coli</i> and even higher when expressed in <i>S. cerevisiae</i> or <i>Pichia pastoris</i> (yeast) [169, 170].
Unique epitopes and targets	Because of their small size, Nbs have access to a wider range of conformational (cryptic) epitopes, including enzymes, small molecule toxins and other haptens, than conventional antibodies [171–176].
Low immune-genicity	Nbs share a high sequence homology to human VH domains, and additional engineering can be performed for further humanization [166, 177, 178].
Affinity and specificity	Due to the <i>in vivo</i> affinity maturation of the HCAs, high specificity and high-affinity Nbs are generally obtained (nano/picomolar range) [167, 179].
Tissue penetration	Nb's small size results in fast tissue penetration (beneficial in solid tumor treatment and <i>in vivo</i> imaging) and in rapid blood clearance (serum $t_{1/2}$ of $\pm$ 2h) (treatment of acute indications) [180–183].



### 4.1.4 Nanobody production

Nanobody generation in camelids is a straightforward process. Weekly, for 5 weeks, the antigen is subcutaneously injected. Following this immunization, the VHH genes are isolated from the camelids lymphocytes and cloned into a phagemid vector. One or several rounds of phage display and panning are then performed to isolate specific and hopefully high affinity binders. Positive clones are withheld. After expression in bacteria or lower eukaryotes - with yields of up to 40-70 mg/l - the nanobodies can be further characterized using several molecular techniques such as ELISA, isothermal titration calorimetry, co-immunoprecipitation, ... [184]. Furthermore, the fact that nanobodies are encoded by single short gene fragments - 450 base pairs - allows easy and straightforward protein engineering, thereby opening the doors for a whole array of research and clinical application.

## 4.2 Applications of nanobodies

### 4.2.1 Research

#### 4.2.1.1 Crystallography

As mentioned earlier, the unique shape of a nanobodies's paratope allows it to bind recognise cryptic epitopes often situated in crevices on the antigens surface. Such interactions may stabilize flexible antigen regions, thereby locking them in a specific conformation. This has rendered nanobodies as ideal chaperones for the crystallization of otherwise uncrystallizable proteins [185, 186]. In the case of amyloidogenic protein research this has been nicely demonstrated in human lysozyme amyloidosis, a hereditary systemic disease associated with at least seven amyloidogenic lysozyme variants [163, 187]. In one specific case  $\beta$ 2-microglobulin-specific nanobodies have been shown to serve as efficient crystallization chaperones for transient intermediate species during fibrillation [188]. The structural data gained from such experiments may provide valuable insights into the mechanisms behind amyloid fibril formation.

#### 4.2.1.2 Intrabodies

The high stability of nanobodies (see **Table 4.1**) allows one to use them intracellularly as an intrabody. More specifically, nanobodies obtained in llama's may be best suited for this application as they are less likely to possess interloop disulfide bonds, thereby reducing the change of intracellular, destabilizing disulfide reduction in the reducing cytoplasm. Intrabodies have been used to produce functional protein knock-outs and inhibit enzymatic activity [189–194]. It is important to note the difference compared to RNAi-based gene knock-outs were the entire protein is removed; intrabodies make it possible to alter a specific function of a protein without disturbing its

other potential interactions/functions. Linked to a signal peptide intrabodies have also been used to lure their targets to a particular cellular compartment different from their normal subcellular location. In this way this kind of intrabodies may indirectly inhibit their targets function [195]. Furthermore, chromobodies - intrabodies fused to a fluorophore - can and have been used to track specific proteins in living cells [196, 197]. In conclusion, due to their high intracellular stability nanobodies hold a clear advantage over other antibody fragments. But before intrabodies can reach their full clinical potential, efficient transduction methods will have to be developed.

## 4.2.2 Diagnostics

### 4.2.2.1 Biosensors

An ideal Biosensor is a highly stable probe which binds its target with a high affinity and selectivity and can be produced in a cost-efficient way on a large scale. Nanobodies definitely meet these requirements (see **Table 4.1**). In fact nanobodies have already been used in HIV and *Trypanosoma* detection [168, 198], quantification of caffeine levels [199] and differentiation between *Brucella* and *Yersinia* infections [200, 201].

### 4.2.2.2 *In vivo* imaging

Via molecular imaging one can visualize molecular biomarkers in a patient's body in a non-invasive way. Equipped with a radionuclide nanobodies can be applied as such an imaging tracer in a single-photon emission computed tomography (SPECT) or positron emission tomography (PET) based setup allowing *in vivo* visualization of tumors, atherosclerotic plaques and rheumatoid arthritis-associated inflammation sites [183, 202, 203]. Indeed, nanobodies are well-suited for imaging purposes. Firstly, their high stability and small size allows a rapid tissue penetration followed by an equally swift clearance of unbound nanobody. Secondly, as their C-terminus is situated on the opposite site of the nanobody paratope [178] it can be readily employed to site-specifically label a nanobody. More specifically, incorporation of a C-terminal His<sub>6</sub>-tag or cysteine allows a straightforward labeling with <sup>99m</sup>Tc or <sup>111</sup>In respectively [204, 205]. Thirdly, a nanobody's low immunogenicity reduces the risk of inflammatory reactions in the case of repeated imaging. Lastly, as highly specific, high affinity nanobodies are fairly inexpensive one may conclude that nanobodies come close to being an ideal imaging format. However, some disadvantages are worth mentioning. First and foremost, their rapid renal clearance results in high kidney and bladder signals, thereby rendering the imaging of nearby targets impossible. Secondly, nanobody-based imaging is limited to extracellular targets and antigens accessible at the cell surface. Intracellular *in vivo* imaging is, at least for the moment, not possible. Lastly, although the production of nanobodies is indeed cheap, they are still more expensive compared to peptide derived tracers.

### 4.2.3 Therapeutics

#### 4.2.3.1 Multidomain nanobodies

Nanobodies, being small and stable, are ideal candidates for various therapeutic applications. Their single-gene/single-domain nature allows one to easily modify, combine or tag a nanobody. As such, bivalent nanobodies - a dimer of two identical nanobodies - to increase the avidity have been created [206].

Bispecific nanobodies on the other hand are a dimers of two different nanobodies which either target two different antigens or two epitopes on the same antigen. Such nanobodies have been used to guide immune effector cells to cancer cells [207], create more potent anti-toxins [208, 209] and extend the overall serum half-life of a nanobody [182, 210]. The latter is achieved via an albumin binding nanobody. More specifically, when bound to albumin the bispecific nanobody-albumin complex is larger than the renal cutoff. As a result, the half-life increases from several hours to several days [100].

#### 4.2.3.2 Cancer therapy

As mentioned several times before, nanobodies have some distinct advantages over conventional antibodies; small size, high stability, long shelf-life and easy to produce. It is therefore not surprising that in recent years a lot of research has been done on nanobody-based cancer therapeutics. However, just as conventional antibodies, nanobodies are unable to freely cross the plasma membrane. As such the targeted cancer antigens still have to be transmembrane or extracellular, cancer specific proteins.

Nanobody-based cancer therapeutics can be effective in three distinct ways. (i) Antagonistic nanobodies which bind to receptors and alter the signaling cascade [211]. (ii) Allosteric nanobodies which alter the enzymatic activity of their target [212]. (iii) Nanobodies can also be deployed as simple carriers of an anticancer drug. This kind of *magic bullet* approach can either be achieved by directly linking the nanobody to the therapeutic moiety [181] or attaching the nanobody to nanoparticles which encapsulate the drug [213].



# **PART II**

## PRECEDING WORK & SCOPE

Adapted from:

Verhelle A. and Gettemans J.

**A Nanobody-Based Approach to Amyloid Diseases, the Gelsolin Case Study, Exploring New Findings on Amyloidosis** *Dr. Ana Maria Fernandez-Escamilla (Ed.), InTech 2016, DOI: 10.5772/63981.*

Available from: <https://www.intechopen.com/books/exploring-new-findings-on-amyloidosis/a-nanobody-based-approach-to-amyloid-diseases-the-gelsolin-case-study>

# 1

## Introduction

This thesis is a continuation of previous work performed by Van Overbeke *et al.*, concerning the development, characterization and therapeutic exploration of both Nb11 and the FAF nanobodies [18, 100]. Therefore it seemed appropriated to provide a concise overview of the rationale behind the development of both types of AGel nanobodies, the performed experiments and the gained insights [214].

# 2

## Preceding work

### 2.1 Extracellular targeting of the AGel pathological pathway

Consecutive aberrant cleavage of PG\* by furin and MT1-MMP-like proteases leads to the production of amyloidogenic fragments which eventually polymerize into fibrils, causing gelsolin amyloidosis pathology. But these two proteases are active in different compartments. Indeed, whereas furin is active in the (intracellular) ER-Golgi compartments, MT1-MMP is inserted in the plasma membrane and oriented to the extracellular environment. This has far reaching consequences in terms of molecular therapeutic avenues that should be followed when gelsolin has to be protected from cleavage by either of these proteases. As the second cleavage step occurs in the extracellular matrix we reasoned that it might be possible to block this process by intraperitoneal administration of C68 chaperone nanobodies [100].

A dromedary was simultaneously immunized with the G2 domain and the 8 kDa fragment of PG\*. Phage panning was also performed with both gelsolin fragments. This yielded three different nanobodies, termed FAF Nb1-3. All three bind to PG, PG\*, C68 and the 8 kDa peptide when tested via immunoprecipitation on crude bacterial lysates, but they did not cross-react with CapG, a protein that is structurally related to gelsolin. Unlike gelsolin, CapG is only capable of capping actin filaments but does not sever. It is the member of the gelsolin superfamily most closely resembling gelsolin. It possesses 49% identity with the N-terminal half of gelsolin.

The hypothesis was that if one of these FAF nanobodies bound to C68 in the vicinity of the MT1-MMP cleavage site, or an important docking area, it would be able to (at least partly) inhibit the production of the 8 kDa fragments. This was indeed confirmed by *in vitro* experiments. C68 was pre-incubated with one of the three FAF Nbs after which MT1-MMP was added to the mixture. Formation of the 8 kDa fragment could be followed by Western blotting and this showed a 70-80% reduction in the presence of a FAF nanobody, attesting to their ability to indirectly prevent MT1-MMP activity on gelsolin (**Figure 2.1a** and **d**). Nb13, a nanobody that binds to



the linker between gelsolin domain 4 and 5 did not show the same effect. Furthermore, the FAF Nbs had no effect on the proteolysis of collagen, another substrate of MT1-MMP. Therefore, it was concluded that a nanobody can be used as a chaperone to prevent degradation of a structural protein by an enzyme without directly inhibiting the activity of the enzyme. In doing so, potential side effects may be prevented. Whether the observed effects are due to a direct inhibition of MT1-MMP docking on C68, shielding of the cleavage site, or rather due to an indirect structural affect caused by the binding of the Nb with C68, still remains to be clarified. A crystal structure of MT1-MMP bound to C68 would bring clarity in this matter.

While these results were promising at first, a new caveat presented itself when considering that nanobodies, because of their small size, are characterized by rapid blood clearance. This could impede their use as a therapeutic *in vivo*. Indeed, although their small size is mostly advantageous, when used as a therapeutic it is rather a burden. Thus it seemed necessary to increase their half life in the circulation as this will improve their probability of binding C68 gelsolin. To achieve this goal, FAF Nb1-3 were coupled to the mouse albumin binding nanobody MSA21 via a short Gly-Ser linker. This linkage did not greatly affect the binding affinity between the Nb and C68 (FAF2 = Kd:  $8.4 \times 10^{-7} \pm 4.7 \times 10^{-8}$  M, FAF2-MSA21 = Kd:  $5.4 \times 10^{-7} \pm 0.6 \times 10^{-7}$  M, determined by Isothermal Titration Calorimetry (ITC) ). The bispecific FAF2-MSA21 Nb binds albumin in the bloodstream and the formation of this larger complex should extend the half-life, resulting in a higher efficiency of the FAF Nb1-3 therapeutic intervention. Serum analysis of injected mice confirmed this assumption. While the monovalent FAF Nb1-3 were no longer detectable after 4h, the bispecific format could still be clearly visualized up until one week post injection (**Figure 2.1d**). Additionally the linkage between FAFNb1-3 and MSA21 did not offset the MT1-MMP inhibiting potential *in vitro*. Hence all requirements were fulfilled to test their effect *in vivo*.

The *in vitro* results were validated using the available AGel mouse model. Over a period of 12 weeks, on a weekly basis, mice were injected with 100  $\mu$ g of either FAF Nb1, FAF Nb2-MSA21 or phosphate buffered saline (PBS). The trial started at the age of 4 weeks, the nanobodies used were the ones which performed best during the *in vitro* set-up. End stage analysis consisted of immunohistochemistry (IHC) and *ex vivo* muscle contractility measurements. IHC revealed a decrease in amyloidogenic gelsolin staining for FAF Nb1 of 15% and FAF Nb2-MSA21 of 30%. Both results were statistically significant. The difference between both nanobody formats shows that a longer half-life is definitely desirable in a therapeutic approach such as this. The reduction seen with IHC in the FAF Nb2-MSA21 treated mice translated into improved muscle contractility and relaxation speed function in the extensor digitorum longus (EDL). Therefore these nanobodies are endowed with a therapeutic quality. It should be noted that the FAF Nbs display an intermediate affinity for their target. Although clear data in support of this contention are wanting, it seems likely that stronger binders might even have stronger effects *in vivo*. Further exploration of the FAF Nb2-MSA21 potential in human gelsolin amyloidosis patients requires two important modification to be made. Firstly the MSA21 nanobody would have to be replaced by a human serum albumin binder. The longer serum half-life of human versus mouse albumin (19 days versus 35 hours) may further lower the administration frequency. Secondly, although nanobodies

are known for their low immunogenicity, humanizing their framework regions can further decrease the risk of an undesirable immune response during therapeutic intervention. More specifically, a universal humanized nanobody scaffold has already been proposed onto which all the CDR antigen-binding loops could be grafted [178].

## 2.2 Intracellular targeting of the AGel pathological pathway

Thanks to their excellent stability, nanobodies are also valuable compounds to be used as intrabodies. The reducing environment of the cytoplasm seems to have little effect on their functionality [215, 216]. As mentioned above, the FAF Nb approach significantly reduced AGel amyloid buildup *in vivo*, but it did not completely halt the 8 kDa peptide production. AGel pathogenesis is a two step process; a furin cleavage of mutant PG produces C68, which is then on its turn cleaved by MT1-MMP, thereby releasing 8 kDa amyloidogenic peptides. This opens the opportunity for a double hit approach.

For that reason we tested whether a different set of gelsolin nanobodies could be applied as a chaperone for gelsolin to divert furin activity in the same manner as we had implemented the FAF Nb1-3 towards C68 [18].

The nanobodies used in this study were not specifically designed for this purpose. Instead, they had been raised against wild type CG and characterized some time ago. Through *in vitro* epitope mapping experiments, Nb11 was shown to interact with the G2-G3 domains (N-terminal half) whereas Nb13 interacts with G4-G5 (C-terminal half). Furthermore, both nanobodies interact with different populations of gelsolin in cells. Indeed, Nb11 binds human gelsolin with high affinity ( $K_d = 3.65 \times 10^{-9} \pm 0.54 \times 10^{-9}$  M, determined by ITC), irrespective of whether  $Ca^{2+}$  is present or not, whereas Nb13 strongly interacts with gelsolin ( $K_d = 9.26 \times 10^{-9} \pm 1.61 \times 10^{-9}$  M, determined by ITC) only when the latter is activated by  $Ca^{2+}$ . Both nanobodies were further shown to act as reliable tracers of gelsolin in MCF-7 cells when expressed as intrabodies. Both gelsolin and nanobody are abundantly present in the cytoplasm of unstimulated MCF-7 cells, preventing straightforward assessment of their co-localization. However, when the cells were stimulated with epidermal growth factor (EGF), both endogenous gelsolin and the nanobodies extensively decorated membrane ruffles [191]. In view of the binding region of Nb11 in gelsolin, it was surmised that it could interfere with furin-mediated degradation. In analogy with the MT1-MMP study, these gelsolin nanobodies were incubated with PG\* and Western blotting showed that only Nb11 reduced furin cleavage of PG\* by 34% when added in concentrations equimolar to PG\* (**Figure 2.1a and b**).

This finding however does not guarantee that the same result will be obtained in mammalian cells. PG will naturally travel through the secretory pathway but simple expression of the nanobody will result in its cytoplasmic and nuclear localization in cells. Hence, the nanobody will not be able to protect gelsolin. For this reason, the nanobody was equipped with an ER-signal peptide

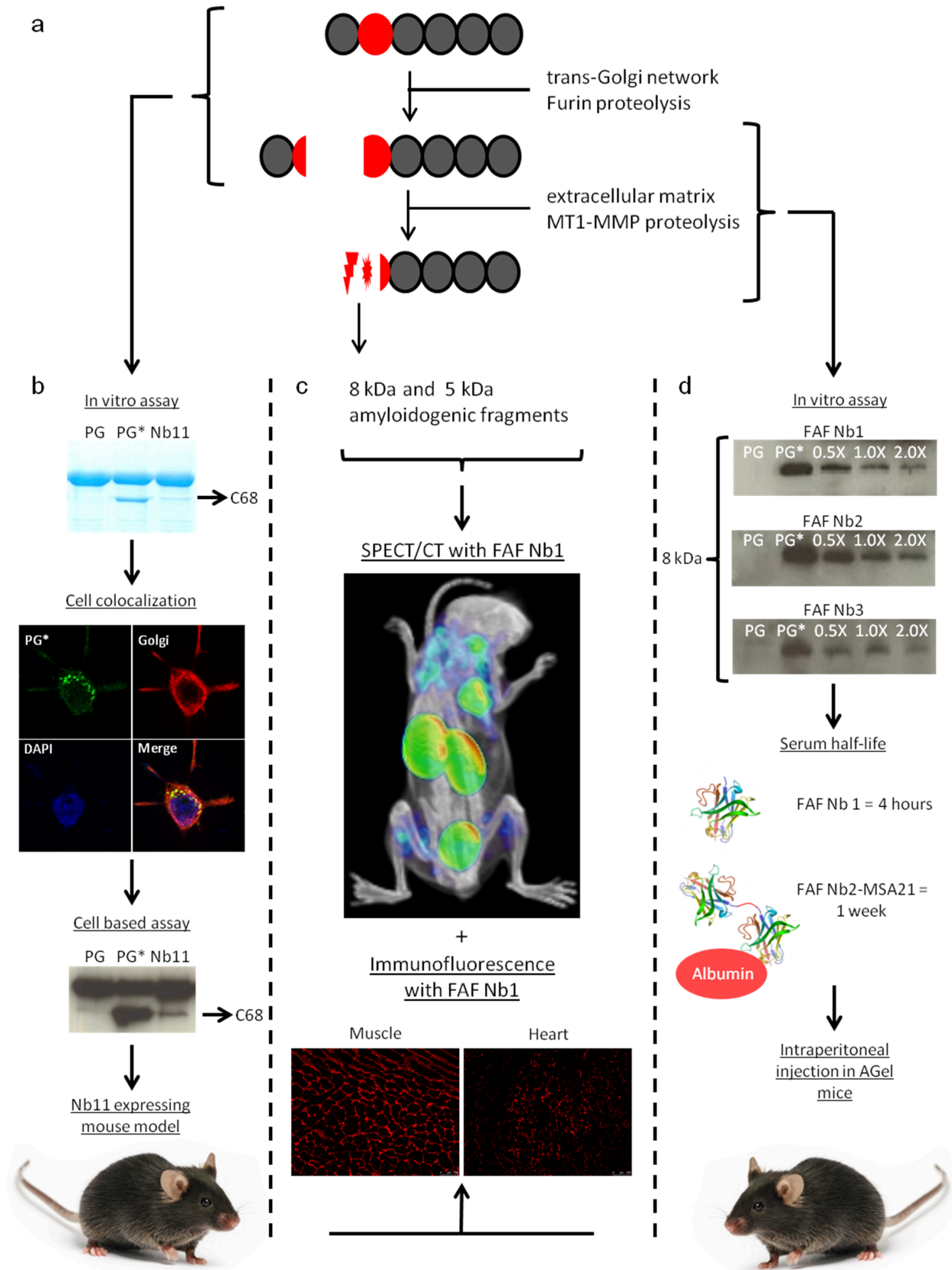


**Figure 2.1: Overview of different diagnostic and therapeutic nanobody-based strategies developed in transgenic mice.** **a:** schematic representation of the steps leading from mutant PG to the 8 and 5 kDa amyloidogenic fragments. **b upper panel:** Gelsolin Nb11 reduces C68 formation *in vitro*: lane 1: PG incubated with furin, lane 2: PG\* incubated with furin, line 3: PG\* incubated with furin and Nb11. **b second panel:** Nb11 co-localizes with mutant gelsolin in the secretory pathway of HEK293T cells. **b third panel:** Nb 11 decreases C68 formation in HEK293T cells: lane 1: medium from cells transfected with PG, lane 2: medium from cells transfected with PG\*, lane 3: medium from cells transfected with PG\* and Nb11. This led to designing the Nb11 expressing mouse model. **c:** Representative images obtained with 99mTc-labeled FAF Nb1 in 9 months old AGel mice. The heart and front and hind leg muscles show a clear signal (blue). Kidneys and bladder signal represents unbound nanobody which is cleared via the urinary system (green and red). FAF Nb1 can also be used as a primary antibody to stain amyloidogenic gelsolin buildup in AGel mice tissue (lower panel). **d upper panel:** FAF Nb1-3 partly inhibits C68 proteolysis *in vitro*. For each nanobody, from left till right, after incubation with MT1-MMP: PG, PG\*, PG\* + 0.5, 1.0 and 2.0 X FAF Nb. Numbers indicate the Nb/PG\* molar ratios. **d middle panel:** Linkage with the albumin binding MSA21 nanobody increases serum half-life from 4 h to more than one week. **d lower panel:** *In vivo* analysis was performed via intraperitoneal injection in AGel mice [23].

to ensure its secretion via the Golgi apparatus. Furin naturally resides in the Golgi apparatus and the first step in the AGel pathology takes place in this compartment. By quantifying the amount of C68 that is secreted in the extracellular environment it could be confirmed that Nb11 exerts a protective effect. The cell media from HEK cells transfected with PG\* and Nb11 contained 80% less C68 compared to HEK cells solely transfected with PG\* (**Figure 2.1b**).

Although nanobodies can, and are, currently being applied in research involving intracellular perturbation of protein-protein interactions, at the moment there is no efficient, fail proof method to introduce them into cells in a recombinant format. Therefore, to test whether the observed effect of Nb11 *in vitro* could be reproduced *in vivo*, a Nb11 expressing mouse model had to be created. To our knowledge this is the first transgenic mammal that contains a therapeutic nanobody in its genome. The ER-directed Nb11 cDNA was cloned in the pROSA-DV2 vector which targets the ROSA26 locus. This locus was identified in 1991 using gene-trap mutagenesis screening on embryonic stem cells. Thanks to its ubiquitous expression in both embryonic and adult tissues, over 130 knock-in mouse lines have been created using this cloning site. G4 ES cells were electroporated and positive colonies were selected via Southern blotting. Next, cells were aggregated with Swiss inner cell mass cells. These blastocysts were transferred into pseudopregnant mice uteri and the resulting chimeric offspring was backcrossed with wild-type C57BL/6 to check for germline transmission. Finally these mice could then be crossed with a non-tissue specific Cre/lox-deleter mouse strain. This resulted in CAGG promoter driven Nb11 expression, resulting in the first Nb11 expressing mice. Nb11 could be visualized and quantified in the serum through co-immunoprecipitation and Western blotting.

The newly developed Nb11 mouse model was crossed with AGel mice. Double positive offspring was evaluated at three distinct time points; 3, 6 and 9 months. Gastrocnemius muscle tissue was stained for AGel buildup. A costaining for laminin was used as an internal control and to discern any potential artefacts. The AGel staining was homogenous in every age group, allowing quantification. Compared to AGel mice or littermates not expressing Nb11, a reduction in AGel staining of 27% and 28% respectively could be detected at 3 and 9 months of age. For the group of 6 months, no significant reduction could be found. The reason for this is unclear. The group of 9 months old mice was also subjected to a muscle performance evaluation. The extensor digitorum longus (EDL) muscle showed a strong attenuation of the typical decrease in contraction speed during the fatiguing protocol. This therapeutic effect was not mimicked by Nb13 that binds to another region in gelsolin (G4-G5 linker) and that had no effect on gelsolin degradation by furin. Neither Nb11 nor Nb13 showed any cross-reactivity with endogenous mouse gelsolin. Thus Nb11 attenuates amyloid buildup by (partly) protecting gelsolin against degradation by furin. One might wonder why the reduction in AGel staining was not as high as expected, given that Nb11 is a strong binder ( $K_d \pm 5$  nM). One possibility involves the relative expression levels of gelsolin and Nb11. Western blotting with internal gelsolin and nanobody standards indicated that both are present at roughly equimolar levels. In the AGel mouse model however, gelsolin is secreted from muscle whereas nanobody expression is thought to be secreted from multiple organs, tissues and cells, because no tissue specific promoter was used to drive expression of the nanobody. Therefore, the nanobody that was detected in the serum of these animals has multiple origins suggesting that its secretion from muscle is significantly lower as compared to gelsolin secretion. This contention however needs to be examined experimentally.

# 3

## Scope of the thesis

Amyloidosis is a group of diseases characterized by the deposition of protein fibrils which exhibit green, yellow or orange Congo red birefringence under polarized light. At the moment, 35 of such proteins are known. In each disease the causative protein will adopt a cross- $\beta$ -sheet structure while forming oligomers and fibrils. Their mode of deposition: systemic or localized greatly influences the type and severity of symptoms in patients. Despite the enormous effort of the global amyloid research community, at the moment no treatments are available<sup>1</sup>.

In this thesis the focus is on gelsolin amyloidosis. Gelsolin amyloidosis is an autosomal dominantly inherited disease caused by a point mutation in the gelsolin gene; G640A and G640T are most common, G580A and C633A were more recently discovered [113, 116, 117]. At the protein level these mutations result in the amino acid substitutions D187N, D187Y, G167R and N184K in gelsolin domain 2. Consequently a  $\text{Ca}^{2+}$  binding site, crucial for the correct folding and function, is lost. As a result, mutant PG adopts an intermediate state between active and inactive, thereby negatively influencing the overall structural stability of the protein and exposing a cryptic, otherwise buried, furin cleavage site [22]. In the trans-Golgi network this intermediate form of mutant PG is susceptible to furin cleavage, giving rise to a 68 kDa C-terminal fragment [20]. On its turn, C68 is cleaved by MT1-MMP-like proteases during secretion into the extracellular matrix. This MMP activity results in the formation of 8 and 5 kDa amyloidogenic peptides which polymerize into mature amyloid fibrils [220]. Patients are generally heterozygous for the mutations and experience a triad of neurological, ophthalmological and dermatological symptoms starting from their thirties [121]. Given the importance of furin and MT1-MMP-like proteases in cell homeostasis, a classical small compound therapy targeting these proteases is unlikely to be successful. Moreover, the gain-of-toxicity nature of this disease rules out replacement gene therapy. In gelsolin amyloidosis, the mutant gelsolin gene still undergoes normal expression.

---

<sup>1</sup>Clinical trials on AL patients using a combination bone marrow transplantation, the drug (R)-1-[6-[(R)-2-carboxy-pyrrolidin-1-yl]-6-oxo-hexanoyl]pyrrolidine-2-carboxylic acid (CPHPC) and anti serum amyloid P IgG appears to be successful and may represent the first ever amyloid therapy [217-219].

---

Curing gelsolin amyloidosis via replacement gene therapy would therefore require the deletion of the mutant gene from every single cell. This is (at the moment) not possible with the available gene therapy technology. Shielding the mutant gelsolin from furin and MT1-MMP-like proteases on the other hand, proved to be a worthwhile approach to tackle this disease.

As described above, two routes to address AGel have already been explored. In a first approach, nanobodies, which partly protect C68 against MT1-MMP, were intraperitoneally injected in AGel mice [100]. In a second approach a mouse model expressing Nb11 was developed [18]. Nb11 binds to mutant PG and shields it from furin degradation. The mouse model secretes this nanobody in its bloodstream. These mice were crossed with AGel mice. Consequently, during the secretion pathway Nb11 encounters PG\* in the trans-Golgi network. Both techniques resulted in a reduced deposition of amyloidogenic gelsolin.

We continued this research in two directions. (i) The nanobodies capable of shielding C68 were generated against the 8 kDa amyloidogenic gelsolin fragment. This characteristic was further explored to develop a  $^{99m}\text{Tc}$  based imaging agent (**Figure 2.1c**). Using the AGel model we selected FAF Nb1 as the most promising candidate based on its superior signal-to-noise ratio and signal specificity. Furthermore, using immunohistochemistry we demonstrated a positive correlation between the generated SPECT signal and *in vivo* amyloid buildup. Indeed using the  $^{99m}\text{Tc}$ -FAF Nb1 we are now able to assess the effect of novel therapeutics under development in a non-invasive manner. (ii) The two therapeutic strategies mentioned above have been merged into a single format; a bispecific Nb11-FAF nanobody capable of (partly) inhibiting both furin and MT1-MMP. Using AAV9 gene therapy we were able to significantly reduce the amyloid burden in the AGel mouse model. Furthermore, here, for the first time, we successfully implemented the  $^{99m}\text{Tc}$ -FAF Nb1 imaging tracer.

Both lines of research have been published and are described in more detail in the following two parts.





# **PART III**

SPECT/CT IMAGING IN THE AGEL  
MOUSE MODEL

Adapted from:

Verhelle A, Van Overbeke W, Peleman C, De Smet R, Zwaenepoel O, Lahoutte T, Van Dorpe J, Devoogdt N, Gettemans J.

**Non-Invasive Imaging of Amyloid Deposits in a Mouse Model of A $\beta$  Using  $^{99m}\text{Tc}$ -Modified Nanobodies and SPECT/CT** *Molecular Imaging and Biology*. 2016 April 29; 18:887-897. DOI: 10.1007/s11307-016-0960-y.

# Non-invasive imaging of amyloid deposits in a mouse model of AGel using $^{99m}\text{Tc}$ -modified nanobodies and SPECT/CT

## 1.1 Abstract

*Purpose:* Gelsolin amyloidosis (AGel), also known as familial amyloidosis, Finnish type (FAF), is an autosomal, dominant, incurable disease caused by a point mutation (G654A/T) in the gelsolin (GSN) gene. The mutation results in loss of a  $\text{Ca}^{2+}$ -binding site in the second gelsolin domain. Subsequent incorrect folding exposes a cryptic furin cleavage site, leading to the formation of a 68-kDa C-terminal cleavage product (C68) in the trans-Golgi network. This C68 fragment is cleaved by membrane type 1- matrix metalloproteinase (MT1-MMP) during secretion into the extracellular environment, releasing 8- and 5-kDa amyloidogenic peptides. These peptides aggregate and cause disease-associated symptoms. We set out to investigate whether AGel-specific nanobodies could be used to monitor amyloidogenic gelsolin buildup.

*Procedures:* Three nanobodies (FAF Nb1-3) raised against the 8-kDa fragment were screened as AGel amyloid imaging agents in WT and AGel mice using  $^{99m}\text{Tc}$ -based single-photon emission computed tomography (SPECT)/X-ray tomography (CT), biodistribution analysis, and immunofluorescence (IF). The quantitative characteristics were analyzed in a follow-up study with a Nb11-expressing mouse model.

*Results:* All three nanobodies possess the characteristics desired for a  $^{99m}\text{Tc}$ -based SPECT/CT imaging agent, high specificity and a low background signal. FAF Nb1 was identified as the most potent, based on its superior signal-to-noise ratio and signal specificity. As a proof of concept, we implemented  $^{99m}\text{Tc}$ -FAF Nb1 in a follow-up study of the Nb11-expressing AGel mouse model. Using biodistribution analysis and immunofluorescence, we demonstrated the validity of the data acquired via  $^{99m}\text{Tc}$ -FAF Nb1 SPECT/CT.

*Conclusion:* These findings demonstrate the potential of this nanobody as a non-invasive tool to image amyloidogenic gelsolin deposition and assess the therapeutic capacity of AGel therapeutics currently under development. We propose that this approach can be extended to other amyloid diseases, thereby contributing to the development of specific therapies.

## 1.2 Introduction

Amyloidosis comprises 35 diseases characterized by the deposition of protein fibrils with a cross-beta sheet structure [101, 221]. Each disease differs from the other in terms of cause, amyloid deposition sites, and clinical features. Gelsolin amyloidosis (AGel) is an orphan disease with worldwide only about 1000 gene carriers of which the majority lives in Finland [121]. As a component of the actin-scavenging system, plasma gelsolin (PG) prevents a drastic increase in blood viscosity after tissue damage [222]. In AGel patients, a point mutation (G654A being most common, D187N) in the gelsolin (GSN) gene results in loss of the  $\text{Ca}^{2+}$ -binding site in the second domain, thereby exposing a furin cleavage site [20]. Mutant PG (PG\*) is cleaved by furin in the trans-Golgi network leading to the production of a 68-kDa C-terminal cleavage product (C68). This C68 fragment is subsequently degraded by membrane type 1-matrix metalloproteinase (MT1-MMP) during secretion, resulting in the release of 8- and 5-kDa amyloidogenic peptides [220]. Patients experience a triad of ophthalmological, dermatological, and neurological symptoms. During disease progression, renal and cardiac complications may also occur [121].

Two routes to address AGel have already been explored in our lab [18, 100]. In the first approach, transgenic gelsolin Nb11- expressing mice were crossed with AGel mice [191]. Nb11 is a gelsolin-binding nanobody that is capable of shielding PG\* furin degradation both *in vitro* and *in vivo*. In the second approach, AGel mice were injected with C68 binding nanobodies (familial amyloidosis, Finnish type (FAF) Nbs) that partly protect against MT1-MMP proteolysis [18, 100]. These findings represent an important step toward a clinically applicable therapeutic. In both approaches however, responses had to be evaluated by immunofluorescence (IF), an end-stage screening method.

In the clinic,  $^{123}\text{I}$ -labelled serum amyloid P (SAP) scintigraphy is implemented to assess the visceral amyloid burden. The non-fibrillar glycoprotein SAP is a member of the pentraxin family and is present in all types of amyloid deposits. Radiolabeled SAP will distribute rapidly and specifically to amyloid, making it a useful imaging tracer. However, it is not capable of visualizing amyloid in neurological tissue and skin, which are two major AGel deposition sites in patients [223]. Other limitations are the relatively high cost of  $^{123}\text{I}$  and the availability of SAP. Furthermore, in AGel patients, the rate of disease progression and the severity of symptoms vary significantly. An individual therapeutic approach and regular assessment of the amyloid burden is thus desirable.

Nanobodies correspond with the variable part of heavy chain antibodies [154]. These fragments are the smallest (15 kDa), intact antigen-binding fragments currently available. Their small size

combined with excellent stability makes them the ideal tool for a plethora of biotechnological applications [224, 225]. Here, we show that nanobodies raised against the 8-kDa amyloidogenic gelsolin peptide can be labeled with  $^{99m}\text{Tc}$  and used as amyloidogenic gelsolin imaging agents *in vivo*. In addition, we provide evidence that this can be done with a low background signal and high specificity. This and other nanobody-based imaging agents may prove useful in drug-screening research and clinical application, especially in those situations where the current imaging platforms expose their limits.

## 1.3 Materials & Methods

### 1.3.1 Antibodies and reagents

Penta-His<sub>6</sub> horseradish peroxidase antibody (1:1000 Western blot) from Qiagen (Venlo, the Netherlands), polyclonal anti-V5 antibody (1:100 IF) from Sigma-Aldrich (Diegem, Belgium), Alexa Fluor 488 goat anti-rat IgG (H + L) and 594 goat anti-rabbit IgG (H + L) from Life Technologies (Merelbeke, Belgium; 1:500 IF), and monoclonal anti-laminin antibody (1:500 IF) from Abcam (Cambridge, UK) were included.

### 1.3.2 Generation of FAF gelsolin-specific nanobodies

Gelsolin-specific nanobodies were obtained in collaboration with the VIB Nanobody Service Facility as described [100]. Briefly, a single dromedary was immunized with synthetic biotinylated human gelsolin 8-kDa AGel peptide and recombinant GST-tagged human mutant (D187N) gelsolin domain 2 (G132-S286). After lymphocyte preparation, a VHH complementary DNA (cDNA) library was subjected to phage panning using the gelsolin 8-kDa peptide or mutant G2 domain as antigen. Three distinct nanobodies could be identified and are referred to as FAF Nb1-3.

### 1.3.3 cDNA cloning

Cloning of the FAF nanobodies in the pHEN6 vector was performed using the Cold Fusion Kit (System Biosciences, Mountain View, CA). The following primers were used: 5' CCAGGTGCAGCTGCAGGAGTCTGGGGGAGGCTC 3' (forward) and 5' GACGCCAGTGAATTCTCAATGGTGATG-GTGATGATG 3' (reverse). This reverse primer incorporated a His<sub>6</sub> tag at the C-terminus of the nanobodies necessary for labeling with  $^{99m}\text{Tc}$ .

### 1.3.4 Purification of the nanobodies

FAF-His<sub>6</sub> nanobodies were produced as previously described [191]. The samples were treated with Pierce<sup>®</sup> High-Capacity Endotoxin Removal Resin according to the manufacturer's instructions

(Thermo Scientific, Erembodegem, Belgium).

### 1.3.5 Serum stability assay

Mouse plasma was obtained by collecting 180  $\mu\text{l}$  blood of WT C57BL/6 mice and mixed with 20  $\mu\text{l}$  of 18 mg/ml EDTA. Serum was collected after 4-min centrifugation at  $1700\times g$  and cleared from albumin with ProMax Albumin Removal Kit following the manufacturer's protocol (Thermo Scientific, Erembodegem, Belgium). Subsequently, 0.5  $\mu\text{g}$  of FAF Nb1-3 was added to 50  $\mu\text{l}$  albumin-cleared plasma and incubated at  $37^\circ\text{C}$ . At different time points, 10  $\mu\text{l}$  was withdrawn. The reaction was terminated by addition of 5  $\mu\text{l}$  Laemmli sample buffer and analyzed by 15% SDS-PAGE followed by western blotting using anti-His<sub>6</sub>-HRP antibody.

### 1.3.6 Radiolabeling with $^{99\text{m}}\text{Tc}$

Nanobodies were radiolabeled with  $^{99\text{m}}\text{Tc}$  using the tricarbonyl method as previously described [226]. Briefly,  $(^{99\text{m}}\text{Tc}(\text{H}_2\text{O})_3(\text{CO})_3)^+$  was synthesized using the Isolink Kit (Mallinckrodt Medical BV). After neutralization with 125  $\mu\text{l}$  of 1 M HCl, 50  $\mu\text{l}$  of 1 mg/ml FAF Nb1-3 and 50  $\mu\text{l}$  of carbonate buffer, pH 8, were added. This mixture was incubated at  $60^\circ\text{C}$  for 90 min. Assessment of the final radiochemical purity was done with instant thin layer chromatography (ITLC) in acetone as a mobile phase and analyzed with a radiometric chromatogram scanner (VCS-201; Veenstra).

### 1.3.7 Single-photon emission computed tomography/X-ray tomography imaging experiments

*Animal models:* Animal experiments were approved by the Animal Experimental Ethics Committee of Ghent University Hospital (ECD 10/32) and the ethical committee for animal research of Vrije Universiteit Brussel, Faculty of Medicine and Pharmacy (project 13-272-12). Animals were housed in individually ventilated cages with food and water ad libitum. Environmental conditions were controlled at  $20\text{--}23^\circ\text{C}$ , 50 % relative humidity, and 12h light/dark cycles. AGel mice were obtained from the Scripps Research Institute (La Jolla, CA, USA). Wild-type C57BL/6 mice were obtained from Charles River (L'arbresle Cedex, France).

*Biodistribution analysis:* Mice were intravenously injected with 50-75 MBq of  $^{99\text{m}}\text{Tc}$ -labeled FAF Nb1-3. One hour postinjection, mice were anesthetized using 18.75 mg/kg ketamine hydrochloride (Ketamine 1000, CEVA) and 0.5 mg/kg medetomidin hydrochloride (Domitor, Pfizer). Animals were positioned in a solid holder with two plastic disks containing three  $^{57}\text{Co}$  (3.7 MBq) sources. Image acquisition was done using a micro-X-ray tomography (CT) scan for 2 min (60 keV, 615 mA,  $360^\circ$ ; Skyscan 1178, Kontich, Belgium) and a dual-headed single-photon emission computed tomography (SPECT) camera (e.cam 180, Siemens, USA) equipped with triple pinhole

collimators (1-mm apertures, focal length of 265.5 mm, and a radius of rotation of 20 mm) for 30 s per projection step and a total scan time of about 40 min. Afterward, the mice were euthanized and dissected.  $^{99m}\text{Tc}$  activity in the individual organs was measured using a Cobra Inspector 5003 gamma-counter (Cannberra-Packard, Downers Grove, IL, USA). Measurements were expressed as percentage injected activity per gram of tissue (% IA/g).

*Image quantification:* After image acquisition, SPECT images were reconstructed using an iterative reconstruction algorithm adapted for the pinhole geometry and reoriented for fusion with CT based on the two plastic disks containing the  $^{57}\text{Co}$  sources. Images were quantified using AMIDE (a Medical Image Data Examiner) software [227]. Ellipsoid regions of interest (ROIs) were drawn around the heart, hind leg muscle, and liver. The same ROI<sub>heart</sub>, ROI<sub>muscle</sub>, and ROI<sub>liver</sub> were used for each individual animal. SPECT signals, obtained/acquired from the ROIs, were calculated and expressed as % IA/cc.

*AGel progression in Nb11-expressing mice using SPECT/CT:* AGel mice expressing therapeutic gelsolin Nb11 (AGel-Nb11) were subjected to SPECT/CT at 2, 5, 7, 9, and 11 months of age [18]. At 9 and 11 months of age, one group was submitted to a biodistribution study. Muscle and heart tissues were analyzed by immunofluorescence as described below. In all the imaging experiments, nanobody BclI10 was chosen as a negative control. The BclI10 ( $\beta$ -lactamase of *Bacillus cereus*) antigen is not present in healthy mice [228].

### 1.3.8 Immunofluorescence

Hind leg muscles and heart were dissected and snap frozen in liquid nitrogen. Cryosections were made and thawed for 15 min followed by 10-min incubation in acetone at  $-20^{\circ}\text{C}$ . After 10 min incubation in PBS, the sections were incubated in 50 mM  $\text{NH}_4\text{Cl}$  followed by PBS for another 10 min followed by an additional PBS washing step. The endogenous peroxidase activity was blocked after 20 min incubation in 0.3 %  $\text{H}_2\text{O}_2$  and then washed in PBS. Sections were incubated with 1 % BSA/PBS for 20 min and with the laminin antibody (1:500) at  $4^{\circ}\text{C}$  overnight, followed by another PBS washing step for 10 min. FAF Nb1-V5 (5  $\mu\text{g}/\text{ml}$ ) was incubated for 1 h at room temperature followed by 10 min incubation in PBS. Polyclonal anti-V5 (1:800) was used as secondary antibody. Alexa Fluor antibodies (488 anti-rat and 594 anti-rabbit, both 1:500) were incubated for 1 h at room temperature. Finally, sections were rinsed with PBS, stained with DAPI (1:500) for 2 min, and mounted with VectaShield. Imaging was performed at room temperature with a Leica DM6000 B microscope. Three sections were made per tissue, and within each section, two images from separate regions were taken for quantification with ImageJ software. This resulted in six technical repeats per tissue, per animal, from which the average was used for further statistical calculations.

### 1.3.9 Statistical analysis

Statistical analysis was performed by SPSS software (SPSS Statistics 22, Chicago, IL, USA) using one-way analysis of variance (ANOVA). Reported values are expressed as mean  $\pm$  SEM (\* $p < 0.05$ ).

## 1.4 Results

### 1.4.1 Nanobody stability and labeling

*In vivo* imaging agents are required to remain stable at 37°C in complex environments such as the blood and extracellular matrix. For this reason, a stability assay was performed. FAF Nb1-3 were incubated in albumin-cleared C57BL/6 mouse serum at 37°C, and samples were taken at different time points. FAF Nb1-3 showed no sign of degradation, even after 24-h incubation (**Figure 1.1**). Next, a test labeling was performed with  $^{99m}\text{Tc}$ . The radiochemical purities of  $^{99m}\text{Tc}$ -FAF Nb1-3 were  $99.7 \pm 1.3 \%$ ,  $99.7 \pm 0.9 \%$ , and  $98.3 \pm 1.0 \%$ , respectively.

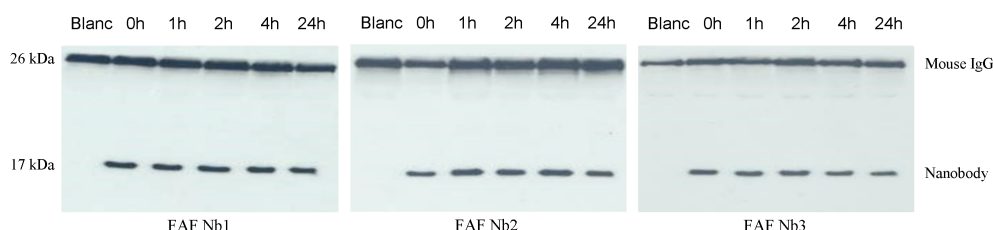


**Figure 1.1: FAF Nb1-3 does not show any deterioration in albumin-cleared mouse plasma.** Western blot analyses shows, from left to right; serum without nanobody (Blanc), FAF Nb1-3 in albumin-cleared mouse plasma after 0, 1, 2, 4 and 24 h incubation at 37°C. The band at 26 kDa is the light chain of mouse Ig. The band at 17 kDa is the nanobody.

$^{99m}\text{Tc}$ -FAF Nb1-3 show no aspecific background signal in WT C57BL/6 mice

To screen for aspecific background signals, 9-month-old WT C57BL/6 mice (three per nanobody) were injected with  $^{99m}\text{Tc}$ -FAF Nb1, 2 or 3. As a negative control, data from previous experiments with the irrelevant control  $^{99m}\text{Tc}$ -Nb-Bcll10 nanobody were used [229]. The SPECT/CT and dissection data show that FAF Nb1- 3 behave similar to the negative control Bcll10 regarding a very low background signal (**Figure 1.2 and 1.6, left panels**). The kidneys and bladder illustrate the typical high uptake of renal-filtered small hydrophilic proteins (**Figure 1.2 and 1.6**). The variability can be attributed to differences in nanobody amino acid sequence [230].



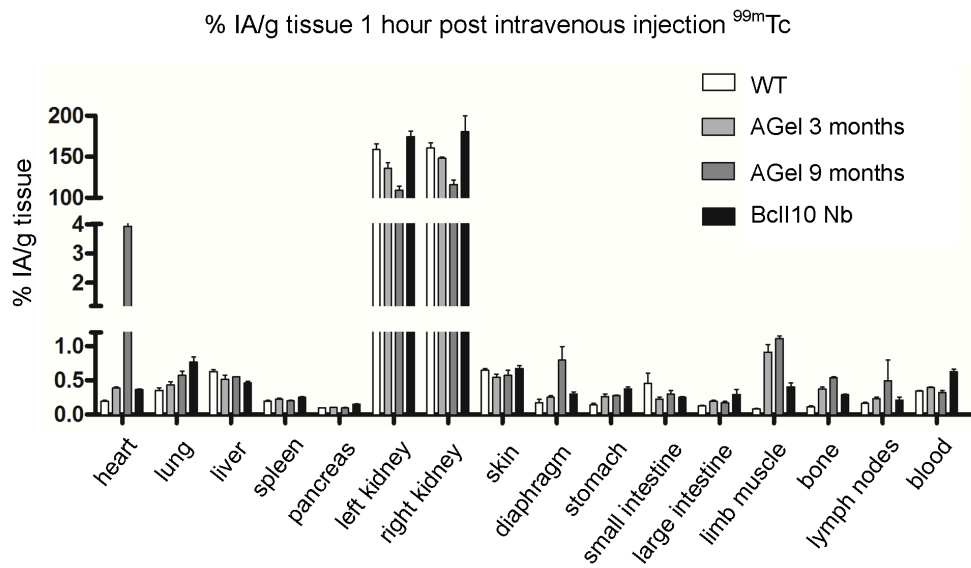


**Figure 1.2: Biodistribution in 9 month old WT C57BL/6 and 3 and 9 month old C57BL/6 AGel mice after SPECT/CT with  $^{99m}\text{Tc}$ -FAF Nb1.** Analysis with  $^{99m}\text{Tc}$ -BcII10 as a control was performed in 9 month old C57BL/6 AGel mice. The kidneys illustrate the typical high uptake of nanobody based imaging agents. The heart, limb muscle and diaphragm show a higher %IA/g tissue for FAF Nb1 compared to BcII10. Data represented as mean  $\pm$  SEM.

$^{99m}\text{Tc}$ -FAF Nb1-3 specifically recognize amyloidogenic gelsolin buildup in the AGel mouse model

A SPECT/CT and dissection analysis was performed on 12 homozygous, 9-month-old AGel mice (3 per nanobody; **Figure 1.6 right panels**). At this age, the animals show significant amyloidogenic gelsolin buildup in muscle tissue [148]. The dissection data showed a specific uptake ( $p < 0.05$ ) in skeletal muscle, heart, and diaphragm for FAF Nb1 and 2. FAF Nb3 did not give a significant signal in the heart nor diaphragm (**Figure 1.3a, c**). BcII10 (negative control) showed statistically significant uptake in the heart (**Figure 1.3a**). The difference is larger in muscle but not statistically significant (**Figure 1.3b**). Also, compared to the WT controls, a significant uptake in the bones ( $p < 0.05$ ) of AGel mice was detected (**Figure 1.3d**).

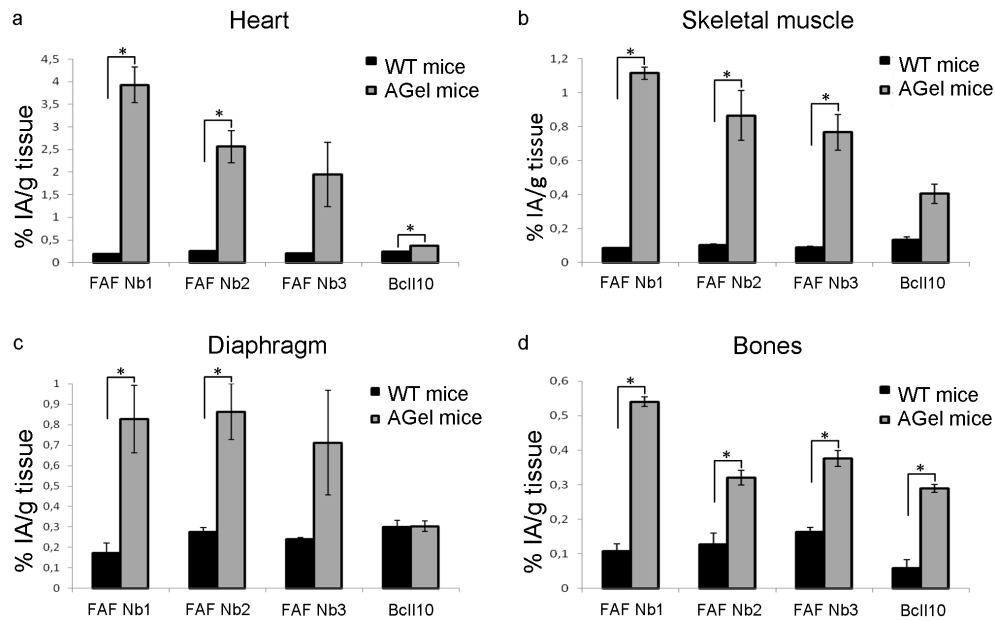


**Figure 1.3: Comparison of biodistribution data between WT and AGel C57BL/6 mice.** FAF Nb1-3 were tested against BcII10 in a biodistribution analysis after  $^{99m}\text{Tc}$ -based SPECT/CT. In the heart (a), skeletal muscle (b), and diaphragm (c), at least two FAF nanobodies showed significant buildup. Bones (d) showed a significant increase for all nanobodies. BcII10 showed a statistical significant difference in the heart (a). The difference in the skeletal muscle (b) was not statistically relevant and significantly smaller than the signal differences acquired with FAF nanobodies. Data were represented as mean  $\pm$  SEM (\* $p < 0.05$ ).

$^{99m}\text{Tc}$ -FAF Nb1 produces the best signal-to-noise ratio and signal specificity in AGel mice

Previous research showed that FAF Nb1 has a slightly higher affinity for the 8- kDa peptide (FAF Nb1 Kd  $3.8 \times 10^{-7} \pm 1.2 \times 10^{-8}$  M, FAF Nb2 Kd  $8.4 \times 10^{-7} \pm 4.7 \times 10^{-8}$  M, and FAF Nb3 Kd  $6.6 \times 10^{-7} \pm 1.7 \times 10^{-7}$  M [100]). Based on these results, it was hypothesized that FAF Nb1 would deliver the best SPECT/ CT result.

The results from C57Bl/6 WT mice and the AGel mice were combined and showed that FAF Nb1 indeed performed best. Using AMIDE software, a ROI around the heart, hind leg muscle, and liver was defined to determine the signal coming from these tissues. FAF Nb1-3 performance was assessed by defining the signal-to-noise ratio as the signals gained with the FAF Nb1-3 in AGel mouse heart or muscle over the signal obtained in AGel mouse liver. Next, signal specificity was defined as the signal obtained with FAF Nb1-3 in AGel mice over the signal obtained with BcII10 in AGel mice. FAF Nb1 has a significantly better ( $p < 0.05$ ; **Figures 1.4** and **1.5**) signal-to-noise ratio and signal specificity score in muscle tissue (**Figures 1.4** and **1.5**). Therefore, FAF Nb1 was designated as the best candidate for a  $^{99m}\text{Tc}$ -based amyloid imaging agent.

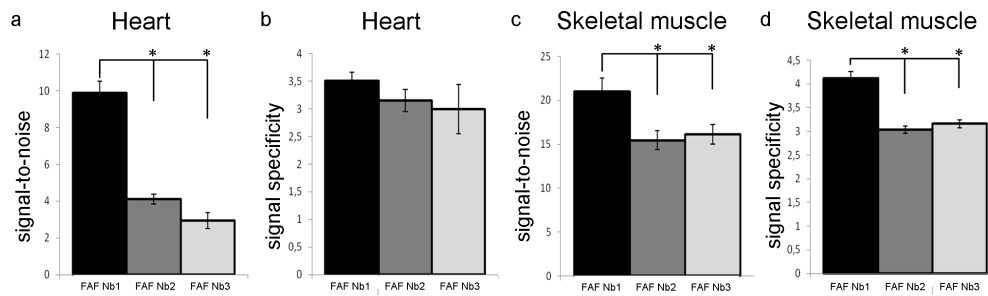


**Figure 1.4: Signal-to-noise ratios and signal specificities for the FAF nanobodies.** Signal-to-noise ratio: signal in AGel mice heart or muscle with FAF Nb1-3/signal in AGel mice liver with FAF Nb1-3 (a, c). Signal specificity: signal in AGel mice with FAF Nb1-3/ signal in AGel mice with BcII10 Nb (b, d). FAF Nb1 significantly outperformed the other two nanobodies in skeletal muscle tissue (c, d). All raw data were gained from 9-month-old mice and are represented in Figure 1.5. Data were represented as mean  $\pm$  SEM (\* $p < 0.05$ ).

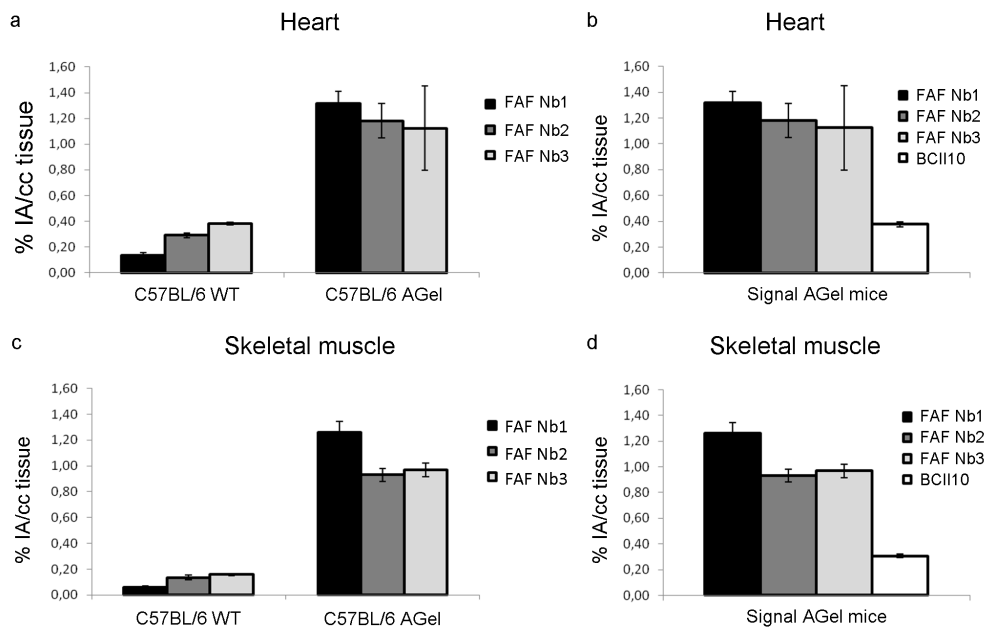


**Figure 1.5: Heart (a,b) and skeletal muscle (c,d) image quantification data via AMIDE software in C57BL/6 WT and AGel mice.** Raw data were used to define the signal-to-noise ratio and the signal specificity as depicted in Figure 1.4. FAF Nb1 outperformed all other nanobodies in the muscle tissue (c, d). All data were obtained from 9 month old mice. Data represented as mean  $\pm$  SEM.

#### $^{99m}\text{Tc}$ -FAF Nb1 shows quantitative features

The AGel mice show progressive amyloidogenic gelsolin buildup over time [148]. A high signal was noted in 9-month-old homozygous AGel mice (Figure 1.6, right panels). Now, 3-month-old homozygous AGel mice were evaluated (Figure 1.6, middle panels). As positive controls, we

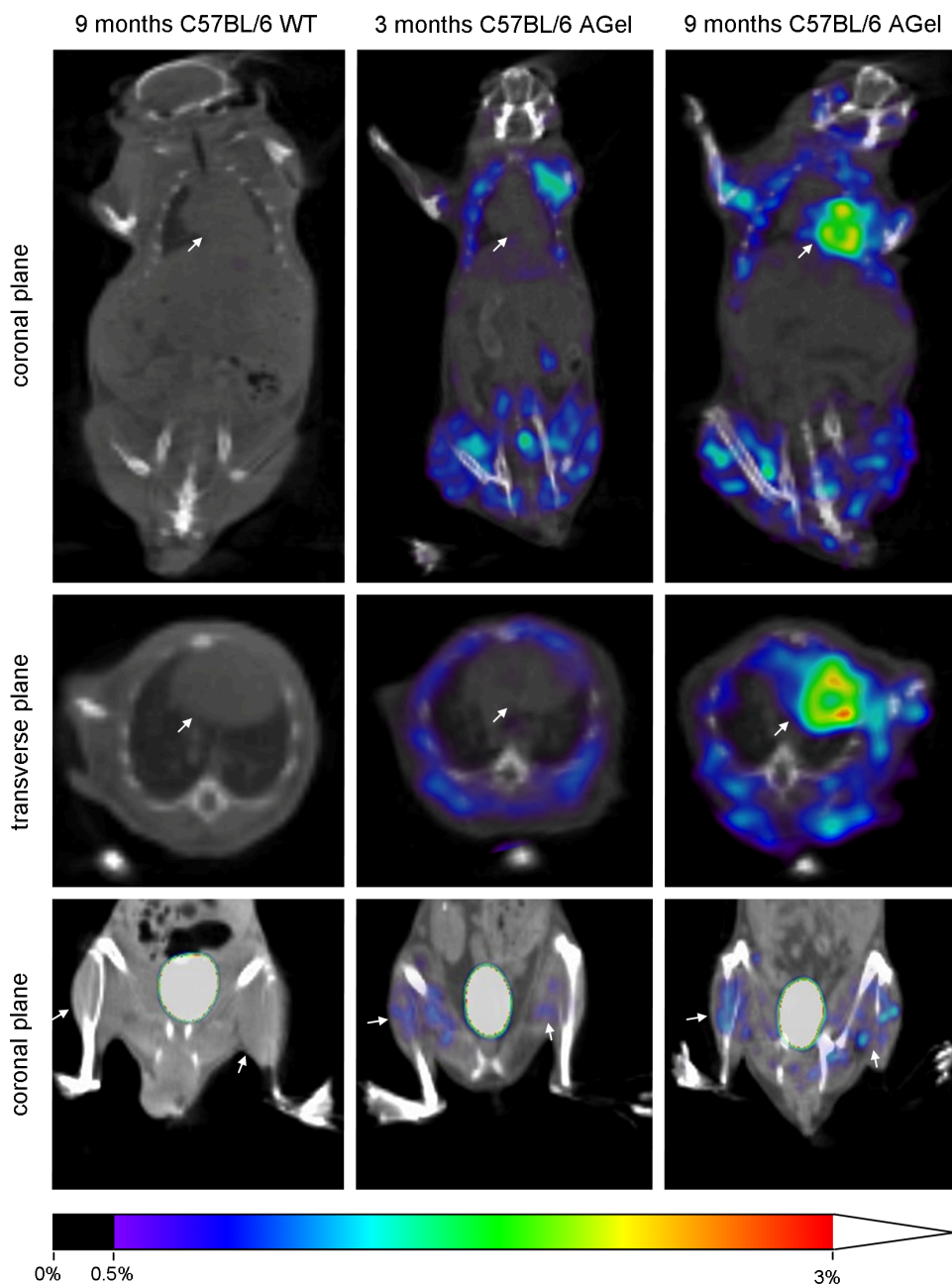


**Figure 1.6: SPECT/CT images obtained with  $^{99m}\text{Tc}$ -FAF Nb1.** In WT mice (left), no significant background signal can be detected. In AGel mice from 3 months onward (middle and right), the major muscle groups clearly light up. The heart however seems unaffected at 3 months (middle) but gives a high signal at 9 months (right). White arrows indicate the heart (upper two panels) and major muscle groups of the hind legs (lower panel). Color scale: NIH (0.5-3%) + white.

used biodistribution data from both the 3- and 9-month-old imaged mice as well as immunofluorescence data from previous experiments [100]. FAF Nb1 showed good quantitative properties as a  $^{99m}\text{Tc}$ -based imaging agent in AGel mice. When comparing data from the heart obtained with IF analysis, biodistribution analysis, and SPECT/CT image analysis, the same pattern of signal increase was found (**Figure 1.7a**). In the muscle, SPECT/CT image analysis shows some deviation from IF and biodistribution controls (**Figure 1.7b**). The first shows the highest signal difference between 3- and 9-month-old AGel mice, whereas the latter two show the highest difference between WT and 3-month-old AGel mice (**Figures 1.6, 1.7 and 1.8**).

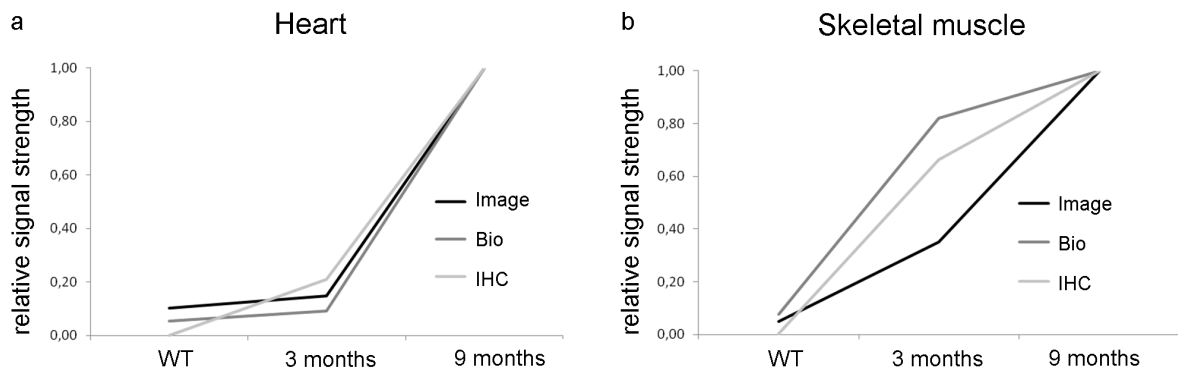


**Figure 1.7: Quantitative characteristics of  $^{99m}\text{Tc}$ -FAF Nb1 in SPECT/CT image and biodistribution analysis.** Heart (a) and hind leg muscle (b) signals were quantified on SPECT/CT images and via dissection after injection with  $^{99m}\text{Tc}$ -FAF Nb1. IF image quantification was used as control. All data were normalized to the maximum signal obtained in 9-month-old C57BL/6 AGel mice per technique. Raw data are presented in **Figure 1.8**. In the heart (a), all three quantification methods show the same pattern of signal increase. In the muscle (b), biodistribution follows the pattern of IF. SPECT/CT image analysis however shows different slopes between the three data points.

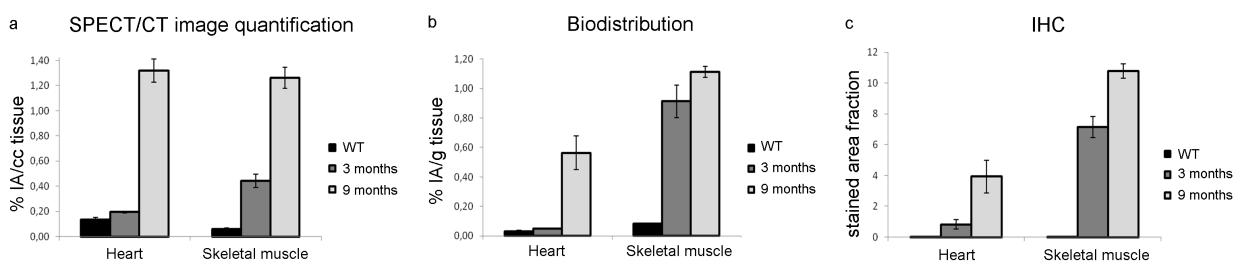


**Figure 1.8: Absolute signal strength in the heart and muscle. SPECT/CT image quantification. (a), biodistribution (b) and IF(c) before normalization.** Raw data were used to determine quantitative features and are depicted in **Figure 1.7**. We analyzed amyloid burden in 9 month old C57BL/6 WT, 3 and 9 month old C57BL/6 AGel mice using SPECT/CT image quantification (ROI) (a), biodistribution analysis (b) and IHC image quantification (c) in both heart and skeletal muscle tissue. Data represented as mean  $\pm$  SEM.

### 1.4.2 Follow-up study of GSN Nb11-expressing AGel mice with $^{99m}\text{Tc}$ -FAF Nb1 SPECT/CT image analysis

In a previous study, we presented a transgenic AGel mouse model that not only expresses mutant PG but also GSN Nb11. GSN Nb11 reduces amyloidogenic gelsolin buildup *in vitro* and *in vivo* due to its ability to interact with the second domain of gelsolin and hence counteract mutant gelsolin proteolysis by furin [18]. Now, as a proof of concept, the study was repeated and the newly developed  $^{99m}\text{Tc}$ -FAF Nb1 amyloidogenic gelsolin imaging agent was used as a means to follow disease progression in a non-invasive manner.

Starting from the age of 3 months, one group of AGel/ GSN Nb11 mice (AGel<sup>+/-</sup> GSN Nb11<sup>+/-</sup>) underwent a SPECT/CT scan every 2 months until the age of 9 or 11 months. Littermates (AGel<sup>+/-</sup> GSN Nb11<sup>-/-</sup>) were used as the control group. At the age of 9 and 11 months, a set of animals was euthanized followed by biodistribution analysis (**Figure 1.9b, d**) and IF (**Figure 1.11**).

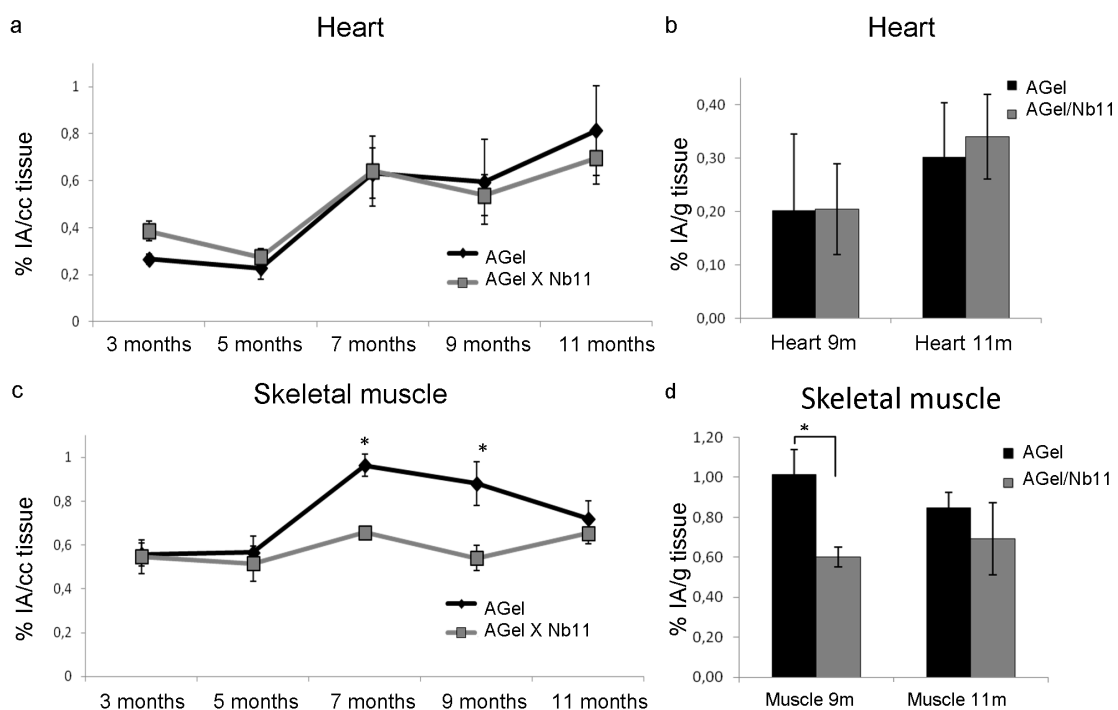


**Figure 1.9: Absolute signal after SPECT/CT image quantification and biodistribution analysis.** After SPECT/CT, using identical ROIs, the absolute signals in the heart (a) and skeletal muscle (c) tissues were determined in 3-, 5-, 7-, 9-, and 11-month-old AGel and Nb11-expressing AGel mice. At 9 and 11 months, a group was euthanized and biodistribution analysis was performed on the heart (b) and skeletal muscle (d). No statistical differences were detected in the heart (a, b). At 7 and 9 months, a statistical difference was detected in the muscle tissue (c, d). Data are expressed as % IA/cc tissue (a, c) or % IA/g tissue (b, d) and represented as mean  $\pm$  SEM (\* $p < 0.05$ ).

The SPECT-CT follow-up revealed no statistical differences in heart amyloidogenic gelsolin buildup during the entire course of the study (**Figure 1.9a**). In muscle tissue, a statistical significant difference ( $p < 0.05$ ) was detected at the age of 7 and 9 months but not at 11 months (**Figure 1.9c**). The same pattern appeared in the biodistribution analysis at 9 and 11 months (**Figure 1.9b, d**).

To validate the results, IF was performed on heart and hind leg muscle tissues from animals in the 9- and 11-month groups. At the age of 9 months, the heart shows diffuse AGel-positive spots, both in the AGel and AGel/Nb11 groups. At 11 months, the staining pattern becomes more evenly distributed (**Figure 1.11a**). In muscles, overall staining can be seen both at 9 and 11 months. Albeit difficult, some differences in staining intensity can be discerned at the age of 9 and 11 months (**Figure 1.11a**). After quantification, the results depict the same pattern as we obtained with the  $^{99m}\text{Tc}$ -FAF Nb1, no statistical difference in the heart, whereas in the muscle, there is a significant difference ( $p < 0.05$ ) at the age of 9 months but no longer at 11 months (**Figure 1.11b and c**).

### 1.4.3 Correlation between SPECT/CT signal and *in vivo* binding site levels

To demonstrate specific binding, we investigated the relationship between *in vivo* radioligand uptake (by SPECT/CT) and binding site expression levels (by IF). To this end, a group of 3-, 5-, and 7-month-old AGel/Nb11 mice underwent SPECT/CT analysis with  $^{99m}\text{Tc}$ -FAF Nb1 after which they were sacrificed. Skeletal muscle tissue was examined by immunofluorescence. Combined with the 9- and 11-month-old AGel/Nb11 mouse data from the follow-up study, a correlation plot between the specific muscle uptake (SPECT/CT signal) and *in vivo* binding site levels was generated (**Figure 1.10**). The trend line ( $R^2 = 0.8447$ ) indicates a positive correlation suggesting that the radioligand binds specifically to its target.

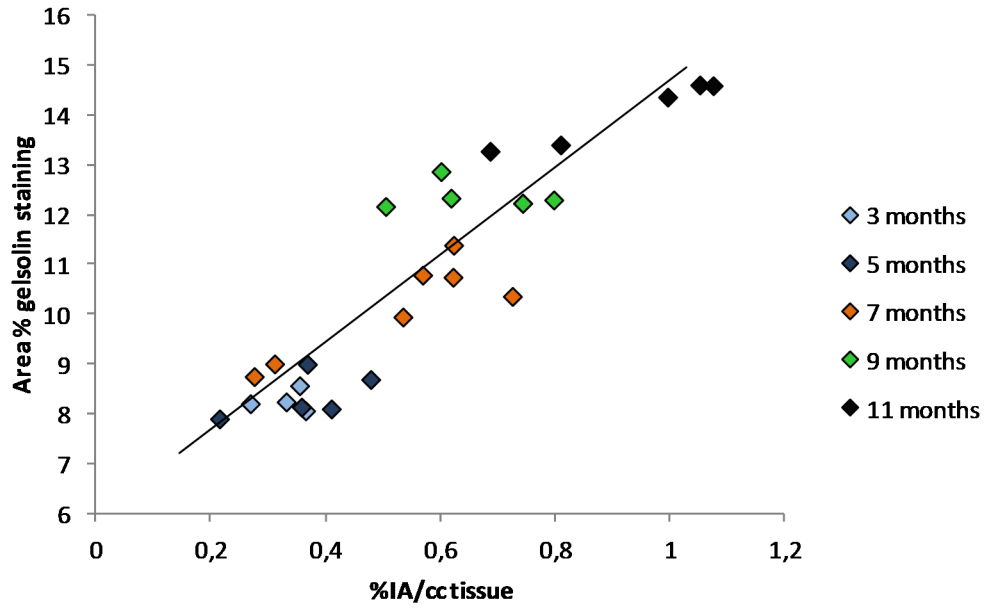


**Figure 1.10: Correlation plot between the SPECT/CT signal (X-axis) and the amount of antigen present (Y-axis, as determined by IHC quantification).** The data points from every age group are color coded. The trend line ( $R^2 = 0.8447$ ) shows a positive correlation between specific muscle uptake (SPECT/CT signal) and *in vivo* expression levels (in proxy determined by IHC).



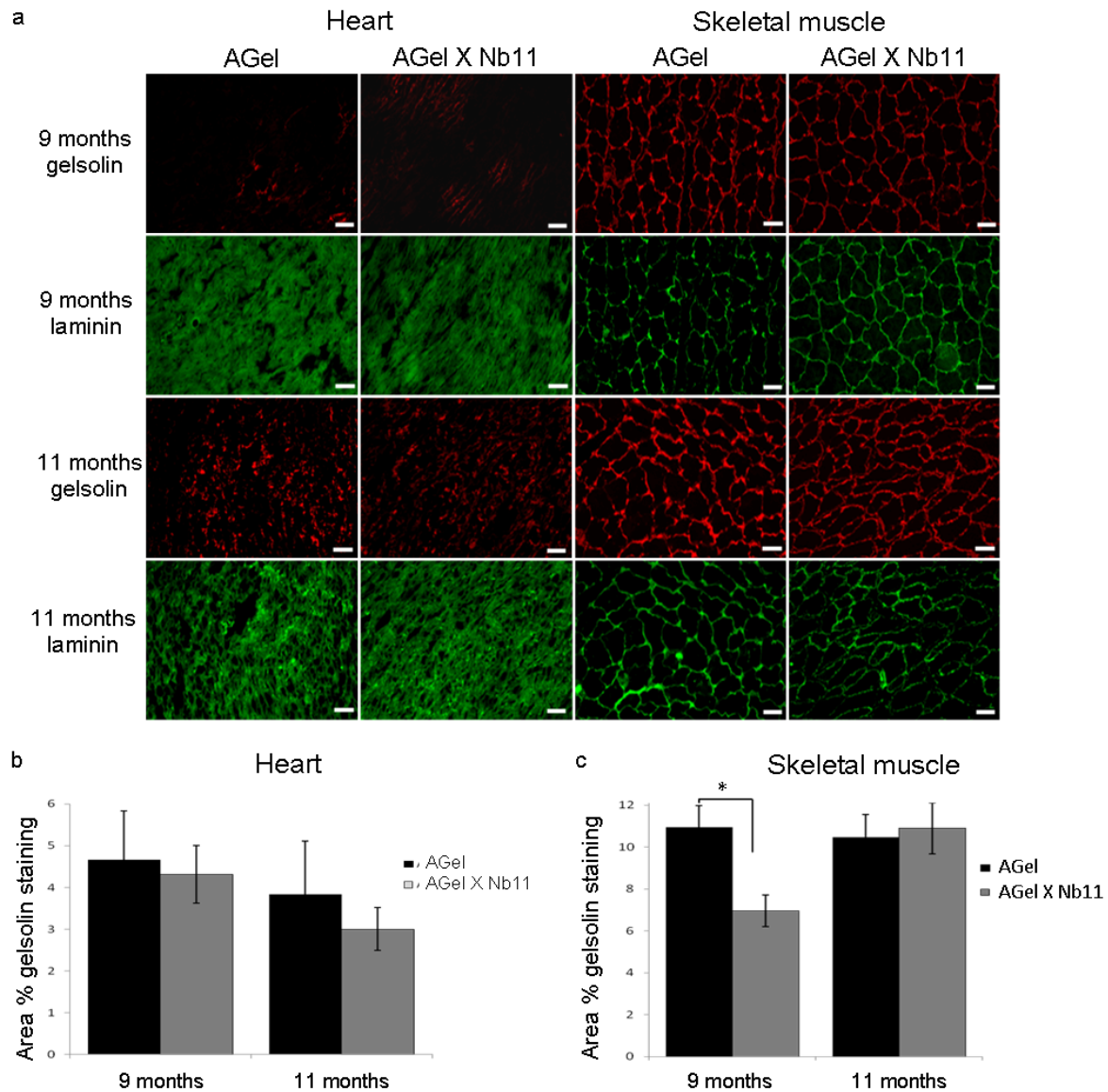


**Figure 1.11: Immunofluorescent analysis and quantification in heart and skeletal muscle in AGel and AGel/Nb11 mice at the age of 9 and 11 months.** Heart and hind leg muscles were dissected from Nb11-expressing AGel mice and their negative littermates as control. IF was done for gelsolin (red) and laminin as a constant control (green). Scale bar = 100  $\mu$ m (a). The staining pattern was quantified (b, c). At 9 months, a statistical difference was detected in the muscle tissue. Results are expressed as mean  $\pm$  SEM (\* $p$ <0.05).

## 1.5 Discussion

In a previous study, three nanobodies, FAF Nb1-3, against the amyloidogenic 8-kDa gelsolin fragment were characterized as part of an intervention study to counteract amyloidogenic gelsolin deposition [100]. Several groups of mice had to be sacrificed at different time points to assess the efficacy of FAF nanobody therapy. In an attempt to circumvent this necessity, we set out to ascertain whether we could implement these same FAF nanobodies as a radionuclide-based amyloid imaging agent.

We showed that the FAF nanobodies possess the characteristics desired for a  $^{99m}\text{Tc}$ -based SPECT/CT imaging agent. We demonstrated their stability in a complex environment for at least 24 h (**Figure 1.1**) and detected no significant background signal when administered in WT C57BL/6 mice (**Figure 1.6, left panels**). In addition, specific uptake was evinced in skeletal muscle, heart, and diaphragm (**Figure 1.3a, b and c**), accompanied by a low circulatory blood signal when administered in AGel mice (**Figure 1.2**). Furthermore, when comparing the nanobodies, FAF Nb1 was identified as the most potent nanobody given its higher signal-to-noise ratio and signal specificity in muscle tissue (**Figure 1.4c and d**). Additionally, we also illustrated the quantitative qualities of  $^{99m}\text{Tc}$ -FAF Nb1 by comparing quantified signals obtained with SPECT/CT, biodistribution analysis, and IF. Similar patterns in signal increase were detected (**Figure 1.7**). Finally, a correlation plot showed a positive relationship between the  $^{99m}\text{Tc}$ -FAF Nb1 uptake and *in vivo* binding site levels (**Figure 1.10**).

Unexpectedly, Bcll10, the negative control nanobody, showed statistically significant uptake in the heart (**Figure 1.3a**). Given the small absolute difference, 0.25 % IA/g in WT versus 0.36 % IA/g in AGel mice, this could represent a biologically irrelevant statistical coincidence. Further research on a larger set of mice might provide a more conclusive answer.

A second unexpected result is the significant uptake in the bones of AGel mice compared to the WT controls. As this was the case for both the FAF Nbs and the Bcll10 control nanobody, it seems logical that this phenomenon is somehow caused by the AGel amyloidogenic buildup. Although in AGel patients, abnormalities have been observed in the bones, gastro-intestinal tract, and thyroid gland [137, 139], there is no evidence at this moment that AGel mice deposit amyloidogenic gelsolin in periosteal or bone marrow. The connection between these findings and AGel is unclear. More specific research, on a larger scale, will be needed to discern whether these findings are just a statistical coincidence or whether there actually is amyloidogenic gelsolin buildup in the bone tissue.

Based on the results discussed above and as a proof of concept,  $^{99m}\text{Tc}$ -FAF Nb1 was implemented in a follow-up study of the Nb11-expressing AGel mouse model. Identical conclusions could be drawn when comparing data obtained with SPECT/CT, biodistribution, and IF analyses (**Figure 1.9** and **Figure 1.11**). No significant difference could be discerned in the heart between the AGel and AGel/Nb11 mice (**Figure 1.9a**). It might be contended that FAF Nb1 does not bind amyloidogenic gelsolin in the heart, but this is not the case since  $^{99m}\text{Tc}$ -FAF Nb1 generates no

signal in the heart of 9-month-old WT mice, proving that Nb1 does not bind aspecifically to a ligand in the heart. Furthermore, Nb11 expression is not driven in a tissue-specific manner, and we therefore expect secretion from different tissues. It is possible that the Nb11 expression cassette is not or less active in the heart. In an attempt to clear this issue, immunofluorescent staining against V5-tagged Nb11 was performed on several tissues. Unfortunately, no clear images could be obtained (data not shown). Most likely, this is due to the overall low expression of Nb11, shown earlier [18]. In muscle tissue, a second intriguing phenomenon was detected; the AGel/Nb11 mice showed significantly less amyloidogenic gelsolin buildup at 7 and 9 months but no longer at 11 months. We know that the amount of Nb11 in the serum diminishes over time [18]. It is possible that the decrease of detectable Nb11 is mainly due to a drop in expression in the muscle tissue, given that, due to the aberrant cleavage of mutant PG, this tissue experiences considerable proteasome stress. Consequently, the therapeutic effect would be lost.

The positive correlation between the specific muscle uptake and *in vivo* amyloidogenic gelsolin expression levels (**Figure 1.10**) hints at a potential use of this nanobody as a noninvasive tool to assess the therapeutic capacity of AGel therapeutics currently under development [231].

Congo red staining is considered the gold standard dye in amyloid research when screening patient biopsies [232]. When amyloid is detected, an evaluation of the global amyloid burden is needed to identify the involved organs, select treatment, and monitor progression of the patient. Currently,  $^{123}\text{I}$ -SAP scintigraphy is the only tool implemented in clinics to assess visceral amyloid burden. Besides the cost of  $^{123}\text{I}$ , there is the unfortunate inability to visualize small, hollow, or diffuse structures like the GI tract, skin, and nervous system [223]. Together with the cornea, these last two form the triad of clinically most affected tissues in AGel amyloidosis [119]. Evidently, there is a need for an alternative. The results described above might be a step in this direction.

The heart, skeletal muscle, and diaphragm (**Figure 1.3**) represent three of the four main tissues in which the AGel mouse model shows amyloidogenic gelsolin buildup [148]. We were unable to identify the fourth tissue, skin, as an organ showing significant uptake (data not shown). In the AGel mouse model however, at least at the age of 18 months, amyloidogenic gelsolin is present in this tissue [148]. Since the skin can be targeted using the  $^{99\text{m}}\text{Tc}$ -nanobody technology [233], we hypothesize that the skin only becomes burdened with amyloidogenic gelsolin somewhere between the age of 9 and 18 months. Future research should test this theory. It is plausible that the significantly smaller size of Nbs compared to SAP (15 versus 127 kDa) helps to probe this tissue and thereby overcomes one of the limitations of  $^{123}\text{I}$ -SAP scintigraphy.

Furthermore, nanobodies have already been applied to the nervous system and showed good biodistribution without causing any significant inflammatory reaction [234]. This makes us confident that when applied in the clinic, the FAF Nbs would also be able to target amyloidogenic gelsolin surrounding the affected facial nerve branches (cranial nerve VII) in AGel patients, thereby surmounting a second tissue barrier of  $^{123}\text{I}$ -SAP scintigraphy. Unfortunately, the AGel mouse model does not allow testing amyloidogenic gelsolin buildup in nervous tissue, although this does occur in human patients.

Finally, nanobodies have already proven to be ideal instruments for imaging carcinomas, arteriosclerotic plaques, and tumor-associated macrophages in mouse models [235–237]. Some studies even suggest that nanobodies, able to cross the blood-brain barrier, can be selected [238–240]. These findings do however require confirmation by other researchers. We showed here that the nanobody approach can also be employed in AGel amyloid. This, together with the fact that nanobodies have been raised against several other amyloidogenic proteins, hints at the potential clinical use of these antibody fragments to monitor global amyloid burden in patients with Alzheimer's or Huntington's disease [187].

In this study, we have used the  $^{99m}\text{Tc}$  and multi-pinhole SPECT technology because of its high resolution when scanning small lab animals [241]. With the clinical application and human patients in mind, we will have to migrate toward a PET-based setup. This should not pose a problem as nanobodies can also be linked with gallium-68 or fluorine-18 to be compatible with PET scanners [237, 242].

Using these  $^{99m}\text{Tc}$ -based nanobody tracers, values of  $1.1 \pm 0.06$  % IA/g tissue in the muscle and  $3.9 \pm 0.68$  % IA/g tissue in the heart were obtained (**Figure 1.3a**). We believe that at least the preclinical values obtained in the heart are high enough to proceed toward clinical PET imaging. Firstly because, similar research with an anti-HER2 nanobody which showed values of  $4.19 \pm 0.47$  % IA/g tissue [183] was recently successfully translated to the clinic in a phase I clinical trial [243]. Secondly image quality is also dependent on good focal uptake, which can be achieved with the  $^{99m}\text{Tc}$ -FAF Nb1 (**Figure 1.6**), and the difference in %IA/g between WT and AGel mice ( $0.2$  % IA/g versus  $3.9$  % IA/g in the heart and  $0.09$  % IA/g versus  $1.1$  % IA in the muscle; **Figure 1.3a and b**).

The AGel mouse model only shows good Congo red birefringence at 18 months of age [148]. The FAF nanobodies are able to bind monomeric and polymeric amyloidogenic 8- kDa gelsolin fragments [100]. It is therefore likely that  $^{99m}\text{Tc}$ -FAF Nb1 predominantly visualizes non-mature amyloidogenic gelsolin deposits instead of fully polymerized, cross-beta sheet AGel amyloid. In recent years, it was evidenced that oligomers may be the major causative agent of cytotoxicity [244, 245]. Therefore, it may prove valuable to visualize the toxic oligomeric intermediates and not just the mature cross-beta fibrils. Future developments will have to reveal which approach is most beneficial or whether a combined strategy is necessary.

## 1.6 Conclusion

Nanobodies against the AGel 8-kDa fragment were tested as non-invasive imaging agents. FAF Nb1 proved to be the most potent candidate. Application in a Nb11 mouse model provided evidence for its qualitative and quantitative characteristics.

## 1.7 Acknowledgements

We thank L. Supply (Ghent University) for investing time in the immunofluorescence experiments and J.W. Kelly, L. J. Page, and A. Guerrero (Scripps Research Institute) for generously sharing the gelsolin amyloidosis mouse model. This work was supported by the Queen Elisabeth Medical Foundation (GSKE, Belgium) the 'Stichting Alzheimer Onderzoek' (SAO, Belgium), and the Amyloidosis Foundation (USA). A. Verhelle is supported by the Agency for Innovation by Science and Technology in Flanders (IWT).



# **PART IV**

NANOBODY GENE THERAPY AGAINST  
GELSOLIN AMYLOIDOSIS VIA  
ADENO-ASSOCIATED VIRUSES

Adapted from:

Verhelle A, Nair N, Everaert I, Van Overbeke W, Supply L, Zwaenepoel O, Peleman C, Van Dorpe J, Lahoutte T, Devoogdt N, Derave W, Chuah K. M, VandenDriessche T, Gettemans J.

**AAV9 Delivered Bispecific Nanobody Attenuates Amyloid Burden in the Gelsolin Amyloidosis Mouse Model.** *Human Molecular Genetics*. 2017 Apr 1;26(7):1353-1364. doi: 10.1093/hmg/ddx056.



# AAV9 delivered bispecific nanobody attenuates amyloid burden in the gelsolin amyloidosis mouse model.

## 1.1 Abstract

Gelsolin amyloidosis is a dominantly inherited, incurable type of amyloidosis. A single point mutation in the gelsolin gene (G654A is most common) results in loss of a  $\text{Ca}^{2+}$  binding site in the second gelsolin domain. Consequently this domain partly unfolds and exposes an otherwise buried furin cleavage site at the surface. During secretion of mutant plasma gelsolin consecutive cleavage by furin and MT1-MMP results in the production of 8 and 5 kDa amyloidogenic peptides. Nanobodies that are able to (partly) inhibit furin or MT1-MMP proteolysis have previously been reported. In this study the nanobodies have been combined into a single bispecific format able to simultaneously shield mutant plasma gelsolin from intracellular furin and extracellular MT1-MMP activity. We report the successful *in vivo* expression of this bispecific nanobody following adeno-associated virus serotype 9 gene therapy in gelsolin amyloidosis mice. Using SPECT/CT and immunohistochemistry, a reduction in gelsolin amyloid burden was detected which translated into improved muscle contractile properties. We conclude that a nanobody-based gene therapy using adeno-associated viruses shows great potential as a novel strategy in gelsolin amyloidosis and potentially other amyloid diseases.

## 1.2 Introduction

Gelsolin amyloidosis (AGel) is an autosomal dominantly inherited disease caused by a point mutation in the gelsolin (GSN) gene (G654A being the most common, D187N) [110, 246]. The resulting destabilization of the second gelsolin domain (gelsolin consist of 6 domains, G1-G6)

results in an aberrant proteolytic cascade, specifically affecting the plasma variant [14, 22, 145, 247]. During its transport through the intracellular secretion pathway, mutant plasma gelsolin (PG\*), is first cleaved by furin in the trans-Golgi network leading to the formation of a 68 kDa C-terminal fragment [20]. When this C68 fragment is secreted, a second proteolytic cleavage by MT1-MMP like proteases results in the release of 8 and 5 kDa amyloidogenic fragments [144]. Over time, particularly the 8 kDa peptide will start to aggregate, forming cross-beta-sheet amyloid fibrils and plaques. Patients experience a triad of neurological, ophthalmological and dermatological symptoms [121, 135]. At the moment, no specific treatments for AGel are available. Instead, patients undergo several symptomatic and aesthetic treatments to improve their quality of life.

Our previous studies have shown that chaperoning nanobodies are able to (partly) inhibit the pathological furin and MT1-MMP cleavages *in vitro* and *in vivo*, resulting in physiological improvements in transgenic mice that recapitulate the proteolytic AGel cascade [18, 100]. In view of the central roles that furin and MT1-MMP undertake in neuropeptide maturation and connective tissue organization/activation of other metalloproteases, respectively, we argue that these proteases should not be considered as therapeutic targets, particularly since familial amyloidosis is a chronic disease. For this reason we used camelid nanobodies that interact specifically with (mutant) gelsolin and shield the protein either from furin [18] or MT1-MMP degradation [100], thus acting as molecular chaperones.

In the present study we combined the two nanobodies into a single bispecific format with the aim of providing simultaneous protection against both proteases simultaneously. The nanobodies were separated by a MT1-MMP-sensitive peptide sequence which was used as an MT1-MMP protease decoy. We investigated if this approach affected the binding characteristics of the individual nanobodies and if this format was able to significantly increase the chaperoning capacity *in vitro*.

Because furin is an intracellular protease, our approach required intracellular delivery of the protective bispecific nanobody. We opted for adeno-associated virus serotype 9 (AAV9) gene therapy considering that AAVs are able to infect both dividing and quiescent cells [248]. Moreover, as only a small fraction of the virus integrates in the genome, the likelihood of insertional mutagenesis is lower compared integrating gene therapy vectors [249, 250].

Using a recently developed nanobody based imaging agent [251] and immunohistochemistry, we provide evidence of a significant decrease in gelsolin amyloid buildup in both the skeletal muscle and heart of AGel mice injected with AAV9-Nb11-FAF1 vector during the neonatal period. These results are further supported by improved muscle contractile properties following treatment.

## 1.3 Materials & Methods

### 1.3.1 Antibodies and reagents

Anti-mouse/rabbit IgG HRP conjugate was purchased from VWR (Leuven, Belgium). Polyclonal anti-V5 antibody (1:100 in IHC) was purchased from Sigma-Aldrich (Diegem, Belgium). Alexa fluor 488 goat anti-rat IgG (H+L) and 594 goat anti-rabbit IgG (H+L) were purchased from Life Technologies (Merelbeke, Belgium) (both 1:500 in IHC). Monoclonal anti-laminin antibody (1:500 in IHC) was obtained from Abcam (Cambridge, UK).

### 1.3.2 Generation of gelsolin-specific nanobodies

Both the anti-gelsolin nanobodies (Nb11 and Nb13) and the anti-8 kDa nanobodies (FAF Nb1-3) were obtained in collaboration with the VIB Nanobody Service Facility as described earlier [100]. In short, dromedaries were injected with either CG or biotinylated human gelsolin 8 kDa AGel peptide and recombinant GST-tagged human D187N gelsolin domain 2. Lymphocytes were collected from the blood, total RNA was extracted and a cDNA library constructed. Phage panning for the anti-gelsolin nanobodies was performed with CG and resulted in two functional nanobodies; Nb11 and Nb13 [191]. Phage panning for the anti-gelsolin nanobodies was performed with the 8 kDa peptide and the mutant G2 domain. Three nanobodies could be identified; FAF Nb1-3.

### 1.3.3 cDNA cloning

All monovalent nanobodies were available in the pHEN6 vector with a C-terminal V5-His<sub>6</sub> tag. The bispecific nanobodies were constructed as followed: the pHEN6 vector containing the FAF Nb1-3-V5-His<sub>6</sub> constructs was cleaved with NcoI, opening the vector between the pelB signal and nanobody N-terminus. The Nb11 sequence was amplified with a double set of primers to introduce a 5' HA-tag and a 3' linker sequence (**Figure 1.1a**). This sequence encodes a MT1-MMP sensitive peptide (SLAPLGLQRR) flanked by two GS linkers. The Cold Fusion Kit (System Biosciences, Mountain View, CA) was used to ligate the PCR fragment in the opened pHEN6 vector.

Primers used in the first PCR cycle: 5' GGT GGT GGT GGT TCT GGT CAG GTG CAG CTG CAG GAG TCT GG 3' (forward) and 5' GAC GCT GCA GAC CCA GCG GCG CCA GAG AAC CAG AAC CAC CAC CAC CGC TGG AGA CGG TGA CCT GGG TCC C 3' (reverse).

Primers used in the second PCR cycle, using the product of the first cycle as template: 5' CGC GGC CCA GCC GGC CAT GGC CTA CCC ATA CGA TGT TCC AGA TTA CGC TGG TGG TGG TGG TTC TGG TCA GGT G 3' (forward) and 5' CCT CCT CCA GAC TCC TGC AGC TGC

ACC TGA CCA GAA CCA CCA CCA CCA CGA CGC TGC AGA CCC AGC GGC GCC AG 3' (reverse).

#### 1.3.4 Purification of recombinant PG\*, C68 and nanobodies

Performed as previously described [100].

#### 1.3.5 ELISA

Enzyme-linked immunosorbent assays (ELISA) were performed in Nunc Maxisorp 96-well plates (Roskilde, Denmark). Target protein was coated in coating buffer (100 mM bicarbonate/carbonate, pH 9.6) at 0.2  $\mu\text{g}$  of protein per well. PBS + 1% BSA was used as a blocking buffer, PBS + 0.5% Tween was used as a washing buffer. Nanobodies were added in a ten-fold dilution series ranging from 1  $\mu\text{g}$  to  $10^{-5}$   $\mu\text{g}$ /well. Anti-V5 antibody followed by anti-mouse HRP +TMB substrate kit (3,3',5,5' tetramethylbenzidine, Thermo Scientific, Erembodegem, Belgium) was used for detection.

#### 1.3.6 WB with bispecific Nb11-FAF nanobodies as primary antibody

Bacterial pellets containing PG, PG\*, C68, 8 kDa peptide or CapG were resuspended in lysisbuffer + 0.5% NP40. Lysis was performed with 0.2 mg/ml lysozyme for 30 min at room temperature followed by sonication (Vibracell, Sonics and Materials, Newtown, CT). The lysates were collected after 30 minutes of centrifugation at  $29.000 \times g$ ,  $4^{\circ}\text{C}$ . 5  $\mu\text{g}$  bacterial protein extract were fractionated by SDS-PAGE. Western blot analysis was performed with V5-tagged Nb11-FAF1, 2 and 3 as primary antibody. Monoclonal anti-gelsolin antibody was used as a positive control.

#### 1.3.7 *In vitro* MT1-MMP sensitive linker assay

*In vitro* MT1-MMP proteolysis of the Nb11-GAF constructs was performed in a total reaction volume of 75  $\mu\text{l}$ . 2.5  $\mu\text{g}$  bispecific Nb11-FAF Nb1-3 was incubated with 100 ng of the catalytic domain of MT1-MMP for 1 hour at  $37^{\circ}\text{C}$  in reaction buffer (50 mM Tris pH 7.5, 5 mM  $\text{CaCl}_2$ , 200 mM NaCl, 20  $\mu\text{M}$   $\text{ZnSO}_4$  and 0.05% Brij-35). At 0, 15, 30, 45 and 60 minutes, samples were taken and the reaction was terminated by adding 5  $\mu\text{l}$  Laemmli sample buffer. Samples were boiled for 5 minutes, fractionated on a 15% SDS-PAGE gel and stained with Coomassie.

#### 1.3.8 *In vitro* Furin/MT1-MMP assay

The *in vitro* proteolytic furin and MT1-MMP reaction was performed in a total end volume of 20  $\mu\text{l}$ . 3  $\mu\text{M}$  purified recombinant PG\* was incubated with an equimolar amount of Nb in furin

reaction buffer (250 mM Tris, 20 mM CaCl<sub>2</sub>, 1 mM  $\beta$ -mercapthoethanol, pH 7.0) for 1 hour at 4°C. Furin was added (0.5 units) and the mixture was incubated for 1 hour at 37°C. Furin Inhibitor I (Merck Millipore, Brussels, Belgium) was added at a final concentration of 100  $\mu$ M together with 50 ng of the catalytic domain of MT1-MMP. The buffer was supplemented with 200 mM NaCl, 0.05% Brij-35 and 20  $\mu$ M ZnSO<sub>4</sub>. After 30 minutes at 37°C the reaction was stopped by adding 5  $\mu$ l of Laemmli sample buffer. The sample was boiled for 5 minutes and separated on an tricine SDS-PAGE gel. Detection of both the C68 and 8 kDa fragment was done via Western blotting with a polyclonal antiserum raised against the 8 kDa AGel fragment. Quantification was done with the Image J software.

### 1.3.9 HEK293T cell culture, transfection and microscopy

Cell culture and transfection

HEK293T cells were grown in DMEM medium (Gibco Life Technologies, Grand Island, NY, USA) supplemented with 10% fetal bovine serum (Thermo Scientific, Erembodegem, Belgium), 10  $\mu$ g/ml streptomycin and 10 IU/ml of penicillin, at 37°C in a humidified 10% CO<sub>2</sub> incubator. Transient expression of both PG and the nanobodies was achieved with Jetprime (Polyplus Transfection Inc., New York, NY).

Microscopy

Cells were fixed with 3% PFA (paraformaldehyde) and permeabilized with 0.1% Triton. Coverslips were blocked with 1% BSA (bovine serum albumin) and incubated with primary antibodies (1 hour at 37°C). The appropriate Alexa Fluor-conjugated secondary antibodies were incubated at room temperature for 30 minutes. Nuclei were stained with DAPI (0.4  $\mu$ g/ml) (Sigma, St. Louis, MO, USA). Cells were mounted with VectaShield (Vector Laboratories, Burlingame, CA, USA) and imaged with a Carl Zeiss Axiovert 200 M Apotome epifluorescence microscope equipped with a cooled CCD AxioCam camera (Zeiss X63 1.4-NA Oil Plan-Apochromat objective; Carl Zeiss, Oberkochen Germany) and Axiovision 4.5 software (Zeiss).

### 1.3.10 HEK293T medium analysis

HEK293T cells were cultured and transiently transfected as described above. 24 hours prior to analysis the cell medium was replaced with a minimum amount of serum free medium. Medium was collected and centrifuged (29.000 x g) for 5 min at 4°C. The cells were washed 2 times with PBS and disrupted in Tris lysis buffer (20 mM Tris-HCl, pH 7.5, 150 mM NaCl, 1% triton-100, 1 mM PMSF and 200  $\mu$ g/ml protease inhibitor cocktail) followed by 10 seconds of sonication. Samples were centrifuged (29.000 x g) for 10 min at 4°C, the supernatant was collected. 20  $\mu$ g of the medium was separated on a 10% SDS-PAGE gel followed by Western blot analysis.

### 1.3.11 AAV9 gene therapy intervention study

The gene encoding the V5-tagged bispecific Nb11-FAF1 nanobody was cloned downstream of a ubiquitously expressed cytomegalovirus (CMV) promoter. This expression cassette was cloned into a self-complementary (sc) AAV backbone (33) to generate the AAV9-Nb11-FAF1 vector **Figure 1.1b**. As before AAV9-Luc2 vector was chosen as viral control [252]. AAV serotype 9 (AAV9) was chosen based on its efficient transduction efficiency in skeletal muscle and heart [252–254]. To produce the AAV9-Nb11-FAF1 vector particles, AAV-293 cells were co-transfected by  $\text{Ca}^{2+}$  phosphate (Invitrogen Corp, Carlsbad, CA, USA) with the AAV9-Nb11-FAF1 vector along with a chimeric AAV Rep2 Cap9 packaging construct and an adenoviral helper plasmid, as described previously [255]. All plasmids were prepared using Qiagen Maxi kits. Two days after transfection, the cells were harvested and lysed by freeze/thaw cycles and sonication, followed by benzonase (Novagen, Madison, WI, USA) and deoxycholic acid (Sigma-Aldrich, St Louis, MO, USA) treatments. The cognate AAV vector particles were then purified by cesium chloride (Invitrogen Corp, Carlsbad, CA, USA) density gradient ultracentrifugation. Fractions containing the AAV vector particles were collected in phosphate buffered saline (PBS) (Gibco, BRL) containing 1 mM  $\text{MgCl}_2$ . The vector titer was determined using quantitative real-time PCR with SYBR Green and primers specific for the CMV promoter. The forward primer sequence was 5' CAT GGT GAT GCG GTT TTG G 3'. The reverse primer sequence was 5' TGG AAA TCC CCG TGA GTC A 3'. To generate standard curves, known copy numbers of the corresponding vector plasmid was used.

The intervention study was performed on 2 groups of mice: WT C57BL/6 and AGel mice. Each group consisted of 3 subgroups (6-12 mice): AAV9-Nb11-FAF1 injected (treatment), AAV9-Luc2 injected (viral control) and PBS injected (negative control). Neonatal mice (2-3 days) were injected with  $4.7 \times 10^{10}$  vg/mouse (viral genomes/mouse) or PBS in the retro-orbital plexus. Over the course of 3 months blood samples were taken from the tail vein at 4, 8 and 12 weeks. After 4 minutes of centrifugation at  $1700 \times g$ , plasma was collected. 1 mg of plasma was incubated with V5-agarose and HA-agarose. Bound protein was separated on an SDS-PAGE gel. HA- and V5-tagged nanobody was visualized via Western blotting.

Animal experiments were approved by the Animal Experimental Ethics Committee of Ghent University Hospital (ECD 14/62). Animals were housed in individually ventilated cages with food and water ad libitum. Environmental conditions were controlled at 20-23°C, 50% relative humidity and 12 h light/dark cycles. AGel mice were obtained from the Scripps Research Institute (La Jolla, California, USA). Wild type C57BL/6 mice were obtained from Charles River (L'arbresle Cedex, France).

### 1.3.12 SPECT/CT imaging

Amyloid burden was visualized using  $^{99m}\text{Tc}$ -FAF Nb1 SPECT-CT imaging (14). Mice were intravenously injected with 51 - 100 MBq of  $^{99m}\text{Tc}$  labeled FAF Nb1. One hour post injection, mice were anaesthetized using 18.75 mg/kg ketamine hydrochloride (Ketamine 1000, CEVA) and 10 mg/kg xylazine hydrochloride (Rompun, Bayer). Animals were positioned in a solid holder with two plastic discs containing three  $^{57}\text{Co}$  (3.7 MBq) sources. Image acquisition was done using a micro-CT scan for 2 min (60 keV, 615 mA,  $360^\circ$ ; Skyscan 1178, Kontich, Belgium) and a dual-headed SPECT camera (e.cam 180, Siemens, USA) equipped with triple pinhole collimators (1.5 mm apertures, focal length of 265.5 mm and a radius of rotation of 20 mm) for 10 s per projection step, 64 projections, and a total scan time of about 10 min. Images were quantified using AMIDE (a Medical Image Data Examiner) software [227]. Ellipsoid regions of interest were drawn (ROIs) around the heart and hind leg muscle. The same ROI<sub>heart</sub> and ROI<sub>muscle</sub> was used for each individual animal. SPECT signals, acquired from the ROIs, were calculated and expressed as % IA/cc.

### 1.3.13 Muscle contractile properties

Muscle contractile properties were determined as described before [256]. In short, mice were anaesthetized with 80% Ketalar/20% Rompun (3.6  $\mu\text{l/g}$  body weight). The soleus and EDL muscles were dissected, wires were attached to the tendons and the muscles were vertically mounted in an Krebs-Heinseleit medium incubation bath with one tendon attached to a force transducer (PowerLab, ADInstruments, Spechback, Germany) and stimulated with capacitor discharges between platinum electrodes. The Krebs-Henseleit incubation medium (10 ml) was continuously gassed (95% O<sub>2</sub>, 5% CO<sub>2</sub>) and maintained at 30°C. After a 15 minutes stabilization period, optimal muscle length was determined by titanic contractions. Next, the force-frequency relation was determined by stimulating at 10, 20, 35, 50, 75, 100, and 125 Hz with 1 minute rest interval for soleus and stimulating at 25, 40 and 55 with 1 minute rest followed by 70, 100, 125 and 150 Hz with 2 minutes rest interval, unless stated otherwise, for EDL. Furthermore, fatigability was evaluated as the percentage decrease in tetanic force, contraction speed (maximum slope) and relaxation rate (minimum slope) values during 8 minutes of repeated tetanic contractions (train duration, 350 microseconds; soleus, 50 Hz every 5 seconds; EDL, 100 Hz every 10 seconds). At the end, mice were euthanized via cervical dislocation.

### 1.3.14 Immunofluorescence

Musculus gastrocnemius and the heart were dissected and snap frozen in liquid nitrogen. Cryosections were made and thawed for 15 min followed by 10 min incubation in acetone at  $-20^\circ\text{C}$ . After 10 min incubation in PBS, the sections were incubated in 50 mM NH<sub>4</sub>Cl/PBS for another 10 min

followed by an additional PBS washing step. The endogenous peroxidase activity was blocked after 20 min incubation in 0.3% H<sub>2</sub>O<sub>2</sub> and then washed in PBS. Sections were incubated with 1% BSA/PBS for 20 min and with the laminin antibody (1:500) at 4°C overnight, followed by another PBS washing step for 10 min. FAF Nb1-V5 (5 µg/ml) was incubated for 1 h at room temperature followed by 10 min incubation in PBS. Polyclonal anti-V5 (1:800) was used as secondary antibody. Alexa Fluor antibodies (488 anti-rat and 594 anti-rabbit, both 1:500) were incubated for 1 h at room temperature. Finally, sections were rinsed with PBS, stained with DAPI (1:500) for 2 min and mounted with VectaShield. Imaging was performed at room temperature with a Leica DM6000 B microscope. Two sections were made per tissue and within each section, 3 images from spate regions were taken for quantification with Image J software. From these 6 technical repeats per animal, per tissue, the average was used for further statistical calculations.

## 1.4 Results

### 1.4.1 Production of the bispecific nanobody

In a previous study we have identified a gelsolin nanobody, Nb11, capable of partly inhibiting the production of C68 by furin [18]. Nb11 binds (mutant) PG irrespective of Ca<sup>2+</sup>, and acts as a molecular chaperone when targeted to the trans-Golgi network where it binds to and protects gelsolin. Further downstream, reduced C68 formation results in a decrease of AGel amyloid buildup. In another study, we followed a different approach and identified three closely related nanobodies, FAF Nb1, 2 and 3, (FAF1-3) capable of binding both C68 and the 8 kDa amyloidogenic gelsolin fragment, thwarting MT1-MMP activity, not furin. *In vivo*, upon binding of C68, these nanobodies once again acted as a chaperone and partly prevented production of the pathological 8 kDa AGel fragment [100]. Here our aim was to combine the two in a clinically applicable way.

Nb11 cDNA was amplified through PCR, introducing a HA-tag at the 5' end and the sequence encoding the MT1-MMP sensitive peptide SLAPLGLQRR [257], sandwiched between two Gly-Ser linkers (GS) at the 3' end. This fragment was linked to the 5' end of FAF Nb1-3 cDNA, already present in the pHEN6-V5-His6 vector, resulting in a final construct where both nanobodies occur in tandem configuration, separated by the MT1-MMP sensitive peptide sequence and GS linker (**Figure 1.1a**).



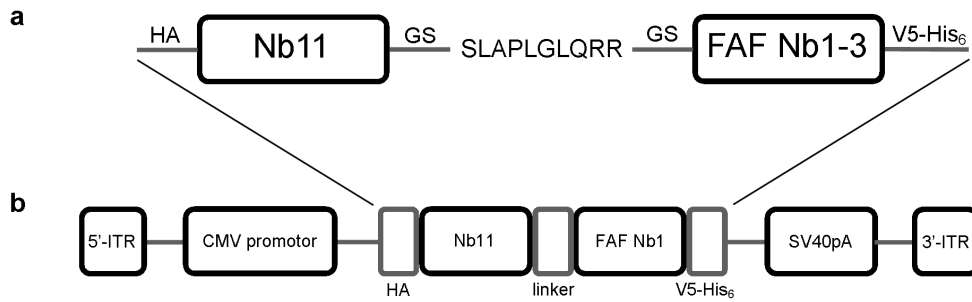


**Figure 1.1: Schematic representation of the bispecific Nb11-FAF format and AAV9-Nb11-FAF1 vector.** The two nanobodies, Nb11 and FAF Nb1-3, are linked via the MT1-MMP sensitive sequence SLAPLGLQRR, flanked between two GS linkers. An N-terminal HA and C-terminal V5-His<sub>6</sub> tag is present (a). The expression cassette was cloned in a self-complementary (sc) adeno-associated virus backbone that was packaged using AAV serotype 9 capsids (AAV9). Expression of Nb11-FAF1 is driven by the CMV promoter. The 5' and 3' inverted terminal repeats (ITR) and SV40 polyadenylation site (pA) are indicated (b).

#### 1.4.2 Bispecific gelsolin nanobodies merge the binding characteristics of their monovalent constituents *in vitro*

The binding characteristics of the bispecific nanobodies were compared to their monovalent counterparts using ELISA. As antigen, PG, PG\*, C68 and the 8 kDa AGel fragment were coated. CapG was chosen as a negative control. This protein belongs to the same family as gelsolin and displays 49% similarity [113]. Nb11 recognized, in decreasing order of magnitude, PG, PG\*, C68 and 8 kDa. The FAF Nbs displayed the opposite binding pattern, as previously described [18, 100]. The bispecific Nb11-FAF combinations exhibited a merge of the Nb11 and FAF1-3 binding characteristics (**Figure 1.2**). No significant binding with the negative control was observed. Furthermore, as previously described [100], FAF Nb1-3 can be used in Western blotting as primary antibodies against PG, PG\*, C68 and the 8 kDa AGel fragment. Linked to Nb11, this ability remained unaffected (**Figure 1.3**).

#### 1.4.3 The MT1-MMP peptide linker is functional in an *in vitro* setup

As mentioned earlier, the linker between Nb11 and FAF Nb1-3 contains the MT1-MMP sensitive peptide SLAPLGLQRR (proteolysis of the GL scissile bond). The purpose of this setup was that, *in vivo*, during secretion, proteolysis of this sequence would release the FAF Nb, enabling it to perform its function without any interference of Nb11. At the same time this mechanism may act as a decoy, luring MT1-MMP away from the (lower amount of) C68 being secreted. This was tested *in vitro* using the recombinant catalytic domain of MT1-MMP. The MT1-MMP sensitive peptide proved to be very efficient in all three bivalent Nb11-FAF constructs and they were readily cleaved upon incubation with MT1-MMP (**Figure 1.4**).

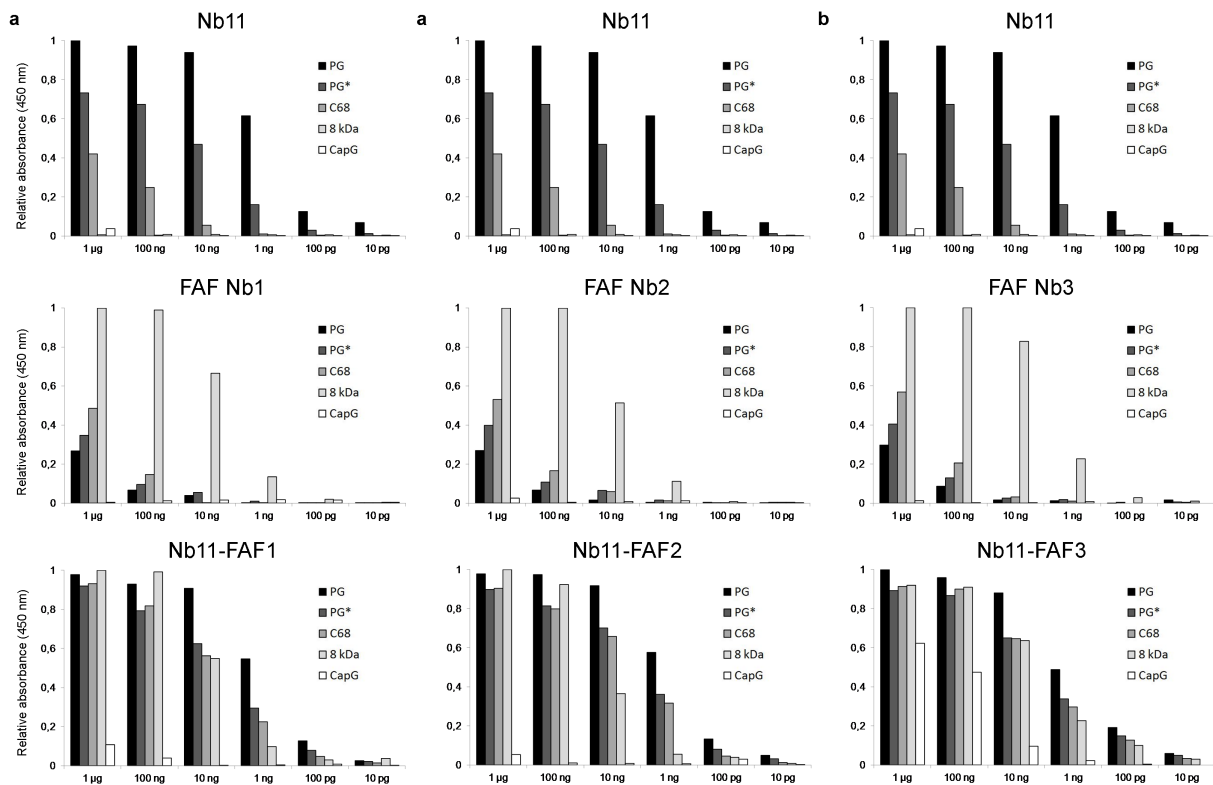


**Figure 1.2: Comparison of the ELISA profiles of monovalent and bispecific nanobodies.** The interaction of monovalent Nb11 and FAF Nb1 with PG, PG\*, C68 and the 8 kDa peptide, in an ELISA setup, are merged in the Nb11-FAF1 construct (a). Each time a tenfold nanobody dilution series was used, starting from 1  $\mu$ g up to 10 pg. Signals are represented relative to the highest value, normalized to 1. FAF Nb2 (b) and FAF Nb3 (c) displayed the same merge of characteristics as FAF Nb1 when merged with Nb11.

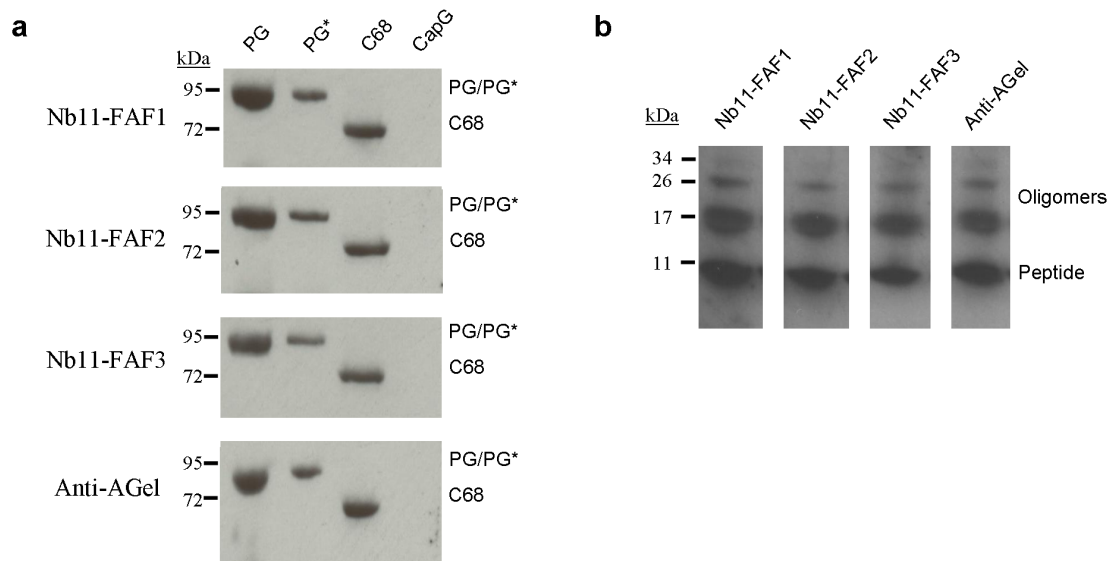


**Figure 1.3: Bivalent constructs can be used as primary antibody for Western blotting.** 5µg bacterial lysate containing PG, PG\*, C68, 8 kDa peptide or CapG was fractionated by SDS-PAGE. Nb11-FAF1-3 can be used as the primary antibody in Western blot analysis (a,b) [100]. Polyclonal anti-AGel antibody was used as a positive control. Both the monomeric and oligomeric forms of the 8 kDa peptide are visualized by the nanobodies (b). Additional bands under the PG/PG\* signal (95 kDa marker) and C68 signal (72 kDa marker) represent degradation products (a).

#### 1.4.4 Bivalent Nb11-FAF Nb protects D187N plasma gelsolin against combined furin/MT1-MMP proteolysis

Since Nb11 can inhibit furin proteolysis of PG\* whereas FAF1-3 counteract MT1-MMP proteolysis of C68 by shielding the substrate, we hypothesized that bivalent Nb11-FAF formats might be able to combine both traits, leading to a synergetic inhibitory effect on 8 kDa amyloidogenic peptide production. An *in vitro* assay was set up wherein the nanobodies were incubated with PG\*, followed consecutively, by furin and MT1-MMP proteolysis. Formation of both C68 and the 8 kDa fragment was assessed by Western blotting (**Figure 1.5a**). Only Nb11-FAF1 could match the inhibitory capacity of Nb11 when looking at C68 formation, the intermediate AGel species formed by furin (**Figure 1.5b**). Quantification of the amyloidogenic 8 kDa fragment showed that all three Nb11-FAF constructs were able to inhibit formation of the 8 kDa AGel peptide more efficiently than their monovalent counterparts (**Figure 1.5c**). Hence, the bivalent format is endowed with a double protective activity, and formation of the 8 kDa fragment in particular is strongly reduced in comparison to monospecific Nb11 or FAF nanobodies.

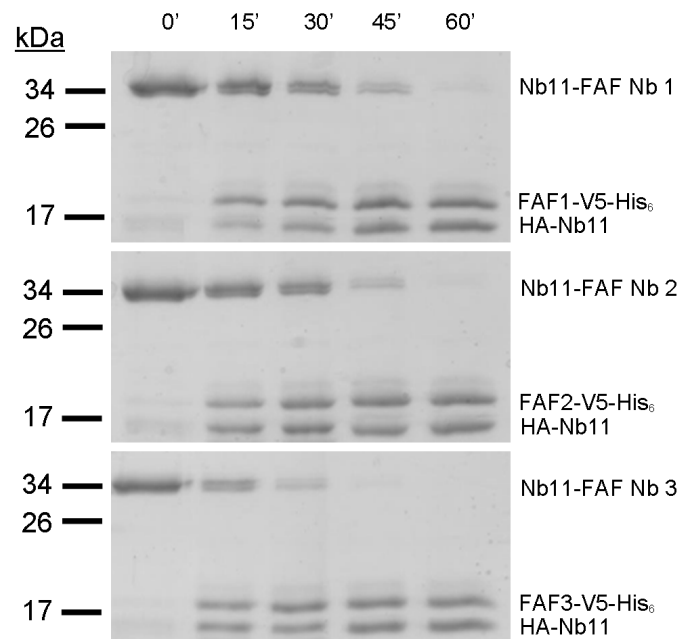


**Figure 1.4: The MT1-MMP linker sequence is cleaved *in vitro*.** The bispecific Nb11-FAF constructs were incubated *in vitro* with MT1-MMP for 1 hour at 37°C. At distinct time points (0, 15, 30, 45 and 60 minutes) samples were taken and the reaction was stopped with Laemmli sample buffer. Samples were boiled for 5 minutes. Visualization was done via Coomassie staining after SDS-PAGE fractionation. MT1-MMP was able to recognize and cleave the SLAPGLQRR sequence, thereby releasing the two individual nanobodies.

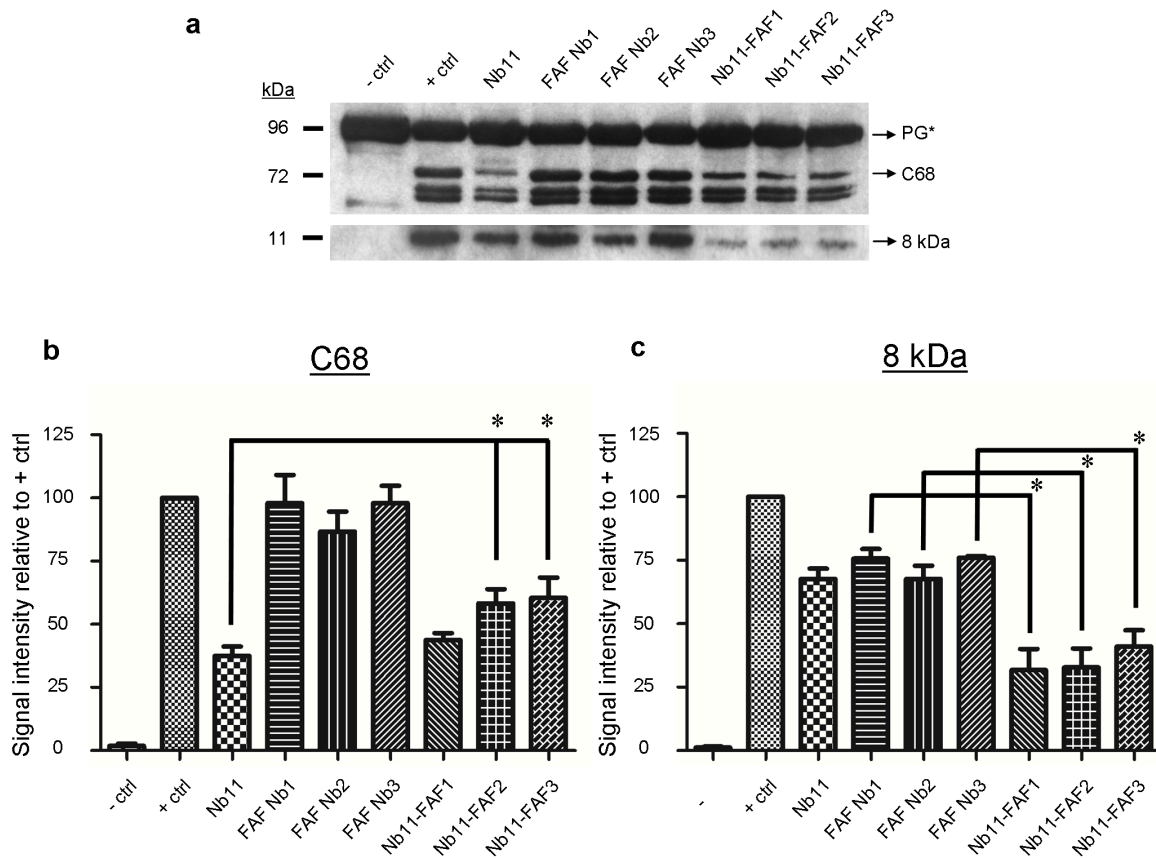


**Figure 1.5: The bispecific Nb11-FAF nanobodies outperform their monovalent counterparts *in vitro* in protecting PG\* against proteolytic degradation.** The AGel degradation was recapitulated *in vitro* through consecutive incubation of PG\* with furin and MT1-MMP. Lane 1: negative control, no furin nor MT1-MMP. Lane 2: positive control, furin and MT1-MMP but no nanobody. Lane 3-9: Furin, MT1-MMP and an equimolar amount of different nanobodies. C68 and the 8 kDa peptide were detected with polyclonal anti-AGel antibody (a) and quantified (b-c). Based on the amount of C68 formed, only Nb11-FAF1 could match Nb11 (b). Quantification of the 8 kDa peptide (c), the end stage of AGel degradation, showed that all three Nb11-FAF constructs performed significantly better than their monovalent counterparts. Data shown are mean of quadruplicates  $\pm$  SE, normalized to the + ctrl sample. \* $p < 0.05$  in a two sided unpaired t-test.

#### 1.4.5 Furrin assay in HEK293T cells - Bivalent Nb11-FAF Nbs inhibit furin proteolysis

In the *in vitro* setup Nb11-FAF1-3 were able to bind their antigen targets and showed a significant protective chaperone activity towards PG\* and C68. As we wanted to confirm this in a more complex environment, PG, PG\* and the Nb11-FAF constructs were transiently expressed in HEK293T cells. Since the first step in AGel pathogenesis, furin cleavage, takes place in the trans-Golgi network, all constructs were equipped with an N-terminal ER-targeting sequence. Co-staining of the constructs followed by epifluorescence microscopy confirmed their colocalisation along the secretory pathway (Figure 1.7). After 24 hours, we analyzed the cell medium via Western blotting (Figure 1.6a). Quantification of the C68 signal revealed a similar pattern

as in the *in vitro* setup; the bispecific Nb11-FAF nanobodies show an inhibitory effect towards furin proteolysis, however none can outperform monovalent Nb11 in this cell based setup (**Figure 1.6b**). We were unable to assess the effect on MT1-MMP proteolysis as no 8 kDa peptide could be detected within the observed timeframe.

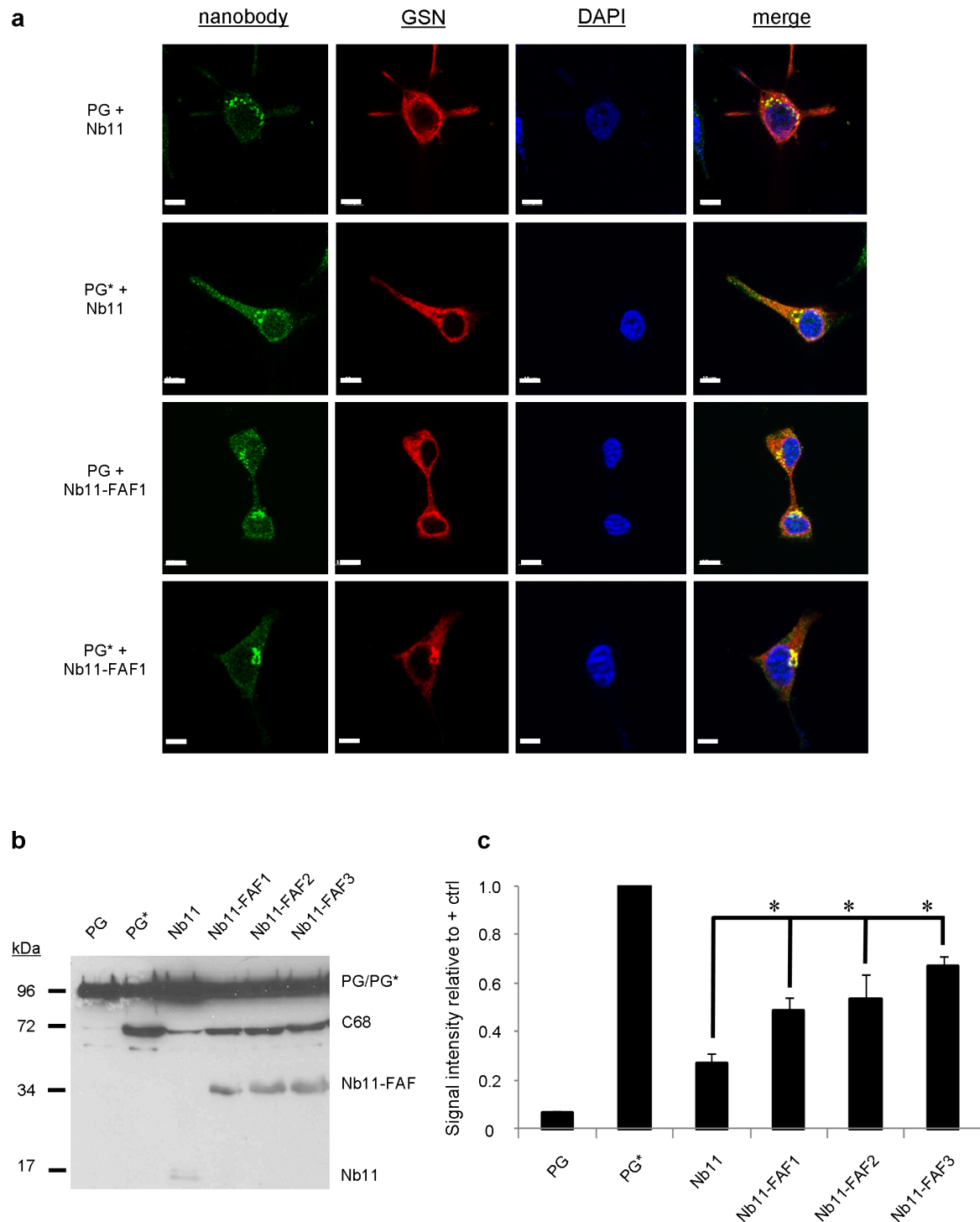


**Figure 1.6: Nb11-FAF nanobodies shield PG\* from furin degradation in HEK293T cells.** PG, PG\*, Nb11 and Nb11-FAF constructs were expressed in HEK293T cells and directed to the secretory pathway using an N-terminal ER signal peptide 1.7. (a) Cell medium of transfected HEK293T cells was collected and analyzed via Western blotting. PG, PG\*, C68, Nb11 and Nb11-FAF nanobodies could all be detected. (b) C68 levels in the cell culture supernatans was quantified using ImageJ. Scale bar = 50  $\mu$ m. Data shown are mean of triplicates  $\pm$  SE, normalized to the PG\* sample. \* $p < 0.05$  in a two sided unpaired t-test.

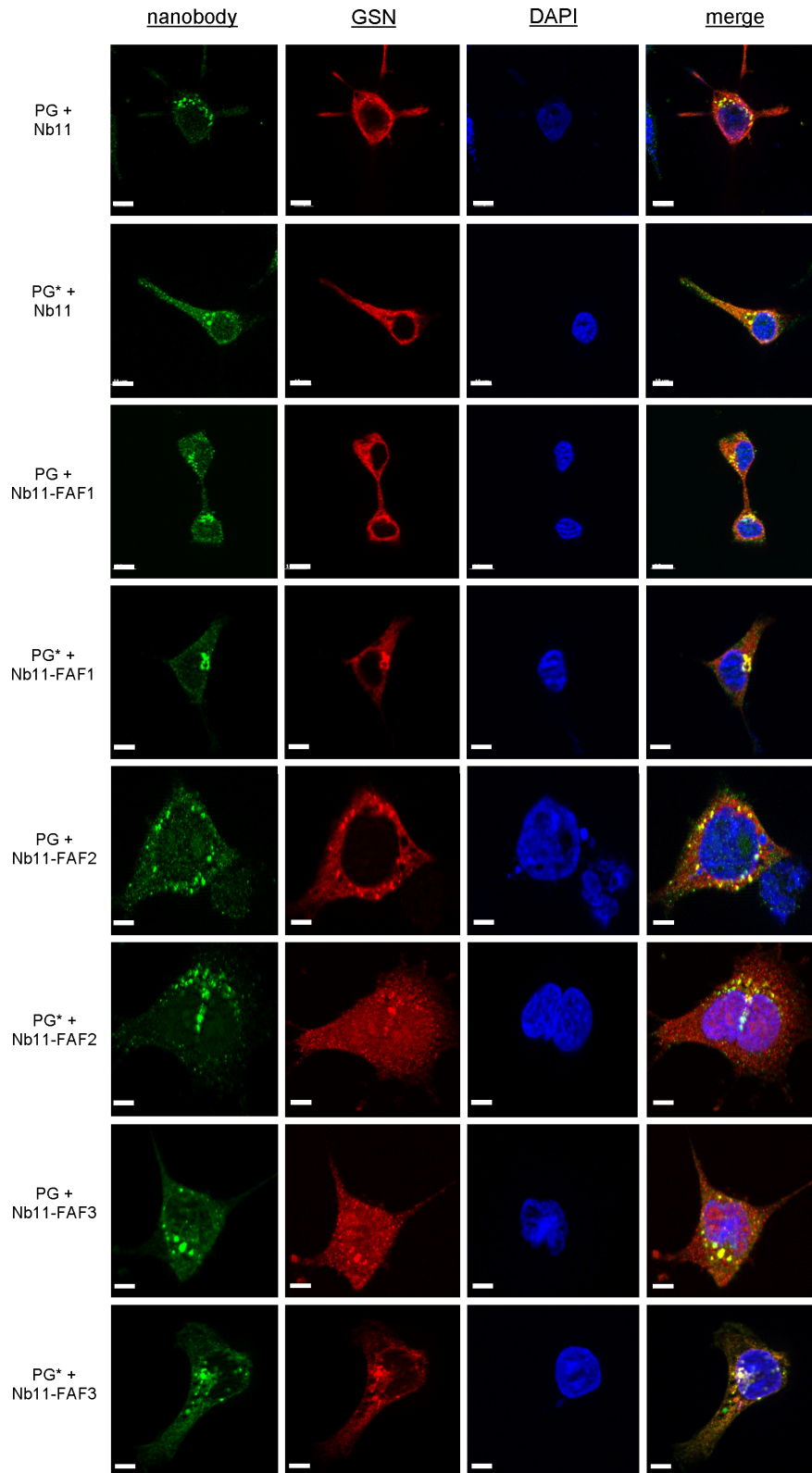


**Figure 1.7: Colocalisation between Nb11-FAF2/3 and PG/PG\*.** Nb11-FAF2, Nb11-FAF3, PG and PG\* were expressed in HEK293T cells and directed to the secretory pathway using an N-terminal ER signal peptide. Via immunohistochemistry the nanobodies (green, first column), PG/PG\* (red, second column) and nucleus (blue, third column) were visualized. Merged images (right column) show colocalisation between the nanobodies and PG/PG\* in the secretory pathway. Scale bar = 50  $\mu\text{m}$ .



### 1.4.6 Bispecific Nb11-FAF1 gene therapy in AGel mice via AAV9

Since the bispecific nanobodies effectively combined the binding and therapeutic characteristics of its monovalent counterparts, an AGel mouse model intervention study was set up. This mouse model recapitulates the pathological AGel pathway in its muscle tissue, leading to extensive, age related, extracellular amyloidogenic gelsolin buildup [148]. Nb11-FAF1 was chosen based on its superior characteristics *in vitro*. Homozygote neonates (2-3 days old) were injected with  $4.7 \times 10^{10}$  vg/mouse of AAV9-Nb11-FAF1, AAV9-Luc2 (viral control) [252, 258] or PBS (negative control) via the retro-orbital plexus. No adverse effects on the development or behavior of the mice were apparent. Nanobody expression was confirmed at 1, 2 and 3 months of age in the plasma of both WT and AGel mice (**Fig.1.8**). The presence of a band at 34 kDa and two at 17 kDa indicates that the MT1-MMP sensitive linker is functional *in vivo* (**Fig.1.8**). At the age of 3 months Nb11-FAF1 gene therapeutic efficacy was determined via SPECT-CT, immunofluorescence and ex vivo muscle performance.

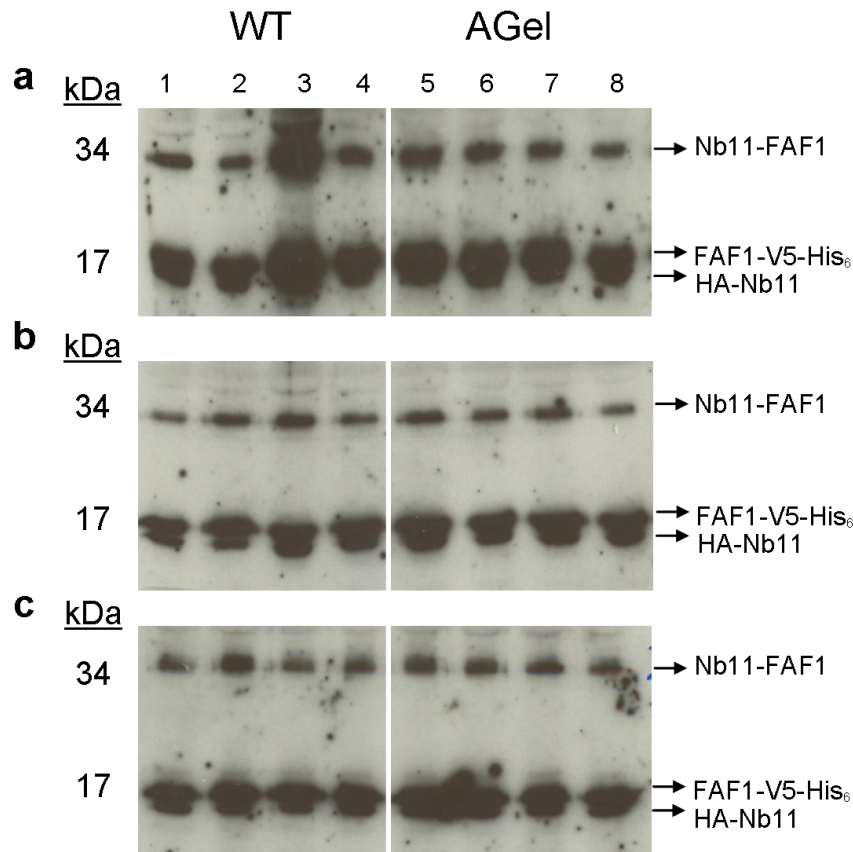


**Figure 1.8: Nb11-FAF1 is expressed in AGel mice after AVV9 gene therapy.** At 1 month of age (a), 1 mg of plasma protein was incubated with anti V5-agarose and anti HA-agarose. Bound protein was visualized via Western blotting after SDS-PAGE. Nb11-FAF1 is visible at the 34 kDa marker. The double band at the 17 kDa marker represents the Nb11 and FAF1 fragments, released after *in vivo* MT1-MMP cleavage. No differences in expression could be detected between WT (lane 1-4, 4 littermates) and AGel mice (lane 5-8, 4 littermates) mice. Nanobody expression remained detectable at 2 (b) and 3 (c) months. At each time point, corresponding lanes represent plasma taken from the same mouse.

#### 1.4.7 AAV9-Nb11-FAF1 displays therapeutic properties in AGel mice

##### SPECT-CT imaging

3 months post treatment, AGel amyloid burden in skeletal muscle and myocardium was determined using SPECT/CT and a recently developed  $^{99m}\text{Tc}$ -FAF Nb1 AGel tracer [251]. In the WT control groups, AAV treatment did not significantly alter the background control signal (**Figure 1.9a** and **b**). In the AGel group however, expression of Nb11-FAF1 resulted in a significantly lower signal (t-test,  $p < 0.05$ ) in the skeletal muscle (25% vs. PBS and 28% vs. AAV9-ctrl) (**Figure 1.9a**) and a significantly lower signal (t-test,  $p < 0.05$ ) in the heart (30% vs. PBS and 36% vs. AAV9-ctrl) (**Figure 1.9b**). This is consistent with a reduction of the characteristic amyloid

burden in the AAV9-Nb11-FAF1-treated AGel mice.

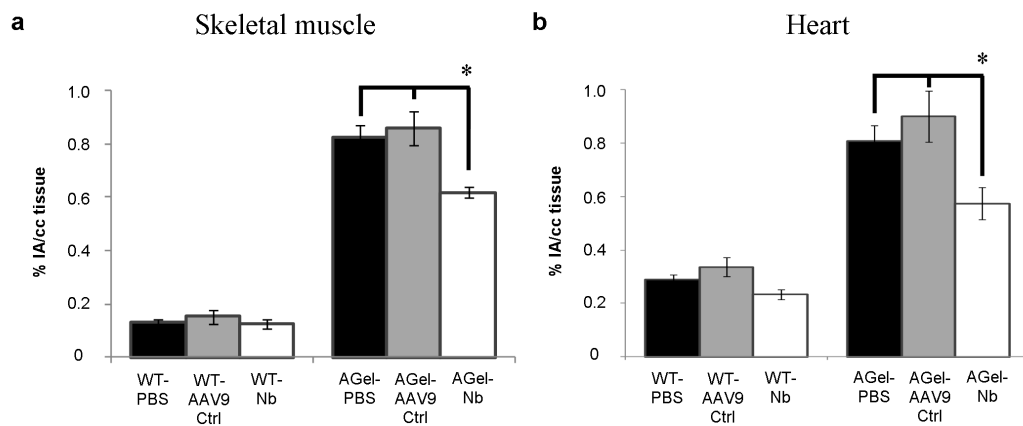


**Figure 1.9: Quantified SPECT-CT data in skeletal muscle and heart.** At 3 months of age all mice underwent a SPECT-CT scan with the  $^{99m}\text{Tc}$ -FAF Nb1 AGel tracer [251]. Identical regions of interest were drawn around hind leg muscles and heart. Signal quantification showed that Nb expression had no effect on WT background signal, neither in skeletal muscle (**a**) nor in heart (**b**). In AGel mice, Nb11-FAF1 expression resulted in a significantly lower signal in skeletal muscle (**a**) and the heart (**b**) compared to PBS and AAV9-control groups. Data shown as mean  $\pm$  SE. \* $p < 0.05$  in a two sided unpaired t-test.

### Immunofluorescence

The mice were sacrificed three months post AAV injection. AGel amyloidogenic buildup in skeletal muscle and heart tissue was stained and quantified. Laminin was used as an internal control. Nb11-FAF1 expression resulted in a significant reduction (t-test,  $p < 0.05$ ) of AGel amyloidogenic buildup in skeletal muscle (39% vs. PBS and 36% vs. AAV9-ctrl) (**Figure 1.10c**) and in the heart (43% vs. PBS and 55% vs AAV9-ctrl) (**Figure 1.10d**) in AGel mice. In contrast, WT control groups expressing Nb11-FAF1 showed no significantly different staining compared to the WT-PBS or WT-AAV9-Ctrl groups (**Figure 1.10a**).

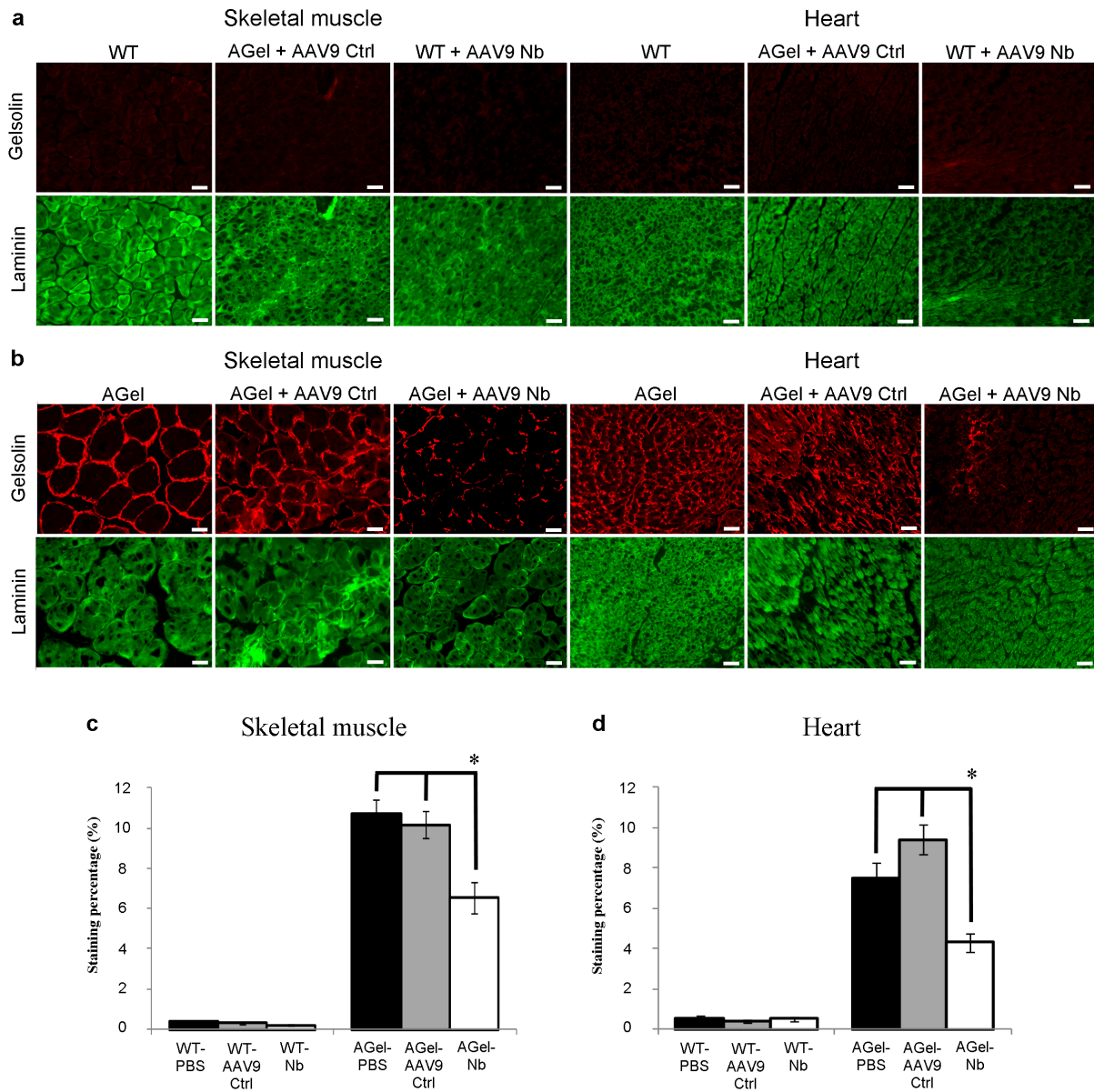


**Figure 1.10: Nb11-FAF1 expressing AGel mice show a decreased immunohistochemistry staining pattern in skeletal muscle and heart tissue.** Mice were sacrificed three months post AAV injection. Skeletal muscle and heart tissue was stained for AGel amyloidogenic buildup (**a-b**, red, scale bar = 50  $\mu\text{m}$ ) and laminin (**a** and **b**, green, control, scale bar = 50  $\mu\text{m}$ ). The staining pattern was reduced in Nb11-FAF1 expressing AGel mice both in skeletal muscle (**c**) and heart tissue (**d**) compared to PBS and AAV9-control groups.

Ex-vivo muscle performance is improved in AAV9-NB11-FAF1 treated mice

At the end of the trial, mice were anaesthetized, the extensor digitorum longus (EDL) and soleus were dissected and their contractile properties were measured. The expression of Nb11-FAF1 in AGel mice resulted in a specific twitch force indistinguishable from the WT control groups (t-test,  $p > 0.05$ ) and significantly different compared to the untreated (PBS or AAV9-ctrl) AGel

groups in EDL muscle (t-test,  $*p < 0.05$ ) but not in the soleus (**Figure 1.11a** and **b**). The amount of force that could be produced for a given frequency (force-frequency) was not affected by the amyloid burden nor by the treatment. Interestingly, fatigue progression was, both in EDL and soleus, significantly more pronounced in the WT versus the (un)treated FAF mice (data not shown). However, the speed of muscle contraction during fatigue in EDL muscle in the Nb11-FAF1 expressing AGel mice showed, as expected, a similar decline as the WT controls in contrast to the untreated (PBS or AAV9-ctrl) AGel mice (**Figure 1.11d**). The soleus seemed unaffected (**Figure 1.11c**).

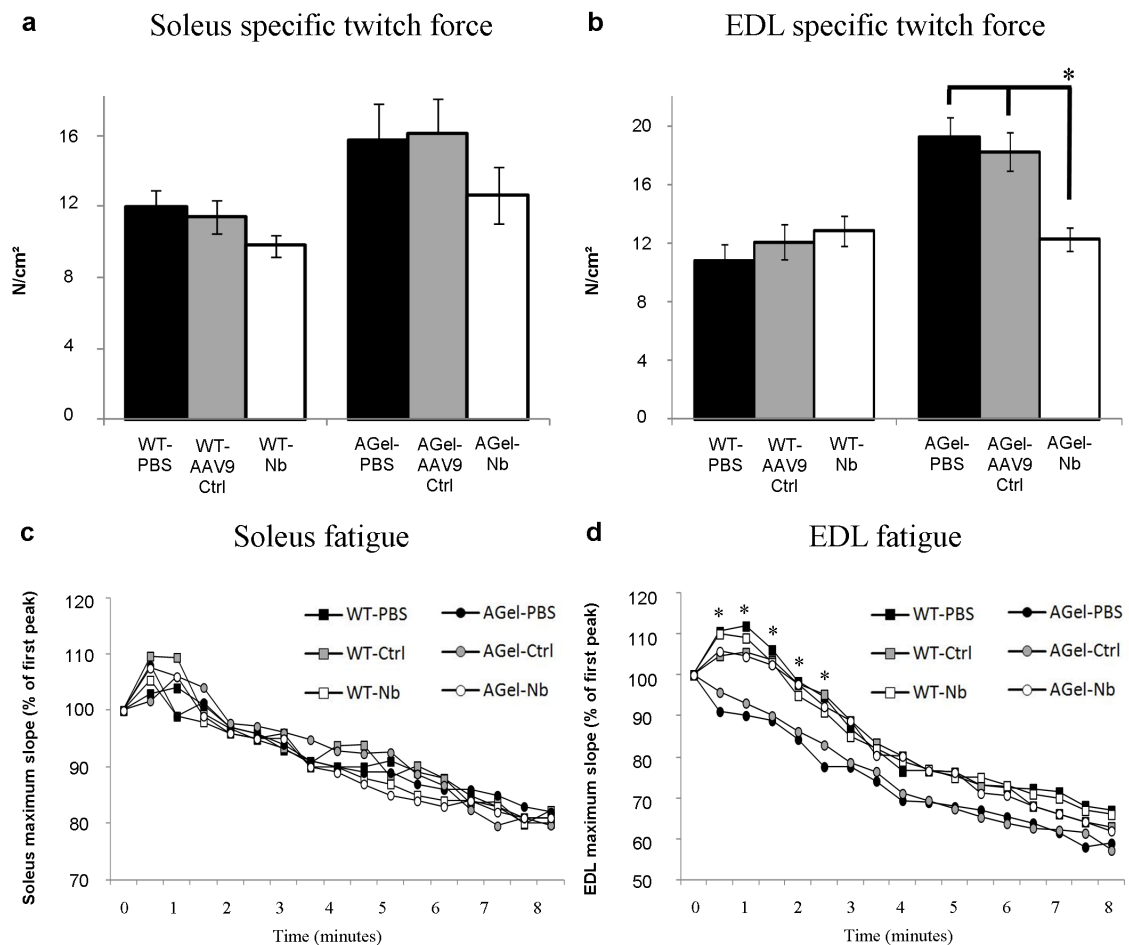


**Figure 1.11: Ex-vivo muscle contractile properties improve after AAV9-Nb11-FAF1 gene therapy.** Soleus and EDL muscles were dissected and their ex-vivo contractile properties measured. Expression of Nb11-FAF1 in AGel mice resulted in a specific twitch force significantly different from AGel control mice (both PBS and AAV9-control) and indistinguishable from the WT-control groups in EDL but not soleus (**a** and **b**, upper panels, data shown as mean  $\pm$  SE.  $*p < 0.05$  in a two sided unpaired t-test). EDL maximum slope (**d**), during the fatigue protocol, in Nb11-FAF1 expressing AGel mice, displayed the same delay as the WT controls. In contrast, AGel PBS and AAV9-control treated mice displayed a significantly faster fatigue onset. The soleus maximum slope during fatigue protocol (**c**) seemed unaffected.  $*p < 0.05$  in a two sided unpaired t-test (**a** and **b**), one way ANOVA (**c** and **d**).

## 1.5 Discussion

As is the case in the majority of amyloid diseases, AGel is characterized by a systemic deposition of amyloid fibrils. The amyloidogenic 8 kDa fragment is produced in a two step process; the first intracellular cleavage of PG\* by furin is followed by an extracellular cleavage of C68 by MT1-MMP like proteases. Both in the present and previous studies, intra- and extracellularly active chaperoning nanobodies have been investigated regarding their potential to inhibit the formation of the amyloidogenic 8 kDa gelsolin fragment. The *in vivo* success of such chaperone based therapeutics strongly depends on the degree in which they distribute throughout the body. In the case of the extracellularly active FAF Nb1, systemic distribution was achieved by intraperitoneal injection [100]. For the intracellularly active Nb11 study, a transgenic mouse model, constitutively expressing Nb11, had to be developed [18]. Here our aim was to combine the FAF Nbs and Nb11 into a single format administered in a clinically applicable way; AAV9 based gene therapy.

Three bispecific nanobodies, Nb11-FAF1, Nb11-FAF2 and Nb11-FAF3 (**Figure 1.1a**), were created. ELISA and Western blot analysis (**Figure 1.2** and **1.3**) showed that, when linked together, the binding characteristics of the constituent nanobodies remained intact. The peptide used to link the two nanobodies was chosen for its susceptibility towards MT1-MMP proteolysis. We envisaged that this approach would result in proteolysis of the amino acid stretch *in vivo* upon secretion of C68, thereby releasing the FAF Nbs, after which they can exert their C68 chaperoning capacity in an unhindered manner. *In vitro*, this peptide sequence performed perfectly; incubation of the bispecific nanobodies with MT1-MMP resulted in the intact release of both constituent nanobodies (**Figure 1.4**).

The chaperone activities of Nb11-FAF constructs were tested *in vitro* in a combined furin/MT1-MMP assay. Quantification of C68 and the 8 kDa peptide revealed that Nb11-FAF1 can rival with Nb11's PG\* chaperoning activity. At the level of the 8 kDa peptide, all Nb11-FAF constructs outperformed their monovalent counterparts (**Figure 1.5**).

To address the *in vivo* problem of amyloid buildup in the AGel mouse model we used a therapeutic approach involving on AAV vector-mediated delivery of the cDNA encoding the Nb11-FAF1 nanobody. AAV is a promising vector for gene therapy yielding long-term expression of therapeutic proteins in clinical trials. The vector tropism is determined by the type of AAV capsid used. We and others had previously demonstrated that AAV serotype 9 is well suited for cardiac and skeletal muscle gene delivery [252–254, 259, 260]. Moreover, the first systemic AAV9 clinical therapy was initiated in 2014, in children up to nine months old, suffering from spinal muscular atrophy type 1 [261], resulting in an apparent sustained therapeutic effect. Since the AGel mouse model recapitulates AGel pathology in skeletal muscle and heart, we therefore also opted for AAV9. *In vivo* transduction with AAV9 vectors encoding the Nb11-FAF1 nanobody resulted in long-term expression of Nb11-FAF1, at least for 3 months post vector-injection, the endpoint of the study (**Figure 1.8**). This is consistent with previous studies showing prolonged expression in the muscle after AAV gene therapy with many different serotypes, including AAV9 [252–254, 259, 260].

Analysis by SPECT/CT and immunohistochemistry revealed a significant decrease in AGel amyloid buildup in both muscle and heart tissue (**Figure 1.10** and **1.11**), consistent with Nb11-FAF1 nanobody expression. The pathological AGel amyloid accumulation could be readily detected using anti-8 kDa antiserum or nanobodies in AGel mice, whereas it was absent in wild-type mice. Most importantly, the observed decrease in AGel buildup translated into improved muscle contractile properties. The EDL showed a specific twitch force indistinguishable from the WT control groups but significantly different from the untreated AGel mice. However, the fact that untreated AGel mice show the highest specific twitch force, and that Nb11-FAF1 treatment reduces this back to the WT base level, is quite counter-intuitive. One would expect that the presence of AGel amyloid between the muscle fibers would negatively influence overall muscle performance. At the moment the molecular mechanisms behind this observation are still obscure. One possibility would be that in AGel affected muscle tissue, the fraction of unaffected muscle fibers somehow overcompensate the functional loss of the more affected fibers. EDL from Nb11-FAF1 treated mice also displayed improved relaxation speeds at the onset of fatigue (**Figure 1.11**). The decline in the speed of muscle contraction during fatigue was identical to the one observed in the wild type mice. In contrast, in the untreated AGel control mice, the presence of AGel amyloid around the muscle fibers most likely hinders an efficient exchange of nutrients and metabolites, adversely impacting the relaxation rate. A reduction in AGel deposition, due to Nb11-FAF1 gene therapy, seems to ameliorate this pathological feature. Our results are consistent with our previous studies, showing that intraperitoneal administration of purified monovalent FAF Nbs or transgenic mice expressing Nb11 following insertion in the ROSA26 locus, also resulted in a significant reduction of the AGel amyloid burden. Head to head studies in the same AGel mouse model are required to compare the relative efficiencies of this Nb11-FAF1 nanobody-based gene therapy approach versus injections of purified nanobodies. Nevertheless, the main advantage of the current nanobody-based AAV9-dependent gene therapy approach is that it enabled sustained *in vivo* nanobody expression that is targeted for secretion following passage through the ER and Golgi apparatus where it binds PG\*. Consequently, the current gene therapy approach is well suited to treat a monogenic disorder like AGel that requires life-long treatment. In contrast, treatment of AGel patients with purified nanobodies, would require life-long, fairly frequent nanobody injections, due to their relatively rapid clearance rates from the circulation. It is particularly encouraging that a long-term therapeutic effect was observed after AAV9-Nb11-FAF1 gene therapy in homozygous AGel mice, which have a more severe phenotype than their heterozygous counterparts (which were used in our earlier studies [18, 100]). In particular, homozygosity of the D187N mutant PG gene results in an earlier onset and higher degree of AGel amyloid deposition leading to a more significant muscle impairment, as opposed to heterozygous AGel mice [148].

Despite the advantages of AAV, some challenges would still need to be addressed to enable its widespread use in patients afflicted by monogenic disorders like AGel. First, there is a high prevalence of pre-existing immunity in the human population (40-80%) against the known AAV serotypes [262]. In time this may be overcome by the discovery of new serotypes against which there is almost no pre-existing immunity or by mutating the antigen epitopes on the AAV capsid.

Using directed evolution, the latter has already proven to be at least partly successful [263, 264]. Secondly, off-target transduction can severely abate the AAV therapeutic efficiency. Any vector taken up by the off-target tissue is essentially lost as it can no longer exert its effect in the desired target tissue. Consequently, this requires higher viral doses, thereby increasing the risk of an immune response. Moreover, since AAV9 also transduces the liver, any nanobody produced in this organ would no longer be able to perform its PG\* chaperone activity. Looking forward to applications in patients, such off-target transductions will have to be minimized. Once again mutagenesis of specific capsid proteins can redirect AAVs more specifically to the tissue of interest [265–267]. In the case of AGel, and more generally in the case of amyloidosis, this may prove useful as the amyloid precursors are quite often formed in a specific cell type, tissue or organ.

Preventing the formation of amyloid precursors, as was attempted here with nanobodies, would be a major step forward in amyloid research. Currently, administration of (R)-1-[6-[(R)-2-carboxypyrrolidin-1-yl]-6-oxo-hexanoyl] pyrrolidine-2-carboxylic acid (CPHPC) followed by anti-SAP antibody is the most promising amyloid removing strategy, as has been proven in patients with AL amyloidosis [268]. Obviously, such interventions are only meaningful if, as is the case in AL amyloidosis, one is also able to stop the production of new amyloid precursors. The development of this bispecific, chaperoning, anti-AGel nanobody, may prove to be a fundamental step towards this goal.

## 1.6 Conclusion

Two types of anti-AGel nanobodies were combined into a single bispecific format; Nb11 which inhibits furin proteolysis and the FAF Nbs which inhibit MT1-MMP proteolysis. *In vitro* studies showed that the Nb11-FAF1 format was most potent. Using AAV serotype 9 gene therapy its therapeutic potential was explored in the AGel mouse model. Expression of Nb11-FAF1 resulted in a reduced amyloid burden and improved muscle contractile properties.

## 1.7 Acknowledgements

We thank Jeffery W. Kelly, Lesley J. Page and Carlos A. Guerrero (Scripps Research Institute) for sharing the gelsolin amyloidosis mouse model. This work was supported by the Queen Elisabeth Medical Foundation (GSKE, Belgium), the 'Stichting Alzheimer Onderzoek' (SAO, Belgium), Ghent University (BOF13/GOA/010), the Research Foundation Flanders (Fonds Wetenschappelijk Onderzoek (FWO) Vlaanderen) and the Interuniversity Attraction Poles Programme of the Belgian State, Federal Office for Scientific, Technical and Cultural Affairs (IUAP P7/13). Adriaan Verhelle is supported by the Agency for Innovation by Science and Technology in Flanders (IWT). Thierry VandenDriessche and Marinee K. Chuah were supported by VUB GEAR IOF (GENECURE), VUB SRP 'Grower' (GENEFIX) and FWO grants





# **PART V**

## DISCUSSION



## Where are we now

Gelsolin amyloidosis, originally discovered in 1969, can sadly still be categorized under 'incurable diseases'. But significant progress has been made in the past several decades. First off all, the underlying molecular mechanism and causative mutations - at the moment four are known - have been thoroughly characterized. Secondly, the phenomenon of amyloidosis has been unraveled. We now know that all amyloid diseases converge towards cross  $\beta$ -sheet amyloid fibrils regardless of the causative protein or protein fragment. Lastly, the creation of the gelsolin mouse model in 2009 [148] allowed us to test potential therapeutic strategies *in vivo*, a milestone in the AGel story.

So why are patients still only receiving symptomatic treatments? What are we missing? Which hurdles still need to be overcome before a groundbreaking therapeutic can be developed?

The fragments responsible for the AGel symptoms are generated from a mutated form of gelsolin. During the secretory pathway of (mutant) gelsolin, it encounters furin in the trans-Golgi network. The AGel mutations result in a partly unfolded variant which reveals an otherwise buried furin cleavage site. Proteolysis generates a 68 kDa C-terminal fragment which, upon secretion, is cleaved by MT1-MMP-like proteases. The latter gives rise to 8 and 5 kDa amyloidogenic fragments able to polymerize into cross  $\beta$ -sheet amyloid fibrils causing the triad of ophthalmological, neurological and dermatological symptoms discussed in Chapter 3, *Introduction to gelsolin amyloidosis*. At first glance, a direct inhibition of furin and/or MT1-MMP with small compounds may seem to be the best therapeutic option. However, these proteases perform key functions in a whole array of crucial biological processes.

Furin is a membrane bound member of the propeptidase family, active in the endosomal and lysosomal pathway. While shuttling between the trans-Golgi network and the cell surface it activates a wide range of serum proteins, hormones and receptors [140–142]. Systemic furin knockout mice proved unviable with embryos dying between days 10.5 and 11.5 [269]. An impaired processing of transforming growth factor  $\beta$  (TGF $\beta$ ) superfamily members has been suggested as the cause [269]. In sharp contrast with its necessity during embryonic development, furin's

---

functions seem partially redundant in adult mice. Inducible furin knockout mice did not develop severe phenotypes; lipoprotein receptor-related protein, albumin,  $\alpha$ V integrin,  $\alpha$ 1-microglobulin, and vitronectin processing was reduced. TGF $\beta$  and PC subtilisin/kexin type 9 processing however seemed entirely dependent on furin [270–273].

MT1-MMP is a membrane bound member of the matrix-metalloprotease family [148] which plays a pivotal role in protein degradation processes during embryonic development and tissue remodeling. MT1-MMP deficient mice suffer from craniofacial dysmorphism, osteopenia, dwarfism, arthritis and fibrosis of soft tissues. The overall cause is the loss of collagenolytic activity essential for the remodeling of skeletal and connective tissue during embryogenesis, growth and tissue maintenance and repair [150].

Taking into account these knockout experiments, in the context of AGel one may expect significant unwanted side effects with a therapy based on furin and/or MT1-MMP inhibition. Especially considering patients would have to take the inhibitors lifelong. At our lab we therefore focused on the development of molecular chaperones with the ability to shield PG\* and/or C68 from furin and MT1-MMP respectively. One nanobody, Nb11, originally developed against CG proved to be able to bind PG\* and shield it from furin degradation [18]. To tackle the MT1-MMP proteolysis, a new set of nanobodies was raised against the amyloidogenic 8 kDa peptide. Three nanobodies, FAF Nb1-3, were selected and all were able to bind and shield C68 from MT1-MMP degradation [100]. In the first article presented in this manuscript the potential of these FAF nanobodies as molecular imaging tools was explored. In the second article Nb11 was combined with the FAF nanobodies, forming a bispecific, therapeutic nanobody applicable via AAV gene therapy.

# 2

## SPECT/CT imaging of amyloid deposits in the AGel mouse model

As stated above, the development of the AGel mouse model in 2009 [148] can be considered a milestone in the AGel research. It expresses D187N human PG under the control of a muscle creatine kinase promoter. From then onwards, new potential therapeutics could, and have been tested *in vivo*. Their efficacy could be evaluated via immunohistochemistry on muscle tissue and analysis of *ex vivo* muscle contractile properties [18, 100]. Nonetheless, the end-stage nature of these experiments leaves many questions unanswered as, over the course of the experiment, the therapeutic mode of actions remains a black box. For example, treatment with FAF Nb1, FAF Nb2-MSA21 - FAF Nb 2 coupled to the albumin binding MSA21 nanobody to enhance the overall half-life - and Nb11 all resulted in a decreased amyloidogenic gelsolin buildup in the AGel mice as determined by immunohistochemistry [18, 100]. From the *in vitro* data we know that this is the result of their chaperoning activity towards C68 and PG\*, respectively, but we have no clue how the resulting lower production of the 8 kDa amyloidogenic fragment influences the amyloid formation process (**Figure 2.1**). Does it delay the nucleation or elongation process? Or does the lower amount simply limit the amount of amyloid which can be formed?

As a first step towards answering these questions we investigated the potential of the FAF nanobodies as an imaging tool. Binding specificity and overall thermal stability are two basic characteristics desired in an imaging agent. The first had already been thoroughly confirmed [100]. The second, thermal stability, was determined via incubation of the nanobodies in mouse serum at 37°C. None of the FAF Nbs showed any degradation up until 24 h of incubation. Moreover, all three nanobodies could be labeled via their hexahistidine tag with  $^{99m}\text{Tc}$  - a process which involves an incubation step at 60°C - with yields over 98%. Technetium was chosen because of its convenient nuclear decay and ideal coordination chemistry for site specific labeling of nanobodies with  $^{99m}\text{Tc}(\text{CO})_3$ . Furthermore, compared to PET isotopes  $^{99m}\text{Tc}$  is relatively cheap and conveniently available from  $^{99}\text{Mo}/^{99m}\text{Tc}$  generators [275].

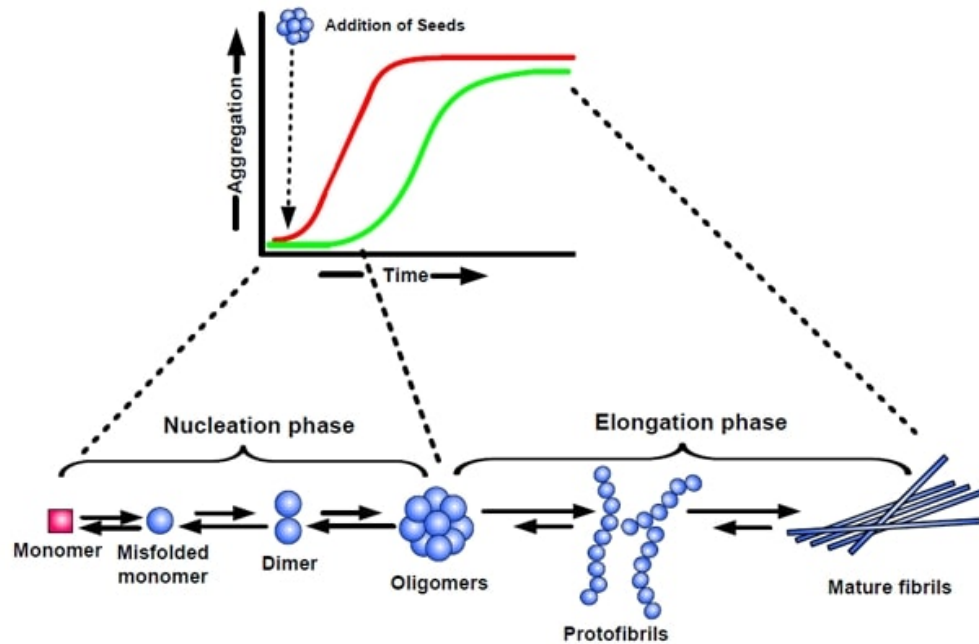


**Figure 2.1:** Amyloid formation happens in two stages: (i) a nucleation phase in which un- or misfolded monomers associate into oligomers and (ii) an elongation phase characterized by a rapid growth of the original oligomers into large fibrils. The nucleation phase is the limiting step due to its unfavorable thermodynamics [274].

A first *in vivo* screening was performed in WT C57BL/6 mice, the WT background of the AGel mouse line. As no aspecific background signals could be detected we began screening the signal-to-noise ratio and signal specificity of the three FAF Nbs. For this 9 month old AGel mice were used and the attained results were compared with the data collected from the WT mice. Given that the AGel mice only produce the D187N gelsolin mutant in their muscle tissue, we specifically focused on the skeletal and cardiac muscle. The liver was chosen as an aspecific control organ. Overall, FAF Nb1 proved superior in both signal-to-noise ratio as signal specificity compared to FAF Nb 2 and 3.

Having selected FAF Nb1 as the best candidate we were interested to see whether or not the SPECT signals generated with  $^{99m}\text{Tc}$ -FAF Nb1 held any quantitative information. After all, the objective was the development of an imaging tool via which we could, non-invasively, access the efficacy of potential FAF therapeutics. In order to do this, the generated SPECT signals would have to correlate with the actual amount of amyloidogenic gelsolin buildup. Therefore a group of 3 month old AGel mice underwent  $^{99m}\text{Tc}$ -FAF Nb1 SPECT/CT analysis. Next, as was also the case for the 9 months old group, the animals were sacrificed and dissected. Tissue specific  $^{99m}\text{Tc}$ -FAF Nb1 retention was determined - biodistribution analysis - and immunohistochemistry - the golden standard in amyloid research - was performed on both skeletal and cardiac muscle. Quantification and comparison of the three techniques revealed a similar pattern of signal increase, thereby confirming that  $^{99m}\text{Tc}$ -FAF Nb1 based SPECT imaging holds quantitative value and correlates with the actual amyloidogenic gelsolin buildup in the tissue.

As a proof of concept an earlier study involving Nb11 expressing mice [18] was repeated. These mice, express and secrete Nb11. In the trans-Golgi network this nanobody encounters PG\* and (partly) shields it from furin degradation, resulting in decreased amyloidogenic gelsolin deposition [18]. Originally, three separate groups were euthanized and analyzed at 3, 6 and 9 months of age. Now, two groups of mice were monitored via SPECT/CT every 2 months up until 9 and 11 months respectively. Next they were euthanized, dissected and analyzed via biodistribution analysis and immunohistochemistry. At these time points the results obtained with all three techniques were identical; Nb11 expressing AGel mice showed significantly less amyloidogenic gelsolin buildup compared to their AGel littermate controls at 9 months, but no longer at 11 months.

To further strengthen our claim that  $^{99m}\text{Tc}$ -FAF Nb1 SPECT imaging can be used for non-invasive assessment of the amyloidogenic gelsolin buildup a set of 5 and 7 month old AGel mice underwent SPECT/CT and immunohistochemistry analysis. Using the already generated data from 3, 9 and 11 month old AGel mice a correlation plot was made between SPECT signal strength and *in vivo* binding site levels, the latter determined in proxy via immunohistochemistry quantification. The trend line ( $R^2 = 0.8447$ ) clearly revealed a positive correlation, thereby supporting our claim.

In conclusion, the study described above has shown that (i) labeling the FAF Nbs with technetium is possible, (ii) none of them recognizes any aspecific target when injected in mice, (iii) that FAF Nb1 is superior in terms of signal-to-noise-ratio and signal specificity and that (iv) with  $^{99m}\text{Tc}$ -FAF Nb1 it is possible to non-invasively assess the amyloid burden in AGel mice. At this point I feel it is important to notice that this study also highlights the pluripotent nature of nanobodies. Indeed, FAF Nb1, originally developed against the 8 kDa amyloidogenic gelsolin fragment can be used both as a molecular chaperone [100] and as a SPECT imaging agent [251].



# 3

## AAV9 gene therapy with bispecific Nb11-FAF1 nanobody in AGel mice

Two types of therapeutic studies had already been performed at our lab. (i) The extracellularly active FAF Nb1 - half-life of one day - and FAF Nb2-MSA21 - half-life of one week - were both intraperitoneally administered for 12 weeks. After diffusion into the tissue these nanobodies could (partly) protect C68 from MT1-MMP degradation [100]. (ii) A Nb11 expressing mouse line has been developed and crossed with AGel mice. As Nb11 works intracellularly the Nb11 gene was accommodated with a N-terminal ER signal ensuring its processing via the Golgi apparatus where it could (partly) protect PG\* from furin [18]. Both approaches led to a reduction of amyloidogenic gelsolin buildup in AGel mice. In theory the easy mode of administration - injection - of FAF Nb2-MSA21 can easily be translated to the clinic. The Nb11 study on the other hand not so much. At the moment, the only truly viable technique is gene therapy, an experimental technique gaining more and more momentum <sup>1</sup> and one which we wanted to explore. If one goes through all the trouble of developing a nanobody gene therapy, would it not be a waste to only deploy half of the available therapeutic potential? More specifically, although the FAF Nb formats are active in the extracellular matrix, and thus can simply be injected, would their efficacy change if we administered them via gene therapy just like Nb11? We thought not. Moreover, we saw a potential extra advantage in combining Nb11 and the FAF nanobodies into a single bispecific format; using a peptide linker sensitive to MT1-MMP proteolysis might lure MT1-MMP away from ( the already lower amount of) C68. Thereby this newly envisioned 'two hit strategy' (**Figure 3.1**) might gain even more therapeutic value. In short, the idea behind the second paper was to combine the therapeutic potential of Nb11 and the FAF Nbs using a mode of administration easily translatable to the clinic.

---

<sup>1</sup>In 2015, Glybera, the first gene therapy that has been approved by the European Commission, has become commercially available.

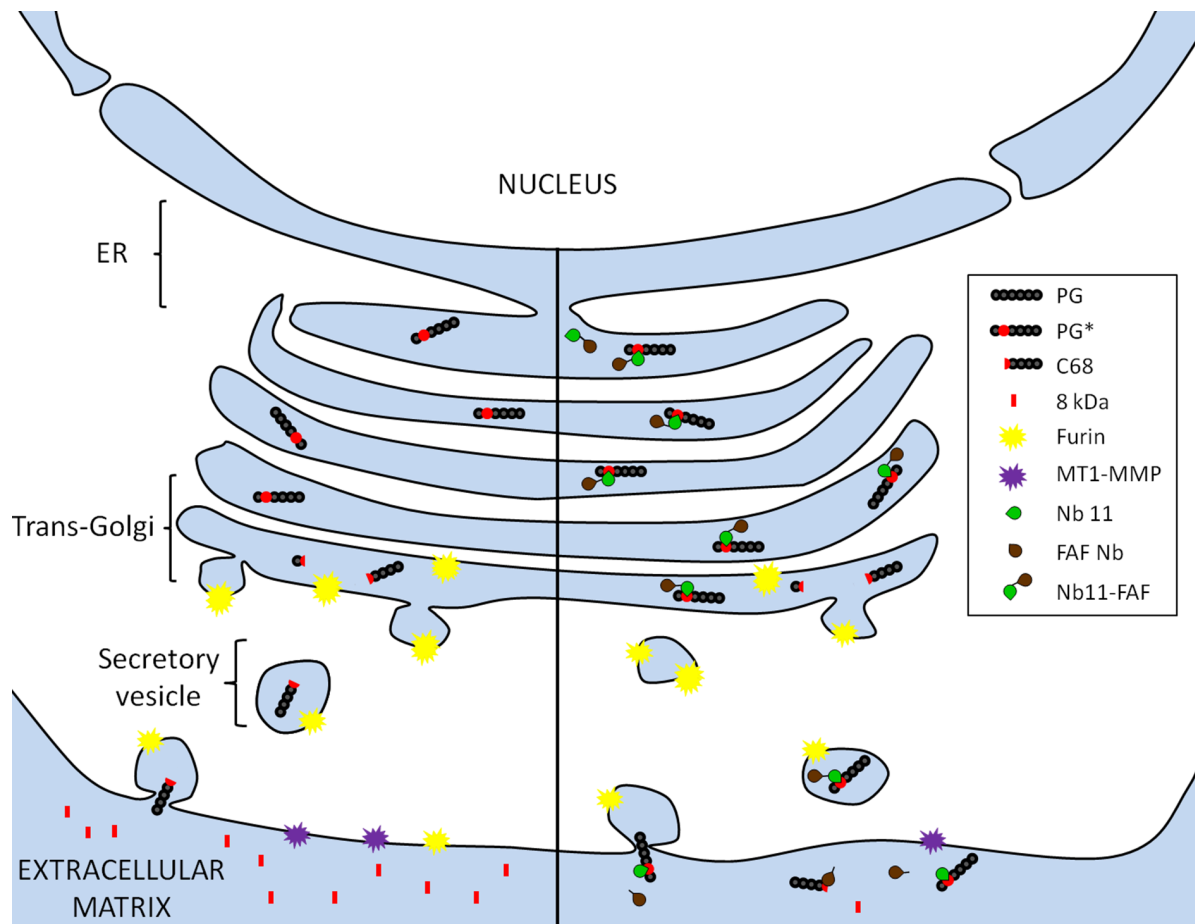


**Figure 3.1: Envisioned molecular mechanism of the therapeutic bispecific Nb11-FAF1.**

The left-hand side depicts the pathological PG\* processing with the formation of C68 in the trans-Golgi network and the 8 and 5 kDa amyloidogenic fragments in the extracellular matrix. On the right-hand side, the intervention with bispecific Nb11-FAF1 is shown. In the trans-Golgi network, the nanobody uses its Nb11 moiety to bind PG\* and (partly) protect it from furin degradation. In the extracellular matrix, the MT1-MMP-sensitive linker between Nb11 and FAF1 serves as a decoy. At the same time, FAF Nb1 is released and is able to perform its C68 chaperoning effect, thereby further decreasing the overall formation of the 8 and 5 kDa amyloidogenic fragments. [23].

We started out by linking Nb11 head-to-tail with each one of the FAF Nbs via the MT1-MMP sensitive peptide SLAPLGLQRR [257]. The latter was sandwiched between two Gly-Ser linkers as a means to limit the constraint of movement each nanobody might inflict on the other. We confirmed via ELISA and Western blot that the bispecific constructs perfectly combine the binding characteristics of their monovalent constituent, hence this strategy seemed effective. Furthermore the incorporated MT1-MMP sensitive peptide proved to remain available and effectively cleavable although interposed between two nanobodies.

A combination of the furin and MT1-MMP *in vitro* assays, presented in earlier publications [18, 100], revealed some interesting insights. (i) Only Nb11-FAF1 could match Nb11's capacity to shield PG\* from furin. (ii) However, based on the amount of 8 kDa amyloidogenic peptide - the main causative agent of the AGel pathology - all three Nb11-FAF constructs outperformed

their monovalent counterparts. This confirms that, at least *in vitro*, a combination of these two types of chaperones is effective. This experiment was repeated in HEK293T cells. Surprisingly Nb11-FAF1 could no longer compete with the inhibitory effect of monovalent Nb11. Perhaps the more complex environment magnifies the (minimized amount of) constraint the two linked nanobodies exert on one another.

Having confirmed that the bispecific nanobody combines the desired characteristics of its monovalent constituents, a gene therapy study in AGel mice was set up. We opted for adeno-associated viruses for their ability to infect both dividing and quiescent cells, their episomal nature after infection and non-pathogenic nature. However some caution regarding the episomal nature is necessary. A small fraction of infecting wild-type AAV genomes integrates in the host genome which can result in insertional mutagenesis. In fact, increased tumorigenesis has been observed in mucopolysaccharidosis VII animal trials [276]. Furthermore, AAV integration has been identified in the testicular tissue of two individuals [277].

AAV9 was our serotype of choice considering its tropism from muscle cells, the afflicted tissue in AGel mice. Three treatments were given, each one to an AGel and WT control group; (i) AAV9-Nb11-FAF1, treatment group, (ii) AAV9-Luc2, viral control group and (iii) PBS, negative control group. The mice were observed for three months, a timeframe during which the expression of Nb11-FAF remained detectable in the serum. At the end of this period the mice were sacrificed and analyzed via SPECT/CT, immunohistochemistry and *ex vivo* muscle performance. The significant reduction in amyloidogenic gelsolin deposition detected with SPECT/CT and immunohistochemistry could be coupled to improved muscle functions. Indeed, the specific twitch force of treated AGel mice was significantly different from the other AGel groups but indistinguishable from the WT control groups. Furthermore, the muscle contractile speed, during fatigue in EDL muscles, showed a similar decline in Nb11-FAF1 treated mice as in WT mice. This correlation hints that the observed reduction in amyloid deposition might be significant enough to alleviate some of the symptoms.

# 4

## General conclusion and future prospects

Considering all of the above, what progress has been made and what are the next steps? First of, the development of the gelsolin amyloid imaging agent -  $^{99m}\text{Tc}$ -FAF Nb1 - is a step forward on two levels. On the one hand, this new tool can significantly boost the overall development of an AGel therapeutic. As we are now able to monitor the amyloidogenic gelsolin buildup non invasively, a significantly lower amount of mice is needed per trial. Moreover, a longitudinal follow-up study might reveal the mode of action of therapeutics under development. For example, SPECT/CT analysis with  $^{99m}\text{Tc}$ -FAF Nb1 in Nb11 expressing AGel mice revealed that deposits are already present at the age of 5 weeks (**Figure 4.1**). We therefore hypothesize that the observed effect of Nb11 expression is mainly due to a deceleration of the elongation phase rather than a delay of the nucleation phase (**Figure 2.1**). This kind of knowledge might prove valuable during the development process. Especially since the majority of cases is only diagnosed in a later stage when significant symptoms start to arise and the nucleation phase is already long past. On the other hand this imaging tracer might also find its way directly into the clinic. A few modifications would have to be made. First, a transition will have to be made from  $^{99m}\text{Tc}$ /SPECT towards a PET-based setup with, for example, Gallium-68 or Fluor-18. Just as  $^{99m}\text{Tc}$ , both can be easily and site specifically linked to nanobodies [237, 242]. Secondly, it would be favorable to humanize the FAF Nb [178]. Given the chronic nature of AGel, patients would most probably be imaged multiple times throughout their life. Despite the low immunogenic nature of nanobodies such repeated exposure could eventually trigger the immune system rendering further use of the FAF Nb1 imaging agent impossible. Experiments regarding the humanization of nanobodies led to the discovery of a universal humanized nanobody; h-NbBCII10<sub>FGLA</sub>. The antigen-binding loops of the FAF Nb1 could be grafted into this humanized nanobody scaffold [178]. Lastly, it is important to acknowledge that in the AGel mouse model deposition occurs in muscle tissue whereas in patients it occurs (mostly) in cranial nerves and the cornea. Whereas the latter can be examined directly by a physician, the cranial nerves however are the tissues to be targeted with Nb/PET imaging. These are comparatively smaller than the skeletal muscles and heart on which we have tested FAF Nb1. Despite the greater sensitivity and resolution which can be achieved with PET

compared to SPECT, visualization of individual nerves is not possible. However, we are hopeful that due to the associated angiopathy in nerve arterioles, amyloid surrounding the facial nerves may be visualized. Indeed, the vascular smooth muscle cells surrounding the facial nerves are heavily loaded with AGel amyloid.

Regarding the Nb11-FAF1 gene therapy approach, the progress is more direct. Both Nb11, FAF Nb2-MSA21 and Nb11-FAF1 have proven to be effective *in vivo* in the AGel mouse model. For FAF Nb2-MSA21 the implementation into the clinic would require a (i) humanization step (as discussed above) and (ii) a replacement of the mouse albumin binding MSA21 nanobody by a variant which binds human albumin. Therapy with Nb11-FAF1 necessitates gene therapy. The here presented AAV-based setup can, and has been implemented in the clinic in various clinical trials [278–288]. Interestingly neural cell lines can be targeted with a wide variety of serotypes; AAV1, 2, 5, 6, 8 and 9. The degree in which they do differs not only in the subset of cell types which they transduce, but also in the efficiency by which they express their incorporated transgene [289]. For example, in rat sensory neurons AAV5 is most effective [290] whereas for spinal motor neurons, AAV2, 6 and 9 proved to be the serotypes of choice [291–295]. At the moment it is hard to say which serotype is the most suitable for treatment of AGel. We know that AGel patients display amyloid deposition in the perineurial sheaths [296] but it is unclear whether the nerve cells, the epithelioid myofibroblasts cells of the perineurium or perhaps both produce the 8 kDa amyloidogenic gelsolin fragment. The answer to this question will determine the desired AAV serotype. Due to pre-existing immunity against AAVs amongst the human population the ultimately selected serotype may be ineffective in a subset of patients. Attempts to avoid this problem via induced mutation of AAV capsid proteins have been (partly) successful [263, 264]. Lastly it will also be desirable to limit off-target transduction as this process increases the required viral doses, which in its turn increases the risk of an immune response. Once again, both the correct serotype selection and induced mutation of capsid proteins are essential to address this issue.

Given the more complex nature of a Nb11-FAF1 gene therapy approach one may wonder whether it is really worth all the trouble. After all, injections with FAF2-MSA21 were effective *in vivo* [100] and this format is more easily translated to the clinic. Although true, we believe that gene therapy with Nb11-FAF1 has several advantages tilting the scale back in its favor. First of all, injections with the FAF Nb would have to be (at least) on a weekly basis [100] whereas in the case of AAV gene therapy adequate gene expression has been observed up until 12 weeks after gene transfer [297]. The latter entails a significant decrease in patient discomfort. Secondly, injected FAF Nb will circulate throughout the body before (eventually, partly) binding its target whereas in the case of gene therapy the bispecific nanobody would only be produced in a subset of cells and secreted directly in the vicinity of the amyloid deposits. Indeed, in the case of gene therapy a much lower dose of nanobody may be needed, thereby decreasing the risk of an immune reaction. Lastly, neither the monovalent FAF Nb approach nor the Nb11 approach [18, 100] could completely stop the formation and progression of gelsolin amyloidosis. Admittedly, neither could the bispecific Nb11-FAF1 Nb. But it could however decrease it to a larger degree compared to

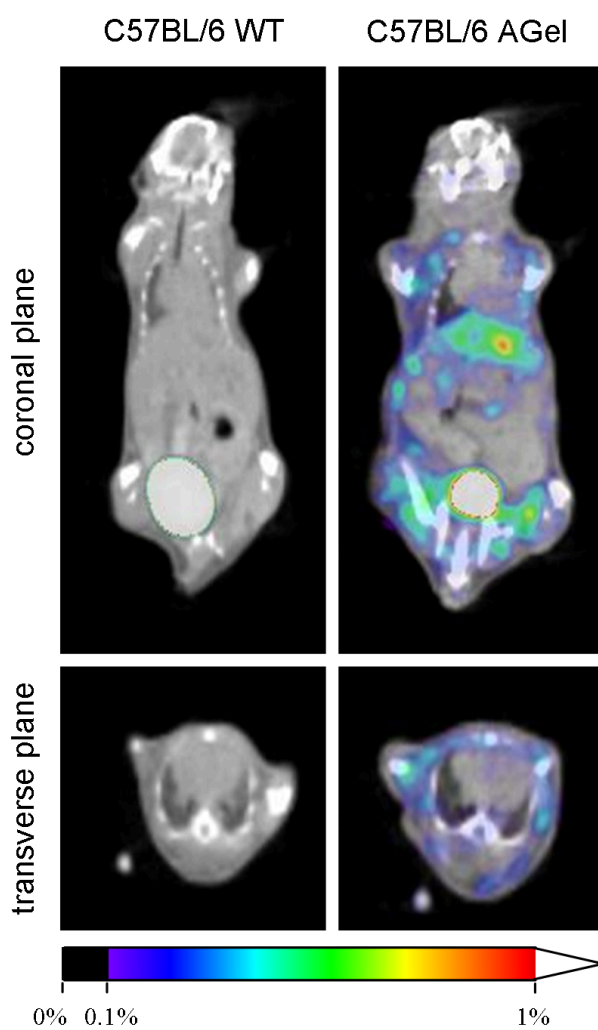


**Figure 4.1:** Using  $^{99m}\text{FAB}$  Nb1 and SPECT/CT, amyloidogenic gelsolin buildup can already be detected in 5 week old mice. CT signal is represented in greyscale. SPECT color scale: NIH (0.1-1%) + white.

its monovalent constituents. Considering the chronic nature and severe symptoms of AGel we therefore believe it to be imperative that each and every effective compound is utilized to its full extent.

Despite all the positive results and prospects mentioned above, the Nb11-FAF1 gene therapy intervention leaves a significant question unanswered; do all three components - Nb11, FAF Nb1, MT1-MMP sensitive linker - contribute to the therapeutic effect? And if so, to what degree? The used setup - PBS controls, vector control, treatment group - does not provide any information regarding these individual components. Neither can we compare with the previously reported studies with monovalent FAF Nb1, FAF Nb2-MSA21 and Nb11 as these were performed in heterozygous AGel mice whereas the AAV-Nb11-FAF1 study was performed in homozygous AGel mice - which show a significantly higher amyloid burden compared to heterozygous mice [148]. As we were able to reduce the amyloid buildup with the bispecific Nb11-FAF1 to a higher degree compared to the monovalent Nb studies it is more than likely that at least more than one of its components was active *in vivo*. Nonetheless, an extensive study encompassing AAV-Nb1, AAV-Nb11 and AAV-Nb11-FAF1 without the MT1-MMP sensitive linker, has to be performed before one can try to answer this question.

The studies performed with the AGel mouse model have shown that nanobodies are useful, potent therapeutics for both extra- and intracellular targets. They also highlighted that nanobodies can be used as an imaging tool in AGel, thereby facilitating the screening of potentially new therapeutic compounds. While AGel is an orphan disease, it should be emphasized that this strategy can be extrapolated to other amyloidogenic afflictions. The most infamous type of amyloidosis, Alzheimer's disease, actually has a quite similar pathogenesis; the sequential proteolysis of Alzheimer precursor protein by  $\beta$ -secretase and  $\gamma$ -secretase results in the release of A $\beta$  amyloidogenic peptides. Nanobodies against this  $\beta$ -secretase have already proven to be therapeutically active in a transgenic AD mouse model [234]. However, we believe that in the long run it would prove more beneficial to target the APP instead of the secretases. Inhibiting a protease will most likely provoke unwanted side effects whereas chaperoning the target, as in the AGel research discussed in this manuscript, is more unlikely to do so.

Raising nanobodies against full length APP, s-APP  $\beta$  or A $\beta$ , may result in nanobodies that bind near the  $\beta$ -secretase cleavage or docking site and that block the formation of s-APP  $\beta$ . A double hit strategy as in the AGel case will most probably be more difficult to achieve. The  $\gamma$ -secretase is a multi unit integral membrane protein. It cleaves transmembrane passes. At the moment there are no reports of nanobodies being able to integrate into the plasma membrane and remain functional. In addition, gamma secretase proteolysis also takes place in the non-pathogenic processing of APP. As the transmembrane part of C-terminal fragment- $\alpha$  and C-terminal fragment- $\beta$  are identical, even a chaperone based intervention may provoke unwanted side effects.

Up until now we have only discussed preventing the formation of amyloidogenic peptides. But directly targeting the amyloidogenic peptides, after their formation, also holds great therapeutic potential. The deposition of amyloid fibrils is the primary pathological feature of this group of

afflictions. In recent years however, scientific insights in the initial processes leading to fibrillation hint that the initial oligomeric aggregates may be the most toxic species in amyloid pathogenesis and mature fibrils may be far less pathogenic than previously thought [244, 245]. These new results hint to new therapeutic strategies. First, one could try to stimulate fibrillation, thus attempting to lower the half-life of small oligomeric aggregates. Secondly, one could try to remove the amyloidogenic peptides altogether as soon as they are formed. Most likely the latter will prove to be the most rewarding in the long run. Because although evidence points at intermediate oligomeric species as highly toxic, the accumulation of amyloidogenic plaques would still impede normal homeostasis of the affected tissue from a certain point in time onwards.

FAF Nb1-3 could be tested for their ability to prevent 8 kDa AGel fibrillation. With transmission electron microscopy (TEM) and/or atomic-force microscopy (AFM) the differences in fibrillation could then be visualized in order to link reduced toxicity to a specific shift in amyloid oligomerization or fibril species.

Once more Alzheimer researchers are also exploring this route. Studying the cytotoxic response of SH-SY5Y cells via LDL release, they found that oligomeric  $A\beta$  provoked a higher cytotoxic reaction compared to monomeric or fibrillar  $A\beta$  [298]. Next the cells were incubated with oligomeric  $A\beta$  formed in the presence of anti- $A\beta$  nanobodies. So far, two distinct nanobodies have been discovered, each binding a specific oligomeric species. Both are able to lower the intrinsic toxicity in SH-SY5Y cells. The first, Nb A4, does so by inhibiting further aggregation of its target. The second, Nb E1, acts in a different manner by binding to smaller  $A\beta$  species than Nb A4, thereby interfering earlier in the fibrillation process. Binding its target stabilizes the formation of small non toxic low-n  $A\beta$  species.

It remains to be demonstrated if these approaches and beneficial effects can be translated in model organisms or even in patients, but the current findings and results obtained with nanobodies in several amyloid diseases indicate that they could represent an instrument of choice in the diagnosis and/or treatment of these debilitating disorders.





# BIBLIOGRAPHY



# Bibliography

- [1] B. Alberts, A. Johnson, and J. Lewis. *Molecular Biology of the Cell*, volume 4th edition. 2002.
- [2] H. E. Harris and A. G. Weeds. Platelet actin: sub-cellular distribution and association with profilin. *FEBS Lett*, 90(1):84–8, 1978.
- [3] T. D. Pollard and J. A. Cooper. Actin and actin-binding proteins. a critical evaluation of mechanisms and functions. *Annu Rev Biochem*, 55:987–1035, 1986.
- [4] L. Bertier. Unpublished figure.
- [5] Patrick van Oostveldt. *Cell biology*. Ghent University, 2010. Course 3<sup>th</sup> bachelor Bio-engineering.
- [6] B. J. Perrin and J. M. Ervasti. The actin gene family: function follows isoform. *Cytoskeleton (Hoboken)*, 67(10):630–4, 2010.
- [7] D. L. Nelson and Cox M. M. *Lehninger Principles of Biochemistry*, volume 5. W. H. Freeman and Company, 2008.
- [8] P. Ranjith, K. Mallick, J. F. Joanny, and D. Lacoste. Role of atp-hydrolysis in the dynamics of a single actin filament. *Biophys J*, 98(8):1418–27, 2010.
- [9] D. Pantaloni, C. Le Clainche, and M. F. Carrier. Mechanism of actin-based motility. *Science*, 292(5521):1502–6, 2001.
- [10] M.V. Dayel and R.D. Mullins. Activation of arp2/3 complex: Addition of the first subunit of the new filament by a wasp protein triggers rapid atp hydrolysis on arp2. *PLoS Biology*, 2(4):e91, 2004.
- [11] C.G. dos Remedios, D. Chhabra, M. Kekic, I.V. Dedova, M. Tsubakihara, D.A. Berry, and N.J. Nosworthy. Actin binding proteins: regulation of cytoskeletal microfilaments. *Physiological Reviews*, 83(2):433–473, 2003.
- [12] H. L. Yin and T. P. Stossel. Control of cytoplasmic actin gel-sol transformation by gelsolin, a calcium-dependent regulatory protein. *Nature*, 281(5732):583–6, 1979.

- [13] P. J. McLaughlin, J. T. Gooch, H. G. Mannherz, and A. G. Weeds. Structure of gelsolin segment 1-actin complex and the mechanism of filament severing. *Nature*, 364(6439):685–92, 1993.
- [14] L. D. Burtnick, E. K. Koepf, J. Grimes, E. Y. Jones, D. I. Stuart, P. J. McLaughlin, and R. C. Robinson. The crystal structure of plasma gelsolin: implications for actin severing, capping, and nucleation. *Cell*, 90(4):661–70, 1997.
- [15] D. J. Kwiatkowski, T. P. Stossel, S. H. Orkin, J. E. Mole, H. R. Colten, and H. L. Yin. Plasma and cytoplasmic gelsolins are encoded by a single gene and contain a duplicated actin-binding domain. *Nature*, 323(6087):455–8, 1986.
- [16] D. Wen, K. Corina, E. P. Chow, S. Miller, P. A. Janmey, and R. B. Pepinsky. The plasma and cytoplasmic forms of human gelsolin differ in disulfide structure. *Biochemistry*, 35(30):9700–9, 1996.
- [17] D. A. Vouyiouklis, T. J. Anderson, H. E. King, D. Kirkham, S. A. Karim, K. J. Johnson, and I. R. Griffiths. Mapping of the dysmyelinating murine hindshaker mutation to a 1.2-cm interval on chromosome 3. *Genomics*, 80(2):126–8, 2002.
- [18] W. Van Overbeke, J. Wongsantichon, I. Everaert, A. Verhelle, O. Zwaenepoel, A. Loonchanta, L. D. Burtnick, A. De Ganck, T. Hochepped, J. Haigh, C. Cuvelier, W. Derave, R. C. Robinson, and J. Gettemans. An er-directed gelsolin nanobody targets the first step in amyloid formation in a gelsolin amyloidosis mouse model. *Hum Mol Genet*, 24(9):2492–507, 2015.
- [19] B. Pope, S. Maciver, and A. Weeds. Localization of the calcium-sensitive actin monomer binding site in gelsolin to segment 4 and identification of calcium binding sites. *Biochemistry*, 34(5):1583–8, 1995.
- [20] C. D. Chen, M. E. Huff, J. Matteson, L. Page, R. Phillips, J. W. Kelly, and W. E. Balch. Furin initiates gelsolin familial amyloidosis in the golgi through a defect in  $ca(2+)$  stabilization. *EMBO J*, 20(22):6277–87, 2001.
- [21] H. Choe, L. D. Burtnick, M. Mejillano, H. L. Yin, R. C. Robinson, and S. Choe. The calcium activation of gelsolin: insights from the 3a structure of the g4-g6/actin complex. *J Mol Biol*, 324(4):691–702, 2002.
- [22] L. D. Burtnick, D. Urosev, E. Irobi, K. Narayan, and R. C. Robinson. Structure of the n-terminal half of gelsolin bound to actin: roles in severing, apoptosis and faf. *EMBO J*, 23(14):2713–22, 2004.
- [23] A. Verhelle and J. Gettemans. *A Nanobody-Based Approach to Amyloid Diseases, the Gelsolin Case Study, Exploring New Findings on Amyloidosis*. InTech, 2016.

- [24] T. Hesterkamp, A. G. Weeds, and H. G. Mannherz. The actin monomers in the ternary gelsolin: 2 actin complex are in an antiparallel orientation. *Eur J Biochem*, 218(2):507–13, 1993.
- [25] S. Nag, M. Larsson, R. C. Robinson, and L. D. Burtnick. Gelsolin: the tail of a molecular gymnast. *Cytoskeleton (Hoboken)*, 70(7):360–84, 2013.
- [26] T. D. Pollard. Regulation of actin filament assembly by arp2/3 complex and formins. *Annu Rev Biophys Biomol Struct*, 36:451–77, 2007.
- [27] F. Bronner. Extracellular and intracellular regulation of calcium homeostasis. *The Scientific World*, (1):919–925, 2001.
- [28] D. Prins and M. Michalak. Organellar calcium buffers. *CSH Perspectives in Biology*, 3(3), 2011.
- [29] S. Chandra, C. Fewtrell, P.J. Millard, D.R. Sandison, W.W. Webb, and G.H. Morrison. Imaging of total intracellular calcium and calcium influx and efflux in individual resting and stimulated tumor mast cells using ion microscopy. *J. Biol. Chem.*, (269):15186–15194, 1994.
- [30] E. de Alba and N. Tjandra. Structural studies on the ca-binding domain of human nucleobindin (calnuc). *Biochemistry*, (43):10039–10049, 2004.
- [31] T. P. Stossel. On the crawling of animal cells. *Science*, 260(5111):1086–94, 1993.
- [32] F. X. Yu, H. Q. Sun, P. A. Janmey, and H. L. Yin. Identification of a polyphosphoinositide-binding sequence in an actin monomer-binding domain of gelsolin. *J Biol Chem*, 267(21):14616–21, 1992.
- [33] P. A. Janmey, J. Lamb, P. G. Allen, and P. T. Matsudaira. Phosphoinositide-binding peptides derived from the sequences of gelsolin and villin. *J Biol Chem*, 267(17):11818–23, 1992.
- [34] V. De Corte, J. Gettemans, and J. Vandekerckhove. Phosphatidylinositol 4,5-bisphosphate specifically stimulates pp60(c-src) catalyzed phosphorylation of gelsolin and related actin-binding proteins. *FEBS Lett*, 401(2-3):191–6, 1997.
- [35] H. Wang and G. Reiser. The role of the ca<sup>2+</sup>-sensitive tyrosine kinase pyk2 and src in thrombin signalling in rat astrocytes. *J Neurochem*, 84(6):1349–57, 2003.
- [36] P. A. Janmey and T. P. Stossel. Modulation of gelsolin function by phosphatidylinositol 4,5-bisphosphate. *Nature*, 325(6102):362–4, 1987.
- [37] S. Ahmed, J. Lee, R. Kozma, A. Best, C. Monfries, and L. Lim. A novel functional target for tumor-promoting phorbol esters and lysophosphatidic acid. the p21rac-gtpase activating protein n-chimaerin. *J Biol Chem*, 268(15):10709–12, 1993.

- [38] M. H. Tsai, A. Hall, and D. W. Stacey. Inhibition by phospholipids of the interaction between r-ras, rho, and their gtpase-activating proteins. *Mol Cell Biol*, 9(11):5260–4, 1989.
- [39] R. Lauener, Y. Shen, V. Duronio, and H. Salari. Selective inhibition of phosphatidylinositol 3-kinase by phosphatidic acid and related lipids. *Biochem Biophys Res Commun*, 215(1):8–14, 1995.
- [40] R. Bucki, P. C. Georges, Q. Espinassous, M. Funaki, J. J. Pastore, R. Chaby, and P. A. Janmey. Inactivation of endotoxin by human plasma gelsolin. *Biochemistry*, 44(28):9590–7, 2005.
- [41] J. A. Lamb, P. G. Allen, B. Y. Tuan, and P. A. Janmey. Modulation of gelsolin function. activation at low ph overrides ca<sup>2+</sup> requirement. *J Biol Chem*, 268(12):8999–9004, 1993.
- [42] K. M. Lin, E. Wenegieme, P. J. Lu, C. S. Chen, and H. L. Yin. Gelsolin binding to phosphatidylinositol 4,5-bisphosphate is modulated by calcium and ph. *J Biol Chem*, 272(33):20443–50, 1997.
- [43] C. C. Cunningham, T. P. Stossel, and D. J. Kwiatkowski. Enhanced motility in nih 3t3 fibroblasts that overexpress gelsolin. *Science*, 251(4998):1233–6, 1991.
- [44] M. Chellaiah, N. Kizer, M. Silva, U. Alvarez, D. Kwiatkowski, and K. A. Hruska. Gelsolin deficiency blocks podosome assembly and produces increased bone mass and strength. *J Cell Biol*, 148(4):665–78, 2000.
- [45] M. Lu, W. Witke, D. J. Kwiatkowski, and K. S. Kosik. Delayed retraction of filopodia in gelsolin null mice. *J Cell Biol*, 138(6):1279–87, 1997.
- [46] T. Azuma, W. Witke, T. P. Stossel, J. H. Hartwig, and D. J. Kwiatkowski. Gelsolin is a downstream effector of rac for fibroblast motility. *EMBO J*, 17(5):1362–70, 1998.
- [47] D. J. Kwiatkowski. Functions of gelsolin: motility, signaling, apoptosis, cancer. *Curr Opin Cell Biol*, 11(1):103–8, 1999.
- [48] G. H. Li, Y. Shi, Y. Chen, M. Sun, S. Sader, Y. Maekawa, S. Arab, F. Dawood, M. Chen, G. De Couto, Y. Liu, M. Fukuoka, S. Yang, M. Da Shi, L. A. Kirshenbaum, C. A. McCulloch, and P. Liu. Gelsolin regulates cardiac remodeling after myocardial infarction through dnase i-mediated apoptosis. *Circ Res*, 104(7):896–904, 2009.
- [49] S. Kamada, H. Kusano, H. Fujita, M. Ohtsu, R. C. Koya, N. Kuzumaki, and Y. Tsujimoto. A cloning method for caspase substrates that uses the yeast two-hybrid system: cloning of the antiapoptotic gene gelsolin. *Proc Natl Acad Sci U S A*, 95(15):8532–7, 1998.

- [50] R. C. Koya, H. Fujita, S. Shimizu, M. Ohtsu, M. Takimoto, Y. Tsujimoto, and N. Kuzumaki. Gelsolin inhibits apoptosis by blocking mitochondrial membrane potential loss and cytochrome c release. *J Biol Chem*, 275(20):15343–9, 2000.
- [51] M. Ohtsu, N. Sakai, H. Fujita, M. Kashiwagi, S. Gasa, S. Shimizu, Y. Eguchi, Y. Tsujimoto, Y. Sakiyama, K. Kobayashi, and N. Kuzumaki. Inhibition of apoptosis by the actin-regulatory protein gelsolin. *EMBO J*, 16(15):4650–6, 1997.
- [52] S. C. Posey, M. P. Martelli, T. Azuma, D. J. Kwiatkowski, and B. E. Bierer. Failure of gelsolin overexpression to regulate lymphocyte apoptosis. *Blood*, 95(11):3483–8, 2000.
- [53] Bulbeck. Two different models for how cells move. a) cytoskeletal model. b) membrane flow model, February 2011.
- [54] J. Gettemans, A. Vanden Abbeele, A. De Ganck, K. Meerschaeert, J. VandeKerckhove, and V. De Corte. *Gelsolin and Tumor Metastasis: Friend or Foe?*, chapter VI, pages 103–121. Nova Science Publishers, 2007.
- [55] N. Sakai, M. Ohtsu, H. Fujita, T. Koike, and N. Kuzumaki. Enhancement of g2 checkpoint function by gelsolin transfection in human cancer cells. *Exp Cell Res*, 251(1):224–33, 1999.
- [56] A. Noske, C. Denkert, H. Schober, C. Sers, B. Zhumabayeva, W. Weichert, M. Dietel, and K. Wiechen. Loss of gelsolin expression in human ovarian carcinomas. *Eur J Cancer*, 41(3):461–9, 2005.
- [57] E. Nishida, K. Iida, N. Yonezawa, S. Koyasu, I. Yahara, and H. Sakai. Cofilin is a component of intranuclear and cytoplasmic actin rods induced in cultured cells. *Proc Natl Acad Sci U S A*, 84(15):5262–6, 1987.
- [58] R. Salazar, S. E. Bell, and G. E. Davis. Coordinate induction of the actin cytoskeletal regulatory proteins gelsolin, vasodilator-stimulated phosphoprotein, and profilin during capillary morphogenesis in vitro. *Exp Cell Res*, 249(1):22–32, 1999.
- [59] J. Chou, D. B. Stolz, N. A. Burke, S. C. Watkins, and A. Wells. Distribution of gelsolin and phosphoinositol 4,5-bisphosphate in lamellipodia during egf-induced motility. *Int J Biochem Cell Biol*, 34(7):776–90, 2002.
- [60] K. Nishimura, H. J. Ting, Y. Harada, T. Tokizane, N. Nonomura, H. Y. Kang, H. C. Chang, S. Yeh, H. Miyamoto, M. Shin, K. Aozasa, A. Okuyama, and C. Chang. Modulation of androgen receptor transactivation by gelsolin: a newly identified androgen receptor coregulator. *Cancer Res*, 63(16):4888–94, 2003.
- [61] A. E. Greijer, P. van der Groep, D. Kemming, A. Shvarts, G. L. Semenza, G. A. Meijer, M. A. van de Wiel, J. A. Belien, P. J. van Diest, and E. van der Wall. Up-regulation of gene expression by hypoxia is mediated predominantly by hypoxia-inducible factor 1 (hif-1). *J Pathol*, 206(3):291–304, 2005.



- [62] P. Chen, J. E. Murphy-Ullrich, and A. Wells. A role for gelsolin in actuating epidermal growth factor receptor-mediated cell motility. *J Cell Biol*, 134(3):689–98, 1996.
- [63] A. S. Lader, J. J. Lee, G. Cicchetti, and D. J. Kwiatkowski. Mechanisms of gelsolin-dependent and -independent egf-stimulated cell motility in a human lung epithelial cell line. *Exp Cell Res*, 307(1):153–63, 2005.
- [64] A. Arcaro. The small gtp-binding protein rac promotes the dissociation of gelsolin from actin filaments in neutrophils. *J Biol Chem*, 273(2):805–13, 1998.
- [65] V. De Corte, E. Bruyneel, C. Boucherie, M. Mareel, J. Vandekerckhove, and J. Gettemans. Gelsolin-induced epithelial cell invasion is dependent on ras-rac signaling. *EMBO J*, 21(24):6781–90, 2002.
- [66] M. A. Chellaiah, R. S. Biswas, D. Yuen, U. M. Alvarez, and K. A. Hruska. Phosphatidylinositol 3,4,5-trisphosphate directs association of src homology 2-containing signaling proteins with gelsolin. *J Biol Chem*, 276(50):47434–44, 2001.
- [67] S. E. Lind, D. B. Smith, P. A. Janmey, and T. P. Stossel. Depression of gelsolin levels and detection of gelsolin-actin complexes in plasma of patients with acute lung injury. *Am Rev Respir Dis*, 138(2):429–34, 1988.
- [68] D. B. Smith, P. A. Janmey, and S. E. Lind. Circulating actin-gelsolin complexes following oleic acid-induced lung injury. *Am J Pathol*, 130(2):261–7, 1988.
- [69] H. Ito, H. Kambe, Y. Kimura, H. Nakamura, E. Hayashi, T. Kishimoto, S. Kishimoto, and H. Yamamoto. Depression of plasma gelsolin level during acute liver injury. *Gastroenterology*, 102(5):1686–92, 1992.
- [70] E. Suhler, W. Lin, H. L. Yin, and W. M. Lee. Decreased plasma gelsolin concentrations in acute liver failure, myocardial infarction, septic shock, and myonecrosis. *Crit Care Med*, 25(4):594–8, 1997.
- [71] K. C. Mounzer, M. Moncure, Y. R. Smith, and M. J. Dinubile. Relationship of admission plasma gelsolin levels to clinical outcomes in patients after major trauma. *Am J Respir Crit Care Med*, 160(5 Pt 1):1673–81, 1999.
- [72] T. M. Osborn, C. Dahlgren, J. H. Hartwig, and T. P. Stossel. Modifications of cellular responses to lysophosphatidic acid and platelet-activating factor by plasma gelsolin. *Am J Physiol Cell Physiol*, 292(4):C1323–30, 2007.
- [73] S. Steyaert. *Developing bioinformatics applications for the analysis of epigenetic next-generation sequencing data*. PhD thesis, Ghent University, 2016.
- [74] G. V. Kryukov and V. N. Gladyshev. The prokaryotic selenoproteome. *EMBO*, 5:538–543, 2004.

- [75] J. Crappé. *Micropeptides as non-classical bioactive peptides in Eukaryotes, a ribosome profiling centered approach*. PhD thesis, Ghent University, 2015.
- [76] H.S. Clackamas. Dna & rna; protein synthesis, March 2016.
- [77] C. B. Anfinsen. The formation and stabilization of protein structure. *Biochem J*, 128(4):737–49, 1972.
- [78] C. B. Anfinsen. Principles that govern the folding of protein chains. *Science*, 181(4096):223–30, 1973.
- [79] L. Goldschmidt, P. K. Teng, R. Riek, and D. Eisenberg. Identifying the amyloids, proteins capable of forming amyloid-like fibrils. *Proc Natl Acad Sci U S A*, 107(8):3487–92, 2010.
- [80] J. Zych. Process: the signal hypothesis, Februari 2014.
- [81] R. Duncan and J. W. Hershey. Identification and quantitation of levels of protein synthesis initiation factors in crude hela cell lysates by two-dimensional polyacrylamide gel electrophoresis. *J Biol Chem*, 258(11):7228–35, 1983.
- [82] N. Lane and W. Martin. The energetics of genome complexity. *Nature*, 467(7318):929–34, 2010.
- [83] M. Piques, W. X. Schulze, M. Hohne, B. Usadel, Y. Gibon, J. Rohwer, and M. Stitt. Ribosome and transcript copy numbers, polysome occupancy and enzyme dynamics in arabidopsis. *Mol Syst Biol*, 5:314, 2009.
- [84] M. A. DePristo, D. M. Weinreich, and D. L. Hartl. Missense meanderings in sequence space: a biophysical view of protein evolution. *Nat Rev Genet*, 6(9):678–87, 2005.
- [85] P. S. Spencer, E. Siller, J. F. Anderson, and J. M. Barral. Silent substitutions predictably alter translation elongation rates and protein folding efficiencies. *J Mol Biol*, 422(3):328–35, 2012.
- [86] M. Kruger and W. A. Linke. The giant protein titin: a regulatory node that integrates myocyte signaling pathways. *J Biol Chem*, 286(12):9905–12, 2011.
- [87] Els Vandamme. *Protein chemistry*. Ghent University, 2009. Course master Cell and Gene biotechnology, Bio-engineering.
- [88] D. Kaganovich, R. Kopito, and J. Frydman. Misfolded proteins partition between two distinct quality control compartments. *Nature*, 454(7208):1088–95, 2008.
- [89] Roggerdodd. The ubiquitination system (showing a ring e3 ligase, January 2011).
- [90] J. R. Glover and S. Lindquist. Hsp104, hsp70, and hsp40: a novel chaperone system that rescues previously aggregated proteins. *Cell*, 94(1):73–82, 1998.

- [91] E. Wirawan, T. Vanden Berghe, S. Lippens, P. Agostinis, and P. Vandenabeele. Autophagy: for better or for worse. *Cell Research*, (22):43–61, 2012.
- [92] E. Lee, A. Ng, Y. Wei, K. Luby-Phelps, A. Juraszek, R.J. Xavier, O. Cleaver, B. Levine, and J.F. Amatruda. Autophagy is essential for cardiac morphogenesis during vertebrate development. *Autophagy*, 10(4):572–587.
- [93] K.J. Kinghorn, A.M. Asghari, and J.I. Castillo-Quan. The emerging role of autophagic-lysosomal dysfunction in gaucher disease and parkinson's disease. *Neural regeneration research*, 12(3):380–384, 2017.
- [94] J.M. Rini. Glycosyltransferases and er quality control, February 2017.
- [95] Virchow R. Uber eine im gehirn und ruckenmark des menschen aufgefundene substanz mit der chemische reaction der cellulose. *Virchows Arch Pathol Anat Physiol*, (6):4, 1854.
- [96] J. B. Cavanagh. Corpora-amylacea and the family of polyglucosan diseases. *Brain Res Brain Res Rev*, 29(2-3):265–95, 1999.
- [97] M. Flanagan. *The Downside of Upright Posture - The Anatomical Causes of Alzheimer's, Parkinson's and Multiple Sclerosis*, volume 1th edition. 2010.
- [98] J.L. Jimenez, J.I. Guijarro, E. Orlova, J. Zurdo, C.M. Dobson, M. Sunde, and H. Saibil. Cryo-electron microscopy structure of an sh3 amyloid fibril and model of the molecular packing. *EMBO*, 18:815–821, 1999.
- [99] M. R. Sawaya, S. Sambashivan, R. Nelson, M. I. Ivanova, S. A. Sievers, M. I. Apostol, M. J. Thompson, M. Balbirnie, J. J. Wiltzius, H. T. McFarlane, A. O. Madsen, C. Riek, and D. Eisenberg. Atomic structures of amyloid cross-beta spines reveal varied steric zippers. *Nature*, 447(7143):453–7, 2007.
- [100] W. Van Overbeke, A. Verhelle, I. Everaert, O. Zwaenepoel, J. Vandekerckhove, C. Cuvelier, W. Derave, and J. Gettemans. Chaperone nanobodies protect gelsolin against mt1-mmp degradation and alleviate amyloid burden in the gelsolin amyloidosis mouse model. *Mol Ther*, 22(10):1768–78, 2014.
- [101] J. D. Sipe, M. D. Benson, J. N. Buxbaum, S. Ikeda, G. Merlini, M. J. Saraiva, and P. Westermark. Amyloid fibril proteins and amyloidosis: chemical identification and clinical classification international society of amyloidosis 2016 nomenclature guidelines. *Amyloid*, 23(4):209–13, 2016.
- [102] P. Westermark. Aspects on human amyloid forms and their fibril polypeptides. *FEBS J*, 272(23):5942–9, 2005.
- [103] D. M. Fowler, A. V. Koulov, W. E. Balch, and J. W. Kelly. Functional amyloid—from bacteria to humans. *Trends Biochem Sci*, 32(5):217–24, 2007.

- [104] C. Bissig, L. Rochin, and G. van Niel. Pmel amyloid fibril formation: The bright steps of pigmentation. *Int J Mol Sci*, 17(9), 2016.
- [105] B. Watt, D. Tenza, M. A. Lemmon, S. Kerje, G. Raposo, L. Andersson, and M. S. Marks. Mutations in or near the transmembrane domain alter pmel amyloid formation from functional to pathogenic. *PLoS Genet*, 7(9):e1002286, 2011.
- [106] S. Mankar, A. Anoop, S. Sen, and S. K. Maji. Nanomaterials: amyloids reflect their brighter side. *Nano Rev*, 2, 2011.
- [107] C. Li and R. Mezzenga. The interplay between carbon nanomaterials and amyloid fibrils in bio-nanotechnology. *Nanoscale*, 5(14):6207–18, 2013.
- [108] U. O. Seker, A. Y. Chen, R. J. Citorik, and T. K. Lu. Synthetic biogenesis of bacterial amyloid nanomaterials with tunable inorganic-organic interfaces and electrical conductivity. *ACS Synth Biol*, 2016.
- [109] J. Meretoja. Familial systemic paramyloidosis with lattice dystrophy of the cornea, progressive cranial neuropathy, skin changes and various internal symptoms. a previously unrecognized heritable syndrome. *Ann Clin Res*, 1(4):314–24, 1969.
- [110] C. P. Maury, J. Kere, R. Tolvanen, and A. de la Chapelle. Finnish hereditary amyloidosis is caused by a single nucleotide substitution in the gelsolin gene. *FEBS Lett*, 276(1-2):75–7, 1990.
- [111] M. Haltia, F. Prelli, J. Ghiso, S. Kiuru, H. Somer, J. Palo, and B. Frangione. Amyloid protein in familial amyloidosis (finnish type) is homologous to gelsolin, an actin-binding protein. *Biochem Biophys Res Commun*, 167(3):927–32, 1990.
- [112] G. Boysen, G. Galassi, Z. Kamieniecka, J. Schlaeger, and W. Trojaborg. Familial amyloidosis with cranial neuropathy and corneal lattice dystrophy. *J Neurol Neurosurg Psychiatry*, 42(11):1020–30, 1979.
- [113] A. de la Chapelle, J. Kere, Jr. Sack, G. H., R. Tolvanen, and C. P. Maury. Familial amyloidosis, finnish type: G654—a mutation of the gelsolin gene in finnish families and an unrelated american family. *Genomics*, 13(3):898–901, 1992.
- [114] K. J. Park, J. H. Park, J. H. Park, E. B. Cho, B. J. Kim, and J. W. Kim. The first korean family with hereditary gelsolin amyloidosis caused by p.d214y mutation in the gsn gene. *Ann Lab Med*, 36(3):259–62, 2016.
- [115] H. P. Solari, M. P. Ventura, E. Anteck, R. Belfort Junior, and Jr. Burnier, M. N. Danish type gelsolin-related amyloidosis in a brazilian family: case reports. *Arq Bras Oftalmol*, 74(4):286–8, 2011.

- [116] S. Sethi, J. D. Theis, P. Quint, W. Maierhofer, P. J. Kurtin, A. Dogan, and Jr. Highsmith, E. W. Renal amyloidosis associated with a novel sequence variant of gelsolin. *Am J Kidney Dis*, 61(1):161–6, 2013.
- [117] Y. A. Efebera, A. Sturm, E. C. Baack, C. C. Hofmeister, A. Satoskar, T. Nadasdy, G. Nadasdy, D. M. Benson, J. D. Gillmore, P. N. Hawkins, and D. Rowczenio. Novel gelsolin variant as the cause of nephrotic syndrome and renal amyloidosis in a large kindred. *Amyloid*, 21(2):110–2, 2014.
- [118] S. Kiuru. Familial amyloidosis of the finnish type (faf). a clinical study of 30 patients. *Acta Neurol Scand*, 86(4):346–53, 1992.
- [119] J. Meretoja. Genetic aspects of familial amyloidosis with corneal lattice dystrophy and cranial neuropathy. *Clin Genet*, 4(3):173–185, 1973.
- [120] M. Tanskanen, A. Paetau, O. Salonen, T. Salmi, A. Lamminen, P. Lindsberg, H. Somer, and S. Kiuru-Enari. Severe ataxia with neuropathy in hereditary gelsolin amyloidosis. *Amyloid*, pages 1–7, 2009.
- [121] S. Kiuru-Enari and M. Haltia. Hereditary gelsolin amyloidosis. *Handb Clin Neurol*, 115:659–81, 2013.
- [122] A. L. Fernandez, J. M. Herreros, A. M. Monzonis, and A. Panizo. Heart transplantation for finnish type familial systemic amyloidosis. *Scand Cardiovasc J*, 31(6):357–9, 1997.
- [123] C. P. Maury, J. Kere, R. Tolvanen, and A. de la Chapelle. Homozygosity for the asn187 gelsolin mutation in finnish-type familial amyloidosis is associated with severe renal disease. *Genomics*, 13(3):902–3, 1992.
- [124] J. Meretoja. Comparative histopathological and clinical findings in eyes with lattice corneal dystrophy of two different types. *Ophthalmologica*, 165(1):15–37, 1972.
- [125] Winkelman J.E., Delleman J.W., and Ansink B.J.J. Ein hereditares syndrom, bestehend aus peripherer polyneuropathie, hautveränderungen und gettriger dystrophie der hornhaut. *Klin Monatbl Augenheilkd*, (159):6, 1971.
- [126] H. S. Stewart, R. Parveen, A. E. Ridgway, R. Bonshek, and G. C. Black. Late onset lattice corneal dystrophy with systemic familial amyloidosis, amyloidosis v, in an english family. *Br J Ophthalmol*, 84(4):390–4, 2000.
- [127] C. Carrwik and U. Stenevi. Lattice corneal dystrophy, gelsolin type (meretoja's syndrome). *Acta Ophthalmol*, 87(8):813–9, 2009.
- [128] R. J. Luttmann, I. Teismann, I. W. Husstedt, E. B. Ringelstein, and G. Kuhlenbaumer. Hereditary amyloidosis of the finnish type in a german family: clinical and electrophysiological presentation. *Muscle Nerve*, 41(5):679–84, 2010.

- [129] S. Akiya, Y. Nishio, K. Ibi, H. Uozumi, H. Takahashi, T. Hamada, A. Onishi, H. Ishiguchi, Y. Hoshii, and M. Nakazato. Lattice corneal dystrophy type ii associated with familial amyloid polyneuropathy type iv. *Ophthalmology*, 103(7):1106–10, 1996.
- [130] Dottorlovisolo. Typical reticulum appearance of diffused latex dystrophy, February 2017.
- [131] E. Klaus, E. Freyberger, and G. Kavka. Familiäres vorkommen von bulbarparalytischer form der amyotrophischen lateralsklerose mit gittriger hornhautdystrophie und cutis hyperelastica bei drei schwestern. *Psychiatr Neurol*, (138):18, 1959.
- [132] Jr. Sack, G. H., K. W. Dumars, K. S. Gummerson, A. Law, and V. A. McKusick. Three forms of dominant amyloid neuropathy. *Johns Hopkins Med J*, 149(6):239–47, 1981.
- [133] R. Hornigold, A. V. Patel, V. M. Ward, and A. F. O'Connor. Familial systemic amyloidosis associated with bilateral sensorineural hearing loss and bilateral facial palsies. *J Laryngol Otol*, 120(9):778–80, 2006.
- [134] K. Makioka, M. Ikeda, Y. Ikeda, A. Nakasone, T. Osawa, A. Sasaki, T. Otani, M. Arai, and K. Okamoto. Familial amyloid polyneuropathy (finnish type) presenting multiple cranial nerve deficits with carpal tunnel syndrome and orthostatic hypotension. *Neurol Res*, 32(5):472–5, 2010.
- [135] T. Pihlmaa, J. Rautio, S. Kiuru-Enari, and S. Suominen. Gelsolin amyloidosis as a cause of early aging and progressive bilateral facial paralysis. *Plast Reconstr Surg*, 127(6):2342–51, 2011.
- [136] N. Chastan, S. Baert-Desurmont, P. Saugier-veber, G. Derumeaux, A. Cabot, T. Frebourg, and D. Hannequin. Cardiac conduction alterations in a french family with amyloidosis of the finnish type with the p.asp187tyr mutation in the gsn gene. *Muscle Nerve*, 33(1):113–9, 2006.
- [137] S. Kiuru. Gelsolin-related familial amyloidosis, finnish type (faf), and its variants found worldwide. *Amyloid*, 5(1):55–66, 1998.
- [138] Jr. Purcell, J. J., M. Rodrigues, M. I. Chishti, R. N. Riner, and J. M. Dooley. Lattice corneal dystrophy associated with familial systemic amyloidosis (meretoja's syndrome). *Ophthalmology*, 90(12):1512–7, 1983.
- [139] M. R. Ardalan, M. M. Shoja, and S. Kiuru-Enari. Amyloidosis-related nephrotic syndrome due to a g654a gelsolin mutation: the first report from the middle east. *Nephrol Dial Transplant*, 22(1):272–5, 2007.
- [140] J. W. Creemers, R. J. Siezen, A. J. Roebroek, T. A. Ayoubi, D. Huylebroeck, and W. J. Van de Ven. Modulation of furin-mediated proprotein processing activity by site-directed mutagenesis. *J Biol Chem*, 268(29):21826–34, 1993.

- [141] S. S. Molloy, P. A. Bresnahan, S. H. Leppla, K. R. Klimpel, and G. Thomas. Human furin is a calcium-dependent serine endoprotease that recognizes the sequence arg-x-x-arg and efficiently cleaves anthrax toxin protective antigen. *J Biol Chem*, 267(23):16396–402, 1992.
- [142] S. S. Molloy, L. Thomas, J. K. VanSlyke, P. E. Stenberg, and G. Thomas. Intracellular trafficking and activation of the furin proprotein convertase: localization to the tgn and recycling from the cell surface. *EMBO J*, 13(1):18–33, 1994.
- [143] H. Kangas, N. G. Seidah, and T. Paunio. Role of proprotein convertases in the pathogenic processing of the amyloidosis-associated form of secretory gelsolin. *Amyloid*, 9(2):83–7, 2002.
- [144] L. J. Page, J. Y. Suk, M. E. Huff, H. J. Lim, J. Venable, J. Yates, J. W. Kelly, and W. E. Balch. Metalloendoprotease cleavage triggers gelsolin amyloidogenesis. *EMBO J*, 24(23):4124–32, 2005.
- [145] H. Kangas, T. Paunio, N. Kalkkinen, A. Jalanko, and L. Peltonen. In vitro expression analysis shows that the secretory form of gelsolin is the sole source of amyloid in gelsolin-related amyloidosis. *Hum Mol Genet*, 5(9):1237–43, 1996.
- [146] S. Kiuru, K. Javela, H. Somer, and R. Kekomaki. Altered platelet shape change in hereditary gelsolin asp187asn-related amyloidosis. *Thromb Haemost*, 83(3):491–5, 2000.
- [147] J. A. Westberg, K. Z. Zhang, and L. C. Andersson. Regulation of neural differentiation by normal and mutant (g654a, amyloidogenic) gelsolin. *FASEB J*, 13(12):1621–6, 1999.
- [148] L. J. Page, J. Y. Suk, L. Bazhenova, S. M. Fleming, M. Wood, Y. Jiang, L. T. Guo, A. P. Mizisin, R. Kisilevsky, G. D. Shelton, W. E. Balch, and J. W. Kelly. Secretion of amyloidogenic gelsolin progressively compromises protein homeostasis leading to the intracellular aggregation of proteins. *Proc Natl Acad Sci U S A*, 106(27):11125–30, 2009.
- [149] N. A. Taylor, W. J. Van De Ven, and J. W. Creemers. Curbing activation: proprotein convertases in homeostasis and pathology. *FASEB J*, 17(10):1215–27, 2003.
- [150] K. Holmbeck, P. Bianco, J. Caterina, S. Yamada, M. Kromer, S. A. Kuznetsov, M. Mankani, P. G. Robey, A. R. Poole, I. Pidoux, J. M. Ward, and H. Birkedal-Hansen. Mt1-mmp-deficient mice develop dwarfism, osteopenia, arthritis, and connective tissue disease due to inadequate collagen turnover. *Cell*, 99(1):81–92, 1999.
- [151] K. Murphy. *Immunobiology*, volume 8th edition. 2011.
- [152] G. Kohler and C. Milstein. Continuous cultures of fused cells secreting antibody of predefined specificity. *Nature*, 256(5517):495–7, 1975.

- [153] A. Beck, T. Wurch, C. Bailly, and N. Corvaia. Strategies and challenges for the next generation of therapeutic antibodies. *Nat Rev Immunol*, 10(5):345–52, 2010.
- [154] C. Hamers-Casterman, T. Atarhouch, S. Muyldermans, G. Robinson, C. Hamers, E. B. Songa, N. Bendahman, and R. Hamers. Naturally occurring antibodies devoid of light chains. *Nature*, 363(6428):446–8, 1993.
- [155] A. S. Greenberg, D. Avila, M. Hughes, A. Hughes, E. C. McKinney, and M. F. Flajnik. A new antigen receptor gene family that undergoes rearrangement and extensive somatic diversification in sharks. *Nature*, 374(6518):168–73, 1995.
- [156] J. P. Rast, C. T. Amemiya, R. T. Litman, S. J. Strong, and G. W. Litman. Distinct patterns of igh structure and organization in a divergent lineage of chondrichthyan fishes. *Immunogenetics*, 47(3):234–45, 1998.
- [157] S. Muyldermans, T. Atarhouch, J. Saldanha, J. A. Barbosa, and R. Hamers. Sequence and structure of vh domain from naturally occurring camel heavy chain immunoglobulins lacking light chains. *Protein Eng*, 7(9):1129–35, 1994.
- [158] S. Muyldermans. Nanobodies: natural single-domain antibodies. *Annual Review of Biochemistry*, 82:775–797, 2013.
- [159] H. Revets, P. De Baetselier, and S. Muyldermans. Nanobodies as novel agents for cancer therapy. *Expert Opin Biol Ther*, 5(1):111–24, 2005.
- [160] S. Muyldermans, T.N. Baral, P. Retamozzo, E. De Baetselier, J. De Genst, J. Kinne, H. Leonhardt, S. Magez, V.K. Nguyen, H. Revets, U. Rothbauer, B. Stijlemans, S. Tilib, U. Wernery, L. Wyns, G. Hassanzadeh-Ghassabeh, and D. Saerens. Camelid immunoglobulins and nanobody technology. *Vet. Immunol. Immunopathol.*, 128:178–183, 2009.
- [161] M. M. Harmsen, C. B. van Solt, A. M. van Zijderveld-van Bommel, T. A. Niewold, and F. G. van Zijderveld. Selection and optimization of proteolytically stable llama single-domain antibody fragments for oral immunotherapy. *Appl Microbiol Biotechnol*, 72(3):544–51, 2006.
- [162] R. H. van der Linden, L. G. Frenken, B. de Geus, M. M. Harmsen, R. C. Ruuls, W. Stok, L. de Ron, S. Wilson, P. Davis, and C. T. Verrips. Comparison of physical chemical properties of llama vhh antibody fragments and mouse monoclonal antibodies. *Biochim Biophys Acta*, 1431(1):37–46, 1999.
- [163] M. Dumoulin, K. Conrath, A. Van Meirhaeghe, F. Meersman, K. Heremans, L. G. Frenken, S. Muyldermans, L. Wyns, and A. Matagne. Single-domain antibody fragments with high conformational stability. *Protein Sci*, 11(3):500–15, 2002.



- [164] J. M. Perez, J. G. Renisio, J. J. Prompers, C. J. van Platerink, C. Cambillau, H. Darbon, and L. G. Frenken. Thermal unfolding of a llama antibody fragment: a two-state reversible process. *Biochemistry*, 40(1):74–83, 2001.
- [165] S. Ewert, C. Cambillau, K. Conrath, and A. Pluckthun. Biophysical properties of camelid v(hh) domains compared to those of human v(h)3 domains. *Biochemistry*, 41(11):3628–36, 2002.
- [166] K. Conrath, C. Vincke, B. Stijlemans, J. Schymkowitz, K. Decanniere, L. Wyns, S. Muyldermans, and R. Loris. Antigen binding and solubility effects upon the veneering of a camel vhh in framework-2 to mimic a vh. *J Mol Biol*, 350(1):112–25, 2005.
- [167] J.A. Kolkman and D.A. Law. Nanobodies - from llamas to therapeutic proteins. *Drug Discovery Today: Technologies*, (7):139–146, 2010.
- [168] D. Saerens, G. H. Ghassabeh, and S. Muyldermans. Single-domain antibodies as building blocks for novel therapeutics. *Curr Opin Pharmacol*, 8(5):600–8, 2008.
- [169] J. M. van der Vaart. Expression of vhh antibody fragments in *saccharomyces cerevisiae*. *Methods Mol Biol*, 178:359–66, 2002.
- [170] F. Rahbarizadeh, D. Ahmadvand, and Z. Sharifzadeh. Nanobody; an old concept and new vehicle for immunotargeting. *Immunol Invest*, 40(3):299–338, 2011.
- [171] M. Lauwereys, M. Arbabi Ghahroudi, A. Desmyter, J. Kinne, W. Holzer, E. De Genst, L. Wyns, and S. Muyldermans. Potent enzyme inhibitors derived from dromedary heavy-chain antibodies. *EMBO J*, 17(13):3512–20, 1998.
- [172] S. Spinelli, L. G. Frenken, P. Hermans, T. Verrips, K. Brown, M. Tegoni, and C. Cambillau. Camelid heavy-chain variable domains provide efficient combining sites to haptens. *Biochemistry*, 39(6):1217–22, 2000.
- [173] A. Desmyter, S. Spinelli, F. Payan, M. Lauwereys, L. Wyns, S. Muyldermans, and C. Cambillau. Three camelid vhh domains in complex with porcine pancreatic alpha-amylase. inhibition and versatility of binding topology. *J Biol Chem*, 277(26):23645–50, 2002.
- [174] B. Stijlemans, K. Conrath, V. Cortez-Retamozo, H. Van Xong, L. Wyns, P. Senter, H. Revets, P. De Baetselier, S. Muyldermans, and S. Magez. Efficient targeting of conserved cryptic epitopes of infectious agents by single domain antibodies. african trypanosomes as paradigm. *J Biol Chem*, 279(2):1256–61, 2004.
- [175] P. J. Doyle, M. Arbabi-Ghahroudi, N. Gaudette, G. Furzer, M. E. Savard, S. Gleddie, M. D. McLean, C. R. Mackenzie, and J. C. Hall. Cloning, expression, and characterization of a single-domain antibody fragment with affinity for 15-acetyl-deoxynivalenol. *Mol Immunol*, 45(14):3703–13, 2008.

- [176] E. De Genst, K. Silence, K. Decanniere, K. Conrath, R. Loris, J. Kinne, S. Muyldermans, and L. Wyns. Molecular basis for the preferential cleft recognition by dromedary heavy-chain antibodies. *Proc Natl Acad Sci U S A*, 103(12):4586–91, 2006.
- [177] K. B. Vu, M. A. Ghahroudi, L. Wyns, and S. Muyldermans. Comparison of llama vh sequences from conventional and heavy chain antibodies. *Mol Immunol*, 34(16-17):1121–31, 1997.
- [178] C. Vincke, R. Loris, D. Saerens, S. Martinez-Rodriguez, S. Muyldermans, and K. Conrath. General strategy to humanize a camelid single-domain antibody and identification of a universal humanized nanobody scaffold. *J Biol Chem*, 284(5):3273–84, 2009.
- [179] S. Schoonooghe, D. Laoui, J. A. Van Ginderachter, N. Devoogdt, T. Lahoutte, P. De Baetselier, and G. Raes. Novel applications of nanobodies for in vivo bio-imaging of inflamed tissues in inflammatory diseases and cancer. *Immunobiology*, 217(12):1266–72, 2012.
- [180] V. Cortez-Retamozo, M. Lauwereys, G. Hassanzadeh Gh, M. Gobert, K. Conrath, S. Muyldermans, P. De Baetselier, and H. Revets. Efficient tumor targeting by single-domain antibody fragments of camels. *Int J Cancer*, 98(3):456–62, 2002.
- [181] V. Cortez-Retamozo, N. Backmann, P. D. Senter, U. Wernery, P. De Baetselier, S. Muyldermans, and H. Revets. Efficient cancer therapy with a nanobody-based conjugate. *Cancer Res*, 64(8):2853–7, 2004.
- [182] B. M. Tjink, T. Laeremans, M. Budde, M. Stigter-van Walsum, T. Dreier, H. J. de Haard, C. R. Leemans, and G. A. van Dongen. Improved tumor targeting of anti-epidermal growth factor receptor nanobodies through albumin binding: taking advantage of modular nanobody technology. *Mol Cancer Ther*, 7(8):2288–97, 2008.
- [183] I. Vaneycken, M. D’Huyvetter, S. Hernot, J. De Vos, C. Xavier, N. Devoogdt, V. Caveliers, and T. Lahoutte. Immuno-imaging using nanobodies. *Curr Opin Biotechnol*, 22(6):877–81, 2011.
- [184] S. Muyldermans. Single domain camel antibodies: current status. *Reviews in Molecular Biotechnology*, 74:277–302, 2001.
- [185] E. Baranova, R. Fronzes, A. Garcia-Pino, N. Van Gerven, D. Papapostolou, G. Pehau-Arnaudet, and H. Remaut. Sbsb structure and lattice reconstruction unveil ca-triggered s-layer assembly. *Nature*, 487(7405):119–122, 2012.
- [186] V. Tereshko, S. Uysal, A. Koide, K. Margalef, S. Koide, and A.A. Kossiakoff. Toward chaperone-assisted crystallography: protein engineering enhancement of crystal packing and x-ray phasing capabilities of a camelid single-domain antibody (vhh) scaffold. *Protein Science*, 17(7):1175–1187, 2008.

- [187] C. Pain, J. Dumont, and M. Dumoulin. Camelid single-domain antibody fragments: Uses and prospects to investigate protein misfolding and aggregation, and to treat diseases associated with these phenomena. *Biochimie*, 111:82–106, 2015.
- [188] K. Domanska, S. Vanderhaegen, V. Srinivasan, E. Pardon, F. Dupeux, J. A. Marquez, S. Giorgetti, M. Stoppini, L. Wyns, V. Bellotti, and J. Steyaert. Atomic structure of a nanobody-trapped domain-swapped dimer of an amyloidogenic beta2-microglobulin variant. *Proc Natl Acad Sci U S A*, 108(4):1314–9, 2011.
- [189] S. A. Jobling, C. Jarman, M. M. Teh, N. Holmberg, C. Blake, and M. E. Verhoeyen. Immunomodulation of enzyme function in plants by single-domain antibody fragments. *Nat Biotechnol*, 21(1):77–80, 2003.
- [190] V. Delanote, B. Vanloo, M. Catillon, E. Friederich, J. Vandekerckhove, and J. Gettemans. An alpaca single-domain antibody blocks filopodia formation by obstructing I-plastin-mediated f-actin bundling. *FASEB J*, 24(1):105–18, 2010.
- [191] A. Van den Abbeele, S. De Clercq, A. De Ganck, V. De Corte, B. Van Loo, S. H. Soror, V. Srinivasan, J. Steyaert, J. Vandekerckhove, and J. Gettemans. A llama-derived gelsolin single-domain antibody blocks gelsolin-g-actin interaction. *Cell Mol Life Sci*, 67(9):1519–35, 2010.
- [192] I. Van Audenhove, K. Van Impe, D. Ruano-Gallego, S. De Clercq, K. De Muynck, B. Vanloo, H. Verstraete, L. A. Fernandez, and J. Gettemans. Mapping cytoskeletal protein function in cells by means of nanobodies. *Cytoskeleton*, 70(10):604–22, 2013.
- [193] K. Van Impe, J. Bethuyne, S. Cool, F. Impens, D. Ruano-Gallego, O. De Wever, B. Vanloo, M. Van Troys, K. Lambein, C. Boucherie, E. Martens, O. Zwaenepoel, G. Hassanzadeh-Ghassabeh, J. Vandekerckhove, K. Gevaert, L. A. Fernandez, N. N. Sanders, and J. Gettemans. A nanobody targeting the f-actin capping protein capg restrains breast cancer metastasis. *Breast Cancer Res*, 15(6):R116, 2013.
- [194] E. Caussin, O. Kanca, and M. Affolter. Fluorescent fusion protein knockout mediated by anti-gfp nanobody. *Nat Struct Mol Biol*, 19(1):117–21, 2011.
- [195] E. Caussin, O. Kanca, and M. Affolter. Fluorescent fusion protein knockout mediated by anti-gfp nanobody. *Nat Struct Mol Biol*, 19(1):117–121, 2012.
- [196] J. Helma, K. Schmidhals, V. Lux, S. Nuske, A. M. Scholz, H. G. Krausslich, U. Rothbauer, and H. Leonhardt. Direct and dynamic detection of hiv-1 in living cells. *PLoS One*, 7(11):e50026, 2012.
- [197] I. Van Audenhove and J. Gettemans. Use of nanobodies to localize endogenous cytoskeletal proteins and to determine their contribution to cancer cell invasion by using an ecm degradation assay. *Methods Mol Biol*, 1365:225–41, 2016.

- [198] I. Habib, D. Smolarek, C. Hattab, M. Grodecka, G. Hassanzadeh-Ghassabeh, S. Muyldermans, and O. Bertrand. V(h)h (nanobody) directed against human glycophorin a: a tool for autologous red cell agglutination assays. *Anal Biochem*, 438(1):82–89, 2013.
- [199] R.C. Ladenson, D.L. Crimmins, Y. Landt, and J.H. Ladenson. Isolation and characterization of a thermally stable recombinant anti-caffeine heavy-chain antibody fragment. *Anal. Chem.*, 78(13):4501–4508, 2006.
- [200] A.Q. Abbady, A. Al-Daoude, A. Al-Mariri, M. Zarkawi, and S. Muyldermans. Chaperonin groel a brucella immunodominant antigen identified using nanobody and maldi-tof-ms technologies. *Vet. Immunol. Immunopathol.*, 146(3-4):254–263, 2012.
- [201] L. Abo Assali, A. Al-Mariri, E. Hamad, and A.Q. Abbady. Immunodetection of the recombinant groel by the nanobody nbbruc02. *Immunodetection of the recombinant GroEL by the Nanobody NbBruc02.*, 28(10):2987–2995, 2012.
- [202] A. Broisat, J. Toczek, L. S. Dumas, M. Ahmadi, S. Bacot, P. Perret, L. Slimani, G. Barone-Rochette, A. Soubies, N. Devoogdt, T. Lahoutte, D. Fagret, L. M. Riou, and C. Ghezzi. 99mtc-cabvcam1-5 imaging is a sensitive and reproducible tool for the detection of inflamed atherosclerotic lesions in mice. *J Nucl Med*, 55(10):1678–84, 2014.
- [203] S. Put, S. Schoonooghe, N. Devoogdt, E. Schurgers, A. Avau, T. Mitera, M. D’Huyvetter, P. De Baetselier, G. Raes, T. Lahoutte, and P. Matthys. Spect imaging of joint inflammation with nanobodies targeting the macrophage mannose receptor in a mouse model for rheumatoid arthritis. *J Nucl Med*, 54(5):807–14, 2013.
- [204] S. Massa, C. Xavier, J. De Vos, V. Caveliers, T. Lahoutte, S. Muyldermans, and N. Devoogdt. Site-specific labeling of cysteine-tagged camelid single-domain antibody-fragments for use in molecular imaging. *Bioconjug Chem*, 25(5):979–88, 2014.
- [205] C. Xavier, N. Devoogdt, S. Hernot, I. Vaneycken, M. D’Huyvetter, J. De Vos, S. Massa, T. Lahoutte, and V. Caveliers. Site-specific labeling of his-tagged nanobodies with (9)(9)mtc: a practical guide. *Methods Mol Biol*, 911:485–90, 2012.
- [206] K. Coppieters, T. Dreier, K. Silence, H. de Haard, M. Lauwereys, P. Casteels, E. Beirnaert, H. Jonckheere, C. Van de Wiele, L. Staelens, J. Hostens, H. Revets, E. Remaut, D. Elewaut, and P. Rottiers. Formatted anti-tumor necrosis factor alpha vhh proteins derived from camelids show superior potency and targeting to inflamed joints in a murine model of collagen-induced arthritis. *Arthritis Rheum*, 54(6):1856–66, 2006.
- [207] C. May, P. Sapra, and H.P. Gerber. Advances in bispecific biotherapeutics for the treatment of cancer. *Biochem Pharmacol*, 84(9):1105–1112, 2012.

- [208] C. Herrera, J. M. Tremblay, C. B. Shoemaker, and N. J. Mantis. Mechanisms of ricin toxin neutralization revealed through engineered homodimeric and heterodimeric camelid antibodies. *J Biol Chem*, 290(46):27880–9, 2015.
- [209] I. Hmila, D. Saerens, R. Ben Abderrazek, C. Vincke, N. Abidi, Z. Benlasfar, J. Govaert, M. El Ayeb, B. Bouhaouala-Zahar, and S. Muyldermans. A bispecific nanobody to provide full protection against lethal scorpion envenoming. *FASEB J*, 24(9):3479–89, 2010.
- [210] M. M. Harmsen, C. B. Van Solt, H. P. Fijten, and M. C. Van Setten. Prolonged in vivo residence times of llama single-domain antibody fragments in pigs by binding to porcine immunoglobulins. *Vaccine*, 23(41):4926–34, 2005.
- [211] R.C. Roovers, M.J. Vosjan, and T. Laeremans. A biparatopic anti-egfr nanobody efficiently inhibits solid tumour growth. *Int. J. Cancer*, 129(8):2013–2024, 2011.
- [212] M.J. Vosjan, J. Vercammen, J.A. Kolkman, M. Stigter-van Walsum, H. Revets, and G.A. van Dongen. Nanobodies targeting the hepatocyte growth factor: potential new drugs for molecular cancer therapy. *Molecular Cancer Therapy*, 11(4):1017–1025, 2012.
- [213] h E. Sadeqzade, F. Rahbarizadeh, D. Ahmadvand, M.J. Rasaei, L. Parhamifar, and S.M. Moghimi. Combined muc1-specific nanobody-tagged peg-polyethylenimine polyplex targeting and transcriptional targeting of thid transgene for directed killing of muc1 over-expressing tumour cells. *Journal of Controlled Release*, 156(1):85–91, 2011.
- [214] W. Van Overbeke. *Keeping mutant plasma gelsolin safe from harm: gelsolin nanobodies act as a chaperone against pathological proteolysis*. PhD thesis, Ghent University, 2015.
- [215] I. Van Audenhove, N. Debeuf, and J. Boucherie, C. Gettemans. Fascin actin bundling controls podosome turnover and disassembly while cortactin is involved in podosome assembly by its sh3 domain in thp-1 macrophages and dendritic cells. *Biochimica et biophysica acta*, 5(1853):940–952, 2015.
- [216] J. Bethuyne, S. De Gieter, O. Zwaenepoel, A. Garcia-Pino, K. Durinck, A. Verhelle, and J. Gettemans. A nanobody modulates the p53 transcriptional program without perturbing its functional architecture. *Nucleic acids research*, 42(20):12928–38, 2014.
- [217] M.B. Pepys, J. Herbert, W.L. Hutchinson, G.A. Tennent, H.J. Lachmann, J.R. Gallimore, L.B. Lovat, T. Bartfai, A. Alanine, C. Hertel, C. Hoffmann, R.D. Jakob-Roetne, R. and Norcross, J.A. Kemp, K. Yamamura, M. Suzuki, G.W Taylor, S. Murray, D. Thompson, A. Purvis, S. Kolstoe, Wood S.P., and P.N. Hawkins. Targeted pharmacological depletion of serum amyloid p component for treatment of human amyloidosis. *Nature*, 417:254–259, 2002.

- [218] J.D. Gillmore, G.A. Tennent, W.L. Hutchinson, J.R. Gallimore, H.J. Lachmann, H.J. Goodman, M. Offer, D.J. Millard, A. Petrie, P.N. Hawkins, and M.B. Pepys. Sustained pharmacological depletion of serum amyloid p component in patients with systemic amyloidosis. *British Journal of Haematology*, 148(5):760–767, 2010.
- [219] D.B. Richards, L.M. Cookson, A.C. Berges, S.V. Barton, T. Lane, J.M. Ritter, D. Phil, M. Fontana, J.C. Moon, M. Pinzani, Gillmore J.D., P.N. Hawkins, and M.B. Pepys. Therapeutic clearance of amyloid by antibodies to serum amyloid p component. *New England Journal of Medicine*, 373:1106–1114, 2015.
- [220] R. C. Robinson, S. Choe, and L. D. Burtnick. The disintegration of a molecule: the role of gelsolin in faf, familial amyloidosis (finnish type). *Proc Natl Acad Sci U S A*, 98(5):2117–8, 2001.
- [221] J. D. Sipe, M. D. Benson, J. N. Buxbaum, S. Ikeda, G. Merlini, M. J. Saraiva, and P. Westermark. Nomenclature 2014: Amyloid fibril proteins and clinical classification of the amyloidosis. *Amyloid*, 21(4):221–4, 2014.
- [222] R. Bucki, I. Levental, A. Kulakowska, and P. A. Janmey. Plasma gelsolin: function, prognostic value, and potential therapeutic use. *Curr Protein Pept Sci*, 9(6):541–51, 2008.
- [223] S. Sachchithanatham and A. D. Wechalekar. Imaging in systemic amyloidosis. *Br Med Bull*, 107:41–56, 2013.
- [224] J. Helma, M. C. Cardoso, S. Muyldermans, and H. Leonhardt. Nanobodies and recombinant binders in cell biology. *J Cell Biol*, 209(5):633–44, 2015.
- [225] P. Vanlandschoot, C. Stortelers, E. Beirnaert, L. I. Ibanez, B. Schepens, E. Depla, and X. Saelens. Nanobodies(r): new ammunition to battle viruses. *Antiviral Res*, 92(3):389–407, 2011.
- [226] L. O. Gainkam, L. Huang, V. Caveliers, M. Keyaerts, S. Hernot, I. Vaneycken, C. Vanhove, H. Revets, P. De Baetselier, and T. Lahoutte. Comparison of the biodistribution and tumor targeting of two 99mtc-labeled anti-egfr nanobodies in mice, using pinhole spect/micro-ct. *J Nucl Med*, 49(5):788–95, 2008.
- [227] A. M. Loening and S. S. Gambhir. Amide: a free software tool for multimodality medical image analysis. *Mol Imaging*, 2(3):131–7, 2003.
- [228] K. E. Conrath, M. Lauwereys, M. Galleni, A. Matagne, J. M. Frere, J. Kinne, L. Wyns, and S. Muyldermans. Beta-lactamase inhibitors derived from single-domain antibody fragments elicited in the camelidae. *Antimicrob Agents Chemother*, 45(10):2807–12, 2001.

- [229] A. Broisat, S. Hernot, J. Toczek, J. De Vos, L. M. Riou, S. Martin, M. Ahmadi, N. Thielens, U. Wernery, V. Caveliers, S. Muyltermans, T. Lahoutte, D. Fagret, C. Ghezzi, and N. Devoogdt. Nanobodies targeting mouse/human vcam1 for the nuclear imaging of atherosclerotic lesions. *Circ Res*, 110(7):927–37, 2012.
- [230] M. D’Huyvetter, C. Vincke, C. Xavier, A. Aerts, N. Impens, S. Baatout, H. De Raeve, S. Muyltermans, V. Caveliers, N. Devoogdt, and T. Lahoutte. Targeted radionuclide therapy with a <sup>177</sup>Lu-labeled anti-her2 nanobody. *Theranostics*, 4(7):708–20, 2014.
- [231] A. Srivastava, P. Arya, S. Goel, B. Kundu, P. Mishra, and A. Fnu. Gelsolin amyloidogenesis is effectively modulated by curcumin and emetine conjugated plga nanoparticles. *PLoS One*, 10(5):e0127011, 2015.
- [232] C. G. Clement and L. D. Truong. An evaluation of congo red fluorescence for the diagnosis of amyloidosis. *Hum Pathol*, 45(8):1766–72, 2014.
- [233] K. De Groeve, N. Deschacht, C. De Koninck, V. Caveliers, T. Lahoutte, N. Devoogdt, S. Muyltermans, P. De Baetselier, and G. Raes. Nanobodies as tools for in vivo imaging of specific immune cell types. *J Nucl Med*, 51(5):782–9, 2010.
- [234] B. Dorresteyn, M. Rotman, D. Faber, R. Schravessande, E. Suidgeest, L. van der Weerd, S. M. van der Maarel, C. T. Verrips, and M. El Khattabi. Camelid heavy chain only antibody fragment domain against beta-site of amyloid precursor protein cleaving enzyme 1 inhibits beta-secretase activity in vitro and in vivo. *FEBS J*, 282(18):3618–31, 2015.
- [235] M. Pruszynski, E. Koumariou, G. Vaidyanathan, H. Revets, N. Devoogdt, T. Lahoutte, and M. R. Zalutsky. Targeting breast carcinoma with radioiodinated anti-her2 nanobody. *Nucl Med Biol*, 40(1):52–9, 2013.
- [236] J. De Vos, I. Mathijs, C. Xavier, S. Massa, U. Wernery, L. Bouwens, T. Lahoutte, S. Muyltermans, and N. Devoogdt. Specific targeting of atherosclerotic plaques in apoe(-/-) mice using a new camelid sdab binding the vulnerable plaque marker lox-1. *Mol Imaging Biol*, 16(5):690–8, 2014.
- [237] A. Blykers, S. Schoonooghe, C. Xavier, K. D’Hoe, D. Laoui, M. D’Huyvetter, I. Vaneycken, F. Cleeren, G. Bormans, J. Heemskerk, G. Raes, P. De Baetselier, T. Lahoutte, N. Devoogdt, J. A. Van Ginderachter, and V. Caveliers. Pet imaging of macrophage mannose receptor-expressing macrophages in tumor stroma using <sup>18</sup>F-radiolabeled camelid single-domain antibody fragments. *J Nucl Med*, 56(8):1265–71, 2015.
- [238] A. Muruganandam, J. Tanha, S. Narang, and D. Stanimirovic. Selection of phage-displayed llama single-domain antibodies that transmigrate across human blood-brain barrier endothelium. *FASEB J*, 16(2):240–2, 2002.

- [239] A. Abulrob, H. Sprong, P. Van Bergen en Henegouwen, and D. Stanimirovic. The blood-brain barrier transmigrating single domain antibody: mechanisms of transport and antigenic epitopes in human brain endothelial cells. *J Neurochem*, 95(4):1201–14, 2005.
- [240] K. S. Rutgers, R. J. Nabuurs, S. A. van den Berg, G. J. Schenk, M. Rotman, C. T. Verrips, S. G. van Duinen, M. L. Maat-Schieman, M. A. van Buchem, A. G. de Boer, and S. M. van der Maarel. Transmigration of beta amyloid specific heavy chain antibody fragments across the in vitro blood-brain barrier. *Neuroscience*, 190:37–42, 2011.
- [241] B. L. Franc, P. D. Acton, C. Mari, and B. H. Hasegawa. Small-animal spect and spect/ct: important tools for preclinical investigation. *J Nucl Med*, 49(10):1651–63, 2008.
- [242] C. Xavier, I. Vaneycken, M. D’Huyvetter, J. Heemskerk, M. Keyaerts, C. Vincke, N. Devoogdt, S. Muyltermans, T. Lahoutte, and V. Caveliers. Synthesis, preclinical validation, dosimetry, and toxicity of 68ga-nota-anti-her2 nanobodies for ipet imaging of her2 receptor expression in cancer. *J Nucl Med*, 54(5):776–84, 2013.
- [243] M. Keyaerts, C. Xavier, J. Heemskerk, N. Devoogdt, H. Everaert, C. Ackaert, M. Vanhoeij, F. P. Duhoux, T. Gevaert, P. Simon, D. Schallier, C. Fontaine, I. Vaneycken, C. Vanhove, J. De Greve, J. Lamote, V. Caveliers, and T. Lahoutte. Phase i study of 68ga-her2-nanobody for pet/ct assessment of her2 expression in breast carcinoma. *J Nucl Med*, 57(1):27–33, 2016.
- [244] C. Cecchi and M. Stefani. The amyloid-cell membrane system. the interplay between the biophysical features of oligomers/fibrils and cell membrane defines amyloid toxicity. *Biophys Chem*, 182:30–43, 2013.
- [245] F. Bemporad and F. Chiti. Protein misfolded oligomers: experimental approaches, mechanism of formation, and structure-toxicity relationships. *Chem Biol*, 19(3):315–27, 2012.
- [246] J. Ghiso, M. Haltio, F. Prelli, J. Novello, and B. Frangione. Gelsolin variant (asn-187) in familial amyloidosis, finnish type. *Journal of Biochemistry*, 15(3):827–830, 1990.
- [247] S. Nag, Q. Ma, S. Wang, H. an Chumnarnsilpa, W.L. Lee, M. Larsson, B. Kannan, M. Hernandez-Valladares, L.D. Burtnick, and R.C. Robinson. Ca<sup>2+</sup> binding by domain 2 plays a critical role in the activation and stabilization of gelsolin. *Proceedings of the National Academy of Sciences of the United States of America*, 106(33):13713–13718, 2009.
- [248] D. Duan. Systemic delivery of adeno-associated viral vectors. *Currunt opinion in virology*, 21:16–25, 2016.
- [249] D.R. Deyle and D.W. Russel. Adeno-associated virus vector integration. *Curr Opin Mol Ther*, 11(4):442–447, 2009.



- [250] L.J. Chang. Vector integration: Pest not guest. *Gene therapy*, (10):193–194, 2002.
- [251] A. Verhelle, W. Van Overbeke, C. Peleman, R. De Smet, O. Zwaenepoel, T. Lahoutte, J. Van Dorpe, N. Devoogdt, and J. Gettemans. Non-invasive imaging of amyloid deposits in a mouse model of agel using 99mtc-modified nanobodies and spect/ct. *Molecular Imaging and Biology*, 18(6):887–897, 2016.
- [252] M. Y. Rincon, S. Sarcar, D. Danso-Abeam, M. Keyaerts, J. Matrai, E. Samara-Kuko, A. Acosta-Sanchez, T. Athanasopoulos, G. Dickson, T. Lahoutte, P. De Bleser, T. VandenDriessche, and M. K. Chuah. Genome-wide computational analysis reveals cardiomyocyte-specific transcriptional cis-regulatory motifs that enable efficient cardiac gene therapy. *Mol Ther*, 23(1):43–52, 2015.
- [253] C. Zincarelli, S. Soltys, G. Rengo, and Rabinowitz J.E. Analysis of aav serotypes 1-9 mediated gene expression and tropism in mice after systemic injection. *Molecular Therapy*, 16(6):1073–1080, 2008.
- [254] T. Vandendriessche, L. Thorrez, A. Acosta-Sanchez, I. Petrus, L. Wang, L. Ma, L. De Weaele, Y. Iwasaki, V. Gillijns, J.M. Wilson, D. Collen, and M.K. Chuah. Efficacy and safety of adeno-associated viral vectors based on serotype 8 and 9 vs. lentiviral vectors for hemophilia b gene therapy. *Journal of thrombosis and haemostasis*, 5(1):16–24, 2007.
- [255] N. Nair, M.Y. Rincon, H. Evans, S. Sarcar, S. Dastidar, E. Samaru-Kuko, O. Ghandeharian, H. Man Viecelli, B. Thöny, P. De Bleser, T. VandenDriessche, and M.K. Chuah. Computationally designed liver-specific transcriptional modules and hyperactive factor ix improve hepatic gene therapy. *Blood*, 123(20):3195–3199, 2014.
- [256] I. Everaert, S. Stegen, B. Vanheel, Y. Taes, and W. Derave. Effect of beta-alanine and carnosine supplementation on muscle contractility in mice. *Medicine and science in sports and exercise*, 45(1):43–51, 2013.
- [257] A. Jabaiah and P.S. Daugherty. Directed evolution of protease beacons that enable sensitive detection of endogenous mt1-mmp activity in tumor cell lines. *Chemistry and Biology*, 18(3):392–401, 2011.
- [258] B. Rasowo, S. Shilpita, S. Ermira, M. Chuah, and T. VandenDriessche. Development of novel muscle-specific adeno-associated viral vector constructs for gene therapy of duchenne muscular dystrophy. *European Scientific Journal*, 10(18):23–37, 2014.
- [259] L.T. Bish, K. Morine, M.M. Sleeper, J. Sanmiguel, D. Wu, G. Gao, J.M. Wilson, and H.L. Sweeney. Adeno-associated virus (aav) serotype 9 provides global cardiac gene transfer superior to aav1, aav6, aav7, and aav8 in the mouse and rat. *Human gene therapy*, 19(12):1359–1368, 2008.

- [260] G.P. Gao, M.R. Alvira, L. Wang, R. Calcedo, J. Johnston, and J.M. Wilson. Novel adeno-associated viruses from rhesus monkeys as vectors for human gene therapy. *Proceedings of the National Academy of Sciences of the United States of America*, 99(18):11854–11859, 2002.
- [261] J. Mendell, S. Al Zaidy, R. Shell, W. Arnold, L. Rodino Klapac, J. Kissel, T. Prior, C. Miranda, L. Lowes, and L. Alfona. Gene therapy for spinal muscular atrophy type 1 shows potential to improve survival and motor functional outcomes. *Molecular therapy: the journal of the American Society of Gene Therapy*, 24, 2016.
- [262] V. Louis Jeune, J.A. Joergensen, R.J. Hajjar, and T. Weber. Pre-existing anti-adeno-associated virus antibodies as a challenge in aav gene therapy. *Human gene therapy methods*, 24(2):59–67, 2013.
- [263] N. Mahesri, J.T. Koerber, B.K. Kaspar, and D.V. Schaffer. Directed evolution of adeno-associated virus yields enhanced gene delivery vectors. *Nature Biotechnology*, 24(2):198–204, 2006.
- [264] D. Grimm, J.S. Lee, L. Wang, T. Desai, B. Akache, T.A. Storm, and M.A. Kay. In vitro and in vivo gene therapy vector evolution via multispecies interbreeding and retargeting of adeno-associated viruses. *Journal of Virology*, 82(12):5887–5991, 2008.
- [265] N. Pulicherla, S. Shen, S. Yadav, K. Debbink, L. Govindasamy, M. Agbandje-McKenna, and A. Asokan. Engineering liver-detargeted aav9 vectors for cardiac and musculoskeletal gene transfer. *Molecular therapy*, 19(6):1070–1078, 2011.
- [266] S. Shen, K.D. Bryant, J. Sun, S.M. Brown, A. Troupes, N. Pulicherla, and A. Asokan. Glycan binding avidity determines the systemic fate of adeno-associated virus type 9. *Journal of virology*, 86(19):10408–10417, 2012.
- [267] S. Shen, E.D. Horowitz, A.N. Troupes, S.M. Brown, N. Pulicheria, R.J. Samulski, M. Agbandje-McKenna, and A. Asokan. Engraftment of a galactose receptor footprint onto adeno-associated viral capsids improves transduction efficiency. *The journal of biological chemistry*, 288(40):28814–28823, 2013.
- [268] M.B. Pepys, L.M. Cookson, S.V. Barton, A.C. Berges, T. Lane, D. Hutt, M. Fontana, J.C. Moon, J.D. Gillmore, A. Weckalekar, P.N. Hawkins, and D.B. Richards. Dose-dependent progressive immunotherapeutic clearance of systemic amyloid deposits by repeated doses of antibody to serum amyloid p component. *Blood*, 126(23):1836–1836, 2015.
- [269] A. J. Roebroek, L. Uman, I. G. Pauli, Robertson E. J., F. van Leuvan, W. J. Van de Van, and D. B. Constam. Failure of ventral closure and axial rotation in embryos lacking the proprotein convertase furin. *Development*, 125(24):4863–4876, 1998.

- [270] L. De Vos, J. Declercq, G.G. Rosas, B. Van Damme, A. Roebroek, F. Vermorken, J. Ceuppens, W. van de Ven, and J. Creemers. Mmtv-cre-mediated fur inactivation concomitant with *plag1* proto-oncogene activation delays salivary gland tumorigenesis in mice. *Int. J. Oncol.*, 32:1073–1083, 2008.
- [271] R. Essalmani, D. Susan-Resiga, A. Chamberland, M. Abifadel, J.W. Creemers, C. Boileau, N.G. Seidah, and A. Prat. In vivo evidence that furin from hepatocytes inactivates pcsk9. *J. Biol. Chem.*, 186:4257–4263, 2011.
- [272] E. Louagie, N.A. Taylor, D. Flamez, A.J.M. Roebroek, N.A. Bright, S. Meulemans, R. Quintens, P.L. Herrera, F. Schuit, W.J.M. van de Ven, and J.W.M. Creemers. Role of furin in granular acidification in the endocrine pancreas: identification of the v-atpase subunit ac45 as a candidate substrate. *Proc. Natl. Acad. Sci. U.S.A.*, 105:12319–12324, 2008.
- [273] M. Pesu, W.T. Watford, L. Wei, L.L. Xu, I. Fuss, W. Strober, J. Andersson, E.M. Shevach, M. Quezado, and N. Bouladoux. T-cell-expressed proprotein convertase furin is essential for maintenance of peripheral immune tolerance. *Nature*, 455:u246–u273, 2008.
- [274] S. Kumar and J. Walter. Phosphorylation of amyloid beta peptides – a trigger for formation of toxic aggregates in alzheimer's disease. *Aging*, 3(8):803–812, 2011.
- [275] W.C. Eckelman. Unparalleled contribution of technetium-99m to medicine over 5 decades. *JACC Cardiovascular imaging*, 2(3):364–368, 2009.
- [276] A. Donsante, D.G. Miller, Y. Li, C. Vogler, E.M. Brunt, D.E. Russell, and M.S. Sands. Aav vector integration sites in mouse hepatocellular carcinoma. *Science*, 317(5837):477, 2007.
- [277] S. Mehrle, V. Rohde, and J.R. Schlehofer. Evidence of chromosomal integration of aav dna in human testis tissue. *Virus Genes*, 28(1):61–69, 2004.
- [278] A.M. Maguire, F. Simonelli, E.A. Pierce, E.N. Pugh, F. Mingozzi, J. Bennicelli, S. Banfi, K.A. Marshal, F. Testa, E.M. Surace, S. Rossi, A. Lyubarsky, V.R. Arruda, B. Konkle, E. Stone, J. Sun, J. Jacobs, L. Dell'Osso, R. Hertle, J. Ma, T.M. Redmond, X. Zhu, B. Hauck, O. Zeleniaia, K.S. Schindler, M.G. Maguire, J.F. Wright, J.N. Volpe, J. Wellman, A. Auricchio, K.A. High, and J. Bennet. Safety and efficacy of gene transfer for leber's congenital amaurosis. *N. Engl. J. Med.*, 358(21):2240–2248, 2008.
- [279] J.W. Bainbridge, A.J. Smith, S.S. Barker, S. Robbie, R. Henderson, K. Balaggan, A. Viswanathan, G.E. Holder, A. Stockman, N. Tyler, S. Petersen-Jones, S.S. Bhattacharya, A.J. Thrasher, F.W. Fitzke, B.J. Carter, G.S. Rubin, A.T. Moore, and R.R. Ali. Effect of gene therapy on visual function in leber's congenital amaurosis. *N. Engl. J. Med.*, 358(21):2231–2239, 2008.

- [280] W.W. Hauswirth, T.S. Aleman, S. Kaushal, A.V. Cideciyan, S.B. Schwartz, L. Wang, T.J. Conlon, S.L. Boye, T.R. Flotte, B.J. Byrne, and S.G. Jacobson. Treatment of leber congenital amaurosis due to rpe65 mutations by ocular subretinal injection of adeno-associated virus gene vector: Short-term results of a phase i trial. *Hum. Gene. Ther.*, 19(10):979–990, 2008.
- [281] L.J. Scott. Alipogene tiparvec :a review of its use in adults with familial lipoprotein lipase deficiency. *Drugs*, 75:175–182, 2015.
- [282] P. Leone, D. Shera, S.W. Mcphee, J.S. Francis, E.H. Kolodny, and L.T. Bilaniuk. Long-term follow-up after gene therapy for canavan disease. *Science Translational Medicine*, 4(165).
- [283] M.G. Kaplitt, A. Feigin, C. Tang, P. Fitzsimons, H.L. and Mattis, and P.A. Lawlor. Safety and tolerability of gene therapy with an adeno-associated virus (aav) borne gad gene for parkinson's disease: an open label, phase i trial. *Lancet*, 369(9579):2097–2105, 2007.
- [284] R.M. Richardson, A.P. Kells, E.A. Rosenbluth, K.H. and Salegio, M.S. Fiandaca, and P.S. Larson. Interventional mri-guided putaminal delivery of aav2-gdnf for planned clinical trial in parkinson's disease. *Mol. Ther.*, 19(6):1048–1057, 2011.
- [285] R.T. Bartus, T.L. Baumann, C.D. Siffert, J. and Herzog, R. Alterman, and N. Boulis. Safety/feasibility of targeting the substantia nigra with aav2-neurturin in parkinson patients. *Neurology*, 80(18):1698–1701, 2013.
- [286] M.S. Rafii, T.L. Baumann, R.A. Bakay, J.M. Ostrove, J. Siffert, and A.S. Fleisher. A phase i study of stereotactic gene delivery of aav2-ngf for alzheimer's disease. *Alzheimers Dement.*, 10(5):571–581, 2014.
- [287] M. Tardieu, M. Zerah, S. Husson, B. and DeBournonville, K. Deiva, and C. Adamsbaum. Intracerebral administration of adeno-associated viral vector serotype rh.10 carrying human sgsh and sumf1 cdnas in children with mucopolysaccharidosis type iiia disease: results of a phase i/ii trial. *Hum. Gene. Ther.*, 25(6):506–516, 2014.
- [288] A.C. Nathwani, U.M. Reiss, E.G. Tuddenham, C. Rosales, P. Chowdary, and J. McIntosh. Long-term safety and efficacy of factor ix gene therapy in hemophilia b. *N. Engl. J. Med.*, 371(21):1994–2004, 2014.
- [289] D.F. Aschauer, S. Kreuz, and S. Rumpel. Analysis of transduction efficiency, tropism and axonal transport of aav serotypes 1, 2, 5, 6, 8 and 9 in the mouse brain. *PLoS One*, 8(9):e76310, 2013.
- [290] M.R. Mason, E.M. Ehlert, R Eggers, C.W. Pool, S. Hermening, A. Huseinovic, E. Timmermans, B. Blits, and J. Verhaagen. Comparison of aav serotypes for gene delivery to dorsal root ganglion neurons. *Molecular therapy*, 18(4):715–724, 2010.

- [291] A.L. Peel, S. Zolotukhin, G.W. Schrimsher, N. Muzyczka, and P.J. Reier. Efficient transduction of green fluorescent protein in spinal cord neurons using adeno-associated virus vectors containing celltype-specific promoters. *Gene Therapy*, 4:16–24, 1997.
- [292] B. Blits, T.P. Carlstedt, M.J. Ruitenbergh, W.T. de Winter, F. and Hermens, and P.A. Dijkhuizen. Rescue and sprouting of motoneurons following ventral root avulsion and reimplantation combined with intraspinal adeno-associated viral vector-mediated expression of glial cell line-derived neurotrophic factor or brain-derived neurotrophic factor. *Experimental Neurology*, 189:303–316, 2004.
- [293] B.R. Snyder, E.T. Gray, S.J. and Quach, J.W. Huang, C.H. Leung, and R.J. Samulski. Comparison of adeno-associated viral vector serotypes for spinal cord and motor neuron gene delivery. *Human Gene Therapy*, 22:1129–1135, 2011.
- [294] J. Homs, L. Ariza, G. Pagès, E. Udina, X. Navarro, and M. Chillón. Schwann cell targeting via intrasciatic injection of aav8 as gene therapy strategy for peripheral nerve regeneration. *Gene Ther.*, 18:622–630, 2011.
- [295] J. Hordeaux, L. Dubreil, J. Deniaud, F. Iacobelli, S. Moreau, and M. Ledevin. Efficient central nervous system aavrh10-mediated intrathecal gene transfer in adult and neonate rats. *Gene Ther.*, 22:316–324, 2014.
- [296] S. Kiuru-Enari, H. Somer, A.M. Seppäläinen, I.L. Notkola, and M. Haltia. Neuromuscular pathology in hereditary gelsolin amyloidosis. *J. Neuropathol. Exp. Neurol.*, 61(6):565–571, 2002.
- [297] A.W. Nienhuis, A.C. Nathwani, and A.M. Davidoff. Gene therapy for hemophilia. *Molecular therapy*, 25(5):1163–1167, 2017.
- [298] S. Kasturirangan, L. Li, S. Emadi, S. Boddapati, P. Schulz, and M.R. Sierks. Nanobody specific for oligomeric beta-amyloid stabilizes nontoxic form. *Neurobiology of Aging*, 19(3):315–327, 2012.
- [299] M. Dumoulin, A. M. Last, A. Desmyter, K. Decanniere, D. Canet, G. Larsson, A. Spencer, D. B. Archer, J. Sasse, S. Muyldermans, L. Wyns, C. Redfield, A. Matagne, C. V. Robinson, and C. M. Dobson. A camelid antibody fragment inhibits the formation of amyloid fibrils by human lysozyme. *Nature*, 424(6950):783–8, 2003.
- [300] M. Arbabi Ghahroudi, A. Desmyter, L. Wyns, R. Hamers, and S. Muyldermans. Selection and identification of single domain antibody fragments from camel heavy-chains antibodies. *FEBS letters*, 414(3):521–526, 1997.
- [301] G. V. Kryukov, S. Castellano, S. V. Novoselov, A. V. Lobanov, O. Zehtab, R. Guigo, and V. N. Gladyshev. Characterization of mammalian selenoproteomes. *Science*, 300(5624):1439–43, 2003.

- [302] K. Meerschaert, V. De Corte, Y. De Ville, J. Vandekerckhove, and J. Gettemans. Gelsolin and functionally similar actin-binding proteins are regulated by lysophosphatidic acid. *EMBO J*, 17(20):5923–32, 1998.
- [303] S. G. Rasmussen, B. T. DeVree, Y. Zou, A. C. Kruse, K. Y. Chung, T. S. Kobilka, F. S. Thian, P. S. Chae, E. Pardon, D. Calinski, J. M. Mathiesen, S. T. Shah, J. A. Lyons, M. Caffrey, S. H. Gellman, J. Steyaert, G. Skinotis, W. I. Weis, R. K. Sunahara, and B. K. Kobilka. Crystal structure of the beta2 adrenergic receptor-gs protein complex. *Nature*, 477(7366):549–55, 2011.
- [304] A.J. Roebroek, N.A. Taylor, E. Louagie, I. Pauli, L. Smeijers, A. Snellinx, A. Lauwers, W.J. Van de Ven, D. Hartmann, and J.W. Creemers. Limited redundancy of the proprotein convertase furin in mouse liver. *J. Biol. Chem.*, 279:53442–53450, 2004.
- [305] I. Vaneycken, N. Devoogdt, N. Van Gassen, C. Vincke, C. Xavier, U. Wernery, S. Muyl-dermans, T. Lahoutte, and V. Caveliers. Preclinical screening of anti-her2 nanobodies for molecular imaging of breast cancer. *FASEB J*, 25(7):2433–46, 2011.
- [306] H. L. Yin, J. H. Albrecht, and A. Fattoum. Identification of gelsolin, a  $Ca^{2+}$ -dependent regulatory protein of actin gel-sol transformation, and its intracellular distribution in a variety of cells and tissues. *J Cell Biol*, 91(3 Pt 1):901–6, 1981.

# PART VI

DANKWOORD





# Bedankt!

Het dankwoord, wat we onszelf ook proberen wijsmaken tijdens het schrijven van een doctoraat, het is en blijft het onderdeel dat finaal het snelst en meest frequent gelezen zal worden. Indien u behoort tot de groep lezers die bij het bemachtigen van dit manuscript meteen naar dit onderdeel doorbladerde, bedankt. Indien u echter eerst de tijd nam (of dit nog van plan bent) om ook de wetenschappelijke hoofdbrok door te nemen, eveneens bedankt. Want, wat voor lezer u ook bent, het feit dat u in het bezit bent gekomen van een kopie betekent hoogstwaarschijnlijk dat u op de één of andere manier, zij het direct of indirect hebt bijgedragen aan de verwezenlijking van mijn doctoraat. Hiervoor dan ook mijn oprechte dank.

Toch had ik ook graag enkele mensen persoonlijk bedankt omdat hun bijdrage er bovenuit springt of omdat zonder hen dit doctoraat nooit mogelijk was geweest. Vooreerst wil ik mijn promotor, Jan Gettemans bedanken. Jan, de voorbije jaren had ik steeds het gevoel dat je vertrouwen had in mijn capaciteiten en je, indien nodig, telkens begripvol en rationeel bijstuurde. De vele uren die je investeerde in het verbeteren van beursaanvragen, wetenschappelijke posters, publicaties en finaal dit manuscript waren onontbeerlijk en niet vanzelfsprekend.

Vervolgens wil ik ook alle co-auteurs die hebben bijgedragen aan de wetenschappelijke publicaties nog eens extra bedanken. Cindy Peleman, Nick Devoogdt en Tony Lahoutte van het ICMI labo van de VUB, om mij in te leiden in de wereld van moleculaire beeldvorming. Rebecca De Smet, Lynn Supply en Jo Van Dorpe van het departement pathologie UZ Gent voor de vele uren geïnvesteerd in het maken van de prachtige weefselcoupes. Nisha Nair, Marinee Chuah en Thierry VandenDriessche van het departement genterapie en regeneratieve geneeskunde VUB voor het creëren en implementeren van het AAV9-Nb virus. Inge Everaert en Wim Derave van het departement beweging- en sportwetenschappen UGent voor de vele dissectieuren en spieranalyses die uitgevoerd werden op de AGel muizen. Co-auteurs, zonder jullie bereidheid om jullie kennis met mij te delen en tijd te willen investeren om mijn wensen om te zetten naar doenbare experimenten was er van dit doctoraat geen sprake geweest. Bedankt!

Als laatste groep binnen de pure academische setting had ik graag mijn juryleden bedankt. Bruno Verhasselt, Elke Decrock, Els Van Damme, Sophie Hernot, Lennart Zabeau en Patrick Santens, jullie kozen er allemaal vrijwillig voor om tijd en moeite te steken in dit doctoraat. Hiervoor mijn oprechte dank. De verschillende opmerkingen hebben dit manuscript naar een hoger niveau getild! Alsook deed het deugd om tijdens de verdediging nog eens te kunnen discussiëren over

de uitgevoerde experimenten en de bekomen resultaten. Jullie kritisch denken zorgde voor een aangename nieuwe invalshoek op het geleverde werk tijdens dit doctoraat.

Uiteraard is dit doctoraat niet enkel en alleen het resultaat van pure, harde wetenschap. De omkadering doorheen de afgelopen 4 jaar zorgde er telkens voor dat de mindere momenten konden overwonnen worden en de piekmomenten gevierd. In eerste instantie wil ik dan ook mijn collega's bedanken die vanop de eerste linie dit avontuur mee hebben beleefd. Bureau boven, doorheen de jaren bestaande uit Ariane, Katrien, Sarah, Ciska, Isabel, Kevin, Laurence, Anneleen en Tim. Alhoewel ik op termijn besepte dat geluid vanuit het nanodrop/ITC lokaal tot boven hoorbaar was, kon ik toch de vele schaterlachen en vloekbuien niet onderdrukken. Ik hoop dat ze ook voor jullie even ontstressend werkten als voor mij. Bureau beneden; Wouter, Jonas, Oliver, Thijs en Els, in jullie directe gezelschap werd elk dood moment meteen opgevuld met de nodige levenswijsheden en woordspelingen. Oorspronkelijk was ons geliefde bureau een mannenbastion, bruisend van de vunzige praat en ongegeneerde conversaties over de meest uiteenlopende onderwerpen. Met de komst van de bedeesde Els leek hieraan abrupt een einde te komen. Alhoewel, reeds snel ontpopte ze zich tot de typische, hardhuidse West-Vlaming die ze is, eiste ze haar plaats op in de pikorde (boven mij!) en nam ze actief deel aan de 'mannenklap'. Prachtig!

Collega's, naast het lief en leed dat we deelden in het labo zullen vooral de minder wetenschappelijke momenten mij bijblijven. De kerstfeestjes, lichtpunten in de éénzame donkere wintermaanden steeds voorzien van de ideale hoeveelheid drank, spijs en entertainment. De traktaties, elke reden was een goeie reden; publicatie, verjaardag, verhuizen, samenwonen,...het moest gevierd worden. De ontbijtmomenten, omdat het kon! De departementele BBQ, nieuwjaarsreceptie en andere doctoraatrecepties die steeds gebruikt werden als uitlaatklep voor alle frustraties over 'den UGent'. De bijna dagelijkse bezoeken aan de SPAR, een noodzakelijk ontspanningsmoment op veel dagen! Daarenboven heb ik het labo ook verlaten met een enorm berg aan levenslessen en wijsheden. Vooreerst, het leven is een stront, je moet er gewoon durven in trappen/bijten! Want het is nu éénmaal een *dog eat dog world* en *science is a bitch!* Als je moe bent is 'het schaap de preute af' en als je klaar bent is 'het spel hespe'. The Doors maken blijkbaar al lang geen nieuwe albums meer maar de soap Thuis is wel nog steeds razendpopulair onder de jeugd?!

Een speciale vermelding voor de collega's behorende tot team eiland is toch wel op zijn plaats. Oorspronkelijk bestaande uit Olivier, Jonas en Wouter tot ik als langharige, blonde snottekeise erbij kwam. Sorry gasten dat ik jullie idee van een blonde, vrouwelijke thesisstudente abrupt de vuilbak in kieperde. Desondanks namen jullie mij meteen volledig op in het team. Geen enkel moment heb ik mij verveeld met jullie aan het eiland.

Wouter, van alle collega's ben jij toch wel diegene die een individuele merci verdient. Als thesisbegeleider leerde je mij vol geduld alle kneepjes van het vak. Serieus, ik heb tot op de dag van vandaag nog geen enkel ander persoon tegengekomen die zo'n eindeloos geduld heeft en frustratie zo vakkundig kan wegwerken voor de medemens. Bedankt dat je mij inleidde in de wondere wereld van het wetenschappelijk onderzoek, de eerste stap richting dit doctoraat. In de daarop volgende jaren was je eveneens de persoon bij uitstek waarbij ik terecht kon met allerhande

vragen en frustraties. Indien een doctoraat een co-auteur kon hebben, stond jouw naam eveneens op deze cover!

Buiten de muren van het Rommelaere complex stonden er eveneens een hele hoop mensen voor mij klaar de voorbije jaren. Eerst en vooral mijn ouders en familie. Bedankt ma, pa en Sander voor het steeds aanwezige luisterende oor gedurende dit grootse UGent avontuur. Steeds was geen enkele moeite jullie teveel om tijdens de moeilijkere (examen)periodes in de bres te springen en alles net dat tikkeltje dragelijker te maken. Ik zeg het nog steeds te weinig, maar jullie hulp werd en wordt steeds geapprecieerd. Evenzeer een dankuwel richting mijn mems, tantes, nonkels, neven en nichten die op elke familiegelegenheid polsten of alles nog steeds vlot verliep aan de UGent.

Bio-ir vriendjes! Eva, Kaat, Bieke, Laurens en Steffie, jullie snapten als geen ander waarom sommige zaken zo frustrerend kunnen zijn en wat er nodig was om die door te komen. Exact; eten, drank en eens goed kunnen zagen over hoe verschrikkelijk irritant de gemiddelde medemens wel niet kan zijn. Het doet mij deugd dat we deze traditie tot op de dag van vandaag nog steeds in ere houden.

Mede Izegemnaren, woorden schieten tekort om jullie significantie te beschrijven! Sinds onze eerste dag in deze studentenstad zijn we door lief en leed extra naar elkaar toegegroeid. We hebben dit avontuur samen beleefd. Een ervaring die niemand ons ooit nog kan afnemen en waar we de komende decennia nog vrij frequent op zullen terugblikken met de nodige nostalgie. Maar het doet mij evenzeer deugd dat we, eenmaal afgestudeerd, gewoon verder bleven en blijven gaan met het maken van prachtige herinneringen! 'Gang', de onverwoestbare vriendschap die ik onder ons voel is voor mij van onschatbare waarde.

Ondanks de trots die ik voel betreffende deze academische verwezenlijking weegt ze niet op tegen de spreekwoordelijke kers op de taart van dit UGent avontuur; Sandra Steyaert, mijn beste vriendin, vrouw en soulmate! Maar eerst een kleine omweg langsheen alle mensen die dankzij haar in mijn leven zijn gekomen.

Betsy, Eric en Nicola, als schoonfamilie aanvaardden jullie mij meteen als een 'echt' lid van de familie. Steeds konden we bij jullie terecht wanneer onze werkdagen iets te lang waren uitgelopen en we de rit naar De Panne of Izegem niet zagen zitten. Telkens mochten we zonder probleem mee aanschuiven aan tafel en vaak ook nog eens mee de menu bepalen. Jullie gastvrijheid heeft ervoor gezorgd dat ik in een mum van tijd een tweede Oost-Vlaamse thuis had. Ook de rest van de Steyaert familie wordt gekenmerkt door deze onvoorwaardelijke gastvrijheid. Op geen enkel moment hebben jullie mij als een buitenstaander aanzien. Bedankt hiervoor!

Hetzelfde kan gezegd worden van de extra vriendengroep(en) die ik erbij kreeg via Sandra. Ondanks de obligatoire West-Vlaamse boerenmopjes en taalgrapjes hebben jullie mij stuk voor stuk aanvaard zoals ik ben. Nooit had ik gedacht om in één slag zo'n verscheidenheid aan individuen als vriend te kunnen bestempelen. Ik vind het fascinerend hoe jullie geen enkele gelegenheid voorbij laten gaan om af te spreken en hoe, zelfs nu we in het "verre Izegem" wonen, de uitnodigingen ook nog steeds onze kant opkomen.

---

Sandra, babe, bolleke, dat jij als laatste aan bod zou komen in dit dankwoord stond reeds lang vast. Het is tenslotte het slotstuk van een wetenschappelijk avontuur en zoals gewoonlijk is in wetenschappelijke literatuur worden de belangrijkste personen laatst vermeld. Sandra, ons avontuur ontsproot in de Vooruit vanuit een gemeenschappelijke interesse in de boeken van Brian Greene. (Djeezes wat zijn wij nerds!) De voorbije 6 jaar waren fenomenaal! Elke dag opnieuw liet je mij zien dat de wereld niet steeds een zwart-wit film hoeft te zijn. Alhoewel in retrospect niet al onze gemeenschappelijke beslissingen de beste waren zou ik geen enkele willen veranderen. Ze hebben tenslotte geleid tot dit moment; getrouwd, beiden gedoctoreerd en samen een huis gekocht! Ik hou ervan hoe je er nog steeds in slaagt om mij tot rust te brengen met een minimum aan sussende woorden en hoe je mij zonder meer aanvaardt op mijn beste en slechtste momenten. Babe, je was, bent en zal steeds de meest intrigerende, fascinerende persoon blijven die ik ken. Wat de toekomst ook brengt, mijn enigste wens is dat ik deze mag doorbrengen met jou!

# CURRICULUM VITAE



# Curriculum Vitae

## General information

	March 9 <sup>th</sup> , 1989, Izegem Belgian Married (to Sandra Steyaert)
	Kouterweg 72 8870 Izegem (Belgium)
	+32 474 38 08 98
	<a href="mailto:adriaan.verhelle@ugent.be">adriaan.verhelle@ugent.be</a> <a href="mailto:adriaan_verhelle@hotmail.com">adriaan_verhelle@hotmail.com</a>
	<a href="http://www.linkedin.com/in/adriaanverhelle">www.linkedin.com/in/adriaanverhelle</a>



## Education

**Ghent University, Faculty of Bioscience Engineering**  
**Ghent, Belgium | 2010-2012**

Master in Bioscience Engineering, cell and gene biotechnology - *magna cum laude*

**Ghent University, Faculty of Bioscience Engineering**  
**Ghent, Belgium | 2007-2010**

Bachelor in Bioscience Engineering, cell and gene biotechnology - *cum laude*

## Experience

**R&D Engineer** | Fromunion NV-Kaasmakerij Passendale  
Passendale, Belgium | March 2017 - PRESENT

**Doctoral researcher** | Medical Biotechnology Center (MBC) - Nanobody lab - Department of Medical Protein Research, Faculty of Medicine and Health Sciences, Ghent University  
Ghent, Belgium | January 2013 - Februari 2017

**Summer Internship** | ILVO - Institute for Agricultural and Fisheries Research  
Melle, Belgium | July 2010 - September 2010

## Publications

Verhelle A, Nair N, Everaert I, Van Overbeke W, Supply Lynn, Zwaenepoel O, Peleman C, Van Dorpe J, Lahoutte T, Devoogdt N, Derave W, Marinee CK, VandenDriessche T, Gettemans J. **AAV9 delivered bispecific nanobody attenuates amyloid burden in the gelsolin amyloidosis mouse model.** Hum Mol Genet. 2017 Feb. doi: ddx056

Verhelle A. and Gettemans J. (2016). **A Nanobody Based Approach to Amyloid Diseases, the Gelsolin Case Study, Exploring New Findings on Amyloidosis.** Dr. Ana Maria Fernandez-Escamilla (Ed.), InTech. DOI: 10.5772/63981. Available from: <http://www.intechopen.com/books/exploringnew-findings-on-amyloidosis/a-nanobody-based-approach-to-amyloid-diseases-the-gelsolin-casestudy>

Verhelle A, Van Overbeke W, Peleman C, De Smet R, Zwaenepoel O, Lahoutte T, Van Dorpe J, Devoogdt N, Gettemans J. **Non-invasive imaging of amyloid deposits in a mouse model of AGel using <sup>99m</sup>Tc-modified nanobodies and SPECT/CT.** Mol Imaging Biol. 2016 Apr. doi: 10.1007/s11307-016-0960-y. PubMed PMID: 27130233

Beghein E, Van Audenhove I, Zwaenepoel O, Verhelle A, De Ganck A, Gettemans J. **A new surviving tracer tracks, delocalizes and captures endogenous surviving at different sub-cellular locations and in distinct organelles.** Sci Rep. 2016 Aug 12;6:31177. doi: 10.1038/srep31177. PubMed PMID: 27514728

Van Overbeke W, Wongsantichon J, Everaert I, Verhelle A, Zwaenepoel O, Loonchanta A, Burt-nick LD, De Ganck A, Hoche-pied T, Haigh J, Cuvelier C, Derave W, Robinson RC, Gettemans J. **An ER-directed gelsolin nanobody targets the first step in amyloid formation in a gelsolin amyloidosis mouse model.** Hum Mol Genet. 2015 May 1;24(9):2492-507. doi:



10.1093/hmg/ddv010. PubMed PMID:25601851

Bethuyne J, De Gieter S, Zwaenepoel O, Gacia-Pino A, Durinck K, Verhelle A, Hassanzadeh-Ghassabeh G, Speleman F, Loris R, Gettemans J. **A nanobody modulates the p53 transcriptional program without perturbing its functional architecture.** Nucleic Acids Res. 2014 Nov 10;42(20):12928-38. doi: 10.1093/nar/gku962 PubMed PMID: 25324313

Van Overbeke W, Verhelle A, Everaert I, Zwaenepoel O, Vandekerckhove J, Cuvelier C, Derave W, Gettemans J. **Chaperone nanobodies protect gelsolin against MT1-MMP degradation and alleviate amyloid burden in the gelsolin amyloidosis mouse model.** Mol Ther. 2014 Oct. 22(10):1768-78. doi: 10.1038/mt.2014.132. PubMed PMID: 25023329

## Conference posters & presentations

Verhelle A, Nair N, Van Overbeke W, Zwaenepoel O, Peleman C, Devoogdt N, Lahoutte T, VandenDriessche T, Chuah M, Gettemans J. **Nanobody gene therapy in the gelsolin amyloidosis mouse model via Adeno-associated virus type 9.**

The XVth International Symposium on Amyloidosis, Uppsala, Sweden, July 2016: *Poster presentation*

Verhelle A, Van Overbeke W, Peleman C, Zwaenepoel O, Devoogdt N, Lahoutte T, Gettemans J. **Prospection of gelsolin-nanobodies as a tool for nuclear imaging in a mouse model for familial amyloidosis of the Finnish type.**

The XIVth International Symposium on Amyloidosis, Indianapolis, USA, April 2014: *Poster presentation*

Van Overbeke W, Verhelle A, Everaert I, Zwaenepoel O, Vandekerckhove J, Cuvelier C, Derave W, Gettemans J. **Gelsolin amyloidosis: gelsolin nanobodies reduce amyloid burden in a transgenic mouse model.**

The XIVth International Symposium on Amyloidosis, Indianapolis, USA, April 2014: *Poster presentation*

